International Committee for Future Accelerators

Sponsored by the Particles and Fields Commission of IUPAP

Beam Dynamics Newsletter

No. 51

Issue Editor:
S. Chattopadhyay

Editor in Chief:
W. Chou

April 2010

Contents

1   Foreword

1.1   From the Chairman

Weiren Chou, Fermilab
Mail to: chou@fnal.gov

The International Committee for Future Accelerators (ICFA) met on February 25-26, 2010 at BNL. Atsuto Suzuki, Director General of KEK and Chair of ICFA, chaired this meeting. The meeting was preceded by an ILCSC meeting earlier on February 25 in the same place.

Jonathan Bagger, the new Chair of ILCSC, gave a report on the status of the ILC. GDE and the detectors are on track for issuing design reports by 2012. There is a growing connection with CLIC activities. Discussion has started on post-2012 plans. It was reported that there was an interesting evolution of the name FALC. It began as *Funding Agencies for Linear Colliders*, then became *Funding Agencies for Large Colliders*, and now stands for *Funding Agencies for Large Collaborations*. This reflects the broadening interest of the funding agencies that joined FALC in order to communicate with each other. Projects of interest to FALC include ILC, CLIC, a muon collider and Super-LHC.

Reports from about 20 laboratory directors and their representatives were presented. Some highlights follow. At Fermilab, the Tevatron is working very well, with delivered luminosity to each experiment approaching 8 fb^{-1}. Muon collider and neutrino factory work have been combined into one coherent US effort with the goal of producing a 5-year feasibility study. At CERN, the LHC will run 6 kA magnet current (7 TeV c.m.) until the end of 2011 with an integrated luminosity of 1 fb^{-1}, followed by a long shutdown in 2012 to prepare for 14 TeV operation. The integrated luminosity over the next 20 years is expected to be 3000 fb^{-1}. . The first improvement in the injector chain will be in the SPS, currently a bottleneck for increasing the luminosity. SPL and PS2 studies have stopped. At SLAC, the LCLS is operational and has received ~200 proposals from users this year. A group has been formed to work on Super-B if that project moves forward. At KEK, the KEK-B reached its goal of 1000 fb^{-1}. Super KEK-B has not yet received final government approval, but there $25M is available for upgrades this year. The first T2K neutrino event has been observed. At DESY, a company has been formed for the XFEL, with 10 countries signed on so far. PETRA3 has reached its emittance and current goals. Both JLab and BNL are designing e-ion colliders. At IHEP/Beijing, BEPC II reached its luminosity goal. Construction is going smoothly on the Daya Bay neutrino facility. CSNS has been approved by the Chinese government.

Four ICFA panels (Beam Dynamics, Advanced and Novel Accelerators, Instrumentation, and Interregional Connectivity) presented reports at the meeting. There will be three ICFA Advanced Beam Dynamics Workshops (ABDWs) this year: *FLS2010*, *HB2010* and *Ecloud2010*. Details can be found on the panel web site (http://www-bd.fnal.gov/icfabd/). ICFA approved the 50th ABDW, *ERL2011*, which will take place in October, 2011 at KEK, Japan. Details will come later.

I'd like to use this opportunity to emphasize again that all ABDWs are required to publish formal proceedings via JACoW. This is a requirement, not an option. An alternative to ABDW is ICFA Mini-Workshops, which are not required to have formal proceedings. Please refer to the panel web site for the requirements of the two different types of ICFA workshops.

This Panel together with the Advanced and Novel Accelerators Panel and the International Committee for Ultra Intense Lasers (ICUIL) has formed a Joint ICFA-ICUIL Task Force chaired by Wim Leemans (LBNL). The task force organized a Joint ICFA-ICUIL Workshop from April 8 to 10, 2010 at GSI, Germany. (https://indico.gsi.de/conferenceDisplay.py?confId=904) The title was "*High Power Laser Technology for Future Accelerators.*" It discussed the laser requirements for applications in future colliders, light sources, medical accelerators and high-intensity hadron machines. A summary report of this workshop can be found in Section 4.1.

The Fifth International Accelerator School for Linear Colliders will be held from October 25 – November 5, 2010 at Villars-sur-Ollon, Switzerland. CERN will host this school. Please see Section 2.1 for the announcement. The school web address is http://www.linearcollider.org/school/2010/.

The editor of this issue is Prof. Swapan Chattopadhyay, a panel member and director of the Cockcroft Institute, UK. Swapan collected 29 excellent articles in the theme section "*Accelerator Science and Technology in the UK.*" These articles give a comprehensive review of a variety of accelerator projects and activities in that country, covering a wide spectrum including particle and nuclear physics, photon science, neutron science, test facilities and accelerator systems R&D, advanced accelerator R&D and new initiatives, applications to energy, health and security, and industrial engagement. In this issue there are also two recent doctoral theses abstracts (Stephen Brooks of Oxford University and Jianjun Yang of Tsinghua University) and three workshop announcements (ELOUD2010, BOD2010 and Cyclotrons2010). I thank Swapan for editing and producing a newsletter of high quality and great value.

1.2   From the Editor

Swapan Chattopadhyay
Cockcroft Institute and Universities of Liverpool, Manchester and Lancaster
Mail to: swapan@cockcroft.ac.uk

This edition of the ICFA Beam Dynamics Newletter is a special one -- rather than focusing on a specific scientific theme, it captures a substantive set of research and development activities in the field of accelerator science and technology in the United Kingdom. The editor thanks the ICFA Beam Dynamics Panel Chair Dr. Weiren Chou for kindly agreeing to this theme which allows exposure of the dynamic and diverse UK activities in the field to the global community.

A very special feature of the UK community is its rather small size of less than 200 full time equivalent (FTE) researchers in the field, aside from the technical operation crews of operating accelerator facilities such as the DIAMOND Light Source in Oxfordshire, the ISIS Neutron Source at Rutherford Appleton Laboratory (RAL) and the R&D Test facility ALICE at Daresbury Lab (DL). Yet this group has a diverse national and international portfolio of activities in colliders and accelerators for Particle and Nuclear Physics, Photon and Neutron sciences and emerging new initiatives in

FFAGs (Fixed Field Alternating Gradient accelerators), Superconducting Radio Frequency (SRF) science and technology, laser-beam-plasma interactions, photonic band-gap structures and meta-matarials, high brightness photoinjectors, advanced diagnostics and instrumentation, mathematical physics of plasmas, particle and laser beams and applications to societal grand challenges in energy, health, security and associated engagement with relevant industries.

Yet another very special feature of this community is the relatively large number of academics from the university sector involved in accelerator R&D. While 60% of the community comes from the two large national laboratories (Rutherford Appleton Laboratory (RAL) and Daresbiury Laboratory (DL), including the Science and Technology Facilities Council's ASTeC centre) and the operating synchrotron radiation facility DIAMOND, the remaining 40% of the community is comprised of faculty, post-doctoral fellows, undergraduate and graduate students from universities such as Imperial College London, University College London, Royal Holloway University London, University of Oxford, University of Cambridge, University of Liverpool, University of Manchester, Lancaster University, University of Durham, University of Birmingham, University of Huddersfield, University of Surrey, University of Warwick, University of York, Leeds Uniuversity, University of Strathclyde, University of Glasgow, University of Dundee, Scottish Universities Physics Alliance and Queens University Belfast. In addition, University of Oxford and Royal Holloway University London are joined up in the collaborative John Adams Institute while a strong collaboration between universities, national labs and local economy/industry makes up the Cockcroft Institute (Universties of Lancaster, Liverpool, Manchester, Science and Technology Facilities Council and the North West economic Development Agency (NWDA)).

The accelerator community in UK is in substantive international collaboration with laboratories such as CERN, DESY (Germany), FAIR (Germany), BESSY (Germany), Sincrotone Trieste (Italy), INFN (Italy), ALBA (Spain), CEA Saclay (France), Soleil (France), MaxLab (Sweden), ESS (Sweden), proposed Turkish Accelerator Centre (TAC), KEK (Japan), J-PARC (Japan), Spring-8 (Japan), RIKEN (Japan), Shanghai Light Source (China), BEPC (China), Pohang Light Source (South Korea), Variable Energy Cyclotron Centre (India), Bhabha Atomic Energy Research Centre (India), Raja Ramanna Centre for Advanced Technology (India), Tata Institute of Fundamental Research (India), Budker Institute of Nuclear Physics (BINP, Russia), Fermilab (USA), ANL (USA), MSU (USA), LBNL (USA), SLAC (USA), Jefferson Lab (USA), Cornell University (USA), BNL (USA), MIT (USA), Harvard University (USA) and TRIUMF Laboratory (Canada). The UK community also plays significant international leadership roles in the International Linear Collider Global Design Effort, the International and European Neutrino Factory Studies and Muon Ionization Cooling Experiment, the emerging initiative in the Large Hadron electron Collider (LHeC) at CERN, the development of non-scaling FFAGs and novel technologies for hadron therapy and accelerator driven subcritical reactors (ADSR). In addition there is a strong activity in the emerging next generation national UK synchrotron radiation facility, the Next Light Source (NLS).

The accelerator community in UK has most recently formed its special Topical Group in the Institute of Physics (IoP), similar to the Division of Physics of Beams of the American Physical Society. There is a strong educational component of the community arising from the Education, Training and Outreach programmes of the

Cockcroft Institute and John Adams Institutes including jointly organized sessions of the Royal Society and ongoing courses at the large number of universities. Recently, there have been proposals to have collaborative accelerator schools with the US particle Accelerator School (USPAS) and CERN.

This edition gives a flavour of the set of diverse activities in accelerator science and technology in the UK. I am thankful to the entire UK community for their contribution and support in the production of this issue of the ICFA Beam Dynamics Newsletter.

2   International Linear Collider (ILC)

2.1   Fifth International Accelerator School for Linear Colliders

Barry Barish, Weiren Chou and Hermann Schmickler
Mail to: barish@ligo.caltech.edu, chou@fnal.gov, hermann.schmickler@cern.ch

We are pleased to announce the *Fifth International Accelerator School for Linear Colliders.* This school is a continuation of the series of schools started four years ago. The first school was held in 2006 at Sokendai, Hayama, Japan, the second in 2007 at Erice, Sicily, Italy, the third in 2008 at Oakbrook Hills, Illinois, U.S.A., and the fourth in 2009 at Huairou, Beijing, China. The school is organized by the International Linear Collider (ILC) Global Design Effort (GDE), the Compact Linear Collider (CLIC) and the International Committee for Future Accelerators (ICFA) Beam Dynamics Panel. The school this year will take place at Villars-sur-Ollon, Switzerland from October 25 to November 5, 2010. It is hosted by CERN and sponsored by a number of funding agencies and institutions around the world including the U.S. Department of Energy (DOE), the U.S. National Science Foundation (NSF), Fermilab, SLAC, DESY, INFN, IN2P3, CEA, Oxford University, KEK, IHEP, KNU and POSTECH.

We will offer a 10-day program, including an excursion and a site visit. There will be 8 days of lectures. The first two days will be an introductory course with an overview of proposed future lepton colliders (ILC, CLIC and the muon collider). This will be followed by two elective courses, one on accelerator physics and the other on RF technology. Both of these will run in parallel for 6 days. Each student is required to take the introductory course and one of the electives. A complete description of the program can be found on the school web site. There will be homework assignments and a final examination but no university credits.

We encourage young physicists (graduate students, post doctoral fellows, junior researchers) to apply. In particular we welcome those physicists who are considering changing to a career in accelerator physics. This school is adopting an in-depth approach. Therefore, former students are welcome to apply if they have a compelling reason to do so. The school will accept a maximum of 70 students from around the world. Students will receive financial aid covering their expenses for attending the school including travel (full or partial). There will be no registration fee. Each applicant should complete the online registration form (which can be found at www.linearcollider.org/school/2010/) and submit a curriculum vita as well as a letter of recommendation from his/her supervisor (in electronic form, either PDF or MS WORD). The application deadline is June 15, 2010. For more information, please

contact: Alexia Augier, CERN, CH-1211, Geneva 23, Switzerland, telephone: +41-22-767-0169, fax: +41-22-767-4194, e-mail: alexia.augier@cern.ch

Organizing Committee
> Barry Barish (GDE/Caltech, Chair)
> Alex Chao (SLAC)
> Hesheng Chen (IHEP)
> Weiren Chou (ICFA BD Panel/Fermilab)
> Paul Grannis (Stony Brook Univ.)
> In Soo Ko (PAL)
> Shin-ichi Kurokawa (KEK)
> Hermann Schmickler (CERN)
> Nick Walker (DESY)
> Kaoru Yokoya (KEK)

Curriculum Committee
> Weiren Chou (Fermilab, Chair)
> William Barletta (USPAS)
> Alex Chao (SLAC)
> Jie Gao (IHEP)
> Carlo Pagani (INFN/Milano)
> Hermann Schmickler (CERN)
> Junji Urakawa (KEK)
> Andrzej Wolski (Univ. of Liverpool)
> Kaoru Yokoya (KEK)

Local Committee
> Hermann Schmickler (CERN, Chair)
> Alexia Augier (CERN)
> Daniel Brandt (CERN)
> Django Manglunki (CERN)
> Barbara Strasser (CERN)

Fifth International Accelerator School for Linear Colliders – Curriculum
(v.3, 03/22/2010)

October 25 – November 5, 2010, Villars-sur-Ollon, Switzerland

Daily Schedule

Breakfast	08:00 – 09:00
Morning	09:00 – 12:30, including ½-hour break
Lunch	12:30 – 14:00
Afternoon	14:00 – 17:30, including ½-hour break
Tutorial & homework	18:00 – 20:30
Dinner	20:30 – 22:00

List of Courses (black: required, red and blue: elective)

	Morning	Afternoon	Evening
October 25		*Arrival, registration*	*Reception*
October 26	Introduction	ILC	Tutorial & homework
October 27	CLIC	Muon collider	Tutorial & homework
October 28	Joint lecture: Linac basics	Course A: Accelerator physics Course B: RF technology	Tutorial & homework
October 29	Course A: Accelerator physics Course B: RF technology	*Excursion*	Tutorial & homework
October 30	Course A: Accelerator physics Course B: RF technology		Tutorial & homework
October 31	Course A: Accelerator physics Course B: RF technology		Tutorial & homework
November 1	Course A: Accelerator physics Course B: RF technology	*Excursion*	Tutorial & homework
November 2	Course A: Accelerator physics Course B: RF technology		Tutorial & homework
November 3	Course A: Accelerator physics Course B: RF technology		Tutorial & homework
November 4	Study time		Study time
November 5	Final exam	*Free time*	*Banquet;* *Student Award* *Ceremony*
November 6	*Departure for a site visit to CERN*		

Program

	Tuesday, October 26	Wednesday, October 27	Thursday, October 28	Friday, October 29
Morning 09:00 – 12:30	**Opening remarks** **Lecture 1 – Introduction** (3 hrs) **Barry Barish** (GDE/ Caltech) • Tera scale physics • ILC and LHC • Layout of the ILC • Parameter choices & optimization • Other possible future lepton colliders: CLIC and the muon collider • Detectors	**Lecture 3 – CLIC** (3 hrs) • Klystron *vs.* beam driven acceleration • CLIC layout • Parameter choices & optimization • Driver beam stability • Comparison of the CLIC and ILC • Technical challenges	**Joint lecture of Courses A & B:** Linac basics (3 hrs)	**Course A: Accelerator physics** Lecture A1 – Linac (cont'd) **Course B: RF technology** Lecture B1 – Room temperature RF (cont'd)
Afternoon 14:00 – 17:30	**Lecture 2 – ILC** (3 hrs) **Barry Barish** (GDE/ Caltech) • e- and e+ sources • Bunch compressors and spin rotators • Damping rings • Main linac • Beam delivery system • Civil construction issues	**Lecture I4 – Muon collider** (3 hrs) • Muon collider basics • Machine layout • Major sub-systems • Challenges	**Course A: Accelerator physics** Lecture A1 – Linac (9 hrs) **Course B: RF technology** Lecture B1 – Room temperature RF (12 hrs)	**Excursion**
Evening 18:00 – 20:30	Tutorial & homework	Tutorial & homework	Tutorial & homework	Tutorial & homework

Program (cont'd)

	Saturday, October 30	Sunday, October 31	Monday, November 1	Tuesday, November 2
Morning 09:00 – 12:30	**Course A: Accelerator physics Lecture A1 – Linac** (cont'd) **Course B: RF technology Lecture B1 – Room temperature RF** (cont'd)	**Course A: Accelerator physics Lecture A2 – Sources** (cont'd) **Course B: RF technology Lecture B2 – Superconducting RF** (12 hrs)	**Course A: Accelerator physics Lecture A3 – Damping rings** (cont'd) **Course B: RF technology Lecture B2 – Superconducting RF** (cont'd)	**Course A: Accelerator physics Lecture A3 – Damping rings** (cont'd) **Course B: RF technology Lecture B2 – Superconducting RF** (cont'd)
Afternoon 14:00 – 17:30	**Course A: Accelerator physics Lecture A2 – Sources** (6 hrs) **Course B: RF technology Lecture B1 – Room temperature RF** (cont'd)	**Course A: Accelerator physics Lecture A3 – Damping rings** (12 hrs) **Course B: RF technology Lecture B2 – Superconducting RF** (cont'd)	Excursion	**Course A: Accelerator physics Lecture A3 – Damping rings** (cont'd) **Course B: RF technology Lecture B3 – LLRF & high power RF** (9 hrs)
Evening 18:00 – 20:30	Tutorial & homework	Tutorial & homework	Tutorial & homework	Tutorial & homework

	Wednesday, November 3	Thursday, November 4	Friday, November 5	Saturday, November 6
Morning 09:00 – 12:30	**Course A: Accelerator physics Lecture A4 – Beam delivery system and beam-beam** (6 hrs) **Course B: RF technology Lecture B3 – LLRF & high power RF** (cont'd)	**Study time**	**08:00 – 12:30 Final exam** (4.5 hrs)	**Departure for a site visit to CERN**
Afternoon 14:00 – 17:30	**Course A: Accelerator physics Lecture A4 – Beam delivery system and beam-beam** (cont'd) **Course B: RF technology Lecture B3 – LLRF & high power RF** (cont'd)	**Study time**	*Free time*	
Evening 18:00 – 20:30	Tutorial & homework	Study time	Banquet at 20:00; Student Award Ceremony	

Notes on the Program:

1. There are a total of 10 school days in this year's program, excluding the arrival day (October 25) and the final examination day (November 5). The time is divided as follows: 2 days for required courses, 6 days for elective courses, 2 half-days for excursion, 1 day for study time for preparation for the final exam. There will also be a site visit to CERN on November 6.
2. The required course consists of four lectures: Introduction, ILC, CLIC and the muon collider. Every student must take this course.
3. There are two elective courses: Course A (the red course) is accelerator physics, Course B (the blue course) is RF technology. They will run in parallel. Each student will choose one of these.
4. The accelerator physics course consists of lectures on four topics: (1) linac, (2) sources, (3) damping rings, and (4) beam delivery system and beam-beam effects.
5. The RF technology course consists of lectures on three topics: (1) room temperature RF, (2) superconducting RF, and (3) LLRF and high power RF.
6. There is a half-day joint lecture on linac basics for students taking both Courses A and B.
7. There will be homework assignments, but homework is not counted in the grade. There will be a final examination. Some of the exam problems will be taken from variations of the homework assignments. The exam papers will be graded immediately after the exam and results announced in the evening of November 5 at the student award ceremony.
8. There is a tutorial and homework period every evening. It is part of the curriculum and students are required to attend. Lecturers will be available in the evening of their lecture day during this period.
9. Lecturers have been asked to cover the basics as well as possible. Their teaching material will be made available online to the students well ahead of time (a few weeks prior to the school). Students are strongly encouraged to study this material prior to the beginning of the school.
10. Lecturers of the elective courses are required to provide lecture syllabus as soon as possible in order to help students make their selection.
11. All lecturers are responsible for the design of homework and exam problems as well as the answer sheet. They are also responsible for grading the exams.
12. The award ceremony will honor the top (~10) students based on their exam scores.

3 Theme Section: Accelerator Science and Technology in the UK

3.1 Overview – an Emerging Paradigm of Collaboration between Universities, National Facilities and Industry

Swapan Chattopadhyay
Cockcroft Institute
Mail to: swapan@cockcroft.ac.uk

3.1.1 Introduction

The UK accelerator programme is presently undergoing a strategic development. The achievements of the UK accelerator community to date have already positioned it as a unique contributor to science internationally. The current effort is devoted also towards applying the underlying knowledge base to the development of solutions to the national and global challenges in energy, environment, health and security. An integrated and comprehensive programme in accelerator science and technology must remain an essential component in the portfolio of investments by the UK in science needed to maintain its position as a leading scientific and industrial nation.

The UK accelerator strategy aims, in the first place, to be intricately linked to a healthy programme in the associated sciences that it enables, namely the particle, nuclear, photon and neutron sciences. It is believed that such fundamental underpinning to the sciences will automatically ensure, with proper motivation and stewardship, a flourishing set of innovations to serve the various societal applications e.g. knowledge exchange and technology transfer in areas of energy, environment, health and security.

3.1.2 Mission of UK Accelerator Science and Technology

The UK accelerator program is based on a sustainable and universal Mission, qualified by means of the following deliverables:

(i)   Innovative and generic R&D at the frontier of accelerator science;
(ii)   Project-specific R&D in accelerators as instruments of science;
(iii)   Leadership and management of national deliverables to international facilities and projects;
(iv)   Competence in crucial and special "transformational" technologies;
(v)   Addressing critical global and national issues in Energy, Health, Environment and Security;
(vi)   Exchange of knowledge with Industry;
(vii)   Staff complement of internationally acknowledged expertise;
(viii)   Seamless involvement of the Universities, National Facilities and Research Councils;
(ix)   Education and training to ensure a healthy next generation of scientists and engineers to benefit society.

3.1.3   The Model: Integrated Accelerator Community and Stakeholders

The aspirational modus operandi of the UK accelerator community is depicted in the figure below showing the essential roles and synergy of the participating sectors. All three of these (the Universities, the National Laboratories (Facilities) and the Industry/Economy) retain their identities and missions within the accelerator partnership providing synergy of fundamental research (academia), scientific and engineering exploitation (national research facilities) and industrial wealth creation. This will require a coordinated national stewardship.
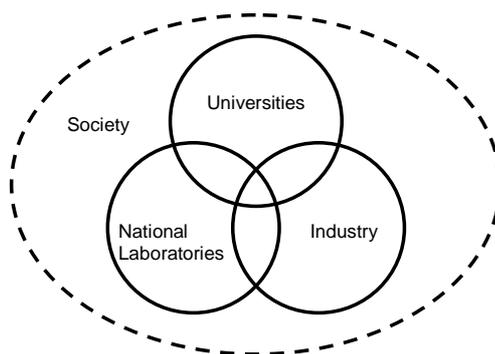
3.1.4   The Research Program Driven by Science

Accelerator-driven, intense, beams of charged particles enable scientists to addresses fundamental questions from sub-atomic to cosmic scales. The "facilities" which result are the grand instruments which make this possible. They range from particle colliders (leptons, hadrons and ions with GeV to TeV energies) to various photon and neutron sources. Present challenges include collisions with luminosities (brightness) up to 10^{36} cm^{-2}.sec^{-1} (ph/s/mm^2/mr^2/0.1% bandwidth), with beam sizes of order nanometres, and with pulse durations in the femto-second to atto-second range. Current and envisioned photon sources that will address electronic, atomic and molecular scale processes will require photon energies from THz and infrared to hard X-rays with varying temporal resolution down to atto-seconds.

Future challenges therefore include achieving stable and ultra-high accelerating fields, producing ultra-cold relativistic beams with very high intensities, developing ultra-fast detection and feedback techniques, producing ultra-short pulses with precise time synchronization and inherent phase-space brightness, and achieving energy efficiency via techniques of energy recovery and re-cycling.

Existing large accelerators facilities such as the LHC, J-Parc, KEK-B, Tevatron and future projects, such as the ILC/CLIC, Super-LHC, LHeC [1], Super-B, FAIR, EURISOL, NF/MC, Project-X, etc. illustrate the scope of particle/nuclear sciences which are possible. Similarly, existing international facilities like DIAMOND in UK, FLASH in Germany and LCLS in USA, facilities under construction such as the XFEL in Germany and the proposed Next Light Source (NLS) in the UK -- all illustrate the scope of the photon sciences which are possible. Finally an equally challenging landscape exists for neutron sciences at existing and upgradeable neutron sources such as the ISIS in UK and the proposed future sources such as the Neutron Source in China and the European Spallation Source (ESS).

3.1.4.1 *Research Focus: Current*

The UK's major accelerator contributions to date in national and international projects and advanced R&D have been focused on: (i) high energy particle physics facilities (e.g. ILC, MICE for Muon Cooling and Neutrino Factory, Super-B); (ii) fourth generation photon sources (e.g. FLASH, DIAMOND, NLS); (iii) prototyping novel concepts and technologies (e.g. SCRF and Energy Recovery in ALICE, electron FFAG in EMMA, Laser-plasma studies at RAL, Imperial College, Oxford, Strathclyde, Queens University Belfast); (iv) fundamental mathematical/computational beam physics; (v) emerging roles in LHC (including upgrades and LHeC), CLIC, Anti-matter research, Neutrino Factory/Muon Collider, Compact High-frequency Linacs and Meta-materials for particle acceleration.

3.1.4.2 *Reasearch Focus: Future*

The UK aspirations and capacity for the future include: (i) extending our linear collider expertise to multiple TeV-scale linear colliders such as CLIC, or other X-band options; (ii) continuing development of novel photon sources/FELs; (iii) contributing to the exploitation of LHC and its upgrades including a novel electron-proton collider (LHeC) spearheaded by UK scientists; (iv) expand our work to facilities serving nuclear and neutron sciences (e.g. HIE-ISOLDE, EURISOL, FAIR, ISIS Upgrade and ESS), (v) expand blue-sky research to include laser-plasma, photonic band-gap structures and meta-materials; (vi) increase our core competency in high current proton beams for applications in neutron sources, intense neutrino beams, particle beam cancer therapy, and in energy and environmental technologies e.g. Accelerator Driven Sub-critical Reactor (ADSR).

The spectrum of activity spans science and technology from the fundamental to the applied. Much of the knowledge generated can immediately be exploited in other areas of endeavour.

3.1.4.3 *Special Comment on the Role of Test Facilities*

The recognition and continuing support of accelerator-based Test Facilities in the UK and development of others in the future are vital to the health of the field. The existing UK facilities such as the High Current Front-end Test Accelerator, ALICE, EMMA, CLF and the Strathclyde ALPHA-X represent first steps in this direction. A national Superconducting RF Test Facility and High Brightness Electron and Ion Source Development Facility will be vital for the future of the NLS, future involvement in Nuclear Physics and Neutron Source Facilities (e.g. HIE-ISOLDE, EURISOL, ISIS Upgrade and ESS), in particle physics (Neutrino factory, Muon Collider and Linear Collider, LHC Upgrades, LHeC) and high-duty factor electron linear accelerators for medical isotope production independent of nuclear reactors.

3.1.5 The Research Program Driven by Applications

3.1.5.1 *Energy and Environment*

It is generally recognised that nuclear fission will have a vital role to play in meeting future energy requirements in the medium term. However, uranium used conventionally will only last a few more decades. Alternative fission technologies must

be sought that can deliver safer power production, lower proliferation risks, and long-term security of supply. ***Accelerator Driven Sub-critical Reactors (ADSRs)*** using thorium, which is plentiful, can secure safe electricity production. The fast-breeder technique pioneered in the UK allows the fuel to be recycled to last thousands of years. A high-power particle accelerator and target can generate the neutrons required to stimulate energy production "on demand", meaning that the reactor cores do not need to rely on their own neutron generation. This greatly reduces the risk of critical accidents. This new generation of nuclear fission technology offers a way of generating low-carbon electricity at low cost. Similar accelerator technology can be applied to the ***Artificial Transmutation of Waste (ATW)*** generated and stored underground, thus reducing environmental risks. Both high current Superconducting Radio Frequency (SRF) linear accelerator technology as well as development of FFAGs will be crucial for this program. In this regard, UK is pioneering the FFAG development program via EMMA electron prototype construction, operation and development.

3.1.5.2   *Health and Medicine*

Proton (and ion) therapy for the treatment of cancer offers significant advantages over other radiation methods. The combination of penetrative power and localised dose (by means of the Bragg peak) allows tumours to be treated with much less damage to surrounding tissue than electron or X-ray-based therapies. At present proton therapy is available at several centres overseas, and there is rapidly growing development of new facilities in Europe. In contrast, in the UK, the only therapy available is with low protons energy which limits the therapeutic use to near-surface cancers such as those of the eye. Cost and availability are major barriers to widespread use of existing accelerator technology to serve UK health needs (2000 patients/year). Higher proton energies are needed to allow therapy throughout the body.

Clinical understanding of radio-therapy must go hand-in-hand with accelerator developments. It is thus essential that any beam therapy facility be tightly coupled to clinical health and safety requirements permit to a university-based medical research centre.

Currently, the UK accelerator community is helping the hospital-based bids for two to three Proton Thereapy Centres in response to a call from the National Health Service (NHS). These will be based on readily available cyclotron or other systems available for purchase from industry today, coupled with an adjacent developmental technical laboratory.

Future compact therapeutic facilities could be based on superconducting cyclotrons (being actively developed at MIT etc.), FFAG-based synchrotrons (being developed in UK and Japan), or recent developments in laser-plasma interactions (being actively developed in Japan under the name Photo-Medical Research Valley, near Nara). The BASROC (the British Accelerator Science for Research in Oncology Consortium) is pursuing R&D at smaller, reliable, flexible, high throughput and cheaper proton/ion sources than those presently available (e.g. the FFAG-based designed pursued in the PAMELA project by UK accelerator scientists and engineers) while the laser-plasma activities in UK, especially the LIBRA project at Queen's University Belfast, could focus on laser-plasma generated protons for cancer therapy. Together, these approaches could give patients much better quality of life after treatment.

Yet another area of accelerators could be in the ***production of the diagnostic radio-isotopes*** matching the world-wide demand, while not depending on the operational

availability of experimental nuclear reactors subject to nuclear regulatory requirements. High current continuous pulse trains of 50 MeV electrons from a specially designed electron accelerator could supply the necessary production rate of the radio-isotopes by photo-fission radio-chemistry of Technicium. Other approaches based on conventional cyclotrons or Molybdinum are also viable and could provide more attractive options. But a design and demonstration via a prototype will be prerequisite to a production facility.

3.1.5.3 *Security*

In today's society, heightened security demands speedy and reliable scanning of materials and people at ports of entry to countries using rapidly scanning X-rays. In addition, compact and mobile security scanning devices are required for use in remote parts of the world in sensitive territories. Much of the technology for these purposes is based on microwave and linear acceleration. However, rapid and repetitive scanning with high reliability depends upon both advanced accelerator and imaging expertise. Neutrons can also be used to identify sensitive materials, conventional explosives and fissile material inside cargo containers. **High power X-ray scanners** based on electron linacs, and **neutron and gamma-ray spectroscopy** using powerful proton beams as neutron sources, all with advanced detector technologies, are areas of expertise that could be developed by the UK accelerator community in close collaboration with partner universities and UK industry.

3.1.6 **Summary and Conclusion**

The UK accelerator enterprise offers a unique paradigm combining academic depth, national laboratory breadth, engineering integration and industrial perspectives, adding to each other in a complementary fashion. Contributing to national and international projects is vital to retaining the skills base and preserves the necessary expertise in the field.

Advancing the frontier of accelerator and science and technology at the cutting edge gives the UK community the critical edge globally. Simultaneously, many of the developments have matured enough to be exploited already. The stakeholders in the field expect the accelerator community to generate value for the science and society at large, who are expecting to benefit from our community. Hence investment in identified "Test Facilities" and "transformational" technologies will be a crucial next step.

The community is seeking long-term sustained national commitment to accelerator science and technology to serve the national and global community further.

3.1.7 **Reference**

1. M. Klein, The Large Hadron Electron Collider Project, Proceedings of DIS09, Madrid, April 2009, arXiv:0909.2877 (2009).

Particle and Nuclear Physics

3.2 The UK LHC, LHeC and ATLAS Forward Physics Programme

Rob Appleby, John Dainton, Federico Roncarolo
Cockcroft Institute/University of Manchester
Mail to: robert.appleby@manchester.ac.uk

3.2.1 The LHC, LHeC and ATLAS Forward Physics

The UK has a strong programme in hadron collider accelerator physics, with key roles in the Large Hadron Collider (LHC) at CERN and in the conceptual design of the LHeC. The UK is also the leading partner in the ATLAS Forward Physics collaboration, which will instrument the forward region of the ATLAS experiment of the LHC and extend the physics capability of the experiment.

3.2.2 The LHC

The UK is active in many areas of the LHC machine. In this section, we describe two areas where the contribution is key - the study of machine-induced backgrounds for the LHC experiments and the LHC machine protection systems.

3.2.2.1 *Background Conditions in the LHC*

The performance of the Large Hadron Collider and the associated experiments is dependent on an understanding and control of particle rates arising in the machine and streaming to the experimental caverns and detectors. The understanding and control of experimental background is crucial to the successful operation of the LHC experiments. This machine induced background (MIB) will be seen with the first few bunches in the machine, and is generally proportional to beam current and dependent on the machine optics, filling scheme, collimation scheme and so on. The various sources of MIB in the LHC can be classified as,

- Halo scattering and subsequent showering, on the tertiary TCT collimators. This contribution arises from beam halo collimation in the long straight sections. It depends on the optics and collimation apertures, and varies greatly depending on the proximity of the experiment from the betatron and momentum cleaning sections of the machine.
- Beam-gas interactions in the long straight section (LSS) of the machine. This contribution depends of the local gas pressure profile, and the produced secondary particles generally have a visible line-of-sight to the interaction point (IP).
- Elastic beam-gas events in the arc. These events will modify the proton loss distribution on the tertiary collimators.
- Cross-talk from other experiment. This background is proportional to luminosity, and is possibly only be a problem for ATLAS and CMS providing a background to the lower luminosity LHCb and ALICE.

The UK is making calculations of the machine induced background to the experiments of the LHC from all sources in the machine, and working with CERN on understanding the measurements of background made at a beam energy of 450 GeV, 3.5 TeV and 7 TeV [1,2].
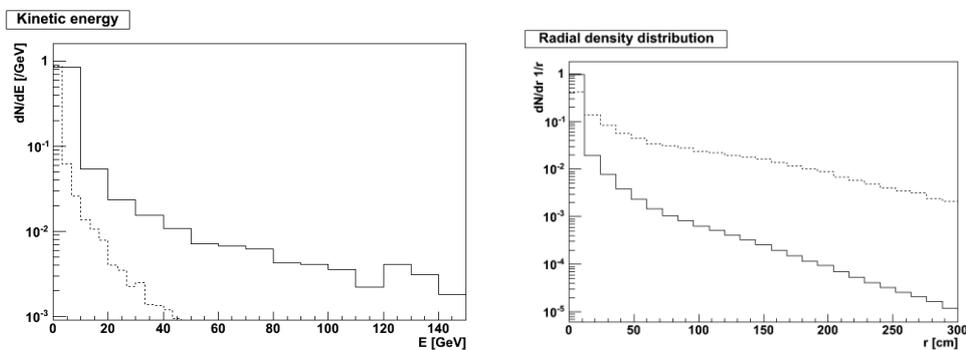
Figure 1: The charged hadron (solid) and muon (dashed) beam-gas background flux from early machine beam-gas interactions flowing to the LHCb cavern of the LHC.

The running at 450 GeV at a beam energy gave the first opportunity of the UK and CERN groups to study measurement of the background conditions. The initial running was made at a beam energy of 450 GeV and few bunches in the machine, and the background conditions into the experiments is dominated by beam-has interactions in the long straight sections of the LHC. Taking LHCb and the backgrounds associated with beam 1 as an example, the rate of inelastic beam-gas interactions in the LSS to the right of LHCb is 2.6 /s for a proton fill of 40E9 protons. The resulting production of forward secondary charged hadrons and muons results in a flux into the experimental cavern of 5.6 /s and 0.4 /s. The spatial and kinetic energy distribution of the charged hadrons (solid line) and muons (broken line) is shown in Figure 1. The UK is studying the measured backgrounds around the LHC to bench mark the calculations and prepare tools to mitigate the background conditions in the machine for 3.5 TeV and 7 TeV running. Features in the calculations such as high multiplicity events and magnitude of non-colliding beam trigger rates are present in the simulation and the data.

3.2.2.2 *Machine Protection*

The Large Hadron Collider (LHC) has a nominal beam momentum of 7 TeV/c per beam, a design luminosity of 1034 cm-2 s-1 in 7 TeV p-p mode and a nominal beam stored energy of 362 MJ, which is enough to cause considerable damage to the elements of the machine and the experiments. To deal with these levels of stored energy a complex system of machine protection has been designed to protect the machine, including beam loss monitors, current monitors and quench monitors, which are connected to a beam dump and interlock system. The strategy of these systems is to manage the continuous losses from the beam, handle failure scenarios over a large range of time scales and provide protection to the machine and the experiments. The system is designed around the beam interlock system (BIS), which receives input from passive and active systems and is capable of triggering a beam dump or inhibiting further injection.

The UK is studying the performance and response of the LHC machine protection systems, both in simulation and with beam [3]. To demonstrate the protection of the near-beam experiments from hardware failures, Figure 2 shows the time-dependent

proton distribution for a 450 GeV beam with collision optics at the TOTEM experiment roman pots located 220 m from the interaction point of CMS. At t=0 the power converter RD1.LR1 powering the separation dipoles D1 fails, the beam orbit distorts around the ring and the beam is lost after about 5 ms on the primary and secondary machine collimators. During this time the beam does not scrape any of the experiments. The machine protection therefore relies on the passive collimator protection combined with beam loss monitors to detect the loss and magnet current monitors to detect the current change. All these subsystems are inputs to the BIS. The commissioning of the LHC in 2009 included time for a study of the machine protections systems. For example, the power converters powering dipoles around the LHC ring were turned off to study the beam and system responses. In all cases, the beam orbit deviation was in agreement in the simulations and the BIS successfully dumped the beam.
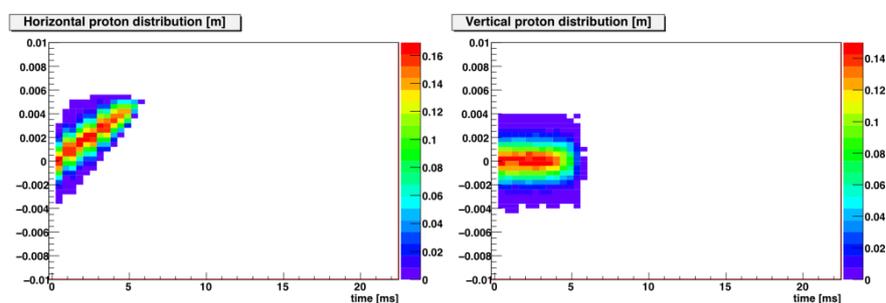
Figure 2: The horizontal and vertical proton distribution at the TOTEM roman pots as a function of time, for a circuit error in RD1.LR1. The calculation was made for a 450~GeV stored beam with nominal collision optics.

3.2.3   The LHeC

The LHeC proposes to collide the LHC 7 TeV proton beam (or ion beam) with a 50-70 GeV electron beam in one of the existing LHC interaction regions, exploiting the LHC beam for high energy lepton-hadron scattering [5]. The physics reach of this machine would allow studies of the parton structure of the proton, new Tera-scale physics, high density matter and many other topics, including a broad nuclear programme from eN collisions. The LHeC CDR is planned for the end of 2010. The LHeC baseline design contains two different possibilities to generate the electron beam. The first, the ring-ring option, installs an electron ring in the LHC tunnel, whilst the linac-ring option proposes a recirculating (and possibly energy recovery) linac to produce the electron beam. Both options are expected to meet the LHeC physics goals and both will be studied for the LHeC CDR.

The UK is contributing to several aspects of the machine design of LHeC, especially in interaction region and optics studies. There are also synergies to the UK programmes in energy recovery linacs, the production of polarised positron beams and crab cavity design.

3.2.3.1   *Interaction Region Design*

The UK is developing the interaction region designs for the LHeC ring-ring option. A key challenge in a ring-ring electron-proton IR is the separations scheme of the two beams, and the associated synchrotron radiation emission of the electron beam. The baseline LHeC physics programme calls for two distinct phases of operation:

- High luminosity of 10^{33} cm $^{-2}$ s $^{-1}$ with low forward acceptance of $10 < \theta < 170$
- Lower luminosity of 10^{31} cm $^{-2}$ s $^{-1}$ with a high forward acceptance of $1 < \theta < 179$

The baseline designs for both interaction regions rely on achieving electron-proton separation using dipole separators, displaced electron final triplet quadrupoles and an electron-proton crossing angle of around 1.5 mrad at the IP. The synchrotron radiation is screened from super conducting elements (specifically the proton inner triplet) by a series of radiation masks. The elements of the layout such as the separation scheme, electron and proton optics, components of the detector and the production of synchrotron radiation are inherently coupled.

The 10-degree acceptance layout is shown in Figure 3, which has a total radiation power of 60 kW. The inner electron triplet is located 1.2 m from the electron-proton IP. Figure 4 shows the 1-degree acceptance IR, which is constrained by the detectors in the forward region and locates the electron triplet 6.2 m from the IP. A variant with a dipole at 6.2 m is under study. The UK is developing both IRs in collaboration with CERN and DESY.
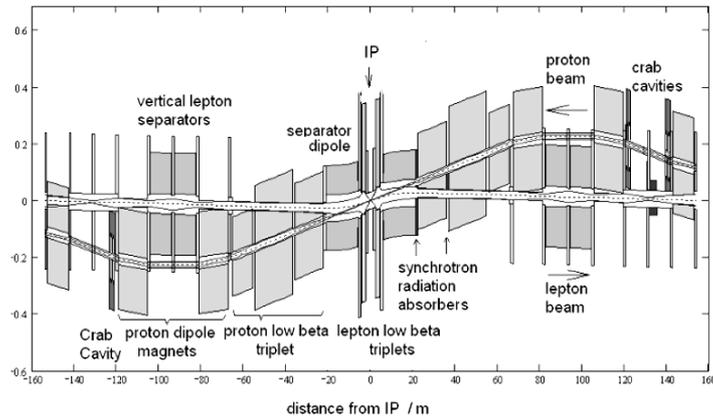
Figure 3: The LHeC 10 degree IR.
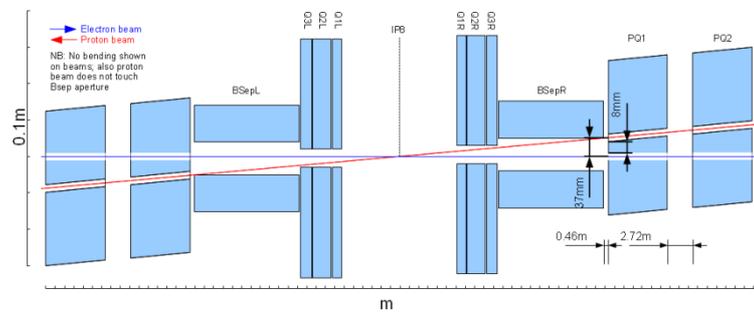
Figure 4: The LHeC 1 degree IR.

3.2.4 **ATLAS Forward Physics**

The ATLAS Forward Proton (AFP) international collaboration is proposing to upgrade the forward region of ATLAS by installing forward proton detectors at 220 m and 420 m from the interaction point on both sides of the LHC ATLAS experiment. The UK is leading the collaboration and coordinating the machine related studies At both the 420 m and 220 m locations it is proposed to install movable beam pipes which will host silicon tracking and fast timing detectors, giving four independent detector stations located on both sides of the ATLAS detector.

The AFP detectors are designed to operate at intermediate and high instantaneous luminosities of up to 10^{34} cm^{-2} s^{-1}. The primary goal is to enhance the ATLAS baseline physics program, particularly the search for and identification of new particles such as Higgs bosons and supersymmetric particles. Full details about the AFP proposal can be found in [4].

3.2.4.1 *The Integration with the LHC Machine*

The experiment acceptance at 220 m is depending upon the setting of two collimators designed to protect the LHC straight section and dispersion suppressor around ATLAS from the physics debris generated at the 2 high luminosity experiments. Such collimators (at about 140 m and 190 m fro the IP) are foreseen to be removed from their parking position (as needed for machine protection) for luminosity higher than a few 10^{33} cm^{-2} s^{-1}. Since the presently foreseen collimators setting would heavily compromise the AFP acceptance, the role and dynamics of the LHC straight section collimators was made. The simulations consist in loss maps from protons generated by ATLAS collisions and tracked along the beam line. Such protons include the AFP signal and background. Figure 4 shows a result example, for which two collimation settings are proposed, either displacing an existent collimator after AFP (red line) or adding a third collimator and relaxing the collimator settings in front of AFP (green line). In both cases all losses in superconducting elements are below the quench limit (blue line).
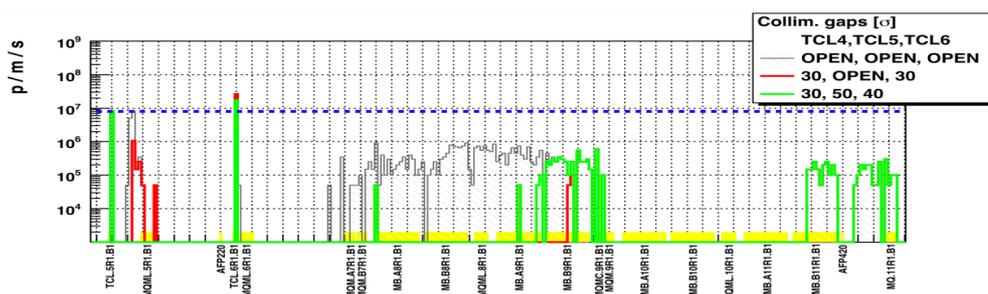
Figure 4: Loss maps generated at the right side of ATLAS in the region 190m-450m. Among the different elements, the collimator (TCL4,5,6) and the proposed AFP positions are indicated.

3.2.5 **References**

1. R.B. Appleby, Y. Inntjore Levinsen, and H. Burkhardt, "Beam-Gas simulations for 2009 LHC running and first comparisons with data", LHC-note-429.
2. R.B. Appleby *et al*, "Betatron halo machine induced background for LHCb at 7 TeV", LHC-report-1180.

3. R.B. Appleby, "LHC circulating beam accidents for near-beam detectors", LHC-report-1176.
4. The FP420 collaboration, "The FP420 R&D Project: Higgs and New Physics with forward protons at the LHC", JINST 4 T10001.
5. M. Klein, The Large Hadron Electron Collider Project, Proceedings of DIS09, Madrid, April 2009, arXiv:0909.2877 (2009).

3.3 LHC, FP420 and SPS Beam Coupling Impedance Studies and Mitigation Methods

Roger M. Jones, on behalf of the MEW group
Cockcroft Institute, Daresbury, Warrington, Cheshire WA4 4AD, UK
University of Manchester, Oxford Road, Manchester, M13 9PL, UK
Mail to: roger.jones@manchester.ac.uk

3.3.1 Introduction

Collimators and kicker magnets within the LHC and SPS have an associated impedance which can cause an appreciable wakefield and will dilute the overall emittance of the beams. The upgrade of the LHC, for example, will feature modified collimators with reduced overall beam impedance. We have been involved with various impedance mitigation techniques and also understanding fundamental models of beam impedance [1-5], in particular, in the low frequency regime for the resistive wall wakefield [1]. Current work is focused on beam impedance of both collimators and kickers for the LHC and SPS. Firstly, the work on impedance of LHC Roman Pots and collimators is discussed.

3.3.2 Analysis of Beam Impedance for LHC and FP420

At the LHC, four Roman Pot (RP) [2] type detectors are installed on both sides of the ATLAS experiment with the aim of measuring elastic scattering at very small angles and determining the absolute luminosity at the interaction point. During dedicated LHC runs, the detectors will be positioned at approximately 1 mm from the nominal beam orbit. Numerical simulations and laboratory wire measurements were carried out to characterize the RP impact on the total LHC beam coupling impedance budget. We also investigated the longitudinal coupling impedance of the FP420 double pocket stations [3-5], which, it turns out, are dominated by a narrow band component with significant modes from 2 to 3GHz. This has been characterized by means of laboratory measurements and numerical calculations that are in good agreement. The already small impact on the LHC impedance budget will be even smaller after implementing in the next design tapering foils at the pockets indentations. The stretched wire technique has been successfully used for determining the characteristic loss factor. This quantity, after scaling for the real LHC bunch shape is used to predict the energy loss.

The work on the low-frequency impedance prediction of the transverse wall beam impedance at the first unstable betatron line (8 kHz) of the CERN Large Hadron Collider (LHC) is particularly important for understanding and controlling the related coupled-bunch instabilities. We performed laboratory measurements and numerical simulations to cross-check the analytical predictions. The experimental results based on

the measurement of the variation of a custom built probe coil inductance in the presence of sample graphite plates and LHC collimator jaws. Both the experimental and simulation component of this work is continuing in detailed experiments being made on both collimators. We have also expanded this area of work to include impedance issues associated with LHC and SPS kicker magnets. This area of work is discussed in the next section.

3.3.3 Current Research: Collimator and Kicker Beam Reduction Research

Current models of the CERN accelerator system attribute a significant proportion of the beam impedance to either the kicker magnet systems (highly prevalent in the SPS) or the beam collimators (expected to dominant in the LHC) and hence present attempts at reducing the beam impedance, both longitudinal and transverse, are focused on for these components. To properly mitigate for these sources of beam impedance losses, accurate models of beam impedance are being developed and applied to structures within the accelerating structures.

In the case of kickers, multiple resonances are being explored. These resonances are the source of reduced rise time in the magnet response. These cause periodic heating in the magnets, potentially above the Curie temperature, and threaten the effective operation of the magnets. A variety of potential impedance reduction methods are under consideration, based on data from existing methods such as using beam screens and implementing serigraphy on internal walls of components, together with new implementations.

We are also studying the impedance of collimators, thought to be the primary source of transverse impedance in the LHC and hence are a significant source of emittance dilution. At present the beam dynamics are severely impacted by the impedance of the collimators and this research will have the potential to make a major impact on the LHC. Means to damp the wakefields in these collimators are being explored, including a consideration of new composite materials specially developed for this application. This work is performed in close collaboration with our CERN colleagues.

3.3.4 Summary

Our earlier work on the impedance of various components in the LHC and FP420 is continuing. We are developing a detailed understanding of the mechanisms behind the existing resonances and operation of the kicker magnets and collimator systems, using theoretical descriptions, computational simulations and experimental measurements. Subsequent to this, further measurements will be made of other magnet systems and collimators to allow a comparison of alternative construction methods; ferrite-loaded magnets, laminated steel-strip magnets, and the existing theoretical models (predominantly assume a continuous aperture of a uniform material). From this comparison it is expected to understand the different sources of resonant phenomena from the components, and if possible expand upon these phenomena and develop new models to more accurately describe the resonance observed.

3.3.5 References

1. F. Roncarolo, F. Caspers, T. Kroyer, E. Metral, , N. Mounet, B. Salvant, B. Zotter,

Comparison between laboratory measurements, simulations, and analytical predictions of the transverse wall impedance at low frequencies. Phys.Rev.ST Accel.Beams 12:084401, 2009.

2. F. Roncarolo, R.M. Jones, F. Caspers, B.D. Girolamo, T. Kroyer, *Characterization of the ATLAS Roman Pots Beam Coupling Impedance and Mechanics.* Proceedings of 11th European Particle Accelerator Conference (EPAC 08), Magazzini del Cotone, Genoa, Italy, 23-27 Jun 2008

3. F. Roncarolo, R. Appleby, R.M. Jones, *Beam Coupling Impedance Studies on LHC FP420 Multi-pocket Beam Pipe Prototype.* Proceedings of 11th European Particle Accelerator Conference (EPAC 08), Magazzini del Cotone, Genoa, Italy, 23-27 Jun 2008.

4. R.B. Appleby, R.M. Jones, F. Roncarolo, *Beam Coupling Impedance Simulations and Laboratory Measurements for the LHC FP420 Detector*, Proceedings of Particle Accelerator Conference (PAC 07), Albuquerque, New Mexico, 25-29 Jun 2007.

5. M.G. Albrow, R.M. Jones, et al., *The FP420 R&D Project: Higgs and New Physics with forward protons at the LHC,* JINST 4:T10001,2009.

3.4 The International Linear Collider

3.4.1 The Positron Source

Jim Clarke, on behalf of the HeLiCal collaboration
STFC Daresbury Laboratory and Cockcroft Institute, Daresbury, Warrington, Cheshire WA4 4AD, UK
Mail to: jim.clarke@stfc.ac.uk

3.4.1.1 *Description of the Source*

The positron source is a highly challenging subsystem of the ILC. In the solution adopted the electron main linac beam passes through a long helical undulator to generate a multi-MeV photon beam.This photon beam is transported ~500 meters to the positron source target hall where it hits a 0.4 radiation length thick Ti-alloy target producing showers of electrons and positrons. The positrons are captured, accelerated, separated from the shower constituents and the unused photon beam and then are transported to the Damping Ring.

More details on the source parameters and layout can be found in a previous newsletter [1]. The UK has leadership responsibility for the complete positron source design effort for the ILC and takes special responsibility for the undulator, the target and the overall system engineering and integration. In addition, the UK group has played a strong role in advancing the development of simulation tools for understanding depolarisation processes in the ILC and hosted an ICFA mini-workshop on Advanced QED Methods for Future Accelerators at the Cockcroft Institute in 2009.

3.4.1.2 *The Undulator*

The undulator must be superconducting to achieve the required parameters of 0.86 T transverse field on-axis with only an 11.5 mm period [2]. Two interleaved helical windings of NbTi spaced half a period apart generate the transverse helical field. The undulator will consist of 4 m long cryomodules containing two separate undulators with an active undulator length per cryomodule of 3.5 m. A number of short superconducting

prototypes have been constructed by a joint collaboration between Daresbury Laboratory and Rutherford Appleton Laboratory (RAL) to help select the optimum undulator parameters. A full scale 4 m long cryomodule has been manufactured at RAL and is now in the final stages of commissioning [3].

The 1.75 m long undulators have been successfully measured magnetically in a vertical cryostat. The tests show that both magnets can deliver the nominal design current of 216A corresponding to 0.86 T. The maximum observed quench current was 301 A and 306 A for magnets 1 and 2 respectively [1]. A photo of the complete cryomodule is given in Figure 1.
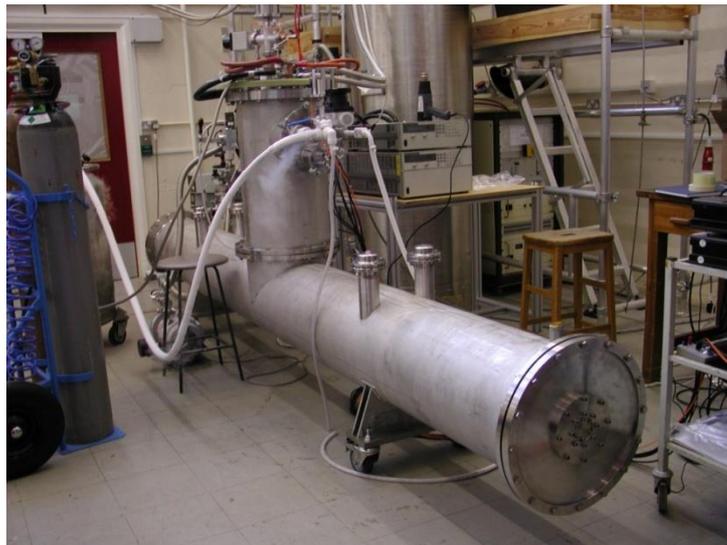
Figure 1. The 4m long cryomodule under commissioning at RAL.

A serious concern for the ILC is the impact of the undulator on the electron beam that travels through it since this electron beam later takes part in the collisions at the Interaction Point. Clearly the emission of synchrotron radiation within the undulator leads to a loss in energy by the electrons. On average the electrons will lose about 3 GeV of their 150 GeV at the undulator and this energy has to be supplied subsequently in the linac. The emission of synchrotron radiation also increases the energy spread of the electron bunches, in this case from a relative value of 0.16% to 0.23% at 150 GeV. The narrow bore of the undulator vacuum vessel (5.85mm diameter) means that strong wakefield effects can also be generated. Fortunately these effects are relatively small so long as a smooth copper beam tube is utilised [4].

3.4.1.3 *The Target*

The positron production target is a rotating wheel made of titanium alloy. The photon beam is incident on the rim of the spinning wheel, whose diameter is 1 m and thickness is 14 mm. During operation the outer edge of the rim moves at 100 m/s. This combination of wheel size and speed offsets radiation damage, heating and the shock-stress in the wheel from the ~130 kW photon beam. A shaft extends on both sides of the wheel with the motor mounted on one shaft end, and a rotating water union on the other end to feed cooling water. The target wheel sits in a vacuum enclosure at 10^{-8} torr. The rotating shaft penetrates the enclosure using two vacuum feed-throughs, one on each end. A strong positron capture magnet is mounted on the target assembly, and requires

an additional liquid nitrogen cooling plant. The motor driving the target wheel is sized to overcome forces due to eddy currents induced in the wheel by this capture magnet.

Several numerical eddy current simulations of the wheel moving in the field of the capture magnet have been carried out using alternative codes and techniques. Whilst broad agreement is found between these studies, showing power loading on the target of ~10 kW for a static 1 T field, it has been decided that this is such a crucial issue that a target prototype has been developed at the Cockcroft Institute and this is being used for eddy current benchmark measurements [5]. A photo of the target test stand is shown in Figure 2. Whilst understanding of the exact eddy current losses is important, equally vital will be the demonstration of stable full speed operation. The experiment is currently taking data and comparison is being made against the numerical models. At present the wheel has operated successfully at up to 1800 revolutions per minute (94 m/s at the rim), no attempt has been made to go beyond this speed at present.
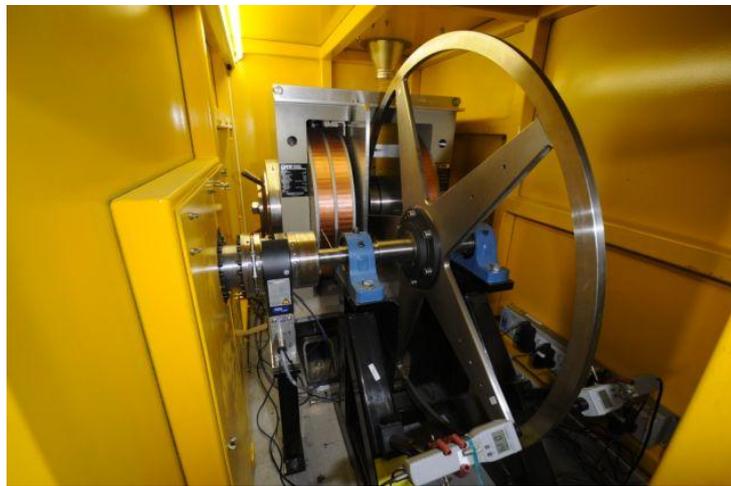
Figure 2. Photo of the 1m target wheel manufactured from Ti passing through the poles of the dipole test magnet. This eddy current experiment is housed inside a solid personnel safety enclosure due to the high rotation speeds being used.

3.4.1.4   *Summary*

The UK has leadership responsibility for the complete positron source design effort for the ILC and takes special responsibility for the undulator, the target and the overall system engineering and integration. A full scale undulator cryomodule has been fabricated and tested as part of a joint collaboration between Daresbury and Rutherford Appleton Laboratories. Additionally, a rotating target test stand has been built at the Cockcroft Institute and this is currently being used to measure the effect of the induced eddy currents on the target performance.

3.4.1.5   *References*

1. ICFA Beam Dynamics Newsletter No. 50, December 2009.
2. D.J.Scott et al, PR-STAB, 10, 032401 (2007).
3. J. Rochford, "The Superconducting Undulator for the ILC Positron Source", PAC 09.
4. D. J. Scott, PhD Thesis, University of Liverpool.
5. I.R.Bailey et al, "A Prototype Target Wheel for the ILC Positron Source", EPAC 08.

3.4.2 **The Beam Delivery System**

D.Angal-Kalinin, ASTeC, STFC Daresbury Laboratory and Cockcroft Institute, UK
N. Watson, Birmingham University, UK
For the LCABD Collaboration
Mail to: deepa.angal-kalinin@stfc.ac.uk

3.4.2.1   *Introduction*

The beam delivery system in the future linear collider will deliver the high energy electron and positron beams to the interaction/collision point. The design of the beam delivery system can essentially be divided in to four main areas, namely: the final focus system to achieve nanometre vertical beam size at the collision point; the collimation system to reduce the background in the detector and provide machine protection; dedicated diagnostics and tuning of the beam and finally post collision extraction line to transport the highly degraded beams after the collision to the beam dumps. The UK programme has contributed to all these areas for the ILC in addition to a few specific areas such as collimation and post collision extraction line for CLIC. We describe here two highlighted topics: interaction region configurations and the collimation studies for the ILC.

3.4.2.2   *ILC Interaction Region Configurations*

The cold technology choice for the ILC implies in principle the possibility of head-on collisions, which has advantages from both the machine and physics point of view. However, to extract the highly disrupted beam after the collision is extremely challenging. The problem of extraction at 800 GeV CM was not solved for TESLA [1,2] when the decision on cold technology was announced in August'04. During the first ILC workshop at KEK (November'04) a working assumption was made to consider two interaction regions, one with a large crossing angle of 20 mrad and one with a small crossing of 2 mrad, due to the pros and cons of both the schemes. In the 2 mrad scheme [3,4,5] as shown in Figure 1, the outgoing beam passes off-axis through the large bore final focus magnet and gets an additional dipole kick. Another scheme named 'modified head-on collision' was proposed during the Snowmass 2005 workshop. This scheme combines the head-on extraction using electrostatic separators with off-axis quadrupoles further down in the final focus to separate the incoming and outgoing beams [6,7] as shown in Figure 2. A careful design of the interaction region is required in both of these schemes to avoid background in the detector and losses in the superconducting magnets. A highly-degraded beam at the collision point with a long low energy tail poses several problems in extracting, avoiding backscattering, transporting and providing polarisation and energy measurements desirable for physics. The machine detector interface evaluation of both the 20 mrad and 2 mrad schemes showed larger backgrounds in the detector due to pairs when the 20 mrad configuration was used with the proposed Detector Integrated Dipole (DID) for correcting the vertical angle at the IP to avoid spin misalignment. As a result of these studies, an intermediate crossing angle of 14 mrad with Anti-DID was proposed [8]. The final configuration chosen for the ILC Reference Design includes one interaction region with 14 mrad crossing angle with two complementary detectors in the push-pull mode [9].
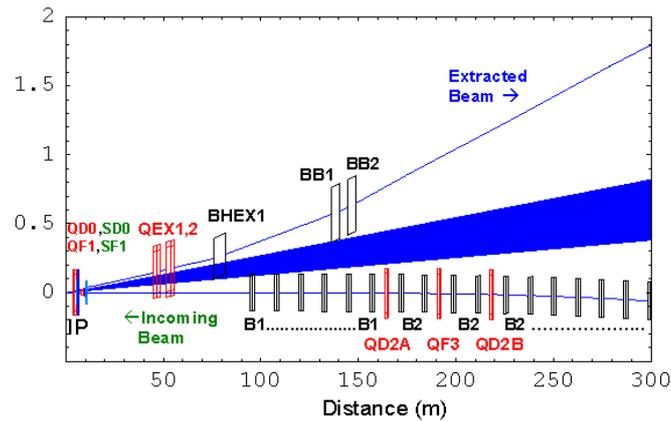
Figure 1: The layout of minimal 2mrad crossing angle configuration. The beamstrahlung photon cone is shown in blue.
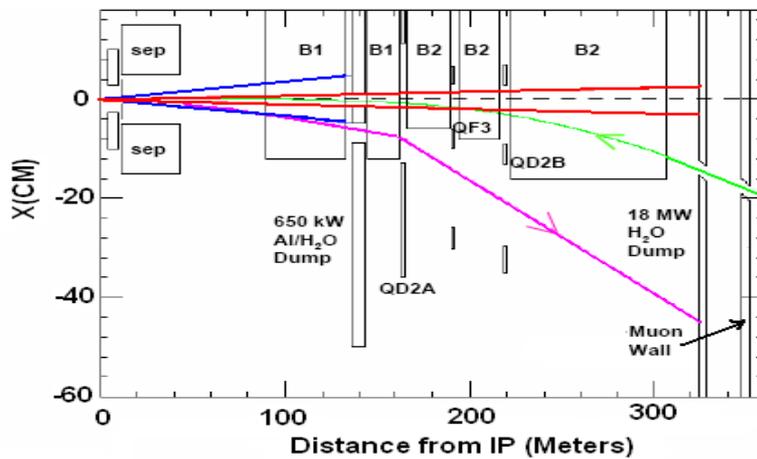
Figure 2: Plan view of modified head-on extraction from interaction point to charged and photon beam dumps. Green line shows the incoming beam, magenta line shows the outgoing beam and red lines indicate the beamstrahlung photon cone.

3.4.2.3   *Collimation Design for the ILC*

A two stage collimation design consisting of thin (<1 radiation length) spoilers and thick absorbers (20-30 radiation lengths) is essential to collimate high energy beams (250-500GeV) in ILC. In order to reduce the background in the detector, very narrow gaps (full gap ~1mm) are required in the spoilers. However, the wakefields generated by a short bunch (300μm) in these collimators degrade the luminosity at the IP.

The studies in the UK with collaborators included the estimations of required collimation depths for different interaction region configurations and different beam parameters [10]; improving the lattice design for improving the collimation efficiency [11]; beam halo tracking to estimate the backgrounds [12] and effect of wake fields on the luminosity [13].

To investigate further the disagreement between the measured and simulated wake fields in the bunch length regime of linear collider [14], an extended experimental programme at SLAC End Station A was undertaken to measure the wake fields from different types of spoiler jaws as shown in Figure 3 and to compare with the simulations [15]. Different materials and geometries were used to separate the geometric and the

resistive effects from these jaws. The relative uncertainty on the reconstructed kick factor was typically less than 10% for most designs considered, with some systematic dependence on the analysis method employed.
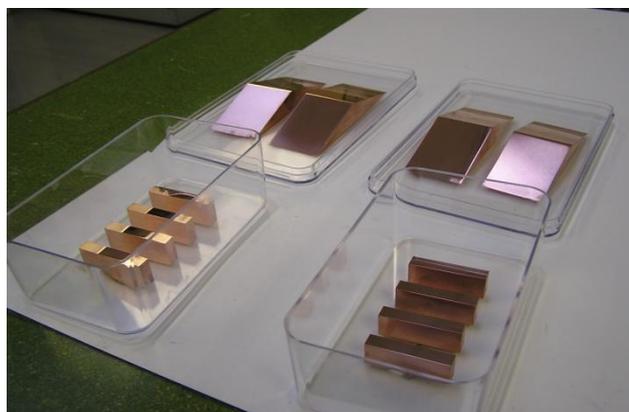
Figure 3: Collimator jaws tested at SLAC ESA for wake field studies.

Different spoiler designs were also investigated for the ILC beam delivery system [16] which can survive impact of two bunches at 250 GeV and one bunch at 500 GeV [17]. Titanium spoiler with Beryllium tapers has been proposed, and a first conceptual mechanical design of the collimator assembly was produced [18].

Experimental work to evaluate the behaviour of the proposed spoiler materials under rapid beam heating are part of the ATF2 programme, following successful first tests at ATF in 2008, and preparation for these tests is currently in progress in the UK [19].

3.4.2.4 *References*

1. Accelerator Physics Design Group meeting, 23rd January'04, TESLA Collaboration meeting, Zeuthen, DESY.
2. R. Appleby et al, Alternative IR geometries for TESLA with a small crossing angle, Proceedings of LCWS04, Paris
3. R. Appleby et al, The 2 mrad crossing-angle ILC interaction region and extraction line, Proceedings of European Particle Accelerator Conference, 2006.
4. D. Angal-Kalinin et al, Optics of the ILC extraction line for 2 mrad crossing angle, EuroTeV Report-2006-001-1, SLAC-PUB-11613.
5. R. Appleby et al, The 2mrad crossing angle scheme for the International Linear Collider, Proceedings of European Particle Accelerator Conference, 2006.
6. J Payet et al, Design of an interaction region with head-on collisions for the ILC, Proceedings of European Particle Accelerator Conference, 2006.
7. O. Napoly et al, Technical challenges for head-on collisions and extraction at the ILC, Proceedings of Particle Accelerator Conference, 2007.
8. A. Seryi et al, IR optimisation, DID and Anti-DID, SLAC-PUB-11662, 2006.
9. International Linear Collider Reference Design Report, ILC-Report-2007-001, 2007.
10. F. Jackson, Collimation aperture for the beam delivery system of the International Linear Collider, Proceedings of European Particle accelerator conference, 2008.
11. F. Jackson et al, Collimation optimisation in the beam delivery system of the International Linear Collider, Proceedings Particle Accelerator Conference, 2007.
12. J. Carter et al, Simulation of the ILC Collimation system using BDSIM, MARS15 and STRUCT, Proceedings of European Particle accelerator conference, 2006.
13. A. Toader et al, Effect of collimator wakefields in the beam delivery system of the International Linear Collider, Proceedings of European Particle Accelerator

Conference, 2008.
14. P. Tenenbaum et al., Phys. Rev. ST Accel. Beams 10, 034401 (2007).
15. J. L.Fernandez-Hernando et al, Measurements of collimator wakefields at End Station A, Proceedings of European Particle accelerator conference, 2008.
16. J.L. Fernandez-Hernando, N.K. Watson, FLUKA simulations of energy density deposition from a ILC bunch in different spoiler designs, EUROTeV-Report-2006-015.
17. G.Ellwood, J.Greenhalgh, Beam Impact Studies on ILC Collimators, Proceedings of Particle Accelerator Conference, 2007
18. B.D.Fell et al., Mechanical Design of Collimators for the ILC, Proceedings of European Particle accelerator conference, 2008.
19. J.L. Fernandez-Hernando et al, Material Damage tests for ILC Collimators, Proceedings of Particle Accelerator Conference, 2007.

3.4.3   **Laser-Wire Transverse Beam Profile Monitor**

Grahame A. Blair, on behalf of the LC-ABD laser-wire collaboration
John Adams Institute, UK
Mail to: g.blair@rhul.ac.uk

3.4.3.1   *Introduction*

The laser-wire transverse profile monitor works by focusing a laser into the particle beam. Laser-wire systems can be employed at H^- machine, such as the Front End Test Stand at RAL, discussed elsewhere in this newsletter. Here, we concentrate on UK involvement in laser-wires at the electron machines ATF and PETRA, at which the laser photons are Compton scattered into the direction of the electron beam, where they can be detected downstream. The laser spot is scanned across the beam and the Compton signal gives the convoluted electron beam-laser spot size. If the laser spot size is known, the electron beam size can be calculated from this measurement provided effects such as Rayleigh range etc. are included; from such measurements the transverse beam emittance can be inferred [1].

3.4.3.2   *PETRAIII Laser-Wire System*

The PETRAII laser-wire system was completed in 2008 and rapid-scanning was achieved in both horizontal and vertical dimensions. Example results are presented in Figure 1 for (Left) a horizontal scan and (Right) a collection of vertical scans [2].
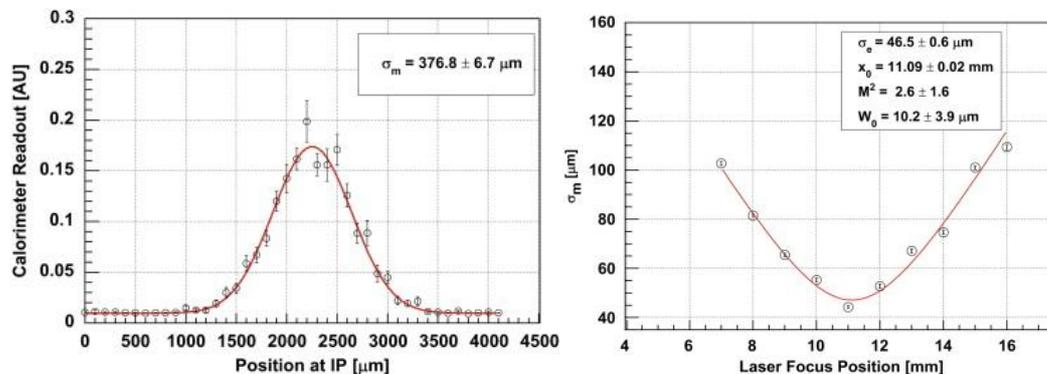
Figure 1: Laser-wire scans performed at the PETRAII machine. Left: a typical horizontal scan. Right: an amalgam of vertical scans with a fit to the laser Rayleigh range profile.

The PETRA laser-wire was upgraded and successfully relocated to its new position in the PETRA ring during the spring of 2009 and first data was taken soon thereafter during the running of PETRAIII.

Very good results have been achieved, building rapidly on the experience gained at the PETRAII system and beam studies with the laser-wire are taking place throughout 2010. A wide-aperture electro-optic scanner based on electrostatic quadrupole fields has been developed [3]; possible implementation of this ultra-fast (~130 kHz laser pulses, ~10 kHz scans) system is being explored as a possibility for PETRAIII and other machines.

3.4.3.3   *ATF Laser-Wire System*

The layout and preliminary results of the first ATF laser-wire system have been described in a previous newsletter [4]. Since then, the results from the runs using the first laser-wire system at the ATF extraction line at KEK have demonstrated electron beam-size measurements of order 3 μm [5]. The optics and light transport system are now sufficiently well understood such that a factor ~2 in improvements seems readily achievable. This can be achieved by reducing the input beam size on the final focus lens to limit the effect of aberrations and by improving the laser system.

The laser system has been commissioned, requiring all services to be installed in a new laser laboratory, located above the ATF2 extraction line. The light transport system from lab to accelerator enclosure final focus line has been installed and the laser is currently (spring 2010) being commissioned. The combination of all the planned upgrades should yield a very good spot size (~1 μm) for laser-wire measurements. In addition a transport line from the ATF2 laser system has been installed so that the UK laser-wire team can also aid the development of the sub-micron profile monitor system (Shintake-monitor).

3.4.3.4   *Fibre Laser R&D*

Lasers for accelerators development in the John Adams Institute at Oxford is currently working specifically on building an innovative fibre laser for the laser-wire experiment at the ATF2 in KEK [6]. This experiment requires a high energy pulses (~ 100μJ) that have a nearly perfect Gaussian spatial, The pulses also have to be at the same repetition rate as the electron bunches, 6.49MHz, and to be approximately the same duration – in the case of the ATF2 ~ 1-30 ps. In addition, the radiation environment of the accelerator restricts the bandwidth of the laser to < 1 nm. These stringent requirements prompted the design of a new laser using doped optical fibres, to exploit the excellent efficiency and beam quality of these systems. The architecture of the final laser system is:

1) a solid state oscillator operating at ~1 μm locked to an external accelerator frequency reference at 52 MHz;
2) reduction of the repetition rate to 6.49 MHz and chirped pulse amplification (CPA) in two stages of ytterbium (Yb) doped double clad fibre up to 1 μJ;
3) final power amplification up to 100 μJ in Yb doped photonic crystal fibre rods;
4) pulse compression to 1 – 10 ps using fused silica gratings; and
5) frequency conversion to ~500 nm.

This laser is under development at Oxford. 100 μJ pulses at 6.49 MHz have not been achieved in fibre systems to date, so high gain photonic crystal fibre (PCF) rods are being used as amplifiers. These are operated in a transient regime, where gain is allowed to build up in the fibre and then extracted by a train of amplified signal pulses. This has proved very successful, with initial experiments showing that the first pulse in a signal train can be amplified from 1 μJ up to ~ 75 μJ (25 dB/m) in a 70 cm fibre.

While this laser has been specifically optimised for beam size measurement in an electron accelerator, the general principle of a seed and amplifier stages is extremely flexible, and the expertise developed in the JAI during this project can be used to design and build laser systems for many applications in accelerator science. The laser team at Oxford is already advising on a fibre laser amplifier for the photoinjector for the CLIC accelerator R&D project at CERN, and on tunable laser systems for interferometric tunnel measurement projects. Additionally, an interdisciplinary research group has been formed at Oxford to investigate laser based acceleration schemes, to which the laser-wire group is contributing expertise in high power short pulse lasers.

3.4.3.5 *References*

1. I Agapov, G. A. Blair, M. Woodley. ""Beam emittance measurement with laser wire scanners in the ILC beam delivery system". Phys. Rev. ST Accel. Beams 10, 112801 (2007)
2. A. Bosco et al. "A two-dimensional laser-wire scanner for electron accelerators" Nucl.Instrum.Meth. A 592 (2008) 162–170.
3. A. Bosco et al. "A large aperture electro-optic deflector". Applied Physics Letters 94, 1 (2009).
4. ICFA Beam Dynamics Newsletter No. 50, December 2009.
5. A. Aryshev et al. "Micron size laser-wire system at the ATF extraction line, recent results and ATF-II upgrade" Proceedings of PAC09 (Vancouver) 2009.
6. "Development of a photonic crystal fibre laser amplifier for particle beam diagnostics". L. Nevay et al. Proceedings PAC09   (Vancouver) 2009.

3.4.4 Beamline Full Simulations Using BDSIM

Grahame A. Blair
Dept of Physics, RHUL, Egham, Surrey. TW20 0EX. UK
Mail to: g.blair@rhul.ac.uk

3.4.4.1 *Introduction*

Traditional particle accelerator tracking codes are mainly concerned with the tracking of the primary particles and are not so concerned with material interactions and tracking of secondary particles, which may be produced when a primary particle hits an aperture in the machine. In an advanced particle transport code such as Geant4 [1] one can in principle describe and simulate single-particle beam dynamics in electromagnetic fields. BDSIM [2] was developed by a UK team to combine the benefits of both techniques. It is based on Geant4, a Monte-Carlo framework, thus giving access to many electromagnetic and hadronic interaction models as well as a powerful geometry description framework. On top of this, fast particle tracking routines and some additional physics processes are introduced, and a high level geometry description language GMAD [3] was added. Since GMAD is an extension of MAD, a standard for

beam optics description, this allows complex accelerator descriptions to be loaded from existing repositories with just a few modifications. BDSIM has been benchmarked against other tracking codes in vacuum to ensure tracking accuracy at the nm level over several kilometers.

3.4.4.2 *Linear Collider Applications*

BDSIM has been applied to the simulations of a future linear electron–positron collider, both for the beam delivery system and for the post-IP line [4], as described elsewhere in this newsletter. It has also been used in the detailed simulation of a laser-wire beam diagnostics system [5], to understand the issues of signal extraction at the ILC; corresponding studies are ongoing for CLIC.

Simulation of beam halo in CLIC collimation system has been studied [6], including the effect of collimator wakefields on the beam halo. An example of the use of BDSIM in the simulation of CLIC is shown in Fig. 1, where the effect of full simulation and tracking of secondary particles is shown, as compared with the "black" collimator approximation normally applied in machine tracking codes.

The simulation of muon production in the spoilers and collimators was performed for the ILC and is now being applied to CLIC. Full simulation of the CLIC tunnel in the BDS will enable realistic tracking of muons from their point of production to the detector. These studies will also be input to the detector working groups as part of the preparations of the CLIC CDR in 2010.
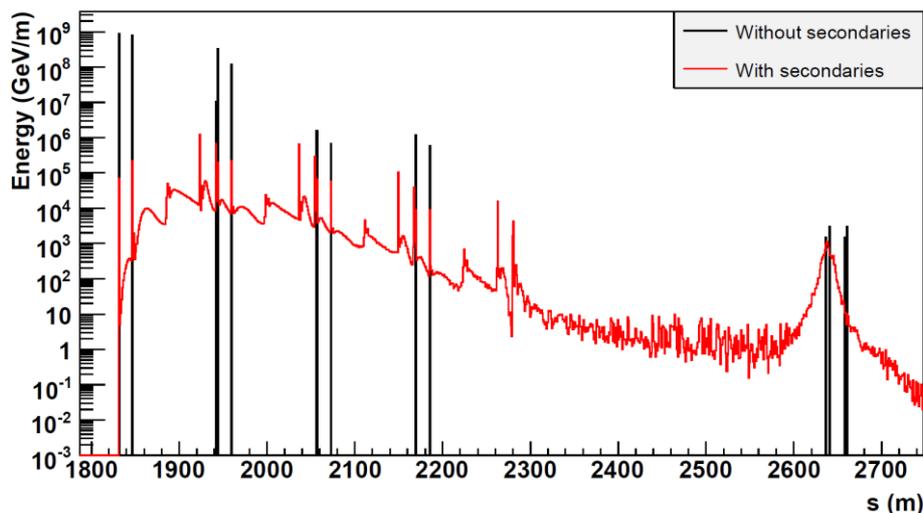
Figure 1: Energy deposition along the CLIC Beam Delivery System using BDSIM with the origin (at 1800 m) being the exit from the linac and the IP at the end. Black: all initial particles hitting a spoiler deposit all their energy immediately without the production of secondary particles. Red: all physics processes are turned on, with full tracking of secondaries [6].

3.4.4.3 *Application to Hadronic Machines*

BDSIM has been applied to the forward detector systems at the Large Hadron Collider [7] and is currently being applied within the LHC background study group and in the LHC collimation working group. For LHC collimation, particle four vectors provided at the collimators by the LHC collimator group are then simulated fully in

BDSIM; this will complement ongoing full simulation using FLUKA and enable new functionality, such as the full simulation of the LHC beam loss monitors, to be included.

3.4.4.4 *References*

1. S. Agostinelli et al. "Geant4—a simulation toolkit". Nucl.Instrum.Meth. **A506** (2003) 250-303.
2. I. Agapov, G.A. Blair, S. Malton, L. Deacon. "BDSIM: A particle tracking code for accelerator beam-line simulations including particle–matter interactions", Nucl.Instrum.Meth. **A606** (2009) 708–712.
3. I. Agapov. "GMAD accelerator description language". EUROTeV-Memo-2006-002-1.
4. R. Appleby et al. "The 2-mrad crossing angle interaction region and extraction line", Proc. of European Particle Accelerator Conference (EPAC 06), Edinburgh, Scotland (26–30 June, 2006).
5. L. Deacon, G.A. Blair. "Laser-wire simulation in the ILC beam delivery system." EUROTeV-Report-2008-018.
6. I. Agapov, G.A. Blair, H. Burkhardt, A. Latina, , S. Malton, J. Resta-Lopez, D. Schulte. Phys.Rev.ST Accel.Beams 12:081001, 2009.
7. F. Roncarolo et al. "Machine induced backgrounds for FP420"., EPAC08-TUPP062, Proc. of 11th European Particle Accelerator Conference (EPAC 08), Magazzini del Cotone, Genoa, Italy (23–27 June, 2008).

3.4.5 **Fast Beam-Based Feedback Systems**

Philip N. Burrows, on behalf of the FONT collaboration
John Adams Institute, UK
Mail to: p.burrows@physics.ox.ac.uk

3.4.5.1 *Introduction*

A number of fast beam-based feedback systems are required at future linear electron-positron colliders. At the interaction point (IP) a very fast system, operating on nanosecond timescales within each bunchtrain, is required to compensate for residual vibration-induced jitter on the final-focus magnets by steering the electron and positron beams into collision. A pulse-to-pulse feedback system is envisaged for optimising the luminosity on timescales corresponding to 5 Hz. Slower feedbacks, operating in the 0.1 – 1 Hz range, will control the beam orbit through the Linacs and Beam Delivery System.

The key components of each such system are beam position monitors (BPMs) for registering the beam orbit; fast signal processors to translate the raw BPM pickoff signals into a position output; feedback circuits, including delay loops, for applying gain and taking account of system latency; amplifiers to provide the required output drive signals; and kickers for applying the position (or angle) correction to the beam. A schematic of the IP intra-train feedback is shown in Figure 1, for the case in which the beams cross with a small angle; the current ILC [1] and CLIC [2] designs incorporate crossing angles of 14/20 mrad respectively.

3.4.5.2 *All-Analogue Systems*

Critical issues for the intra-train feedback performance include the latency of the system, as this affects the number of corrections that can be made within the duration of

the bunchtrain, and the feedback algorithm. We have built all-analogue feedback system prototypes in which our aim was to reduce the latency to a few tens of nanoseconds, thereby demonstrating applicability for 'room temperature' Linear Collider designs with very short bunchtrains of order 100ns in length, such as CLIC. We achieved total latencies (signal propagation delay + electronics latency) of 67 ns (FONT1) [3], 54 ns (FONT2) [4] (Figure 1) and 23ns (FONT3) [5].
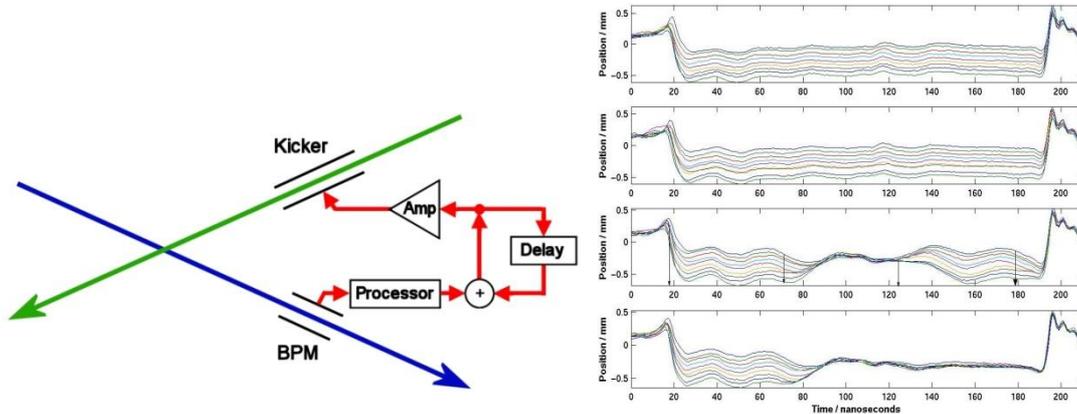
Figure 1: Left: Schematic of IP intra-train feedback system with a crossing angle. The deflection of the outgoing beam is registered in a BPM and a correcting kick applied to the incoming other beam. Right: Feedback performance of FONT2 [4].

3.4.5.3 *Digital Systems*

More recently we have developed and tested ILC prototype systems that incorporate a digital feedback processor based on a state-of-the-art Field Programmable Gate Array (FPGA). The use of a digital processor allows for the implementation of more sophisticated algorithms which can be optimised for possible beam jitter scenarios at ILC. However, a penalty is paid in terms of a longer signal processing latency due to the time taken for digitisation and digital logic operations. This approach is now possible for ILC given the long, multi-bunch train, which includes parameter sets with 3000/6000 bunches separated by 300/150 ns respectively. Performance results have been reported [6,7,8,9].

FONT4 was designed [7] as a bunch-by-bunch feedback with a latency goal of less than 140ns. This meets the minimum ILC specification of c. 150ns bunch spacing, as well as the smallest spacing allowed in beam tests at ATF. This will allow measurement of the first bunch position and correction of both the second and third ATF bunches. The correction to the third bunch is important as it allows test of the 'delay loop' component of the feedback, which is critical for maintaining the appropriate correction over a long ILC bunchtrain.

The design of the front-end BPM signal processor is based on that for FONT3 [5]. The top and bottom (y) stripline BPM signals were added and subtracted using a hybrid, to form a sum and difference signal respectively. The resulting signals were band-pass filtered and down-mixed with a 714 MHz local oscillator signal which was phase-locked to the beam. The resulting baseband signals are low-pass filtered. The hybrid, filters and mixer were selected to have latencies of the order of a few nanoseconds, in an attempt to yield a total processor latency of around 10 ns [7,8].

44

The custom digital feedback processor board is shown in Figure 2. There are two analogue signal input (output) channels in which digitisation is performed using Analog Devices ADCs (DACs) which can be clocked at up to 105 (210) Ms/s. The digital signal processing is based on a Xilinx Virtex4 FPGA which can be clocked at up to 500MHz. The FPGA is clocked with a 357 MHz source, derived from the ATF master oscillator and hence locked to the beam. Logic operations are triggered with a pre-beam signal. The ADC/DAC are clocked at 357/4 Ms/s. The analogue BPM processor output signal is sampled at the peak to provide the input signal to the feedback. The gain stage is implemented via a lookup table stored in FPGA RAM, alongside the reciprocal of the sum signal for charge normalisation. The delay loop is implemented as an accumulator on the FPGA. The output is converted back to analogue and used as input to the driver amplifier.

The driver amplifier was specified to provide +-30A of drive current into the kicker, whose striplines were shorted at the upstream end (nearer the incoming beam). The risetime, starting at the time of the input signal, was specified as 35ns to reach 90% of peak output. The output pulse length was specified to be up to 10 microseconds. Although current operation is with only 3 bunches in a train of length c. 300ns, it is planned in future to operate ATF with extracted trains of 20 or 60 bunches with similar bunch spacing; the design allows for this upgrade. The feedback performance (correction of bunch 3) is illustrated in Figure 2.
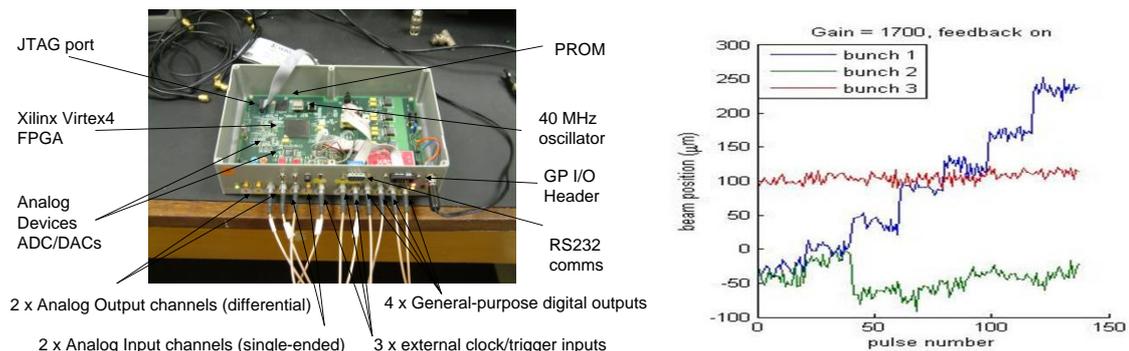
Figure 2: Left: FONT4 digital feedback processor. Right: Feedback performance of FONT4 [9].

3.4.5.4 *References*

1. ILC: http://www.linearcollider.org/cms/
2. CLIC: http://clic-study.web.cern.ch/CLIC-Study/
3. P.N. Burrows et al, Proceedings PAC03, Portland, Oregon, May 2003, p. 687.
4. P.N. Burrows et al, Proceedings EPAC04, Lucerne, July 2004, p. 785.
5. P.N. Burrows et al, Proceedings PAC05, Knoxville, TN, May 2005, p. 1359.
6. P.N. Burrows et al, Proceedings EPAC06, Edinburgh, UK, June 2006, p. 849.
7. P.N. Burrows et al, Proceedings PAC07, Albuquerque, NM, June 2007, p. 416.
8. P.N. Burrows et al, Proceedings EPAC08, Genoa, June 2008, p. 3245.
9. R. Apsimon et al, Proceedings PAC09, Vancouver, May 2009.

3.5 CLIC Main Linac HOM Wakefield Suppression through Novel Cavity Design

Roger M. Jones, on behalf of the MEW group
Cockcroft Institute, Daresbury, Warrington, Cheshire WA4 4AD, UK.
University of Manchester, Oxford Road, Manchester, M13 9PL, UK.
Mail to: roger.jones@manchester.ac.uk

3.5.1 Introduction

It is generally agreed within the particle physics community that a lepton collider will be the successor to the LHC and to prevent excessive synchrotron radiation losses, this will necessitate a linear collider. The compact linear collider (CLIC) design accelerates leptons and collides them at a 3 TeV centre of mass energy. CLIC features normal conducting (NC) cavities with accelerating electric field gradient of 100 MV/m at an X-band frequency of 12 GHz.

The passage of a charged particle beam within a cavity, results in the excitation of an electromagnetic field, which can be decomposed into a series of modes which affect both the longitudinal and transverse motion of the beam. In linear colliders the beam is travelling ultra-relativistically and these modes constitute the wakefield excited by the beam. It is important to ensure this wakefield is kept to within acceptable limits. The short-range wakefield, or the wakefield along the bunch, is tied to the average radius of the individual cells and the long-range wakefield, or the wakefield along a train of bunches, can be suppressed by both modifying the cell geometry and by adjusting the damping Q.

There are two main approaches being followed to damp the long-range wakefield for CLIC: firstly, heavy damping (Q~10) and secondly, moderate damping (Q~500) combined with detuning of the individual cell frequencies of each structure. The CLIC baseline design focuses on the former option and this entails attaching large damping waveguides to each individual cell. We are spearheading the effort of a damped detuned structure (DDS) which incorporates a pair of higher order mode (HOM) manifolds and modifying the frequencies of each cell in a precise manner. It is notable that monitoring a small fraction of the manifold radiation allows both the beam position and the structure alignment to be inferred.

The structure bears comparison to those structures used in NLC programme [1-2] but it is quite different in the degree of interleaving of structures required and in the detuning characteristics. The detuning has been obtained by carefully modifying the cell geometry. In designing these cells attention has to be paid to two main issues: firstly, that the accelerating field and frequency are largely unaffected, and secondly, that the surface electromagnetic field and pulse surface temperature rise are kept within acceptable limits. These two issues, and in particular the latter, constrain the design considerably.

This research is conducted in close collaboration with our CERN colleagues. An overview of work in this area was presented at the 44th ICFA structures and beam dynamics workshop [3], hosted by the Cockcroft Institute. The damped and detuned design being applied to the CLIC main linac is now described in the next section.

3.5.2 **Wakefield Suppression with CLIC_DDS**

We have investigated a design which entails strong detuning of the cell frequencies and moderate damping (Q ~ 500-1000). The latter is reflected through four manifolds running along the walls of the accelerator. Several potential structures have been considered to suppress the wakefield in this manner [4-5]. This included structures closely tied to the CLIC baseline geometry, suitably modified to facilitate detuning of cell frequencies, and structures relying on a zero crossing in the wakefield. However, the present optimised structure relies on interleaving of the frequencies of 8 successive structures and has relaxed the CLIC baseline design of 6 rf cycles to 8 rf cycles. The
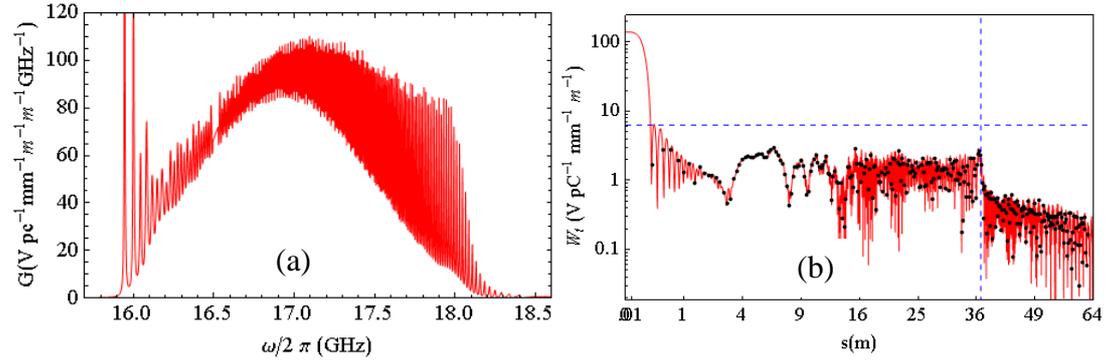
Figure 1: Spectral function (a) and wakefield (b) prediction for 8-fold interleaved CLIC_DDS. Points indicate the position of each bunch in the train.

spectral function and the overall wakefield for this structure, effectively consisting of 192 cells, is illustrated in Fig. 1. Detailed simulations on the passage of a train of electron bunches through 21 km of main linacs puts a limit on the wakefield that will not cause appreciable emittance dilution and this is indicated by the horizontal dashed line in Fig 1(b). The vertical dashed line denotes the point at which the modes in the structure recohere (36m) and also corresponds to the minimum mode separation in the spectral function (8 MHz).
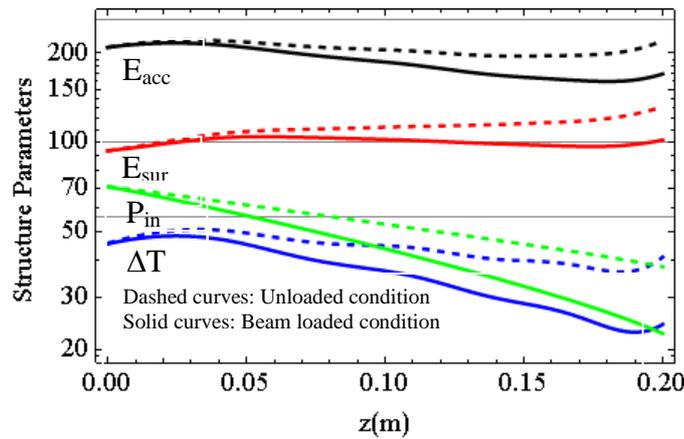
Figure 2: Rf properties of single accelerating CLIC_DDS suitable for high power experimental evaluation. The input power, accelerating electric field gradient, surface pulse temperature rise, and surface electric field, are indicated by P_{in} (MW), E_{acc}(MV/m), ΔT (°K), and E_{suf} (MV/m), respectively. Those corresponding to a structure without beam, the unloaded case, are indicated by dashed curves.

An initial structure will be fabricated this year and will focus on the ability to withstand high accelerating field gradients. This will be tested at the CTF3 or high power test facility at CERN. The rf properties of the fundamental mode are illustrated in Fig 2. This design is being finalised and a representative set, suitable for high power testing and requiring an input power of ~71 MW, is illustrated in Fig 3. In this structure there will be no attempt to ensure the wakefield is adequately suppressed from the perspective of emittance dilution in the complete CLIC main linac, as it will not include interleaving of adjacent structure frequencies. However, the cells will be precisely machined and a comparison between experimental measurement of the modes to that predicted is anticipated. Particular parts in the structure are especially sensitive to fabrication errors [6] and this will form part of the experimental study. Subsequent structures will incorporate full damping and detuning features, including HOM couplers and damping materials.
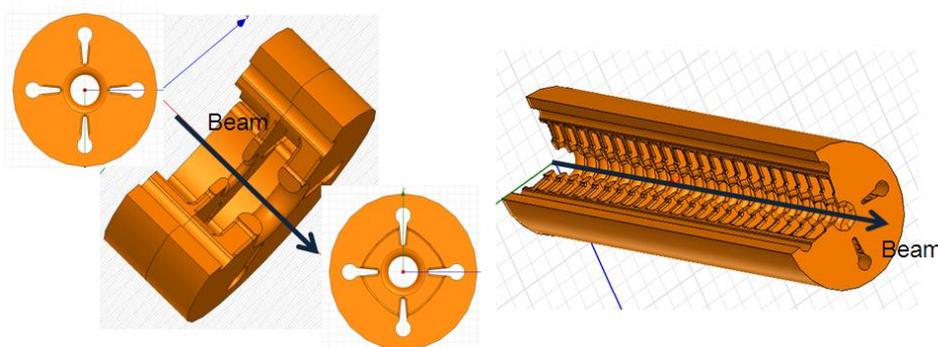
Figure 3: CAD representation of a CLIC_DDS prototype.

3.5.3 **Summary**

Studies on an alternative means of long-range wakefield suppression scheme for the main linacs of CLIC is now sufficiently mature to enable an initial prototype structure to be built. This will verify the ability of the damped and detuned structure to withstand high accelerating gradients for CLIC. The main cells of a complete 8-fold interleaved structure have also been designed and adequate wakefield suppression is predicted. These DDS accelerators achieve the dual purpose of suppressing the wakefield and, through monitoring of the radiation of the modes, allows remote diagnosis of the beam position and inter-cell alignments [7]. Results of this work were presented at the 44th ICFA X-Band Structures Collaboration meeting [8]. This research has received funding from the European Commission under the FP7 Research Infrastructures grant agreement no.227579.

3.5.4 **References**

1. R.M. Jones, C. Adolphsen, Z. Li, J. Wang, *Wakefield damping in a pair of X-band accelerators for linear colliders*. Phys.Rev.ST Accel. Beams 9:102001, 2006.
2. R.M. Jones, V. A. Dolgashev, and J. W. Wang, *Dispersion and energy compensation in high-gradient linacs for lepton colliders*, Phys. Rev. ST Accel. Beams 12, 051001 2009.
3. http://www.cockcroft.ac.uk/events/X-Band/programme.htm   and   http://prst-ab.aps.org/speced/XB2008.
4. R. M. Jones, *Wake field Suppression in High Gradient Linacs for Lepton Linear*

Colliders, Phys. Rev. ST Accel. Beams 12, 104801, 2009.

5. V.F. Khan and R.M. Jones, I*nvestigation of an alternate means of wakefield suppression in the main linacs of CLIC*, Presented at Particle Accelerator Conference (PAC 09), Vancouver, BC, Canada, 4-8 May, 2009.

6. R.M. Jones, C.E. Adolphsen, R.H. Miller, J.W. Wang , T. Higo, I*nfluence of fabrication errors on wake function suppression in NC X-band accelerating structures for linear colliders*, New J.Phys.11:033013,2009.

7. R.M. Jones, M. Seidel, N.M. Kroll, R.H. Miller, C. Adolphsen, K.L.F. Bane, R.D. Ruth, J. Wang, *Analysis and application of microwave radiation from the damping manifolds of the SLAC Damped Detuned Structures (DDS)*. Proceedings of 17th IEEE Particle Accelerator Conference (PAC 97): Accelerator Science, Technology and Applications, Vancouver, British Columbia, Canada, 12-16 May 1997, pp 554-556.

8. V.F. Khan, R.M. Jones, *An Alternate design for CLIC main linac wakefield suppression, p*roceedings of 44th ICFA Advanced Beam Dynamics Workshop: X-Band RF Structure and Beam Dynamics, Warrington, United Kingdom, 1-4 Dec 2008.

3.6 Development of Crab Cavity Systems at the Cockcroft Institute

P. Ambattu, G. Burt, A. Dexter, P. Goudket, C. Lingwood, P. McIntosh and I. Tahir
Cockcroft Institute, Daresbury, Warrington, Cheshire, WA4 4AD, UK
Mail to: graeme.burt@stfc.ac.uk

3.6.1 Introduction

Crab cavities are a subset of transverse deflecting cavities, utilised for rotating particle bunches in order to align them for head-on collisions in colliders with finite crossing angles. This idea was first proposed in 1988 by Palmer [1] however was not realised until 2007 at the KEKB collider in Japan [2]. After this successful proof of principle experiment many colliders have included crab cavities in their baseline designs. Of particular interest are the big future colliders SLHC, ILC and CLIC which all propose the use of crab cavities. The Cockcroft Institute (CI) has a major role in the design of the crab cavities and their control systems for all three of these accelerators.

3.6.2 ILC Crab Cavity Development

The 1st crab cavity system investigated at the CI was the ILC crab cavity. The CI led a collaboration including FNAL and SLAC which were responsible for the design of the cavities and LLRF control system. The cavity was based on the FNAL superconducting Kaon separator [3]. This was a 13 cell niobium cavity resonant at 3.9 GHz. A study of mode spacing, cavity tuning and higher order modes concluded that 13 cells would be problematic for the ILC requirements hence a 9-cell version was adopted (see Figure 1).

Operating π mode: f=3.90304GHz
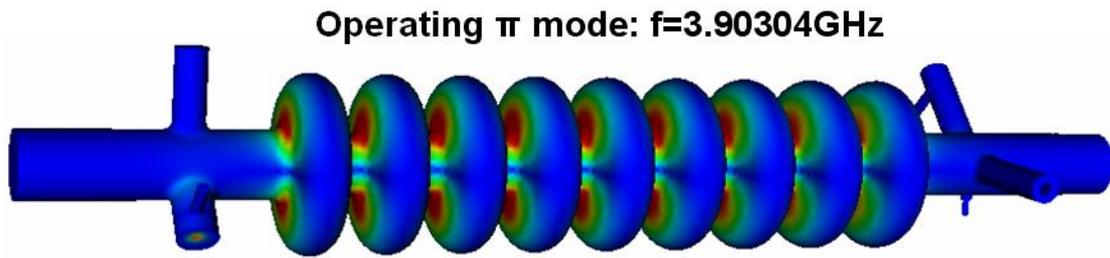
Figure 1: 9-cell ILC crab cavity design

A major part of the design would focus on the excitation of unwanted cavity modes and their removal. Crab cavities operate using the first dipole mode of the system, meaning that the fundamental accelerating mode of the system is now unwanted and can lead to beam instabilities, in addition the dipole mode is degenerate and has a 2nd polarisation which also strongly couples to the beam, these modes are referred to as the lower-order-mode (LOM) and same-order-mode (SOM) respectively. In addition the regular higher-order-modes (HOMs) of the system must also be considered. A study of the 1st 200 monopole and dipole modes of the cavity suggested that a set of problematic dipole modes existed at 8.0 GHz which should be the main focus of the HOM dampers.

For the ILC a new set of couplers were required to remove these modes. Initially a separate coupler was envisioned each for LOM, SOM and HOMs. The LOM coupler was a hook type coaxial coupler where the inner conductor was bent towards the cavity at the tip. This coupler was supported by a single stub which impedance matched the coupler to the LOM. The SOM coupler was a large diameter coaxial coupler. Both these couplers relayed on geometry to avoid coupling to the crabbing mode, as this mode is highly polarised by two dents made on the cavity equator. A HOM coupler was designed at the CI, based around an integrated LOM/SOM coupler. This coupler was again a hook type coupler, but the diameter was increase to improve coupling, and a second stub was added to improve impedance matching at both frequencies. This freed up space on the beam-pipes to include two HOM couplers (see Figure 2).
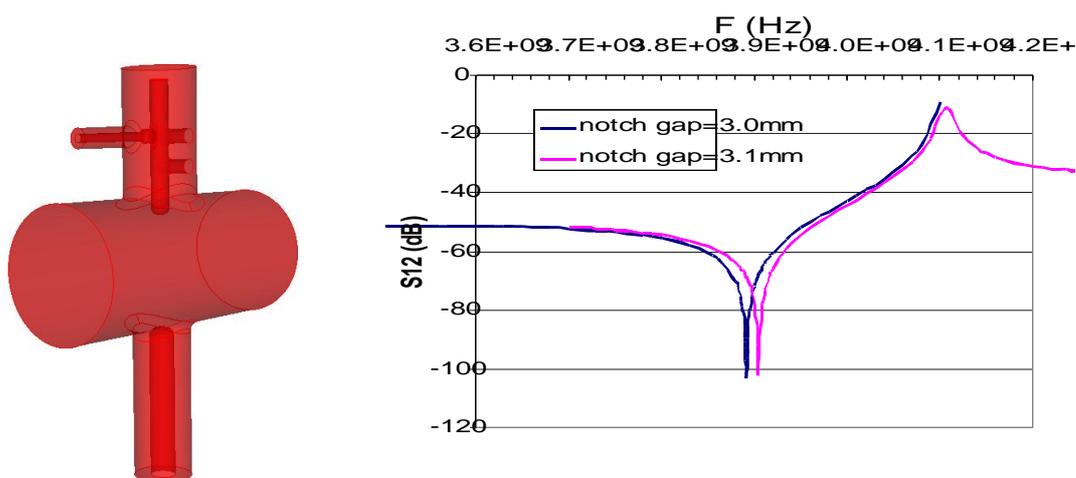
Figure 2: HOM coupler and and notch filter sensitivity. A 0.1-MHz/micron notch sensitivity achieved with the new design.

The 1st HOM coupler was the original SLAC HOM coupler as this mode had excellent damping of lower frequency HOMs near the operating frequency. The 2nd

coupler was a small waveguide coupler designed specifically to damp the dipole modes at 8.0 GHz, it was found that these modes were optimally damped when the waveguides cut-off was near to their resonant frequency.

After the cavity was designed a normal conducting prototype including the 1st version of the couplers was constructed. Bead-pull, wire testing and coupler measurements were made to fully characterise the cavity. Measurements were in good agreement with the simulations (see Figure 3) and in addition, the CI performed major development and testing of the LLRF control system (see later).
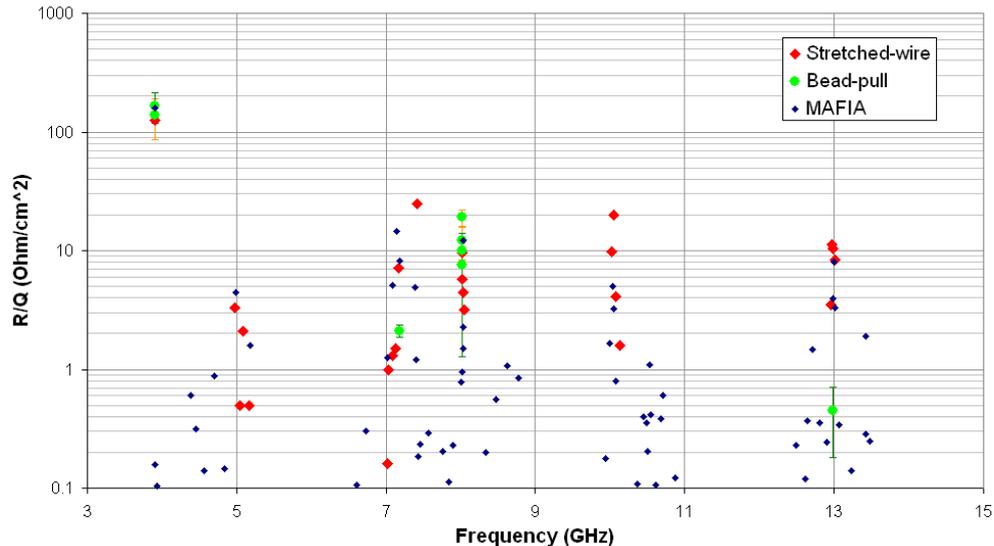
Figure 3: Model impedance characterisation, including damping couplers

3.6.3   CLIC Crab Cavity Development

Having made advances in the ILC crab cavity progression into the CLIC crab cavity [4] seemed natural. However as the beam structure was very different for CLIC a different technology was required. The smaller transverse bunch size required a tighter phase tighter phase tolerance, and hence a higher frequency was needed to counteract this. Also the bunch spacing was very short meaning a lower Q factor and higher frequency was required to reduce the effects of beam loading. This led to the decision to base the CLIC crab cavity of normal conducting X-band technology, similar to the CLIC accelerating structures.

Due to the very tight phase tolerances a major focus of the cavity design was focussed on reducing beam loading. The chosen solution was to use a low shunt impedance structure, with a high group velocity and use a very high power RF source to drive it, in this way any perturbations were quickly removed from the system. The cavity optimisation was based on maximising group velocity and R/Q, while minimising the peak surface fields. Short range wakefield calculations were performed to set a minimum iris radius, which is a very important parameter in crab cavities due to the large surface current flowing around the iris. This leads to the design of a $2\pi/3$ travelling wave structure with a 5 mm radius iris, and an iris thickness of 2 mm (see Figure 4).
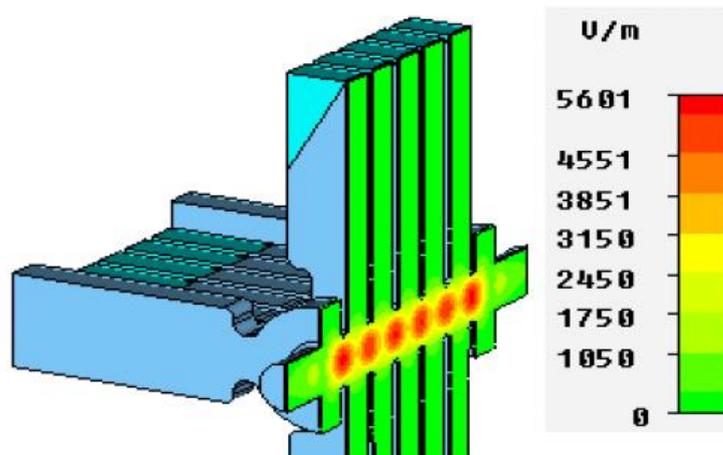
Figure 4: Multi-cell 11.9942 GHz CLIC crab cavity design

To investigate the high power performance of this cavity a copper prototype is under construction at Shakespeare Precision Engineering in the UK [5]. The Cockcroft Institute has been in collaboration with Shakespeare on the construction of X-band cavities and the company has been upgrading its infrastructure and experimenting in order to meet the stringent manufacturing requirements. This cavity is expected to be tested at high power at SLAC at some point in 2010.

The small transverse bunch size at the IP in CLIC, means that the luminosity is very sensitive to transverse offsets at the the IP. Due to the large R12 between the crab cavity and the IP, and perturbation at the cavity can have a huge effect on the luminosity, hence the long range wakefield must be reduced by severe damping of any spurious modes excited. The LOM and SOM of the CLIC crab cavity are particularly dangerous and must be damped to Q values of around 10-100 (see Figure 5).
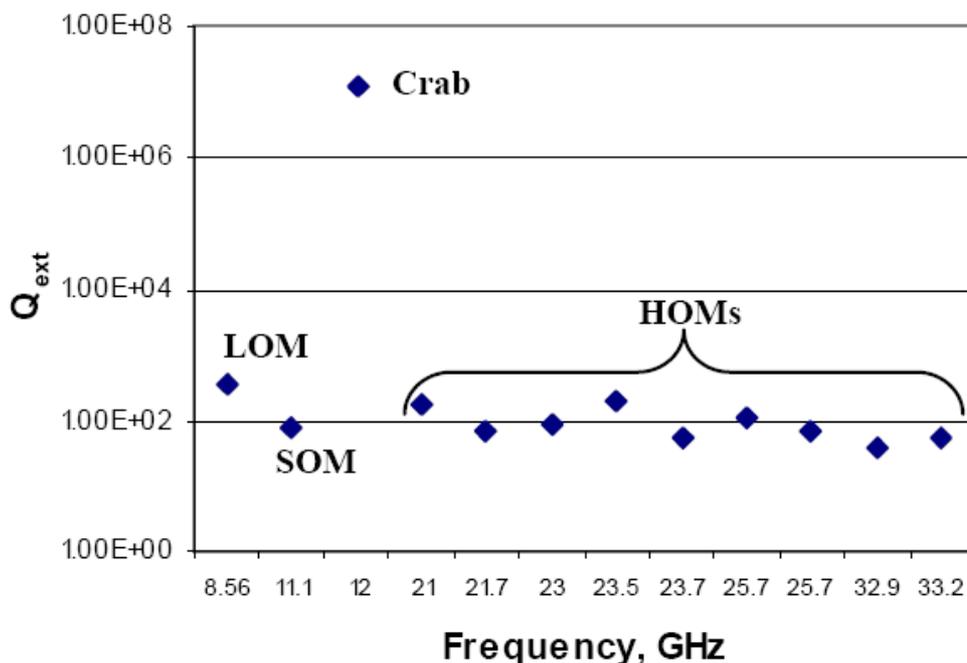
Figure 5: Optimised 7-cell, waveguide damped design

A major study is underway into the different damping methods possible, it is envisioned that waveguide damping will be utilised however, choke mode and manifold damping has also been considered. In addition we are investigating the use of damped detuned structures similar to the scheme envisioned for NLC [6], however such a scheme would only be effective for either the LOM or the SOM, not both, hence we must first investigate which mode is likely to cause the largest problems [7].

3.6.4 LHC Crab Cavity Development
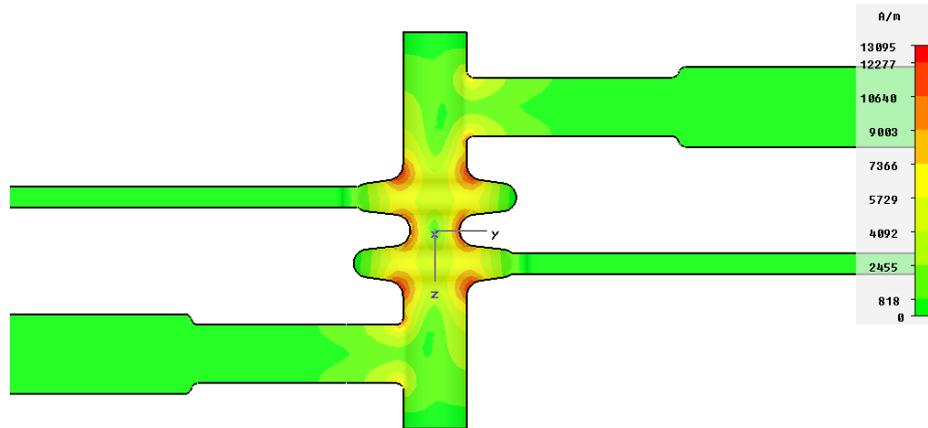
Figure 6: 800MHz Phase –I 'Global' test structure

The Cockcroft Institute are also involved in the design of the LHC crab cavity [8]. As the LHC is a working accelerator, any crab cavities installed as part of an upgrade will have to fit into the existing system, this places tight requirements on the transverse size of the cavity and it's beampipe diameter. Initially efforts were focused on a Phase-I test of an 800 MHz elliptical cavity similar to the KEK-B cell shape [9], as it was initially envisioned that a prototype could be tested in the LHC in the near future (see Figure 6). Such a test would have a single crab cavity installed, which would rotate the beam around the entire circumference of the LHC ('Global'), aligning collision at the Interaction Point (IP) and dealing with the rotation with appropriately positioned collimation systems around the ring.

The LHC crab cavity initially had three teams working on separate elliptical designs. One of these teams was a collaboration between Cockcroft, TJNAF and TechX. The LHC crab cavity needs significant damping of the LOM and SOM modes, to loaded Q factors of around 100. As such the optimisation of the UK-TJNAF-TechX design focused on the damping structures. The final design utilised novel on-cell waveguide damping (originally proposed for the APS crab cavity [10]), where two waveguide dampers are connected to the cavity equator such that it damps the SOM and LOM but does not couple to the operating mode (see Figure 7). This scheme also benefits from a large frequency separation between the SOM and the operating mode caused by the waveguide dampers. Multipactor simulations were carried out in VORPAL [11] and Particle Studio [12]. These studies revealed a two-point multipactor at the peak magnetic field on the iris, the on-set of this multipactor was found to occur when the peak magnetic field reached a value consistent with the operating frequency being double the cyclotron frequency.

However, such 'Global' tests are now unlikely and efforts have been shifted to a novel parallel rod cavity operating at 400 MHz. For a more compact 400 MHz crab cavity design, there are four teams each with a separate solution. The Cockcroft is collaborating with TJNAF and TechX on a 4-rod crab cavity based on an SRF version of the current CEBAF separator [13] (see Figure 7). The cavity utilises a thick conical rod geometry to minimise microphonics, and has an optimised profile to reduce surface fields. Owing to its more compact design, installation tests on LHC will allow for 'Local' crabbing at individual IP's, ensuring no change is required for machine collimation systems.

Type	H-Field (peak)
Monitor	Mode 1
Component	Abs
Maximum-3d	17554.5 A/m at 45.1613 / 45.1613 / 163.043
Frequency	0.400055
Phase	90 degrees
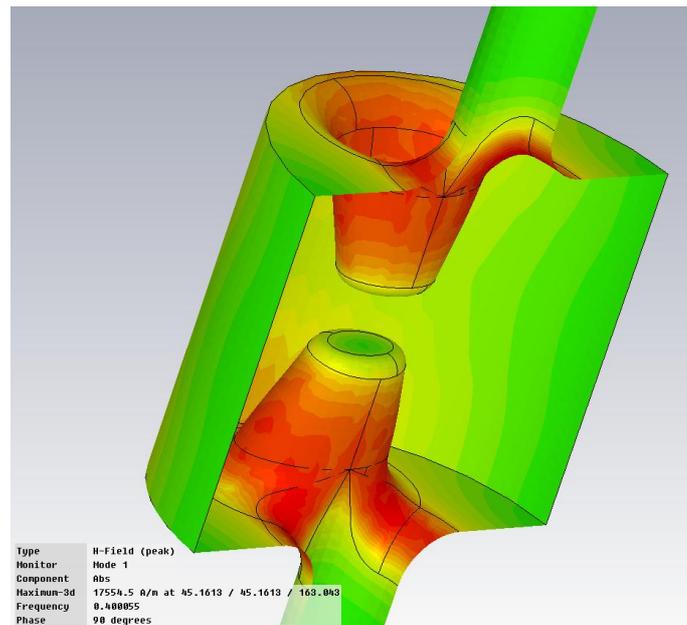
Figure 7: 4-rod Phase-II 'Local' test structure

3.6.5 **Crab Cavity LLRF System**

The choice of RF technology for crab cavities must respect constraints determined by beamloading. Figure 8 illustrates electric and magnetic fields inside a single cell dipole cavity. It is immediately apparent that beam loading only occurs when the bunch is off axis. Beamloading changes its sign depending on which side of the centre that the beam passes.
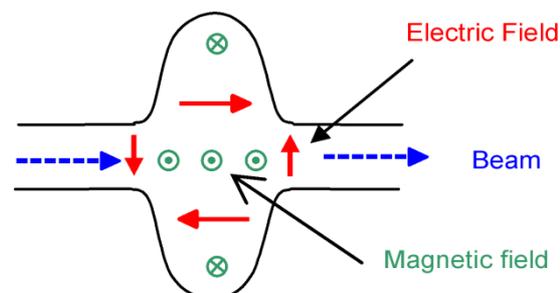
Figure 8: Dipole mode cavity fields

At crab cavity locations bunch offsets are typically large. For a chosen machine the deflecting voltage required in the crab cavity is determined as $V_\perp \cong \dfrac{\theta_r E_o c}{\omega R_{12}}$ where θ_r is half the crossing angle, ω is the cavity RF frequency, E_o is the beam energy and R_{12} is the ratio of offset at the IP to deflection angle at the crab cavity.

When a bunch of charge q passes through a dipole cavity with repetition f_{rep} , phase ϕ and horizontal offset α, the power extracted from the cavity is $P_b = qV_\perp \left(\dfrac{\alpha \omega}{c} \right) f_{rep} \cos \phi$

hence at the perfect crabbing phase $\phi = 0$ we obtain $P_b = \dfrac{\alpha \theta_r q f_{rep} E_o}{R_{12}}$. We note that beamloading is zero for a bunch which is perfectly on axis. How much power one requires in practice to provide the kick depends on the loaded Q factor of the cavity. For optimum power transfer one matches the loaded Q to worst case beamloading and cavity losses. For superconducting cavities the cavity losses can be neglected. For copper cavities there is the option to make losses much larger than worst case beam losses which minimizes amplitude errors in the absence of control action [14].

Table 1 computes this peak power requirement P_b for the ILC at 1 TeV c.o.m, for CLIC at 3 TeV c.o.m and the LHC at 14 TeV c.o.m.. Before any consideration of cavity frequency is made one realizes that the ILC, LHC and CLIC crab cavities will be low, medium and high power installations respectively.

Table 1: Crab cavity peak power requirements

	Max bunch offset (α)	half crossing angle θ_r	bunch charge	bunch repetition	Beam energy	R12	Crab peak power
ILC	0.6 mm	0.0070 rad	3.2 nC	3.03 MHz	0.5 TeV	16.4 m/rad	1.24 kW
LHC	0.2 mm	0.00016 rad	18.4 nC	40.0 MHz	7.0 TeV	30.0 m/rad	8.12 kW
CLIC	0.4 mm	0.0100 rad	0.6 nC	2.00 GHz	1.5 TeV	25.0 m/rad	288.0 kW

A key issue for crab cavity RF systems is phase synchronisation between cavities on opposing beams so that bunches in each do not miss in the crabbing plane [15] (horizontal for linear colliders) as illustrated in Figure 9.
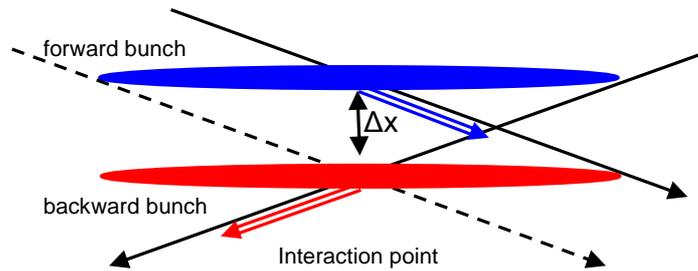
Figure 9: Crab cavity synchronisation

For circular machines one needs in addition extremely low phase noise at offset frequencies from the cavity RF frequency that coincide with betratron resonances. The cavity to cavity phase synchronization requirement can be estimated as

$$\text{synchronisation} = \frac{360\ \sigma_x f}{c\,\theta_r}\sqrt{\frac{1}{S_{rms}^4}-1}\quad\text{degrees}$$

where σ_x is the bunch width in the crabbing plane, f is the cavity RF frequency and S_{rms} is the minimum acceptable luminosity loss factor (usually about 0.98). The cavity frequency has to be equal to the bunch repetition frequency or one of its harmonics. For the ILC, the crab cavity frequency was chosen to be three times the linac RF frequency so that it would fit between the beam lines. For the LHC the crab cavity frequency has been chosen to be equal to the accelerating RF frequency to cater for long bunches. For CLIC the frequency was chosen to be 12 GHz to meet availability of high power Klystrons. Table 2 gives nominal parameters for ILC, LHC and CLIC crab cavity applications.

Table 2: Collider nominal parameters

	Luminosity fraction S	f (GHz)	σ_x (nm)	θ_c (rads)	ϕ_{rms} (deg)	Δt (fs)	Pulse Length (μs)
ILC	0.98	3.9	655	0.014	0.1271	90.5	1000.00
LHC	0.98	0.40	16500	0.000316	14.4	99800	CW
CLIC	0.98	12.0	45	0.020	0.0188	4.4	0.14

For crab cavity applications one must consider flexibility of the power supply [16]. At the arrival of each bunch train, the power supply does not know whether it will need to deliver power into the cavity or provide a 180° phase shift to assist power leakage from the cavity through a circulator to a load. Without compensation beamloading gives amplitude fluctuations in the cavity. Amplitude fluctuations change the crabbing angle, however small changes in the crabbing angle have a very much smaller effect on luminosity compared to phase fluctuations that move the bunches out of alignment.

For the ILC, amplitude fluctuations of 1% or more are acceptable. For superconducting cavities operating with external Q factor above 10^5 microphonics give large undesirable phase shifts which require active compensation with the RF power. Control implementation with an FPGA or DSP opens the possibility for feedforward or adaptive control. For sub microsecond bunch trains (CLIC for instance) timing latency rules out digital control.
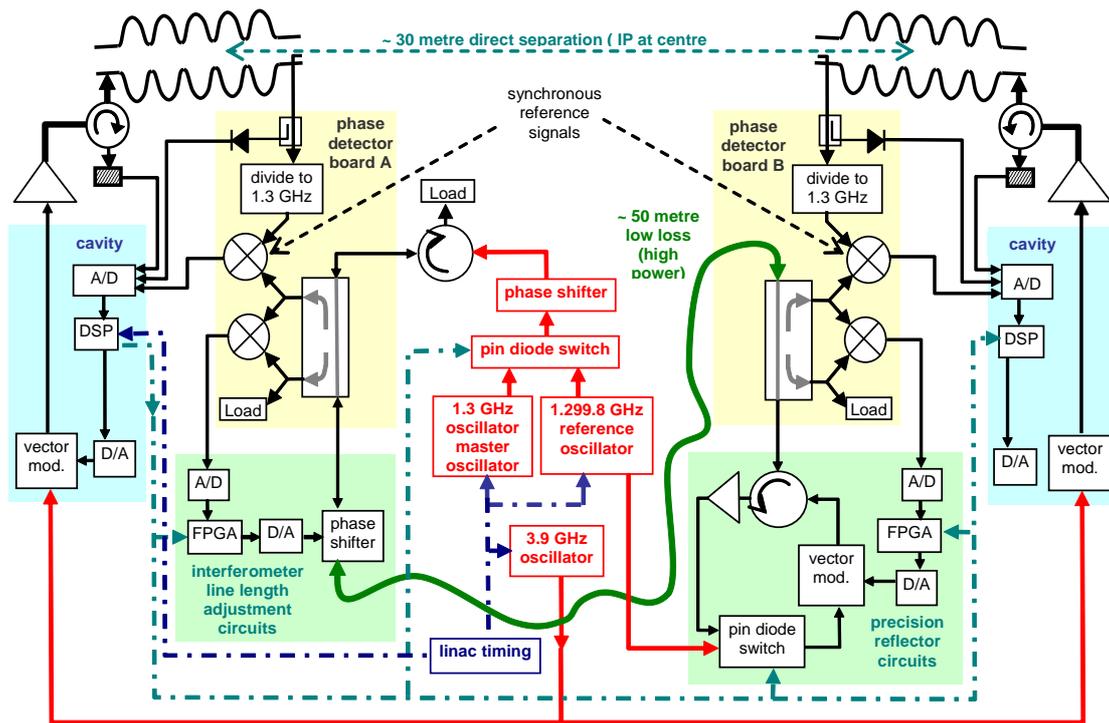
Figure 10: ILC crab cavity LLRF concept

The critical parameter for a linear collider crab cavity scheme is the cavity to cavity phase error. As long as the two cavities are in perfect phase with each other there can be a small phase error to each beam. Phase errors between cavities and beams cause lateral and longitudinal displacement of the IP. Limits on the phase error are determined from defocusing and vertex detection. The control system must have cavity synchronization as an integral feature. The strategy we have adopted for testing phase synchronisation concepts for ILC Crab cavities is set out in Figure 10.

The scheme takes a timing signal from the linac to ensure the cavities are synchronised to the beam. This signal stablises a 1.3 GHz master oscillator for the crab system. The reference oscillator shown alongside in the figure is only used in between bunch trains to determine and cancel amplifier offset errors. The master oscillator is used to establish a standing wave on a coaxial cable between the control systems for the two cavities, effectively forming an interferometer. A control circuit adjusts a two way phase shifter on the coaxial line to compensate for cable fluctuations. The desired outcome is a standing wave whose phase is identical at the mixers comparing cavity phase for each beamline.

In the adopted measurement scheme we chose to measure phase and amplitude of each cavity separately. Control action of digital signal processer (DSP) for each cavity is on the I and Q power components of each cavity and hence the first action of the DSP is to convert amplitude and phase to I and Q. This avoided the complexities of direct digital sampling of a down converted cavity signal. A distinctive feature of the control system used for the tests to date is the use of Hittite HMC439QS16G digital phase detectors on the phase detector boards (shown with mixer symbols). These detectors were investigated as their linearity offer advantages with respect to system calibration. Their phase jitter performance however is significantly worse than double balanced

mixers. The phase noise at 1280 MHz is about -135 dBc/Hz and is relatively flat with offset. Noise in 1 MHz bandwidth is about -80 dBc. corresponding to an r.m.s. phase jitter of 1.41×10^{-4} radians = 8 milli-degrees and a timing jitter of 17 fs. This is quite large but still significantly less than the ILC crab cavity to cavity timing requirement. Frequencies greater than 1 MHz have virtually no effect on the cavity phase jitter performance where a superconducting cavity with a bandwidth near to or less than 1 kHz is used.

Digital phase detectors only operate up to a frequency of 1.3 GHz hence they must be used either after down conversion or with frequency dividers. Down conversion adds the complexity of generating multiple phase locked frequencies. For simplicity we chose to divide the frequency using HMC437MS dividers; these generate an additional 2 milli-degrees r.m.s. phase jitter at 1.3 GHz. The big drawback of frequency dividers is that the phase gets divided hence 8 milli-degrees of phase jitter at 1.3 GHz implies 24 milli-degrees of phase jitter at 3.9 GHz. The LLRF system in figure 3 with its interferometer uses four digital phase detectors. Assuming that their noise is uncorrelated they contribute 48 milli-degrees of phase jitter at 3.9 GHz. The dividers add a further 2.82 milli-degrees hence system performance cannot be expected to exceed 51 milli-degrees of phase jitter. Another source of jitter is the digitization error. The sixteen bit ADCs used, have just 13 significant bits on a sample to sample basis. Without averaging, one nominally resolves the angular range into 8192 levels. For convenience of obtaining the lock a phase range of 100° at 3.9 GHz was mapped to the 8192 levels hence the digitization error for two uncorrelated channels is approximately 9 milli-degrees.

In tests using a slightly simplified version of the circuit in Figure 10 where two single cell cavities were mounted in the same cryostat, the cavity phase to phase jitter measured with a double balance mixer between the cavity outputs and for a measurement bandwidth of 1 MHz achieved 80 milli-degrees RMS. A sample output is shown in Figure 11.
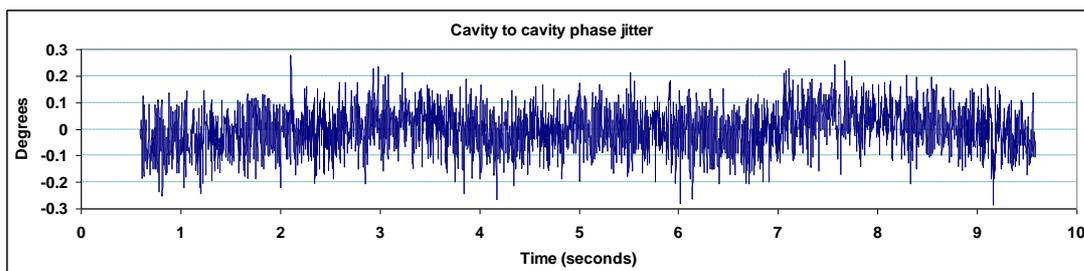
Figure 11: The cavity phase to phase jitter measurement.

Phase synchronisation for the LHC is trivial and no interferometer is needed. Suppression of noise at specific frequencies will be the key challenge for the LHC crab cavity system. The phase control specification for the CLIC crab cavities is well beyond anything that has been demonstrated at the 100 kW input power level. Given that beam loading is likely to be completely unpredictable for CLIC, our proposed solution is to have a power flow into and through the cavity that is significantly higher than the maximum beam loading power requirement. This is most easily realized with a high group velocity travelling wave cavity.

A reason for not favouring standing wave (SW) over travelling wave (TW) cavities is that measurement of phase in multi-cell cavities can have inaccuracies at the level of

milli-degrees caused by the excitation of modes adjacent to the operating modes [17] and we expect these to be somewhat smaller for TW cavities. This is because the TW cavity will have lower Q factors and we expect that the phase shift when the cavity is not precisely on frequency will be distributed along the structure rather than being all across the input coupler as it would be for the SW cavity. Beamloading calculations for a preliminary cavity design have been made to ensure that the amplitude fluctuations in the uncontrolled cavity are acceptable. In this case the TW cavity has 16 cells and operates in the $2\pi/3$ mode, R/Q = 53.92, group velocity = 0.0295c, Q = 638. Table 3 gives estimated power balances for maximum offsets and the consequential kick. Figure 12 shows the calculated fill and amplitude dip when an offset bunch train arrives.

Table 3: RF power balances for maximum deflection kick offsets

Beam offset (mm)	-0.4	0.0	0.4
Power entering cell 1 (MW)	6.388	6.388	6.388
Power leaving cell 16 (MW)	5.619	5.341	5.063
Ohmic power loss (MW)	1.071	1.047	1.023
Beamload power loss (MW)	-0.302	0.000	0.302
E max for cell 1 (MV/m)	51.1	51.1	51.1
Efficiency	12.04%	16.39%	20.74%
Kick (MV)	2.428	2.400	2.372
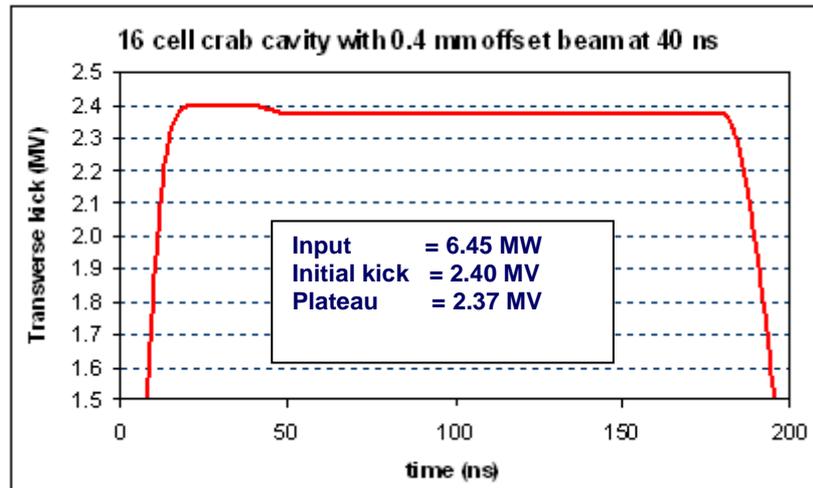
Figure 12: Calculated fill and amplitude dip for offset bunch.

The proposal for synchronising the cavities is to use the scheme proposed for the NLC by J. Frisch where the output from a klystron is split and carried along equal lengths of temperature controlled waveguide to the crab cavities on opposing beams. With an advanced optical interferometer it may be possible to provide reference phases at the cavities that are synchronized to 1 fs [18]. The strategy is then to design a cavity which follows the input phase as closely as possible. To do this one might for instance mount the cavity centrally so that expansion gives phase errors that cancel. Careful attention to cavity temperature control will be needed so that the two systems perform in an identical fashion.

It is unlikely that cavity phase could ever be measured to an accuracy of milli-degrees and then corrected on the timescale of a few bunches (say 40 ns). If after

actively matching waveguide paths to the input couplers it turns out that the relative phase of the two crab cavities drift with respect to each other during the pulse then the only possible correction scheme is to mix an RF power correction with the main split power using feed forward estimation from the previous bunch train.
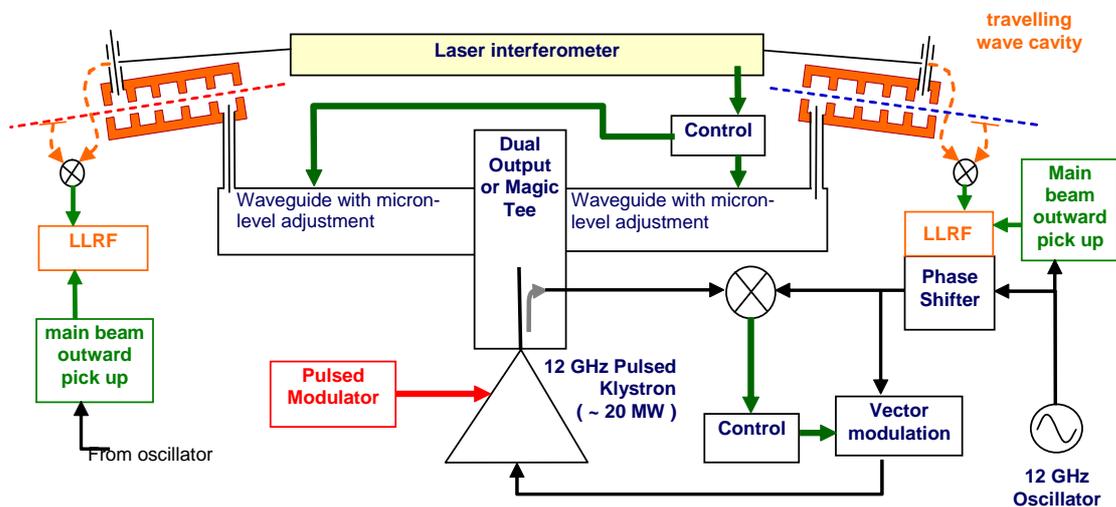
Figure 13: Calculated fill and amplitude dip for offset bunch.

The control procedure might run as follows:

1. Send pre-pulse to cavities and use interferometer to measure difference in RF path length
2. Perform waveguide length adjustment at micron scale
3. Measure phase difference between oscillator and outward going main beam
4. Adjust phase shifter in anticipation of round trip time and add offset for main beam departure time
5. Klystron output is controlled for constant amplitude and phase
6. Record phase difference between returning main beam and cavity
7. Alter correction table for next pulse

3.6.6   **Outlook**

The application of crab (or deflecting mode) cavities for next generation colliders and storage rings, to facilitate beam manipulation for optimising luminosity, shortening bunches or to enable precision diagnostics, is now widespread, and the CI is playing a major role in the design of these systems for ILC, CLIC and LHC. Having demonstrated that working tolerances can be maintained to within required ILC stability margins, the CI has utilised such development skills to determine appropriate crab cavity system solutions for both CLIC and LHC. As part of the FP7 European Framework programme, 'EuCARD – European Coordination for Accelerator Research & Development [19]', the CI is leading the development in these areas, with an intention to design optimised crab structures, with effective wakefield management attributes and to also understand and determine appropriate mechanisms for providing precise, synchronised control of the deflecting cavity fields.

3.6.7 **References**

1. R. B. Palmer, Energy scaling, crab crossing and the pair problem SLAC-PUB-4707, 1988
2. T. Abe et al, Compensation of the crossing angle with crab cavities at KEKB, MOZAKI01, PAC07, Albuquerque
3. L. Bellantoni, H.T. Edwards and M. McAshan, "Design and measurements of a deflecting mode cavity for an RF separator", PAC 2001
4. I. Wilson, "The compact linear collider CLIC", Physics Reports 403-404 (2004) 365 – 378.
5. Shakespeare Engineering Group. Unit 91, Haltwhistle Road, South Woodham Ferrers, Essex CM3 5ZA, UK.sales@shakie.demon.co.uk
6. Z. Li et al, "RDDS Cell Design and Optimisation for the Linear Collider Linacs", PAC99, New York, 1999, pp. 3480 – 3482.
7. C. Nantista, S. Tantawi, and V. Dolgashev, "Low-field accelerator structure couplers and design techniques", Phys. Rev. ST Accel. Beams 7, 072001 (2004)
8. F. Ruggiero and F. Zimmermann, "Possible scenario for an LHC upgrade", CARE-Conf-05-002-HHH, Proceedings of the HHH 2004 Workshop, Geneva, November 2004, http://care-hhh.web.cern.ch/care-hhh/HHH-2004/Proceedings/proceedings_hhh2004.htm.
9. K. Hosoyama et al. "Crab cavity development", SRF 2005, Ithaca, 2005.
10. M. Borland et al., "Planned Use of Pulsed Crab Cavities at the Advanced Photon Source for Short X-ray Pulse Generation", PAC07, Albuquerque, USA, 2007.
11. VORPAL, Tech-X Corporation, 5621 Arapahoe Ave. Suite A, Boulder, CO 80303, www.txcorp.com/products/VORPAL/
12. Particle Studio, CST GmbH, Darmstadt, [online] http://www.cst.com/.
13. K. Hovator et al, "The CEBAF RF Separator System", LINAC96, Geneva, 1996, pp. 77 – 79.
14. G. Burt, R.M. Jones, A. Dexter, "Analysis of Damping Requirements for Dipole Wake-Fields in RF Crab Cavities." IEEE Trans. Nuc. Sci. Vol. 54, 2007
15. A. Dexter and G. Burt "Phase and Amplitude Control of Dipole Crabbing Modes in Multi-Cell Cavities", EUROTeV-Report-2008-064, 2008
16. G. Burt, A. Dexter , P. Goudket, A.C and A. Kalinin, "Effect and tolerances of phase and amplitude errors in the ILC Crab Cavity", EUROTeV Report 2006-098
17. D. Alesini, A. Gallo, B. Spataro, B. Marinelli A. and L. Palumbo L. Nuclear Instruments and methods in physics research A 580 (2007) 1176-1183
18. J. W. Staples, R. Wilcox and J. M. Byrd, "Demonstration of femto-second phase stabilization in 2 km optical fibre", Proceedings of PAC07, Albuquerque, New Mexico, USA.
19. https://eucard.web.cern.ch/EuCARD/index.html

3.7   Neutrino Factory Studies

C. Prior[1], K. Long[2], R. Edgecock[1], J. Pasternak[2], J. Pozimski[2]

[1] STFC Rutherford Appleton Laboratory, Didcot, Oxon OX11 0QX, UK

[2] Imperial College London

Mail to: chris.prior@stfc.ac.uk

3.7.1   Introduction

The neutrino is, perhaps, the most mysterious of the particles that make up the Standard Model. It has long been known that neutrinos carry spin ½ and occur in three flavours: ν_e, ν_μ, and ν_τ. One of the most exciting developments in particle physics over the past decade has been the establishment of the phenomenon of neutrino oscillations in which neutrinos produced in a particular state of flavour (say ν_μ) may be observed to have evolved (oscillated) into a different state (say ν_τ) by the time they are detected. The implications of these observations are far reaching for, not only do neutrino oscillations require the Standard Model to be extended to include neutrino mass and mixing between the flavour states, but, neutrino oscillations open the possibility that neutrinos violate the matter-antimatter (CP) symmetry. Indeed, the possibility of CP-violation in the lepton sector means that the interactions of neutrinos may be responsible for the matter-dominated Universe. The Neutrino Factory, in which intense, high-energy neutrino beams are produced from the decay of stored muon beams, has been shown to be the 'facility of choice' for the study of neutrino oscillations [1].

The idea of a Neutrino Factory (NF) was first put forward as far back as the 1970's when it was suggested that neutrino beams might be generated from the decay of kaons and muons in the straight sections of large storage rings. However, predicted intensities were well below the required level of about 10^{21} neutrinos a year. The first viable scenario was published by Steve Geer in 1997 [2], followed by a seminal paper by Bob Palmer, Colin Johnson and Eberhard Keil [3] that prompted major design reviews. The first review, undertaken by Fermilab in April 2000 and known as US Study I [4], demonstrated the feasibility of the NF concept. A design with improved performance, through changes in the target and the muon cooling and accelerating systems, was completed by Brookhaven in 2001 (US Study II [5]). Additional studies were carried out at CERN in 1999 [6] and in Japan in 2001 (Nufact-J [7]). The Japanese study was notable for its use of very large acceptance fixed field alternating gradient (FFAG) accelerators, which seemed to obviate the need to cool the muon beam. A revised US Study IIa [8] subsequently included FFAGs of the recently developed non-scaling type, but with the cooling retained.

August 2005 saw the setting up of a one-year review, called the International Scoping Study (ISS), which assessed the status of Neutrino Factory work and identified a fully self-consistent and viable accelerator scenario. The ISS Accelerator Working Group Report [9] made recommendations for all parts of the Neutrino Factory complex, ranging from a high intensity proton driver, through muon production, control and acceleration, to the design of the storage rings that direct the neutrino beams through the Earth to distant detectors. The ISS scheme has subsequently been adopted by its successor, the International Design Study for the Neutrino Factory (IDS-NF) [10], which is due to deliver a Reference Design Report (RDR) by 2012-13 [11]. This should

include a detailed specification of the accelerator complex, some engineering plans, identification of R&D and costing.

The UK has been involved in Neutrino Factory accelerator studies from the outset, initially through work on the proton accelerator that drives the complex, and then developing into ideas for muon capture and acceleration schemes. The UK Neutrino Factory R&D activity is now established as the UK contribution to the IDS-NF. The following paragraphs outline the UK contributions to the international effort.

3.7.2 The Neutrino Factory Accelerators

The IDS-NF baseline for the Neutrino Factory is shown in Figure 1 [12]. A high intensity proton driver directs a multi-megawatt beam onto a pion production target. Charged pions are captured in a focusing channel at low energy; they decay to muons, whose phase space is controlled and reduced in size by ionisation cooling. The resulting muon beam is then accelerated rapidly to an energy of 25 GeV. Finally the muons are
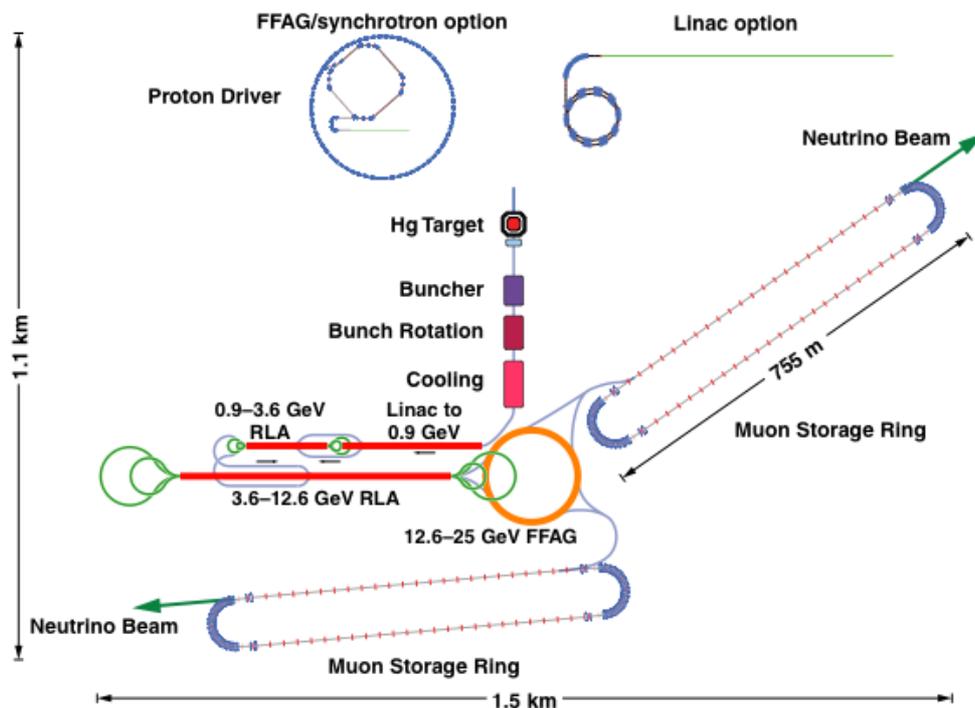
Figure 1: Layout of the Neutrino Factory, showing the component accelerators drawn to relative scale.

stored in designated storage rings with long straight sections, where the neutrinos produced by their decay can be directed towards the detector sites. The proton driver, target station, and muon front end of the Neutrino Factory have been proposed as part of the accelerator facility required to deliver multi-TeV lepton-antilepton collisions at the Muon Collider. The Neutrino Factory may therefore be seen as a step on the way to a Muon Collider, conceivably the next big particle accelerator project after the LHC.

3.7.2.1 *Proton Driver*

At the start of the accelerator chain, a proton driver capable of delivering a peak power of 4 MW at a repetition rate of 50 Hz is required. The proton-beam energy must be in the multi-GeV range in order to maximise the pion production. In addition, the Neutrino Factory requires a particular time structure consisting of three very short bunches separated by about 100 µs. The short bunch length of 2 ns rms is dictated by the efficiency of the muon-beam capture and the bunch separation is constrained by beam loading in the downstream muon accelerator and the disruption time of the mercury-jet target. In order to achieve such short bunches, a dedicated bunch compression scenario needs to be carefully designed in order to deal with very strong space-charge forces. Several proton driver schemes fulfilling these requirements have been proposed. Typically they consist of an H⁻ ion source followed by an RFQ, chopper, and a linear accelerator. The main hardware R&D activity for the front-end of the multi-MW proton driver, the Front End Test Stand (FETS) is described elsewhere in this newsletter. The final energy of the proton driver may be obtained directly in the linac, as in the CERN design based on the SPL [13] or in the recent studies based on the Project-X at Fermilab [14]. In these scenarios the beam time structure is obtained with the help of charge exchange injection into the accumulator ring followed by fast phase rotation in the dedicated compressor ring. Alternatively, the beam from the linac may be accumulated and further accelerated in a Rapid Cycling Synchrotron (RCS) as in the solution proposed at RAL in the ISS study [15,16]. In this proposal, bunch compression is accomplished adiabatically in the second RCS or, alternatively, in the FFAG ring, see Figure 2 (left). Recently the attractive idea of the common proton driver for the
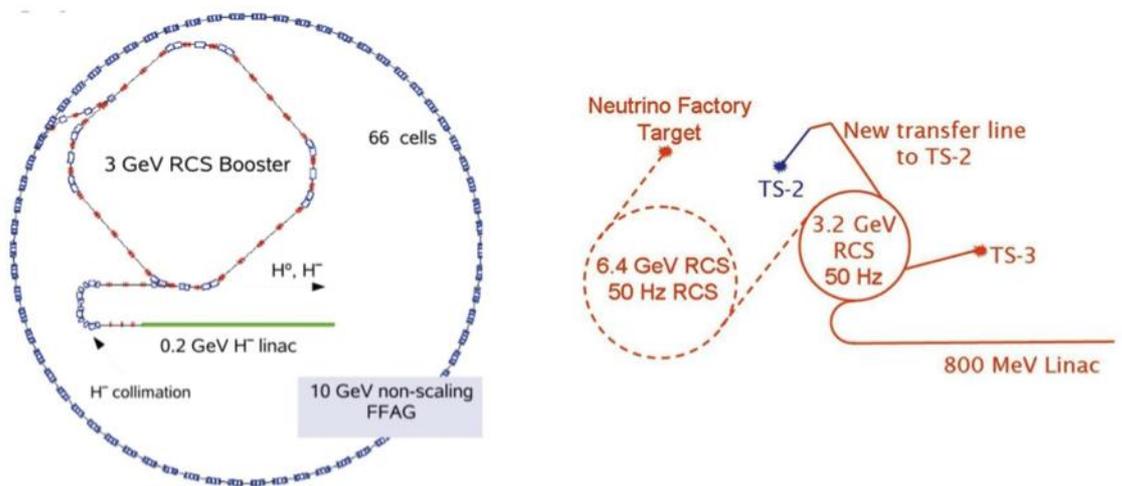
Figure 2: Left: Layout of the proton driver based on an RCS and an FFAG. **Right:** Layout of the common proton driver for ISIS and the Neutrino Factory.

spallation neutron source and the Neutrino Factory was proposed [17] in the framework of the ongoing megawatt ISIS upgrade programme. In such a scenario (see Figure 2, right panel), the proton drivers for both facilities share the same source, chopper, linac, accumulation and RCS acceleration to 3.2 GeV. After extraction, three bunches will be sent directly to the neutron-spallation target while three others will be injected into a

second RCS where, after acceleration and bunch compression, the beam will be extracted towards the Neutrino Factory pion production target.

3.7.2.2 *Target*

The Neutrino Factory target station presents a formidable engineering challenge. It must efficiently produce and capture sufficient pions, while simultaneously dissipating the 4 MW of proton beam power. The IDS-NF baseline calls for a free-flowing liquid-mercury jet target. The free-flowing jet has the advantage that the portion of the jet disrupted by the beam is replaced in time for the next proton-beam pulse. The measurements made by the MERIT collaboration [18] indicate that the mercury-jet technology is capable of operating successfully at the Neutrino Factory. However, the liquid-mercury technology has the disadvantage that the mercury delivery and re-circulation system is complex and the mercury itself presents substantial safety issues that must be overcome in the design of the target station.

In view of the high level of the technical risk associated with the Neutrino Factory target, work in the UK has focused on the development of alternatives to liquid mercury. A novel 'powder jet' scheme, in which tiny tungsten balls are 'fluidised' in a high-velocity 'carrier' gas, offers some of the advantages of the mercury jet while avoiding the chemical and some of the radiological issues associated with mercury. A prototype of a powder-jet target has successfully been built and operated. Initial results of the power-jet tests are promising.

The possibility that a solid target for the Neutrino Factory can be designed is also being energetically investigated. The principal issue that must be faced in the design of a solid target is that of beam-induced shock caused by the enormous power density deposited by the short proton pulses. The shock induced in the target can exceed the mechanical strength of materials such as tantalum or tungsten if the target is operated at room temperature. Experiments have been carried out to study the response of tantalum and tungsten to shock at high temperatures. The passage of the beam through the Neutrino Factory target is simulated using a high-current pulse in a thin wire. Results obtained to date indicate that tungsten is a better choice of target material that tantalum. Extrapolation of the measurements indicates that a solid target system for the Neutrino Factory could be designed using solid tungsten rods, so long as a mechanism to exchange the tungsten rods at an appropriate frequency can be implemented.

The simulated shock studies are now being augmented with studies of the modes of excitation of the tungsten wire by the current pulse. Measurements using a Laser Dople Vibrometer are being compared with dynamic finite element analysis, the calculations are performed using LS-DYNA. By comparing the measurements with the LS-DYNA simulation it will be possible to understand the lifetime measurements and to extrapolate more precisely to the Neutrino Factory configuration. In parallel, design work on a solid-target station based on a rotating wheel bearing a number of tungsten rods has been initiated.

3.7.2.3 *Muon Capture and Cooling*

Pion production and the distribution of the dissipated power in the target area have been studied for solid and liquid-mercury targets as shown in Figure 3. Yield calculations have been used to optimise the proton-driver energy to be in the range between 6 GeV and 10 GeV. While for a proton energy of 10 GeV, nearly all energy is

dissipated near the target area with the consequence of an improved shielding of the superconducting solenoids, for higher proton energy the power dissipation is maximum in the mercury beam dump raising concerns about mercury splashes damaging the containment vessel.

The muon front-end is designed to optimise the number of muons that can successfully be transmitted through the downstream accelerator complex. The baseline
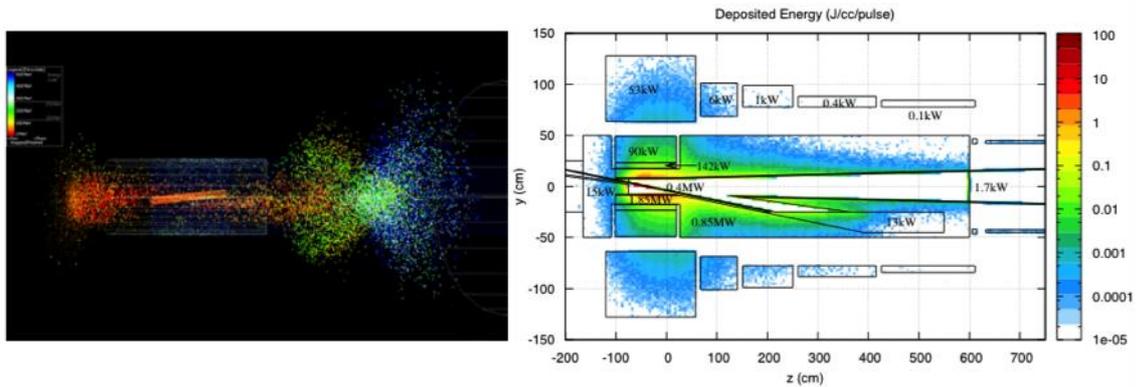
Figure 3: Left: Simulation of the pion distribution delivered by a solid target (*courtesy S. Brooks*). **Right:** Simulation of the power distribution dissipated in the baseline liquid mercury target area for a 10 GeV proton beam (*courtesy J. Back*).

design has a 12 m solenoid capture channel with fields tapering from 20 T down to 1.75 T (see also Figure 3 left), and a decay section of about 100 m, after which the muons undergo adiabatic bunching in a system of RF cavities of fairly modest gradient. This is followed by RF phase rotation with higher gradients and frequencies that decrease with progress down the channel. The energy spread is reduced and the beam is formed into trains of about 50 interleaved $\mu^\pm$ bunches [19]. This process is shown in Figure 4 (left). An approximately 80 m section of ionisation cooling channel - a novel
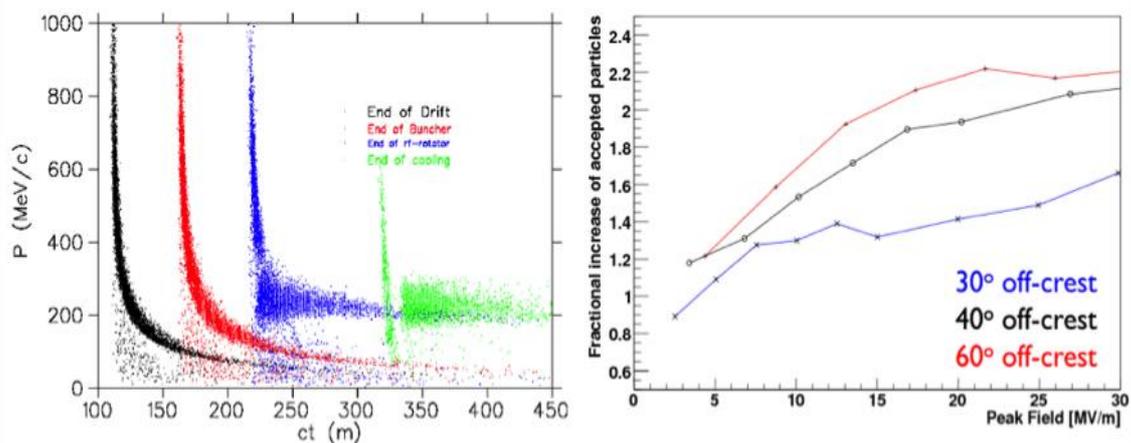
Figure 4: Left: Simulation of the muon Front-End showing the formation (left to right) of a train of interleaved $\mu^\pm$ bunches (*courtesy D. Neuffer*). **Right:** Influence of achievable RF gradient in the cooling section on particle yield for different RF phases (*courtesy C. Rogers*).

concept and the proof-of-principle experiment, MICE, is described elsewhere in this issue - is used to increase the number of muons that can be accepted by the accelerators. Experiments at the MTA at Fermilab showed that the strong magnetic fields required to

transport the muon beam may have a seriously detrimental effect on the effective gradients that can be achieved. Quantifying this effect and finding appropriate solutions form a major R&D project that is being carried out by the MuCOOL collaboration.

3.7.2.4 *Muon Acceleration*

The muon accelerators have a transverse phase space acceptance of 30 π mm.rad to be able to accelerate the beam, which is enormous compared with conventional beams in proton and electron machines. In their rest-frame, muons have a half-life of only 2.2 μs, so acceleration has to be very rapid to benefit from the effects of time dilation and to reduce losses through decay. FFAG accelerators are promising in this respect but work less efficiently at low energies. The chosen system, the central part of Figure 1, therefore starts with a 201 MHz pre-accelerator linac, which accelerates the beam to
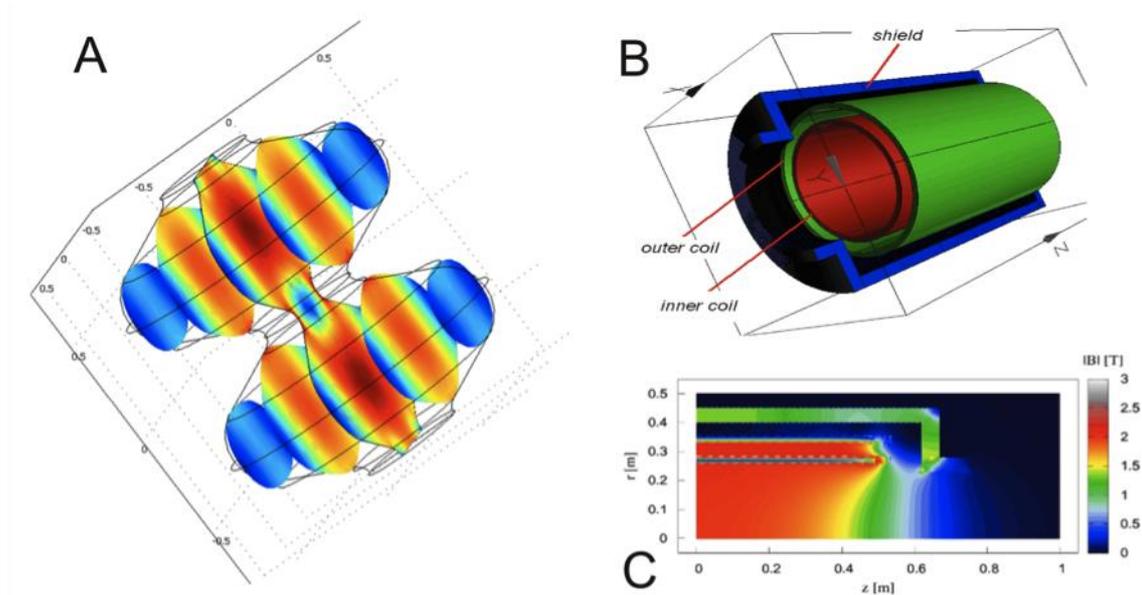
Figure 5: A: Simulation of the electric field distribution in a 2-cell SC linac cavity running in π-mode at 201.25 MHz using *COMSOL*. **B:** The design of the linac solenoids consists of two SC coils with opposite excitation and an iron shield to reduce stray and fringe field effects. **C:** Magnetic field distribution in one quadrant of the solenoid simulated with *ROXIE* (*courtesy M. Aslaninejad and C. Bontoiu*).

0.9 GeV while adiabatically reducing the phase-space volume. The linac has been developed by A. Bogacz (JLab) and confirmed using MAD-X. Design and EM simulations of the linac components (solenoids and cavities) have been completed and the results are shown in Figure 5. While the design of the niobium sputtered superconducting cavities is straightforward, the solenoid design is optimised to reduce the magnetic fringe field at the position of the cavities (to avoid degradation of achievable field) by using a counter-excited outer shell together with an iron shield. Multi-particle simulations based on the results of the EM simulations have been performed using GPT. The output distribution of the longitudinal phase space after the cooling section is shown on Figure 6A. The huge momentum spread in the bunch results in particle losses in the first part of the linac of roughly 5% but this assumes a

very preliminary matching section between the cooling section and the linac. The results of these simulations are shown in Figure 6B.
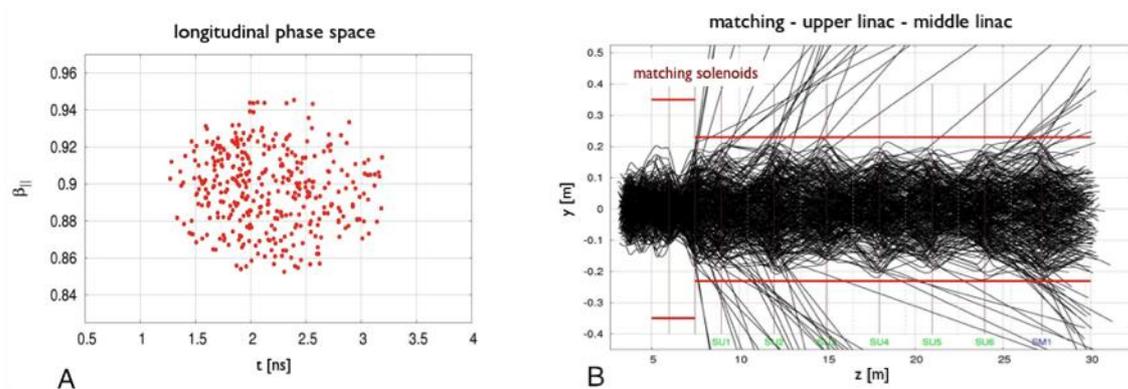
Figure 6: A: Longitudinal phase space distribution of the acceptable part of the muon beam at the end of the cooling section (*courtesy C. Rogers*). **B:** Result of a multi-particle tracking using the code GPT with field maps from the end of the cooling section to the linac (*courtesy C. Bontoiu*).

At the end of the linac the beam has an energy of 0.9 GeV. Use of a recirculating linear accelerator is now possible and the phase slip, caused by the variation in time-of-flight with energy, is tolerable. The beam is accelerated in two dogbone RLAs, making 3.5 passes in each, gaining energy to 3.6 GeV in the first, and 12.6 GeV in the second. Dogbone RLAs give improved cost efficiency over normal linacs and racetrack RLAs, but features such as the non-zero energy spread in the beam, the transverse beam size and the space required for magnet coils restrict the number of separate return arcs into which the beam can be directed and so limit the number of passes through the accelerating structures.

A non-scaling FFAG (NS-FFAG) accelerator has been proposed for the final muon acceleration from 12.6 GeV to 25 GeV as a quasi-isochronous design allows for up to 8-12 turns. The lattice is filled with 201 MHz RF cavities, increasing the muon acceleration efficiency and lowering the overall cost of the facility. As confirmed in numerous beam dynamics simulations, a linear strong-focusing NS-FFAG lattice can transport large emittance muon beams using relatively compact magnets since orbit excursion is very small. The linear design of the NS-FFAG lattice candidates was recently optimised with respect to cost and performance. One remaining difficulty is that the variation in time-of-flight for particles with large transverse amplitude causes phase slip at the RF cavities, which can lead to longitudinal phase space distortion and increased final energy spread. Although this increase of the energy spread is much higher than the effect of beam loading, the resulting beam can still be accepted by the decay ring. However, it has been shown chromaticity correction, by introducing non-linear magnetic field components (see Figure 7, right panel), can reduce the longitudinal distortion and the final energy spread. The disadvantage of this solution is the reduction in the dynamic acceptance. The degree of chromaticity correction finally adopted may be a compromise between these two effects and still needs to be defined. Other important issues addressed in recent studies are the beam injection and extraction [20]. Several lattice candidates were carefully considered and current results favour the triplet solution with 3 m long straight sections. This solution allows the field requirements on the kicker and septum magnets to be reduced. In the proposed injection/extraction geometries, several kicker units are distributed in several lattice cells, assuming mirror

symmetry in order to reuse the same kickers for both signs of muons. In this way, as shown in Figure 7 (left), sufficient orbit separation can be created. This allows the use of septum magnets whose strength requires the use of superconducting technology. Another approach to facilitate injection/extraction has been studied using a lattice with a special 7 m long drift-insertion cell. Whether the dynamic acceptance is sufficiently large in such a lattice remains to be demonstrated. Since non-scaling FFAGs are very much in their infancy, the results from EMMA, the electron model under construction at the Daresbury Laboratory (*q.v.*), will be of great interest and relevance to the Neutrino Factory study.
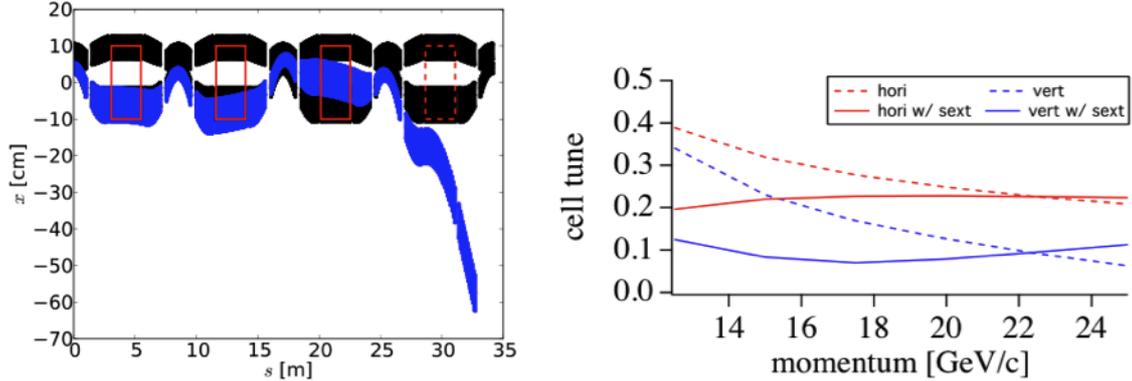
Figure 7: Left: Geometry of injection into the NS-FFAG triplet lattice. The superimposed rectangles indicate the kicker positions; the dashed rectangle shows the position of the septum (*courtesy D. Kelliher*). **Right:** Cell tunes with and without chromaticity correction using sextupoles (*courtesy S. Machida*).

3.7.2.5 *Muon Storage Rings*

Intense bursts of neutrinos and anti-neutrinos are generated by the decays of the μ^+ and μ^- bunches in long straight sections in dedicated storage rings according to

$$\mu^- \to e^- + \bar{\upsilon}_e + \upsilon_\mu \qquad \mu^+ \to e^+ + \upsilon_e + \bar{\upsilon}_\mu$$

The neutrinos are directed through the Earth to detectors at distances of about 3000 km and 7500 km at angles to the surface of 18° and 36° respectively. Three ring geometries have been studied, of which the most flexible are based on racetrack lattices (Figure 8A), which can be built to point towards any fixed detectors. The shown is designed for either µ+ or µ- with a single production straight pointing into the ground. The return straight is used for collimation, RF and tune control. However a development of this ring is in progress to double the neutrino rate by storing counter-rotating muons of both signs. An alternative is a triangular lattice (Figure 8B) with two production straights that can be pointed in different directions and so send neutrinos to combinations of detectors (dictated by the apex angle) [21]. Two triangular rings would be built side by side in the same tunnel, one serving μ^+ and the other μ^-. A third option, a bow-tie ring (Figure 8C), could similarly point at two separate detectors but will preserve the muon polarisation, which may interfere with the accuracy of the beam instrumentation. The choice of the decay ring depends on the efficiency (the ratio of the total length of the neutrino production straights to the circumference), and the depth of the tunnels, which has geological and cost implications. The production straights for the

racetrack design are 600.2 m long, giving an efficiency of 37.5% for single sign muons, and higher (perhaps 60%) for counter-rotating bunches of μ^+ and μ^-. The corresponding figures for the racetrack and bow-tie lattices are 398.5 m (2×24.8%) and 469 m (2×29.2%) respectively. The tunnel depths for rings of this size are 444 m for the racetrack, 493 m for the triangle and 312 m for the bow-tie. To keep the neutrino beams
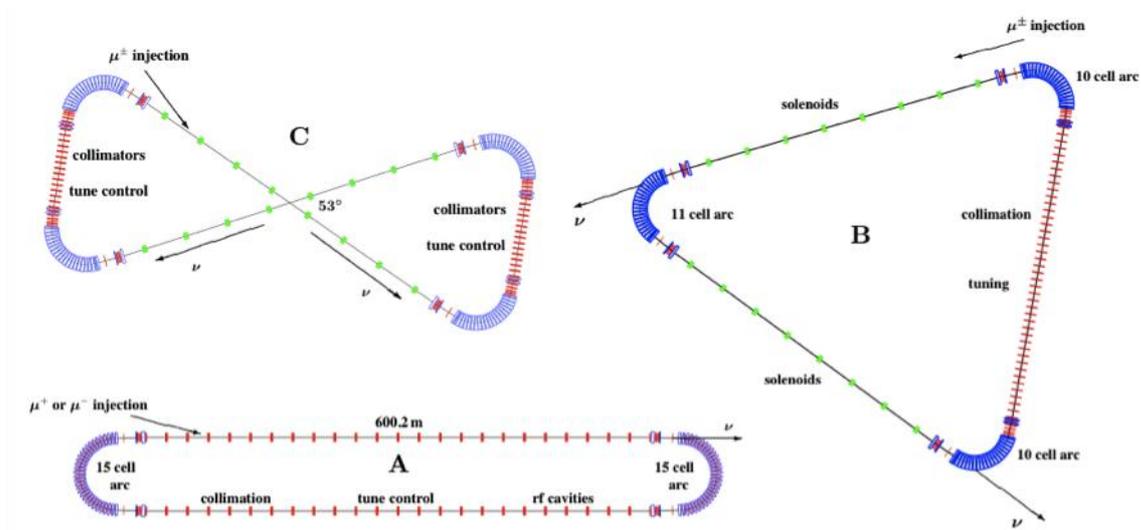
Figure 8: Different designs of muon storage ring. **A:** Racetrack structure that can send simultaneously neutrinos from both sign muons to one detector; this is the baseline design. **B:** A design based on triangular geometry, able to send neutrinos to detectors in two different directions (but only for one muon sign). **C:** A bow-tie design, similar to B but requiring less tunnel depth.

reasonably well focused, the muon beam's rms divergence angle should not add more than about 10% to the natural $1/\gamma$ angle of the decay cone. This means that the β-functions, which should be small (~14 m) in the arcs, have to be matched to much larger values (100-150 m) at the start of the long production straights.
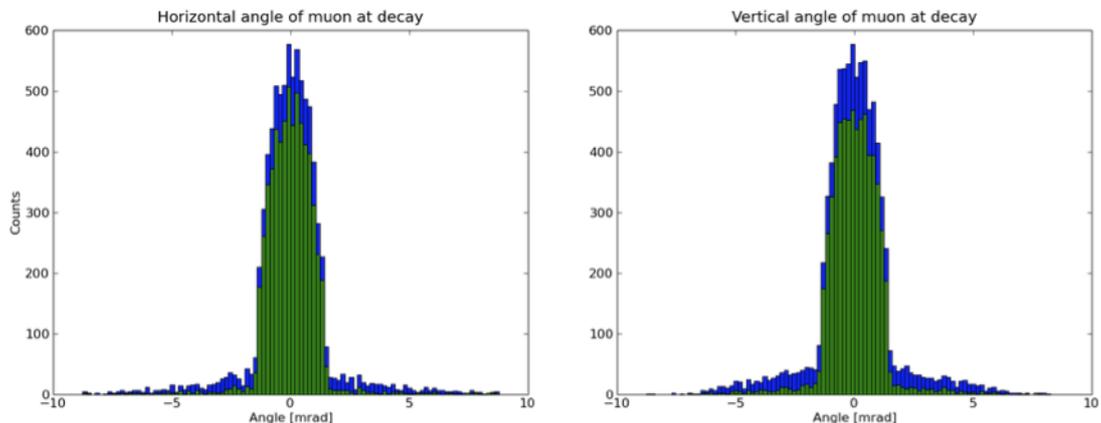
Figure 9: Neutrino angular distribution from horizontal and vertical muon decay angles.

Simulations of the racetrack decay ring have been carried out using the code Zgoubi [22]. These predict the neutrino angular distribution shown in Figure 9. Studies of the beam instrumentation in the decay ring (beam current and beam divergence),

essential for the correct prediction of the expected neutrino flux at the far detector, have been started and an efficient collimation systems needs to be developed to cope with the megawatts of muon beam power the rings have to sustain.

3.7.2.6　*Detector Sites*

Provided there are detectors at the right distances from the Neutrino Factory site, the racetrack lattice has the greatest flexibility in that it can be pointed in any direction. Two separate tunnels would be needed with a total of four transfer lines, in order to handle both μ^+ and μ^- in each of two rings. Depending on the NF site, the triangle or bow-tie may prove more suitable geometries because of their enhanced neutrino production efficiency, the use of only one tunnel and a reduced number of transfer lines. For these configurations, several suitable Neutrino Factory (CERN, RAL, Fermilab) and detector (Gran Sasso, Norsaq, INO) sites have been identified. Another option that the IDS-NF is currently investigating is a Neutrino Factory with a much lower muon energy (~4 GeV) and a smaller storage ring with reduced tunnel depth. In all scenarios, a geological survey of the sub-terrain of any proposed Neutrino Factory site is essential.

3.7.3　**Acknowledgements**

3.7.4　**References**

1. The ISS Physics Working Group, Rept.Prog.Phys.72:106201, 2009.
2. S. Geer, FERMILAB-PUB-97-389, 1997; Phys.Rev. D 57, 6989, 1998.
3. R.B. Palmer, C. Johnson, E. Keil, Nucl. Instr. Methods A 451, 265, 2000.
4. N. Holtkamp, D. Finley (eds), FERMILAB-PUB-00/108-E, http://www.fnal.gov/projects/muon_collider/nu-factory
5. S. Osaki, R. Palmer, M. Zisman, J. Gallardo (eds), BNL-52623, http://www.cap.bnl.gov/mumu/studyii/FS2-report.html
6. B. Autin, A. Blondel, J. Ellis (eds), http://muonstoragerings.web.cern.ch/muonstoragerings
7. Y. Kuno, Y. Mori (eds), http://www-prism.kek.jp/nufactj/index.html
8. J.S. Berg et al, Phys.Rev.ST.Accel. Beams 9, 011001, 2006; http://www.cap.bnl.gov/mumu/study2a/.
9. The ISS Accelerator Working Group, JINST **4** PO7001, 2009.
10. https://www.ids-nf.org/wiki/FrontPage
11. The IDS-NF Steering Group, IDS-NF-001 http://www.ids-nf.org/wiki/FrontPage/Documentation#ids
12. The IDS-NF Steering Group, IDS-NF-002 *ibid.*
13. R. Garoby, E. Benedetto, M. Aiba, M. Meddahi, "Linac-based Proton Driver for a

Neutrino Factory", CERN-NEUTRINO-FACTORY-NOTE-157, Dec 2009.

14. http://projectx.fnal.gov/
15. C.R. Prior & G.H. Rees, "RAL Proton Driver Studies for a Neutrino Factory", Proceedings of NUFACT'00, Monterey, California, 2000.
16. G.H. Rees, "An FFAG Proton Driver for a Neutrino Factory", ICFA Beam Dynamics Newsletter 43, August 2007.
17. J. Pasternak, M. Aslaninejad, K. Long, J. Pozimski, "Feasibility of a Common Proton Driver for a Neutron Spallation Source and a Neutrino Factory", Proceedings of the Particle Accelerator Conference, PAC'09, Vancouver, Canada, May 2009.
18. H.G. Kirk, "The MERIT High-power Target Experiment at the CERN PS", WEPP169, Proceedings of the XIth European Particle Accelerator Conference, EPAC'08, Genoa Italy, June 2008.
19. D. Neuffer, NFMCC-doc-181-v1, 2000; NFMCC-doc-269-v1, 2003.
20. J. Pasternak, M. Aslaninejad, J. Scott Berg, D. Kelliher, S. Machida, "Injection and Extraction Studies for the Muon FFAG", Proceedings of NUFACT'09, Chicago, USA, 2009.
21. C.R. Prior, "Muon Storage Rings for the Neutrino Factory", Proceedings of the Particle Accelerator Conference, PAC'09, Vancouver, Canada, May 2009.
22. F. Méot, "6D Beam Dynamics Simulations in FFAGs using the ray-tracing code ZGOUBI", ICFA Beam Dynamics Newsletter 43, *op.cit.*

3.8   The Muon Ionisation Cooling Experiment MICE

Chris Rogers

STFC Rutherford Appleton Laboratory, Didcot, Oxon OX11 0QX, UK

Mail to: chris.rogers@stfc.ac.uk

3.8.1   Introduction

The Muon Ionisation Cooling Experiment (MICE) is currently under construction at the Rutherford Appleton Laboratory. MICE will prove the technology necessary for muon ionisation cooling. In ionisation cooling, particle beam emittance is reduced by passage through an energy absorbing medium and RF cavities.

In its final configuration, MICE will consist of a 5.5 metre cell of an ionisation cooling channel, containing two 4-cavity linacs and 8 coils producing an overlapping solenoid field in an SFoFo arrangement. Detector systems at each end of the cooling channel will measure the 6-dimensional phase space vector of individual muons enabling the reconstruction of the full 6D beam distribution. A schematic of the cooling channel in its final configuration is shown in Figure 1.
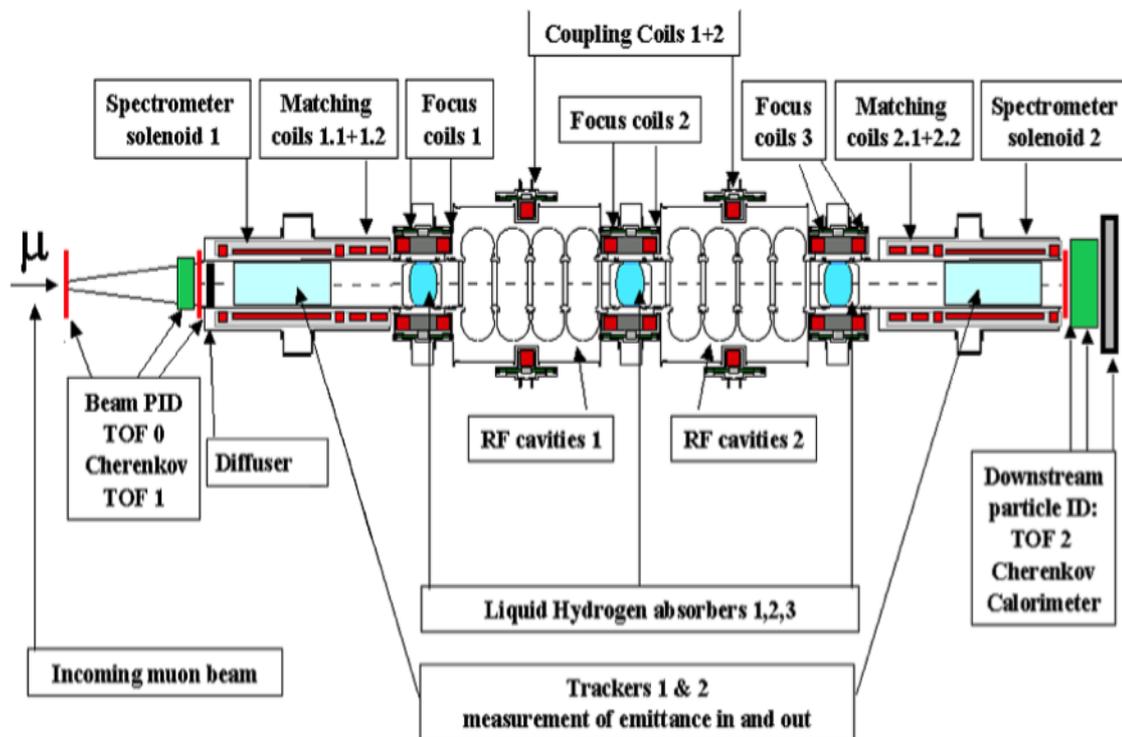
Figure 1: Schematic of the Muon Ionisation Cooling Experiment in its final configuration

MICE seeks to demonstrate: that the physics of ionisation cooling works as expected; that it is possible to contain very high emittance beams typical of the Neutrino Factory muon front end; and that the construction and operation of the cooling channel is feasible.

3.8.1.1 *Transverse Cooling Theory*

In its most basic form, ionisation cooling reduces the transverse emittance of a particle beam. On passing through an absorber the momentum of the particle is reduced non-symplectically resulting in a reduction in normalised emittance. Subsequently muons pass through RF cavities where the momentum is restored in the longitudinal direction only and the geometric emittance of the beam is reduced.

The cooling effect is ruined by stochastic effects, principally multiple Coulomb scattering transversely and energy straggling longitudinally. Additionally the curvature of the Bethe Bloch curve can provide additional longitudinal cooling or heating.

For a cylindrically symmetric beam, the change in transverse RMS emittance ε_n and longitudinal RMS emittance $\varepsilon_{//}$ on passage through a thin absorber of thickness dz are given by [1]

$$\frac{d\varepsilon_n}{dz} = -\frac{1}{\beta_{rel}^2}\frac{dE}{dz}\frac{\varepsilon_n}{E_\mu} + \frac{\beta_\perp \left(13.6[MeV]\right)^2}{2\beta_{rel}^3 E_\mu mc^2 L_R}$$

$$\frac{d\varepsilon_P}{dz} = -\frac{g_L}{\beta_{rel}^2 E}\frac{dE}{dz}\varepsilon_L + \frac{\beta_P}{2}\frac{d}{dz}\left\langle \Delta E_{rms}^2 \right\rangle \tag{1}$$

Here $\beta_\perp$ and $\beta_{//}$ are the optical Twiss functions of the beam, β_{rel} is the relativistic velocity, E_μ is the energy and m is the mass of the particle, while L_R is the radiation length, g_L is the partition function and $<dE/dz>$ is the mean energy loss in the medium. When the change in emittance is zero, the beam is at the equilibrium transverse emittance that represents the minimum emittance the cooling channel can provide,

$$\varepsilon_n = \frac{\beta_\perp \left(13.6[MeV]\right)^2}{2\beta_{rel} mc^2 \frac{dE}{dz} L_R} \tag{2}$$

For most cases of interest, β_{rel} is near 1 so the equilibrium emittance is determined by material parameters and the amount of focussing that can be provided. Typically, materials with low atomic number create the least scattering per energy loss, with liquid Hydrogen providing an especially beneficial parameter set. In MICE, liquid Hydrogen, Lithium Hydride and Polyethylene absorber materials will be studied; other materials are under consideration.

For these transverse ionisation cooling schemes, the challenge is to design focussing lattices capable of containing large transverse and longitudinal emittances while simultaneously providing a tight focus on the absorber such that the equilibrium emittance is small.

3.8.1.2 *Transverse Optics and Transverse Cooling*

Muons are produced as tertiary particles, produced from pion decay which are produced in turn from protons incident on a target [2]. This results in large emittances, typically 10 mm transverse and 50 mm longitudinal (RMS). In order to achieve the requirement of containing such a large beam while simultaneously keeping tight focussing on the absorbers, an SFoFo solenoid arrangement is chosen in MICE.

The MICE lattice is a 5.5 m cell based on the lattice presented in the Neutrino Factory Feasibility Study II (FS2) [2]. The MICE magnets have been designed to operate in a number of modes:

- The sign of the magnetic field can be reversed at the absorbers; this prevents the build-up of canonical angular momentum, which would result in a mismatch and spoil the cooling performance; and
- The strength of the focus can be increased or decreased, resulting in various lattice acceptances and equilibrium emittances.

The on-axis solenoid field for the baseline MICE case is shown in Figure 2. Cooling hardware is in the region between -2.75 metres and +2.75 metres, while detector systems sit outside this region. In this case the absorbers sit at a field flip to prevent angular momentum build-up. RF cavities sit in a rather strong magnetic field and this may have some impact on their function.
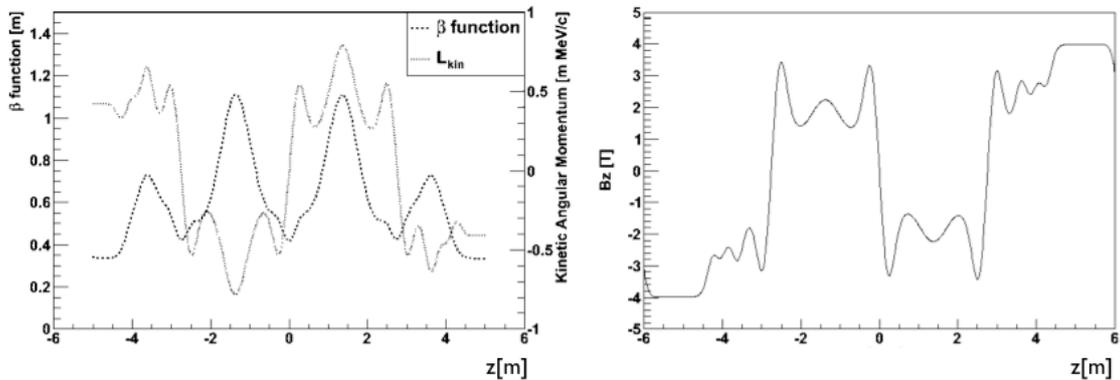
Figure 2: (Left) β-function and kinetic angular momentum, (Right) On-axis field for a particular MICE configuration.

The lattice β-function is shown in Figure 2. β is 0.42 m at the absorbers giving an equilibrium transverse emittance of about 2 mm when only the Hydrogen absorbers are considered. Additional material for Hydrogen windows and RF cavity irises increases the equilibrium emittance. The transverse emittance change as a function of input emittance between upstream and downstream detectors is shown in Figure 3 together
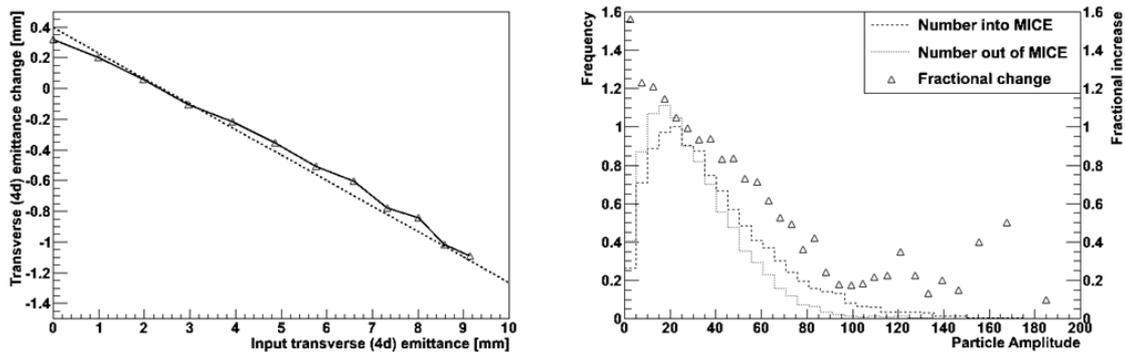
Figure 3: (Left) Transverse emittance reduction as a function of input emittance and (Right) transmission as a function of particle amplitude and fractional change in transmission.

with the RMS emittance reduction predicted by the analytical expression above. The emittance reduction is broadly in line with the theoretical expectation, although some non-linear effects reduce the performance.

The other ingredient of a good ionisation cooling channel is aperture. The transmission of MICE as a function of particle amplitude is also shown in Figure 3, where transverse four dimensional particle amplitude is calculated using

$$A^2 = \varepsilon_n \underline{u}_{4D} \underline{V}^{-1} \underline{u}_{4D}^T \qquad (3)$$

where $\underline{u}_{4D}$ is the transverse phase space vector $\underline{u}_{4D}=(x,p_x,y,p_y)$ and $\underline{V}_{4D}$ is a matrix with elements $V_{ij}=$covariance(u_i,u_j).

The target system of the Neutrino Factory captures muons with transverse amplitudes as large as 200 mm. In FS2, a tapering scheme was envisaged where a 2.75 m, higher acceptance lattice was used initially and then the beam was passed into the MICE-like 1.65 m lattice. Nonetheless, it can be seen that particles with amplitudes of order 50 mm can be contained in the MICE lattice. Additionally the cooling effect of MICE can be observed here; the transmission at small amplitudes is higher after passage through MICE, indicating that particles at high amplitude have been moved to lower amplitude, i.e. the beam has been cooled.

3.8.1.3 *Suppression of Chromatic Aberrations*

The harmonic content of the MICE magnetic field has been chosen rather carefully. The phase advance and β-function are shown in Figure 4 for the nominal configuration detailed above. β is very flat with momentum in the region between the 2π and 4π resonance indicating that chromatic aberrations have been successfully removed. As the focussing strength goes with B_z^2, the periodicity of the focussing function is even for the cooling period of 5.5 m so that the 3π resonance is suppressed.
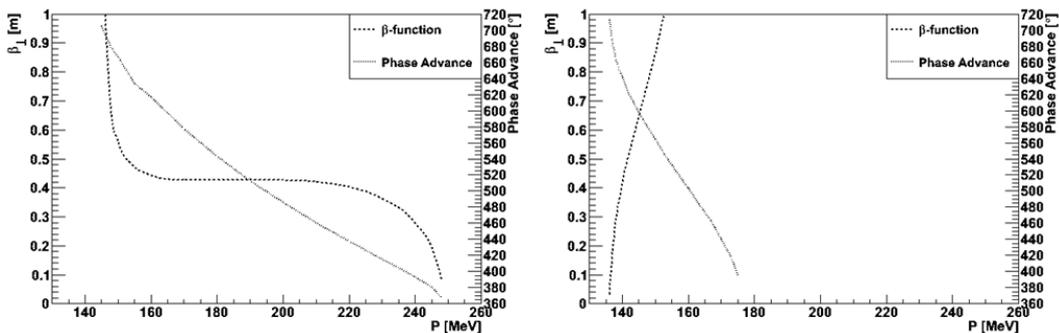
Figure 4: Transverse β-function and phase advance for (left) the full MICE cooling cell, and (right) the case where only the Coupling Coil is present.

The harmonic content of the magnetic field can be related to the β-function and phase advance [3]. As a demonstration of these effects the phase advance and β-function are shown in Figure 4 for the case where only a single focussing coil is present, giving a sine-like field with periodicity 5.5 m. The fields are scaled so that the total focussing strength of the cell is the same. In this case, the 2π and 4π linear resonances are much closer and the β-function is highly momentum dependent. This results in a poor momentum acceptance and would give poor cooling performance.
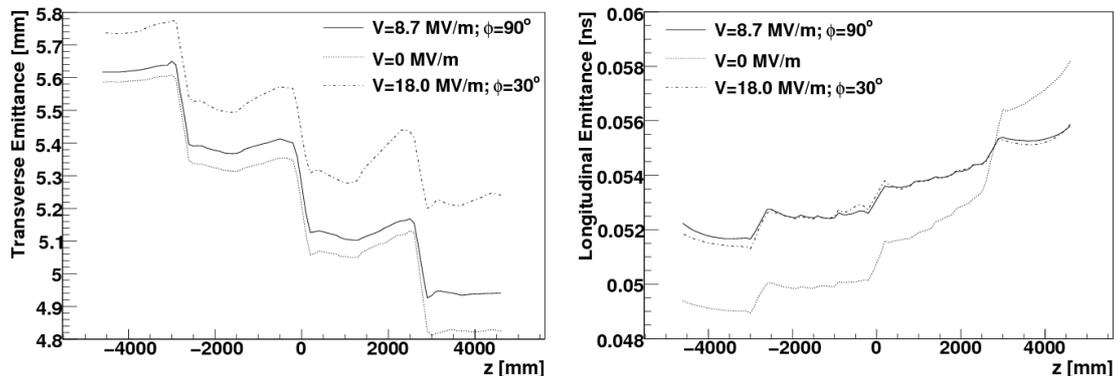
Figure 5: Emittance along the MICE beam axis for different RF arrangements.

3.8.2 Longitudinal Dynamics and RF

MICE has two 4-cavity linacs operated in TM010 mode at 201.25 MHz. In long cooling channels it is necessary to replace energy lost in the absorbers while retaining a bunch structure. As muons are only partially relativistic, maintaining a good bunch structure requires that RF be operated somewhere between on-crest and bunching mode. Unfortunately, financial constraints mean MICE cannot afford to operate RF cavities at peak gradient and so to replace the energy lost in the absorbers, MICE will operate on-crest. In a long cooling channel this would affect performance, but simulation results plotted in Figure 5, show the emittance reduction is not seriously reduced.

Some empirical evidence has revealed that siting RF cavities in strong magnetic fields may induce RF breakdown at somewhat lower peak fields than expected [4,5]. The peak field on the MICE cavities in the baseline configuration is around 8 MV/m, well below the Kilpatrick limit of 17 MV/m, so it is hoped that the MICE cavities will be able to operate at their nominal gradient. However, further studies are underway to understand the full impact of this issue.

3.8.3 Emittance Exchange and Longitudinal Cooling

It is possible to reduce longitudinal emittance using ionisation cooling by transferring emittance from longitudinal to transverse phase space through emittance exchange [6]. In emittance exchange, a dispersive beam is passed through a wedge-shaped absorber. Higher energy particles pass through more material and so lose more energy, resulting in a reduction in energy spread. This is a shear in *x-energy* space, resulting in emittance transfer from longitudinal to transverse phase space. Simultaneously, transverse emittance is reduced resulting in the appearance of longitudinal cooling.

Such a thing can be demonstrated in MICE, but only with some difficulty. The large emittances typical of MICE and the significant non-linear effects in solenoidal channels mean that without care the cooling signal would be drowned by optical heating. By using bespoke, fully six-dimensional statistical weighting algorithms to select a beam that transports symmetrically about the centre of MICE, these non-linear effects can be reduced [7].

In Figure 6 two beams are tracked through MICE; a natural beam from the MICE beamline; and an ideal beam generated to be well-matched to the MICE lattice and with a dispersion suitable for emittance exchange. Tracking is performed using the lattice for MICE step IV, an early configuration of MICE before the installation of RF cavities where only one absorber is present. The emittance change for the natural beamline beam is also plotted with statistical weights applied so that experimental data can be made to resemble the ideal beam. For the ideal beam and the weighted beam, a clear longitudinal cooling signal can be observed indicating that the emittance exchange was successful.
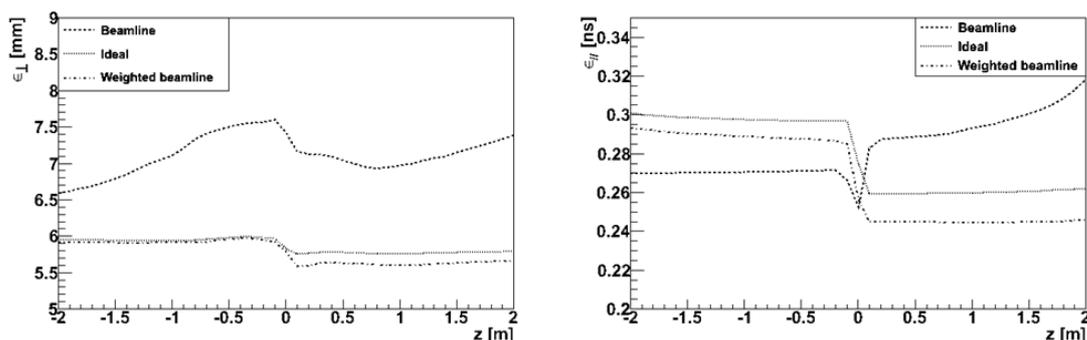
Figure 6: (Left) Transverse emittance and (Right) longitudinal emittance for a wedge-shaped absorber. The emittance change for a natural beam from the MICE beamline, an ideal beam and with the beamline beam statistically weighted to mimic the ideal beam are shown.

3.8.4 Detector Systems

MICE has a set of fine resolution detector systems. Production of a high intensity muon beam with the desired properties is impractical and measurement of the full six dimensional correlations required to demonstrate 6D emittance reduction is difficult. Instead, MICE will measure the 6D phase space vector of individual particles. Separate measurement devices enable independent measurement of particles upstream and downstream of the cooling channel.

Transverse position and momentum will be measured using a scintillating fibre tracker placed in a 4 T field. By measuring the helical path of muons at five planes, the position and momentum can be reconstructed with precision of a few hundred microns and about 1-2 % *dp/p* [8,9]. The time-of-flight of individual muons and their phase relative to the RF cavities is measured using 50 ps resolution plastic scintillators [10].

Discrimination between muons, undecayed pions and electrons is provided by:

- Time of flight detectors that enable the comparison of measured momentum with time-of-flight, enabling the calculation of mass and hence particle type.
- Cerenkov transition detectors (CKOV) emit Cerenkov radiation with different momentum thresholds for different particle species.
- The Kloe Light (KL) and Electron-Muon Ranger (EMR) discriminate between muon and electron energy loss properties in matter.

3.8.5 Modelling Codes

Several modelling codes have been used to simulated ionisation cooling channels, such as ICOOL [11] and G4Beamline [12]. Due to the unprecedented combination of high resolution single-particle detector equipment and accelerator hardware, the MICE collaboration has designed a custom modelling and reconstruction code, G4MICE [13], that enables detailed modelling of accelerator hardware, beam optics, multiple Coulomb scattering and ionisation energy loss, together with effects important to the detector systems such as Cerenkov radiation, scintillation and detector electronics effects. G4MICE also contains libraries for pattern recognition and detector reconstruction. enabling the modelling of both the accelerator and detector performance. G4MICE has also been used for general accelerator lattice development, simulating a variety of solenoid and multipole lattices in both ring and linac arrangements [14,15].

A visualisation of the simulation of MICE, as implemented in G4MICE, is shown in Figure 7. Note that details such as the curved shape of the absorbers and RF windows and subtleties of the quadrupole aperture are modelled with good precision. Muon tracks together with electron and photon secondaries are shown.
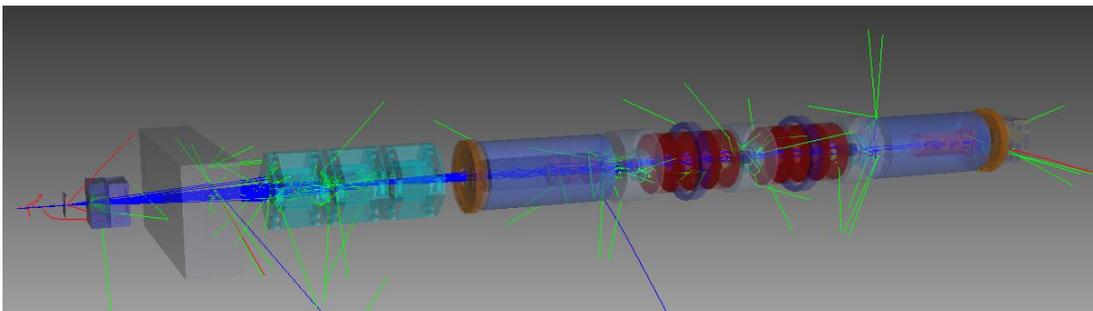
Figure 7: Visualisation of the MICE simulation in G4MICE.

3.8.6 Status, Schedule and Plans

MICE is under construction at Rutherford Appleton Laboratory. The MICE beam line, TOF detectors, CKOV, KL and EMR detectors are in place and commissioned. The scintillating fibre trackers have been constructed. The spectrometer solenoids, within which the trackers sit, are expected to arrive in 2010, followed by Absorber Focus Coil modules that will enable the first measurement of muon ionisation cooling.

3.8.7 Acknowledgements

I am indebted to the international MICE collaboration, which has provided the motivation for and the context within which the work reported here is being carried out. I also gratefully acknowledge the ISIS Division at the STFC Rutherford Appleton Laboratory for providing beam and essential support. Support for the UK contributions to the MICE experiment is provided by the Science and Technology Facilities Council and through SLAs with STFC supported laboratories.

3.8.8 **References**

1. D. Neuffer, Introduction to Muon Cooling, Nuclear Instruments and Methods in Physics Research A, 532, (2004) pp 26-31.
2. Ed. S. Ozaki, R Palmer, M Zisman and J Gallardo, Feasibility Study-II of a Muon-Based Neutrino Source, BNL-52623, 2001.
3. C. Wang and K. Kim, Recursive Solution for Beam Dynamics of Periodic Focussing Channels, Phys. Rev. E 63, 56502, 2001.
4. A. Moretti et al, Effects of high solenoidal magnetic fields on rf accelerating cavities, Phys. Rev. STAB 8, 072001, 2005.
5. R. Palmer et al, RF Breakdown with and without External Magnetic Fields, Phys. Rev. STAB 12, 031002, 2009.
6. V. Balbekov, Solenoid-Based Ring Coolers, MUCOOL Note 232, 2002.
7. C. Rogers & P. Snopok, Wedge Absorber Simulations for the Muon Ionisation Cooling Experiment, Proc. COOL 2009, 2009.
8. C. Rogers & M. Ellis, High Precision Measurement of Muon Beam Emittance in MICE, Proc. PAC 2006.
9. M. Ellis et al, The design, construction and performance of the MICE scintillating trackers, *in preparation*.
10. R. Bertoni et al, The design and commissioning of the MICE upstream time-of-flight term system, NIM A 168, 9002, 2010.
11. R. C. Fernow, ICOOL: A simulation code for ionization cooling of muon beams, Proc. PAC 1999.
12. T. Roberts et al, G4Beamline Particle Tracking in Matter-Dominated Beamlines, Proc. EPAC 2008.
13. C. Rogers & R. Sandstrom, Simulation of MICE Using G4MICE, Proc. EPAC 2006.
14. C. Rogers, A Dogbone Cooling Channel, Proc. NuFact 2007.
15. C. Rogers, Recirculating Ring for an Ionization Cooling Channel, Proc. EPAC 2008.

3.9   **HIE-Linac Development at the Cockcroft Institute**

A. D'Elia, M. Fraser, R. Jones and P. McIntosh
Cockcroft Institute
Mail to: peter.mcintosh@stfc.ac.uk

3.9.1 **Introduction**

Radioactive ion beam production at the ISOLDE facility, CERN, illustrated in Figure 1, is based on the ISOL (Isotope Separation On-Line) method where a proton beam with an intensity of about 2 µA is extracted from the Proton-Synchrotron Booster (PSB) and impinges upon a thick, high-temperature target. The radioactive nuclei can be produced in two different target stations (GPS and HRS) via spallation, fission or fragmentation reactions. ISOLDE has been continuously developing targets and ion sources for four decades, introducing several new technologies (e.g. the resonance ionization laser ion source) so that there are now available 700+ radioisotopes from 65 elements. These beams are accelerated to 60 keV and steered to different experimental stations. In the present REX-ISOLDE facility, the RIBs are prepared in a low-energy preparatory stage before injection into the normal conducting linear accelerator. This stage consists of a Penning trap (REXTRAP), a charge breeder (REXEBIS) and an achromatic A/q separator of the Nier spectrometer type (see Figure 2). The

chargebreeding efficiency depends critically on the quality of the injected beam, i.e., its longitudinal and transverse emittance in particular. The purpose of the trap is to collect and to cool the radioactive ions delivered by ISOLDE before they are sent in bunches into the EBIS. In the EBIS the ions are charge-bred into charge states so that the mass to charge ratio is always $3 \leq A/q \leq 4.5$. The normal conducting linear accelerator then provides an accelerating voltage for a corresponding A/q maximum of 4.5.

Figure 1: Schematic of the ISOLDE facility at CERN, showing the existing hall extension that is allocated to the new accelerator HIE-LINAC.

Presently, the REX-ISOLDE linac delivers beams with a mass to charge ratio of $3 < A/q < 4.5$ at a final energy of 2.8 MeV/u using a combination of several normal conducting structures. After charge breeding, the first acceleration stage is provided by a 101.28 MHz 4-rod radio-frequency quadrupole (RFQ) which takes the beam from an energy of 5 keV/u up to 300 keV/u. The beam is then re-bunched into the first 101.28 MHz interdigital drift tube (IH) structure which increases the energy to 1.2 MeV/u. Three split-ring cavities are used to give further acceleration to 2.2 MeV/u, and finally a 202.58 MHz 9-gap IH-type cavity is used to boost and to vary the energy between $2 < E < 2.8$ MeV/u. Figure 2 illustrates the scheme of the present REX-ISOLDE linac.
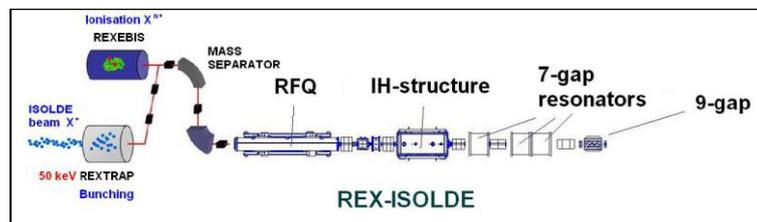
Figure 2: Schematic of the present REX-ISOLDE accelerator.

This acceleration method was developed in order to deliver beams at specific energies whilst taking advantage of the high accelerating gradient that pulsed Normal-

Conducting (NC) IH-structures could achieve. This concept is nevertheless not without some limitations:

- Very limited energy flexibility.
- The operation is restricted to pulsed mode.
- Longitudinal beam parameters, such as energy spread and bunch length, are nonvariable.
- Extension to higher energies is difficult due to the low reliability of the present machine (if an RF system fails there is no compensation scheme and the beam is lost)

Moreover, during this staged acceleration process, the transverse emittance grows by almost a factor of 2. This uncontrolled emittance growth is also confirmed from experiments which indicate that halo particles result in an increased background noise. The requirement for beam energies of up to 10 MeV/u whilst retaining, at the same time, the flexibility to deliver the beam at all intermediate energies starting at 1.2 MeV/u drives the choice for a superconducting (SC) linear accelerator. Examples of SC linear accelerators that provide energetic heavy ions include ATLAS (Argonne National Laboratory) [1], ALPI (INFN Legnaro) [2] and ISAC2 (TRIUMF) [3].

3.9.2 The HIE-ISOLDE Linear Accelerator: HIE-LINAC

The HIE (high intensity and energy)-ISOLDE [4] project embraces new developments in radioisotope selection, improvements in charge-breeding and target-ion source development, as well as construction of the new injector for the PS Booster, LINAC4. For extending the physics reach of the facility, the most significant component is the SC linear accelerator with a maximum energy of 10 MeV/u (HIE-LINAC) which will replace most of the existing REX structure. It will be based on independently phased quarter wave resonators (QWRs). The alternative to a SC QWR is a normal conducting IH-structure. The SC option has the following features [5]:

- The final beam velocity can be tailored to the ion so that particles of lower A/q can be accelerated to higher final velocities;
- SC quarter-wave cavity apertures are only limited by transit time factor and peak surface field concerns and in general can be bigger than apertures in normal conducting IH structures;
- The RF frequency can be kept lower than in room temperature machines yielding a larger longitudinal acceptance;
- The accelerating gradients are significantly larger than those that can be realized in a room temperature CW machine.

Figure 3 shows the schematic layout of HIE-LINAC. The replacement of part of the normalconducting structures will enable the final transverse emittance to be improved with stable acceleration and well defined accelerating structures. The low-β sections contain 6 cavities, and two solenoids within each cryostat, with one diagnostic station. The high-β sections contain 5 cavities, 1 solenoid and a diagnostic station. The aim of this project is to realise all six sections together with the necessary power supplies, RF amplifiers and control systems.
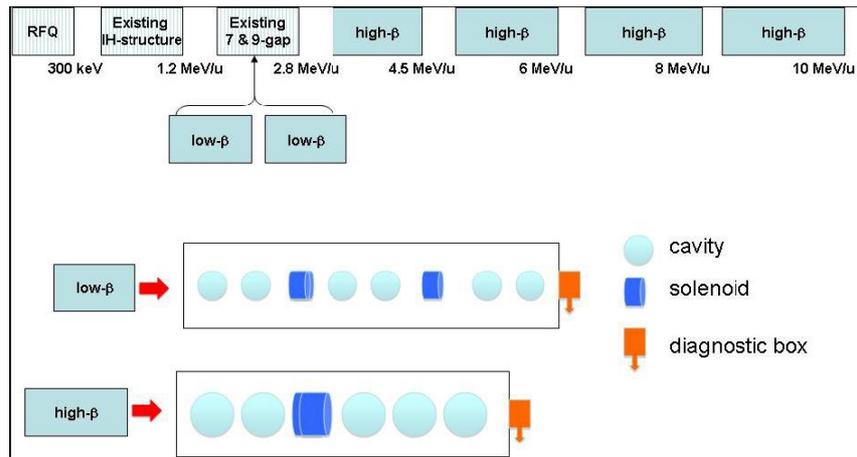
Figure 3: schematic layout of HIE-LINAC. The existing REX structure is shown with a light blue background.

Table 1 compares the fundamental beam characteristics of the new SC linac facility with that of the existing facility (REX-ISOLDE). In addition to these, a benefit of SC technology is that the machine has built-in redundancy, i.e. the beam can be transmitted with small losses if one cavity fails by compensating elsewhere.

Table 1: SC Linac Capability Comparison with Existing REX-ISOLDE Facility

	Existing facility REX-ISOLDE	HIE-LINAC	Physics Reach/impact on techniques
Maximum energy	2.8 MeV/u	10 MeV/u (higher for A/q < 4.5)	Multiple Coulex, transfer reactions, soft dipole modes
Range of beams; intensity	8Li . 188Hg (50 isotopes so far accelerated)	Beams continuously developed; increased intensity from multi-q acceptance[a]	Increased scope and sensitivity for experiments
Energy variation	Fixed per experiment	Variable, extend to low	Study of resonances, energies excitation functions, astrophysics
Emittance & beam spot	0.5 ð.mm.mrad at 3 MeV/u; large halo	0.3 ð.mm.mrad; 1mm beam spot at 10 MeV/u	Precision Spectroscopy - better angular definition
Time structure	Pulsed with no bunching	CW[a] or bunched beam	Reduced random background *or* beam timing possible
Longitudinal parameters	Fixed	Variable	Required for lifetime & g-factor meas'mts
Beam identification	Z identification limited to Z~40	Switching to 10 MeV/u increases Z range	Improved Z identification of beam contaminants

[a] in superconducting part of linac

The necessary research and development, prototyping, construction, installation and commissioning will be carried out by the Cockcroft Institute. The Institute (Both STFC/ASTeC and university staff) has a wealth of skills, recently applied within the ERLP/ALICE and EMMA projects, which are well matched to the requirements of the HIE-LINAC project: cryogenics, RF, beam dynamics, cavity fabrication, control systems and UHV technology.

3.9.3 Superconducting Cavities

For the quarter-wave cavities there are two competing technologies that can be used for the production of the cavity itself. The first is based on sheets of high grade niobium, 3mm in thickness. The shape can be obtained by deep-drawing, rolling, or hydro-forming. All the parts are subsequently electron beam welded. An external vessel is also made in order to contain the liquid helium. This technology is in general referred to as bulk niobium technology.

An alternative technology is based on a copper cavity in which a layer of a few microns of niobium is deposited via a sputtering technique. In this case only the internal conductor is cooled directly by liquid helium since the excellent thermal conductivity of copper assures a homogeneous temperature distribution in the cavity. This technology is in general referred to as sputtered niobium. Figure 4 shows an example of the two technologies available for superconducting quarter-wave cavities.
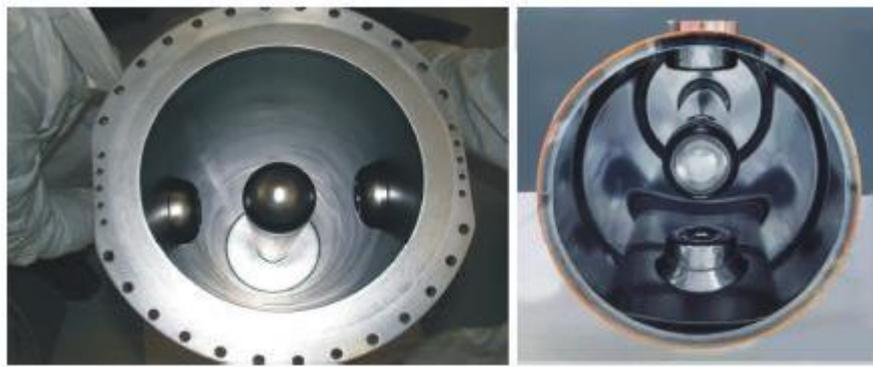
Figure 4: Photographs of cavities made with two technologies. Bulk niobium is shown left and sputtered niobium to the right.

The nominal parameters for the SC cavities are quite demanding. Nowadays bulk niobium technology has demonstrated that values of $Q_0 \sim 5 \cdot 10^8$ can be reached for accelerating gradients larger than 6MV/m [6] (with associated peak electric fields larger than 30 MV/m). This corresponds to a dissipated power of roughly 7W at the temperature of liquid helium. Sputtering technology has reached similar values on test cryostats and, to date there are no fundamental scientific impediments to achieve similar gradients in an operational machine. In Figure 5, the measurements of the quality factor versus the accelerating gradient of 4 cavities installed into a cryomodule at the Legnaro National Laboratory (LNL-INFN) are displayed [7]. The curves represent the functions of the quality factor with a constant dissipated power. A distinct advantage of sputtering technology is that because of the dominant copper base with a higher thermal conductivity, the cavities can be made with thicker walls and hence are mechanically

more stable than their bulk niobium counterpart. The consequence of this is that the resonant frequency of the accelerating mode is hardly affected at all by external noise sources (vibrations, liquid helium pressure variations) and this allows substantial simplification in the tuning system. This leads to a more robust overall accelerator with no appreciable sensitivity to microphonics. Moreover, the cryogenic system is not as demanding as for the bulk niobium cavities since there is also an absence of .Q-disease. which will allow a slower cool down. Finally, there are substantial cost savings as sputtering onto copper is expected to be at least a factor of two less expensive than fabricating bulk niobium cavities. The disadvantage of sputtered niobium cavities is a drop off of ohmic Q with gradient. However as the HIE-ISOLDE has a requirement for a relatively low Q at a moderate gradient this is not a problem in this case. Integration of tuners in the design of the cryomodules housing the cavities in order to minimise microphonics will be an essential feature of the R&D efforts in their design.

Two cavity geometries, *low* and *high β*, will be used to cover the whole energy range. As the first part of the upgrade will consist in the realization of the high energy section, the R&D effort have been focused on the study and production of a prototype of the *high β* cavity. The electromagnetic study and realization of the cavity prototype has been carried out in different steps. The definition of the cavity main parameters derives directly from beam dynamics studies (beam aperture, gap to gap distance, RF field asimmetry) [8] from the upstream linac (RF frequency) and from manufacturing technique (Nb sputtering). Given the above constraints, the electromagnetic study has been performed in order to minimize the surface peak electric and magnetic field, maximizing the *Rsh/Q* and the *g* factor. In addition a particular attention has been payed to the study of the frequency sensitivity of the different geometric parameters, in order to evaluate a suitable tuning range. During the fabrication of the cavity prototype, after each significant step (machining, welding, deep pressing) an RF measurement has been performed and results are reported after in the paper. Given the limited frequency range of the tuner, the final dimension of the external conductor has been set only after the final frequency measurement. Figure 5 shows the prototype built at CERN and, presently, under sputtering tests. In the following we will show the main electromagnetic parameters for the optimized geometry of the cavity and we will compare them to the ones of similar structures as in TRIUMF and SPIRAL2.
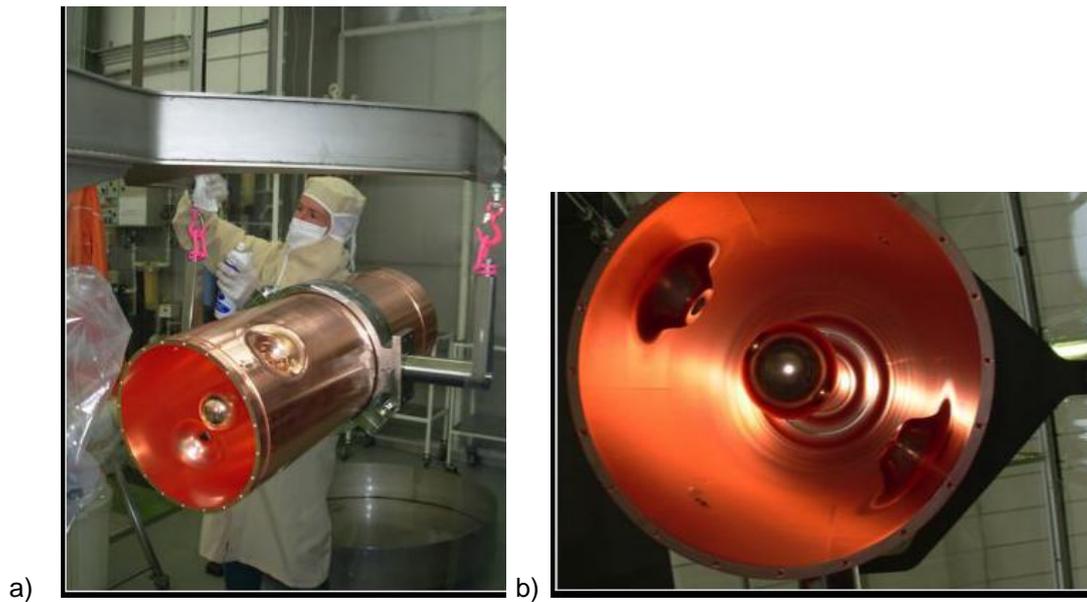
Figure 5: The prototype of the high β cavity produced at CERN, (a) the cavity during the cleaning process (b) internal view of the cavity.

3.9.4 Electromagnetic Simulations

The electromagnetic design of the cavity aims to minimize the surface peak fields, both electric and magnetic. As mentioned above the geometry has also been optimized for the sputtering process [9]. In particular beam ports on the external conductor have been shaped in order to avoid any hidden edges on surface to the Nb cathode. Similarly, the region of the maximum magnetic field has been rounded in order to have a better homogeneity of the Nb film and this shape gives also a regular surface current paths minimizing the magnetic fields on these positions. The electric peak field, located at the bottom part of the resonator antenna, can be varied by changing the distance of the bottom part of the antenna from the bottom plate of the cavity (tipgap). The tipgap has been chosen of 70mm but the cavity, at the beginning, has been manufactured with a tipgap of 90mm. This gives the opportunity of tune up the frequency at the end of the machining procedures if needed. The simulations presented in the following have been carried out with the nominal value of 70mm. Figure 6 shows a cut-view of the CAD model and the positions of the maximum electric and magnetic field.
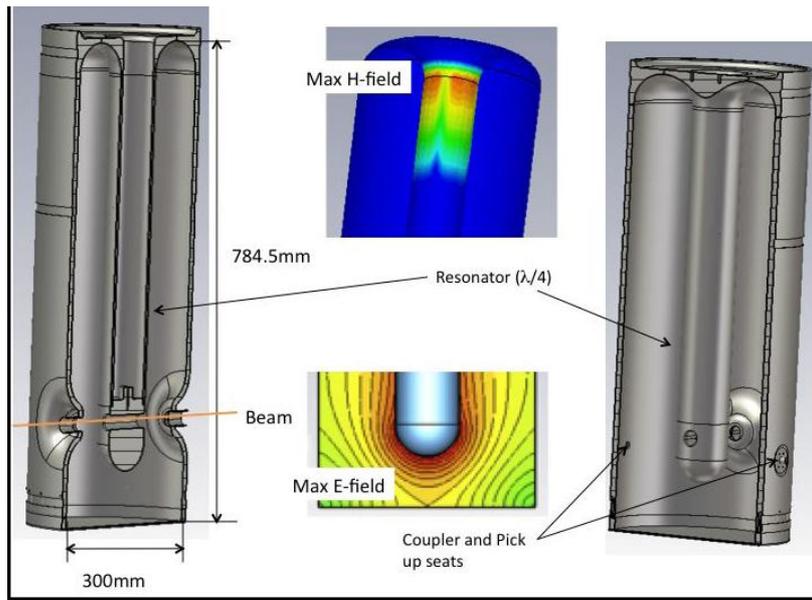
Figure 6: Cut-view of the cavity showing the internal geometry and also coupler and pick-up seats; in the middle, the regions of the maximum electric and magnetic fields are shown.

Because of the cavity geometry is not azimuthal symmetric, 3D electromagnetic codes need to be used to evaluate its RF properties. In order to pin down reliable results, a *calibration* of the simulation tools have been performed. A simpler geometry without beam ports has been designed in order to get a comparison between Ansoft HFSS [10], CST Microwave [11] and POISSON SUPERFISH (see Figure 7). For this kind of structures, we consider the data from SUPERFISH as the reference one.
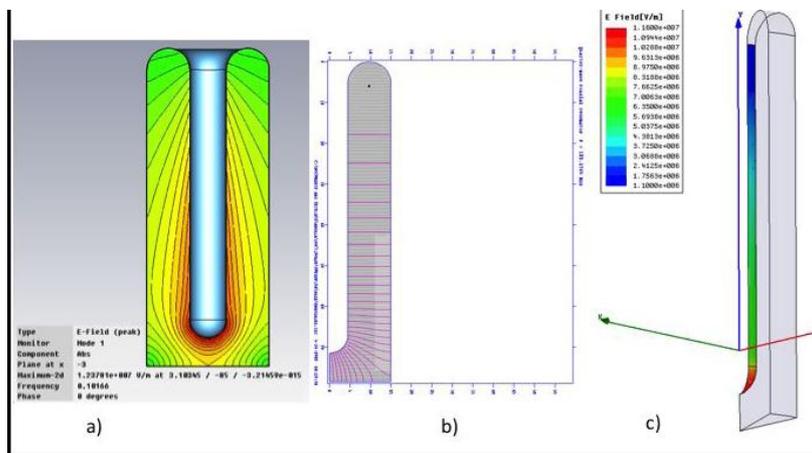
Figure 7: Models used for simulations: a) MWS, b) SUPERFISH, c) HFSS.

Considering the azimuthal symmetry of this simpler structure, only one quarter has been simulated in CST and the mesh refinement has been used. The higher step in the refinement corresponds to about 1.000.000 of meshcells. In HFSS, only a slice of one sixteenth has been simulated. The results have been obtained by considering a surface refinement of the meshes of 2μm, the total number of tetrahedral is about 110.000. The mesh stepsize for SUPERFISH is of 2.5mm (finer meshing does not change the results).

The comparison terms have been the maximum electric and magnetic field and the $Q0$. The results for peak fields are shown in Figure 8.
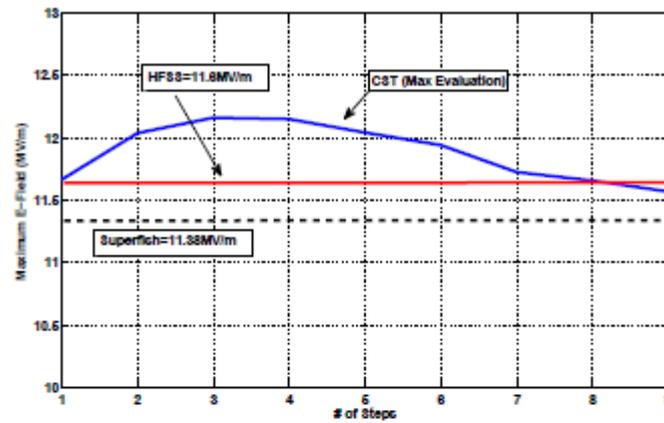
(a) Max E-field
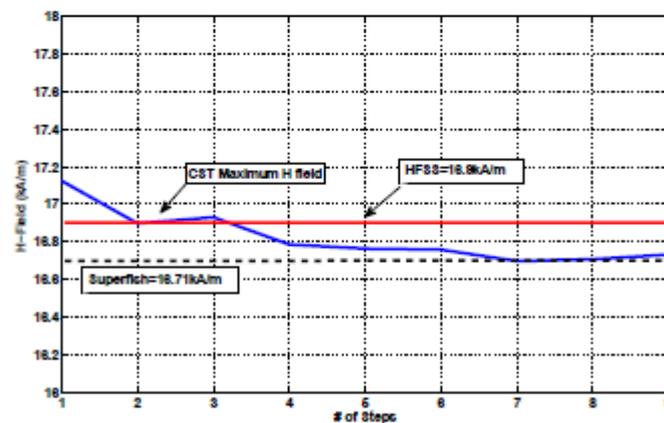
(b) Max H-field

Figure 8: Peak surface fields.

The fields are normalized to give 1J stored energy in the cavity (CST normalization). The plots show consistent results between the three codes. A summary of the results, included $Q0$ values are listed in Table 1. When the beam ports are added to the structure, the results are expected to stay consistent with the ones found previously. For this structure, Superfish is no longer possible to use and then the results are extracted only from HFSS and CST. Actually *Epeak* and *Hpeak* are consistent between HFSS and CST and also with the previous plots, but the value of $Q0$ found by CST is overestimated, about 14000, and not consistent with the HFSS simulations, about 11700. Probably this is due to some geometry problem in the CST model around the noses. In fact, when the racetrack shape of the noses is changed to a simpler circular geometry, the value becomes compatible with other simulations.

Table 2: Simulation Comparison

	Superfish	CST	HFSS	CST − SF %	HFSS − SF %
Frequency (MHz)	101.674	101.666	101.674	-	-
H_{peak} (kA/m)	16.711	16.733	16.763	0.1	0.3
E_{peak} (MV/m)	11.38	11.57	11.6	1.7	1.9
Q_0	11795	11844	11746	0.4	-0.4

Finally, the electromagnetic cavity parameters are shown in Table 2 in comparison with TRIUMF and SPIRAL2.

Table 3: Cavity parameters in comparison with TRIUMF and SPIRAL2.

	ISOLDE	TRIUMF	SPIRAL2
Frequency (MHz)	101.28	141.4	88
β (%)	11.4	11.2	12
E_{acc} (MV/m)	6	6	6.5
L_{norm} (mm)	300	180	410
E_{peak}/E_{acc}	5.4	4.9	4.9
B_{peak}/E_{acc} [G/(MV/m)]	96	99	90
R_{sh}/Q_0 (Ω)	554	545	518
$g = R_s \cdot Q_0$ (Ω)	30.34	25.6	37.5
P_{cav} (W)	7	7[a]	10[b]

[a] Measurements on a cavity prototype showed results exceeding the design parameters: $Q0 = 7 \cdot 10^8$ for $Eacc = 8.5$MV/m with $Pcav = 7$W [12].
[b] Measurements on a cavity prototype showed: $Q0 = 10^9$ for $Eacc = 6.5$MV/m with $Pcav = 10$W [13]

3.9.5 The Tuner Plate

For the tuning system it has been decided to follow the concept that has been developed at TRIUMF [14]. An *oilcan* shaped diaphragm of CuBe has been hydroformedwith a pressure up to 120 bar. All radial slots necessary for the elongation and contraction of the diaphragm are performed with a laser beam. The same plate can be mounted directly on the low β cavity or welded to a flange in the case of the high β cavity. The actuator is designed to have no backlash. A pictorial view of the tuner is presented in Figure 9. The useful stroke of the tuner plate is of 20 mm. From the *manufacturing* position the plate can be pushed up towards the central resonator of 5mm (position +5) and down, in the other direction, of 15mm (position -15). In Table 4 the results of the simulations are listed for the nominal value of the tipgap of 70mm and for a tipgap of 90 mm. The coarse range of the tuner plate for tipgap = 70 mm is foreseen to be of 245 kHz for a moveable range of 20mm giving an average $\Delta tunerplate \approx 12.25$ kHz/mm. The value for tipgap = 90 mm is of 5.2 kHz/mm and the correction is

less efficient as expected (coarse range of only 140 kHz). However, both coarse ranges largely cope with frequency detuning coming from machining errors, listed in Table 5, considering that mechanical tolerances are in the order of the tenth of mm.
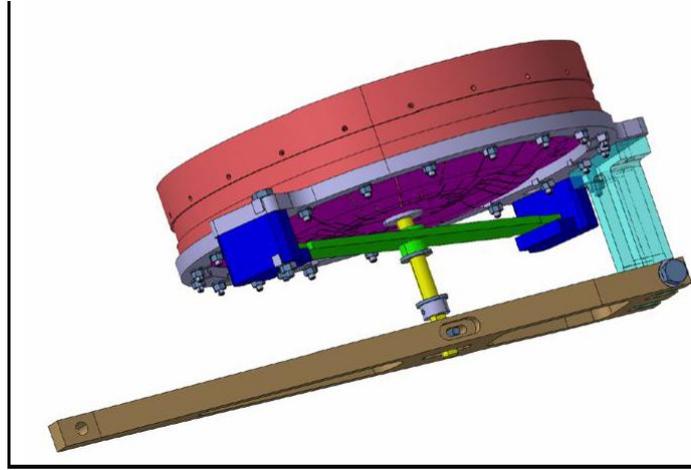
Figure 9: Tuner plate with its actuator.

Table 4: Simulated frequency values of the tuning plate when all up (Position +5) or all down (Position -15); in yellow the values for the nominal tipgap value.

	Tipgap 70mm	Tipgap 90mm
Position +5	100.684 MHz	101.235 MHz
Position -15	100.929 MHz	101.339 MHz
$\Delta_{\text{tuner plate}}$	12.25 kHz/mm	5.2 kHz/mm

Table 5: Simulations results of the frequency detuning due to the main possible machining errors.

Type of error	Δ_{freq} (kHz/mm)
Cavity diameter	≈ 65
Resonator length	≈ 160
Nose length	≈ 50

Another important aspect to take into account is the radiation pressure acting on the tuner plate. Because of the high number of cuts and the reduced thickness of the diaphragm, a strong force could irreversibly modify the tuner shape leading to an unrecoverable frequency shift. The radiation pressure can be calculated by evaluating both electric and magnetic field on the plate surface by the following equation:

$$P = \frac{1}{4}\left(\mu_0|\mathbf{H}|^2 - \epsilon_0|\mathbf{E}|^2\right)$$

The result is shown in Figure 10 in the case of a flat plate: the total force is quite low, equal to -1.77 N.
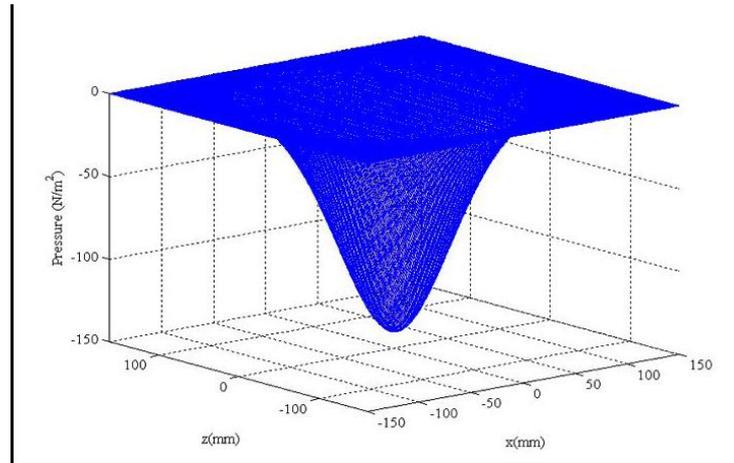
Figure 10: Radiation pressure on a flat plate.

3.9.6 **Frequenc Measurements**

The working frequency of the cold cavity has to be 101.28 MHz. Taking into account the scaling factors due to the superconducting mode of operation (shortening of the length of the central resonator, skin depth variation, etc...) and due to the vacuum-air environment change, the *hot* frequency at room temperature in air should be ≈ 100.900 MHz. As described before we have left the value of the tipgap as a *free* parameter in order to compensate possible errors coming from the machining process. During the welding of the top part of the cavity, a problem occurred and the result has been a change of the length of the internal conductor, which is now shorter of 0.4 mm, with a foreseen increase of the frequency of about 65 kHz. The measured variation is of 77 kHz. Table 6 shows the measured values before and after welding the inner conductor to the outer. It is also shown the value of Q_0 which is significantly improved after welding as expected. Furthermore the measured value is consistent with simulations giving a value of about 11700.

Table 6: Measurements before and after welding the inner conductor to the outer with tipgap = 90 mm.

	Before welding	**After welding**
Frequency	101.147	101.224
Q_0	5908	11380

The last step is to finally define the length of the outer conductor. An intermediate cut of 75 mm has been performed and the subsequent frequency measurement confirmed the final cut position as from design value. The results are shown in Table 7 the values both of the simulations and of the measurements have been properly scaled (values in bold) to get a comparison. The effect of the shorter central conductor can be accepted and the cut has been done at the nominal tipgap length of 70 mm.

Table 7: Set of measurements for different cut of the tipgap and different coupler insertion; bold values are scaled to get a comparison.

Coupler in=64mm and Pickup in=22mm		
	Simulation	Measurement
Tipgap 90	101.233MHz	101.246MHz
	(-32kHz air)	(-77kHz res)
	101.201MHz	**101.169MHz**
	Simulation	Measurement
Tipgap 75	101.013MHz	101.000MHz
	(-32kHz air)	(-77kHz res)
	100.981MHz	**100.923MHz**
	Simulation	Measurement
Tipgap 70	100.899MHz	100.916MHz
	(-32kHz air)	(-77kHz res)
	100.867MHz	**100.839MHz**
Coupler in=22mm and Pickup in=22mm		
	Simulation	Measurement
Tipgap 90	101.410MHz	101.483MHz
	(-32kHz air)	(-77kHz res)
	101.378MHz	**101.406MHz**
	Simulation	Measurement
Tipgap 75	101.191MHz	101.240MHz
	(-32kHz air)	(-77kHz res)
	101.159MHz	**101.163MHz**
	Simulation	Measurement
Tipgap 70	101.083MHz	101.150MHz
	(-32kHz air)	(-77kHz res)
	101.051MHz	**101.073MHz**

Finally the measurement with the tuning plate has been done. The value is shown in Table 8 in comparison with simulation results opportunely scaled and goal frequency and all the values are fully compatible.

Table 8: Frequency measurement at room temperature with tuner plate in rest position.

Measured frequency	100.885 MHz
Simulation	100.816 MHz (-32kHz air) (+77kHz res) 100.861MHz
Goal frequency	≈100.900 MHz

3.9.7 **Conclusion**

The use of superconducting cavities will tremendously facilitate the provision of variable-energy beams of exotic ions at considerably improved beam quality. In order to meet the specification of the linac (energy tuning, resolution, duty cycle, emittance, etc.), R&D is being carried out in several areas. One research area is to explore state-of-the-art cavity preparation techniques using niobium sputtered onto copper quarter-wave accelerating cavities rather than bulk niobium in order to substantially bring down the

overall cost of the machine and serve to provide an ideal technological base for the construction of future accelerators. RF cavity and beam dynamics studies is being conducted to both design the overall system and simulate the progress of the beam in a 'cradle to grave' simulation. In particular the influence of transverse kicks to the beam has been carefully investigated by designing the geometry of the quarter wave cavities with precise RF computer codes. A sensitivity study is to be conducted in order to anticipate any possible dilution in beam emittance and beam instability. The high β cavity for ISOLDE upgrade has been fully designed and built. The cavity parameters have been derived showing values comparable to other similar structures (TRIUMF and SPIRAL2). The foreseen Q_0 should be 6.6×10^8 with a surface resistance $Rs = 46$ nΩ giving a power dissipation on the cavity wall of 7 W. A prototype tuner plate has been built. The total coarse range in simulation is of 245 kHz for a stroke of 20 mm giving 12.25 kHz/mm. The frequency measurements at room temperature show a perfect agreement with the designed frequency: the measured frequency is 100.885 MHz, the design frequency at room temperature should be ≈ 100.900 MHz (the simulations give 100.861 MHz).

3.9.8 **References**

1. http://www.phy.anl.gov/atlas/
2. http://www.lnl.infn.it/~tandem/TAgeneral_info.html
3. R.E. Laxdal, `Initial Commissioning Results from the ISAC-II SC Linac', LINAC06, Knoxville, Aug. 2006
4. HIE-ISOLDE: the technical options (ed. M. Lindroos, T. Nilsson) http://cdsweb.cern.ch/record/1001782, M. Lindroos, P.A. Butler, M. Huyse, and K. Riisager, Nucl. Instr. Meth., to be published.
5. Report of International Advisory Board for the REX-ISOLDE LINAC energy upgrade (A. Mueller, R Laxdale and O. Kester) http://hie-isolde.web.cern.ch/HIE-ISOLDE/Documents/HIE%20REX%20IAB%20Report%20final%20mod.pdf
6. R.E. Laxdal, Commissioning and early experiments with ISAC-II, proceedings of PAC07, Albuquerque (2007)
7. A. M. Porcellato *et al.*, Proceedings SRF 2005, Cornell (2005)
8. G. Lanza et al., "The HIE-ISOLDE Superconducting Cavities: Surface Treatment and Niobium Thin Film Coating", SRF09, Berlin, 2009, pp. 801 - 805.
9. M. A. Fraser et al., "Compensation of Transverse Field Asymmetry in the High-Beta Quarter-Wave Resonator of the Hie-Isolde Linac at CERN", SRF09, Berlin, 2009, pp. 604 -608.
10. http://www.ansoft.com/products/hf/hfss/
11. www.cst.com
12. V. Zvyagintsev et al., "Development, Production and Tests of Prototype Superconducting Cavities for the High Beta Section of the Isac-ii Heavy Ion Accelerator at Triumf", RuPAC 2008, Zvenigorod, Russia.
13. G. Olry et al., "Tests Results of the Beta 0.12 Quarter Wave Resonators for the Spiral2 Superconducting Linac", LINAC 2006, Knoxville, Tennessee USA.
14. T. Ries et al., "A mechanical Tuner for the ISAC-II QuarterWave Superconducting Cavities", PAC03, Portland, USA, May 2003.

Photon Science

3.10   Developments at Diamond Light Source

R. Bartolini

Diamond Light Source, Harwell Science and Innovation Campus, Chilton, Didcot, OX11 0DE and
John Adams Institute, U. of Oxford, Keble Road, OX1 3HR, Oxford, UK
Mail to: riccardo.bartolini@diamond.ac.uk

3.10.1 Introduction

Diamond Light Source started user operation in January 2007 with an initial complement of seven Phase I beamlines [1]. Today Diamond is well into the Phase II of the project. Seventeen beamlines are operational, ten of which are based on radiation from in-vacuum insertion devices operated at 5 mm minimum gap, and a further two are in commissioning. The installation of the new beamlines is progressing towards twenty-two beamlines at the end of Phase II in 2012. Phase III with a further ten beamlines is currently at the final stage of approval.

Since January 2007 Diamond has already undergone two important development programmes: Top-Up operation and short bunch generation in low-alpha lattices for time resolved X-ray studies and the generation of coherent THz radiation. Ongoing developments include the design and implementation of customised optics for dedicated straight sections for high coherence applications and for fast polarisation switching. Also, a better understanding of the machine performance has been achieved in various areas including beam optics, beam stability and collective effects.

3.10.2 Beam Optics

A careful implementation of both the linear and the nonlinear optics of the machine is essential to guarantee the best performance of the synchrotron light source at its design parameters.

3.10.2.1   *Linear Optics*

The linear optics of the machine was analysed and corrected with the LOCO programme [2] which uses the closed orbit response matrix to detect any deviation of the linear optics from the nominal model. The nominal optics was implemented with very high precision as shown in Figure 1, with a residual β-beating of less than 1% peak to peak. The quadrupole gradients shifts required by the LOCO programme to correct the optics were below 2%, as reported in Figure 2. Emittance and energy spread measurements based on two X-ray pinhole camera systems, confirmed the nominal values of 2.7 nm emittance and 10^{-3} relative energy spread.

The linear coupling was easily corrected to 1% which is the value used for normal users' operation. This corresponds to a vertical emittance of 27 pm. Despite the fact that users do not at present require better correction of the linear coupling, a number of machine physics studies have been devoted to understanding the minimum vertical emittance achievable in the storage ring and to devise experimental procedures to

accurately measure such small vertical emittances [3]. It was possible to show that coupling correction strategies based on the analysis of the off-diagonal terms of the orbit response matrix were capable of reducing the linear coupling to below 0.1% with a measured vertical emittance of 2.2 pm. This value constitutes one of the best ever achieved at synchrotron light sources and corresponds the target requirement for low emittance damping rings for future colliders [4].
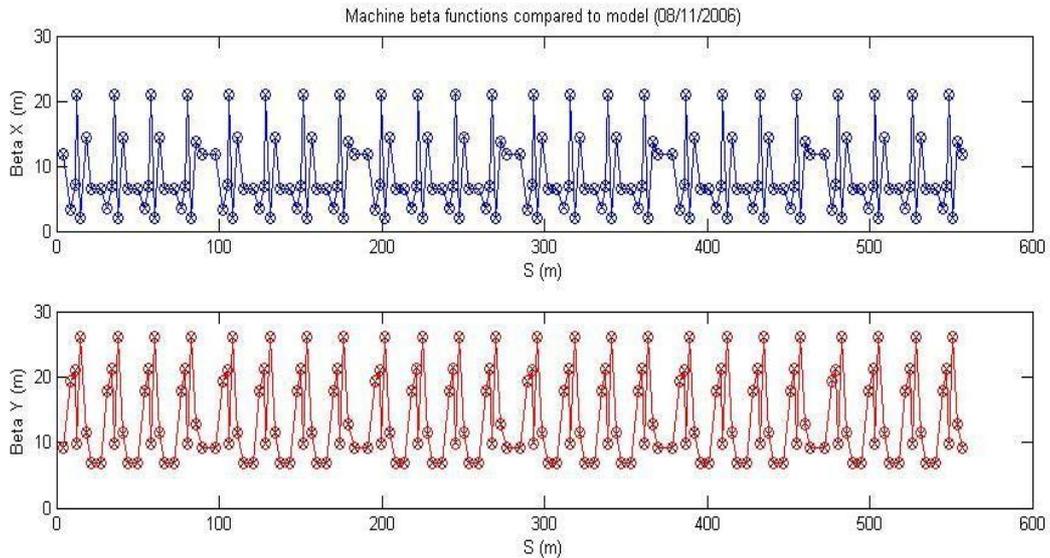
Figure 1: Comparison of measured (circle) and model (cross) beta functions at the BPMs. Top is the horizontal plane, bottom is the vertical plane.
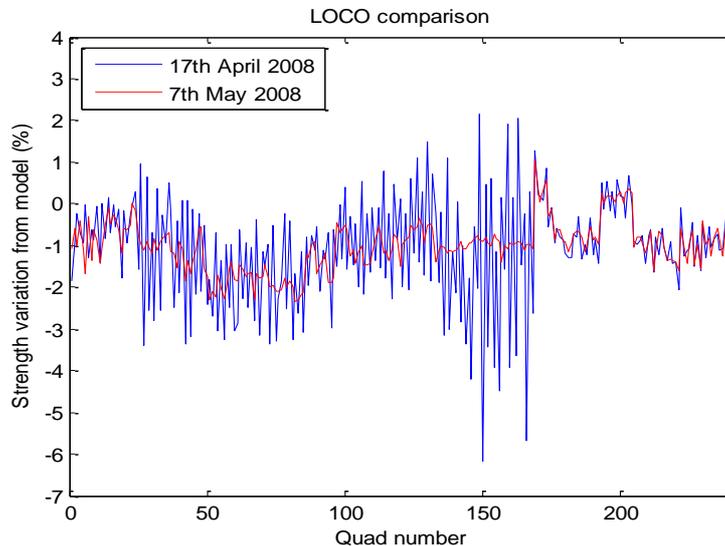
Figure 2: Quadrupole variation for LOCO correction of the linear optics. The quadrupole variations in blue are from LOCO with unconstrained algorithm to fit the quadrupoles. In red is LOCO's output with constraints on the quadrupole variations as described in [5].

The beam sizes measured at the X-ray pinhole camera before and after the best coupling correction are reported in Figure 3. In the coupling corrected case, the vertical beam size is 6 μm at the source point in the dipole.
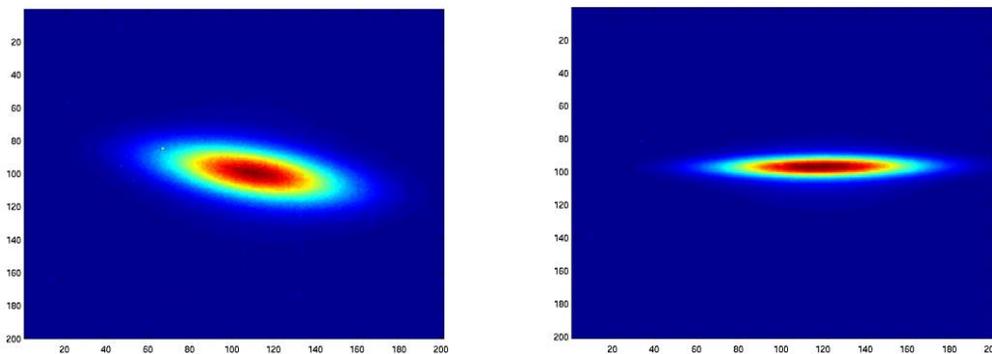
Figure 3: Beam size at the X-ray pinhole camera before (left) and after (right) coupling correction with LOCO.

3.10.2.2 *Nonlinear Optics*

Extensive campaigns of measurements were devoted to understanding and correcting the nonlinear motion of the electron beam with the aim of implementing correctly the nonlinear machine model. The dynamics quantities used in this comparison were detuning with amplitudes, dynamic aperture (DA) and momentum apertures (MA) measured through injection efficiency, beam lifetime and loss distribution. A combination of relatively new techniques such as the Frequency Map Analysis (FMA) and the nonlinear resonant driving terms was used to establish the correct nonlinear model of the storage ring. To this aim the Diamond storage ring has been equipped with a pair of pinger magnets which can excite betatron oscillations in the horizontal and vertical planes independently. Furthermore all beam position monitors (BPMs) have turn-by-turn capabilities.

In Figures 4 and 5 we report the comparison of the Frequency Map measured in the machine with the one obtained from tracking particles in the computer model of the storage ring. Data refer to the operation of the machine without Insertion Devices (IDs). The remarkable agreement is the result of a very careful description of the machine model which takes into account all the measured multipolar errors in the dipoles, quadrupoles, sextupoles and includes the fringe fields in the dipole and quadrupoles. The only parameters adjusted in this comparison were the calibration of the magnetic field vs applied current for the eight sextupole families and the magnitude of the assumed normal octupolar term in the dipole magnets.

An alternative technique for the analysis of the betatron motion based on the measurement of the nonlinear resonant driving terms was also developed at Diamond. This is based on the measurements of the amplitude and phase of the spectral lines excited in the spectrum of the betatron oscillations by the nonlinear resonance driving terms. These measurements can be compared with the same information obtained from tracking data in the computer model of the storage ring and thus provide a method to compare the nonlinear beam dynamics on the real accelerator with the model. The discrepancies can be corrected by fitting algorithms which use the sextupole gradients as fit parameters. In this way the nonlinear machine model can be correctly implemented in the real accelerator. The results of the application of this technique to the Diamond storage ring are reported in [6].
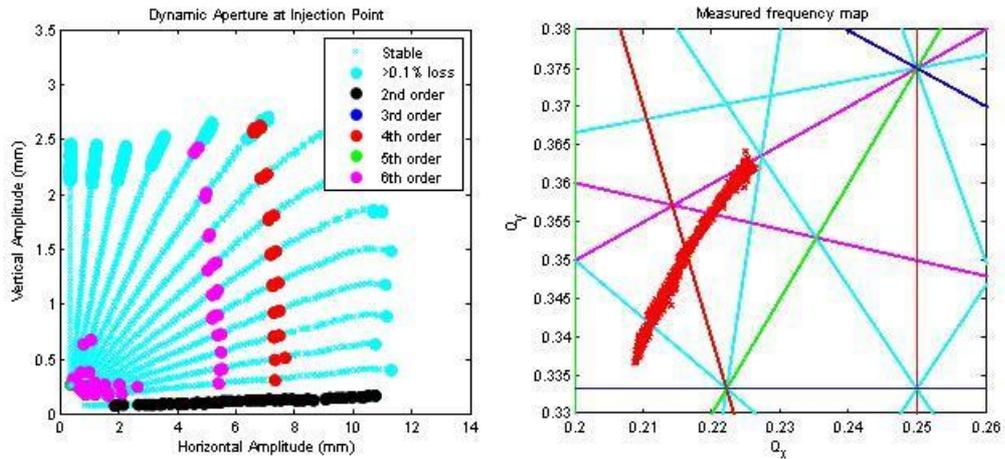
Figure 4: Measured DA (right) and measured FM (left): the magenta dots in the left graph correspond to initial beam conditions which are on a 6th order resonance, the red points are the initial beam conditions which correspond to the 3Qx + Qy resonance.
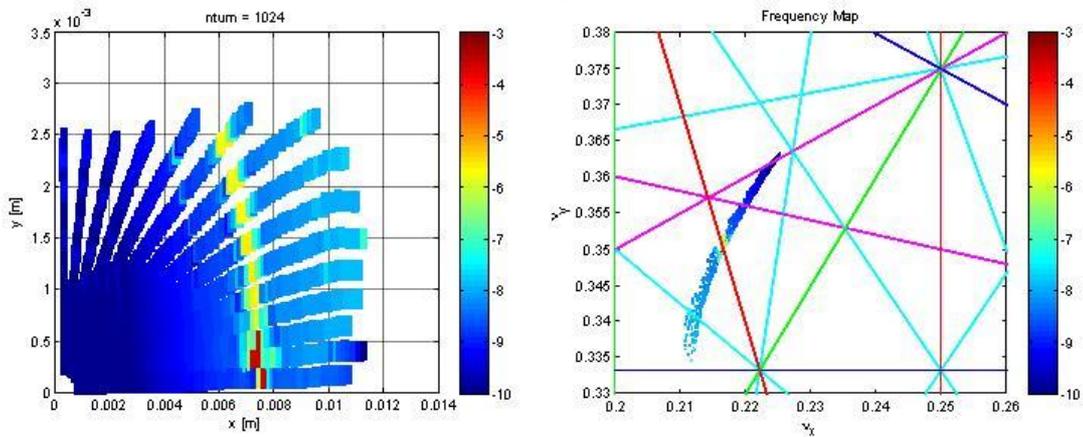
Figure 5: same as Figure 4 but data obtained form tracking particle in the accelerator model

3.10.2.3 *Beam Dynamics with IDs*

A good understanding of the beam dynamics in the bare machine (without IDs) is a prerequisite to the understanding of the beam dynamics in the machine when all IDs are operational. The analysis of the effect of the IDs is an active area of investigation, in particular since the user's demand that the minimum gap of the in-vacuum IDs was reduced from 7 mm to 5 mm.

In terms of linear optics the only IDs which produce significant perturbations are the two Superconducting (SC) wigglers I15 and I12 operating at 3.5 T and 4.2 T maximum field respectively. While perturbation of the orbit is corrected locally by means of trim coils, the β-beating introduced by the SC wigglers is corrected by feed-forward tables which adjust the quadrupoles located in the corresponding straight sections. Theses table follow the ramp of the magnetic field of the two SC wigglers and restore the optics to below 5 %.

In terms of nonlinear dynamics we have found that most of the IDs do not produce any significant change in the DA except the in-vacuum ID I04, which has a significant impact on the DA as shown in Figure 6. The reduction of the dynamic aperture was identified to be due to the crossing of the 3Qx + Qy resonance. A simple shift of the

betatron tune to a working point below this resonance was sufficient to restore the injection efficiency.
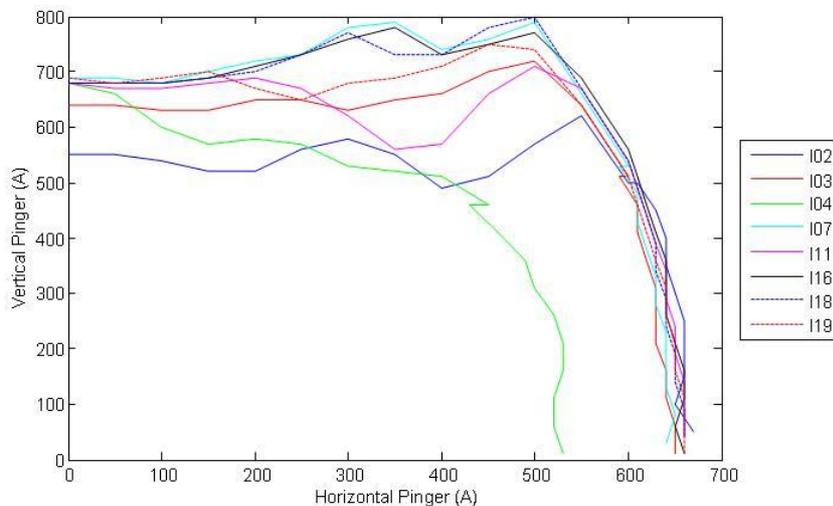
Figure 6: Dynamic aperture with individual in-vacuum IDs closed to 5 mm gap as a function of the pinger voltage. The reduction of the DA with I04 closed is sufficient to impact the injection efficiency.

3.10.3 Collective Effects

Diamond operates usually in multibunch mode with a gap for ion clearing which can be made wider to accommodate a hybrid bunch for dedicated time resolved experiments. The nominal operation requires a chromaticity of 2 units in both planes to damp the multibunch instabilities. The main source of instability was identified to be Resistive Wall although evidence of fast-ion instability has been reported [7]. A transverse multibunch feedback is installed and allows operation of the ring in full fill at 300 mA with zero chromaticity [8].

Several campaigns of measurements were performed at Diamond to understand the machine impedance. Single bunch measurements allowed extracting the longitudinal and transverse broadband impedances. At the same time the results were compared with multiparticle tracking codes, e.g. sbtrack [9], to reproduce numerically the instability threshold and define an effective model of the impedance of the ring based on measurements with the beam.

Bunch lengthening and energy widening curves and their comparison with numerical simulations are reported in Figure 7. The impedance required to reproduce the measurement consists of a broadband resonator (BBR) with R_s=20 kΩ, f_{res}=48 GHz and Q=1 and purely inductive impedance $Z(\omega)=iL\omega$ with L = 149 nH. Through the measurement and fit of the vertical TMCI (Transverse Mode Coupling Instability) at zero chromaticity in Diamond, a BBR impedance with R_T=1 MΩ/m, f_{res}=6 GHz and Q=1 was obtained [7]. These parameters were used in the sbtrack tracking code to investigate the dependence of the TMCI current threshold with the chromaticity including the effect of the bunch lengthening induced by the longitudinal wake and a first simplified modelisation of the Landau damping effect induced by the tune spread in the transverse planes due to the sextupoles magnets. The inclusion of these effects significantly improves the agreement with the experimental data as shown in Figure 8.
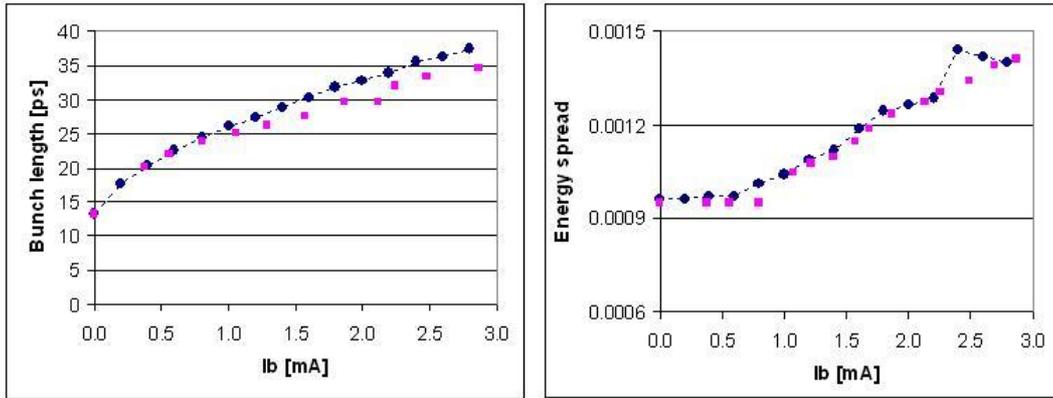
Figure 7: Bunch lengthening (left) and energy spread widening (right) calculated with *sbtrack* (circles), in comparison with measurement (squares) in Diamond. See text for details.
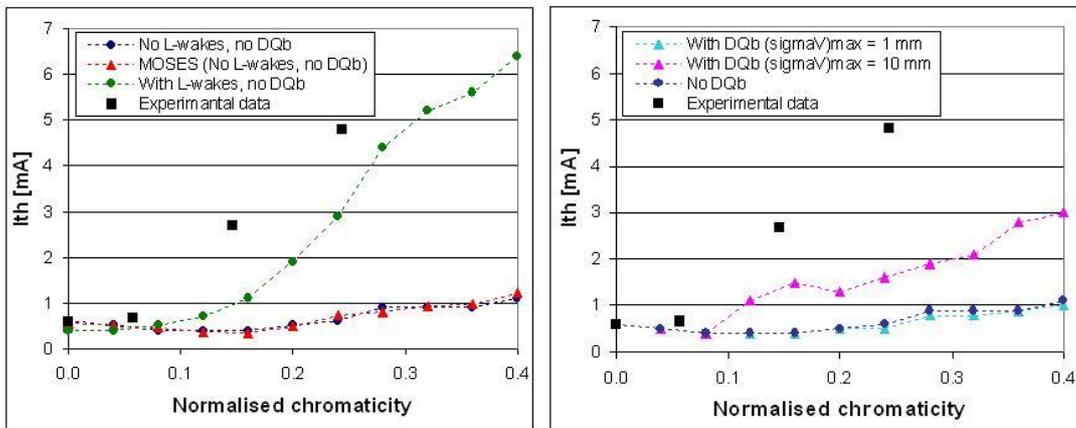
Figure 8: Measured (black squares) and calculated vertical thresholds versus chromaticity in Diamond. Left graph includes longitudinal wakefields, right graphs includes transverse tune spread due to sextupoles [9].

The analysis of single bunch instabilities was also performed by using ultra fast mm-wave detectors using Schottky Barrier Diodes in collaboration with Royal Holloway University London [10]. It was possible to clearly detect bursting above a current threshold of 1.9 mA per bunch in nominal operating condition for the storage ring. This bursting was also clearly correlated to quadrupole oscillations in the bunch length as measured simultaneously by a streak camera as shown in Figure 9. The analysis of the coherent emission bursting is now concentrating on the low-alpha mode (see later section).

The vertical multibunch thresholds were measured and computed from the mbtrack code [9] including the resistive-wall and the BBR wake fields described above. A comparison of the results obtained is shown in Figure 10. Unlike with *sbtrack* where the beam current was explicitly ramped up until the threshold is reached, here the growth rate evaluated at a given current was used to deduce the threshold via equilibrium with the radiation damping. The experimental data show that increasing the chromaticity allows operation at 250 mA already with 1.5 units of vertical chromaticity (0.12 normalised chromaticity) in a two third fill. The comparison with the simulated data is still in its preliminary stages: the discrepancies with the measured data is likely to be due to the fact that only BBR impedance obtained via the TMCI estimates was used in

the description of the impedance and no resistive wall contribution was considered so far.
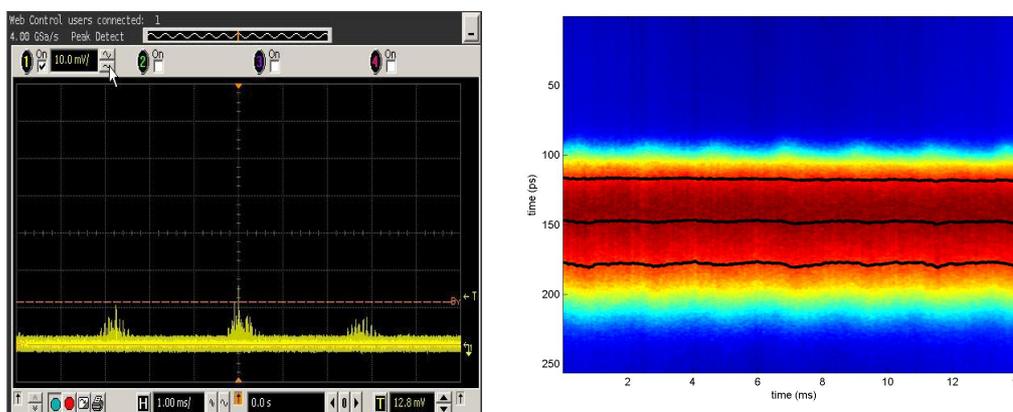
Figure 9: Oscilloscope traces of THz bursting of single bunch detected from a Schottky diode (left) and corresponding streak camera image (right).
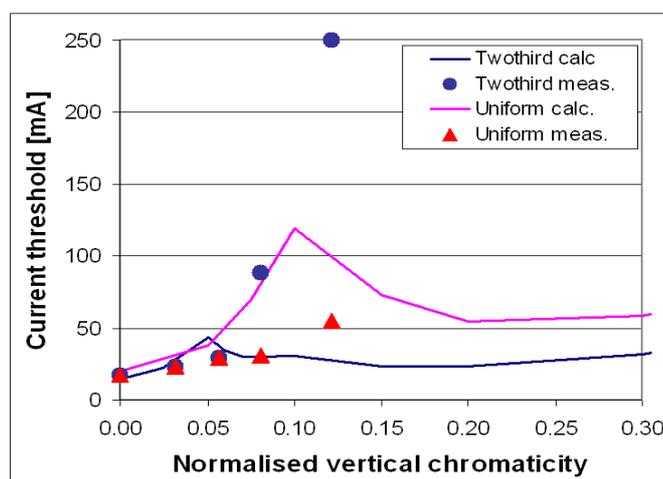
Figure 10: Calculated vertical multibunch threshold versus chromaticity in comparison with measurements

3.10.4 **Top-Up Operation**

Top-Up operation consists in the continuous injection of electrons in the storage ring to restore the operating current and make up for the lifetime losses. Injection occurs with the beamline shutter open, so that the experiments can continue their data acquisition during injection. In this way the experiments benefit from a constant photon flux with higher average values with respect to the previous "beam decay" mode. At the same time, the constant heat load on the vacuum chamber of the storage ring and beamline optics allows a much improved long term stability of the electron and photon beams. Top-Up operation was introduced for the first time in October 2008 and Figure 11 reports the current stability achieved over more than 4 days of continuous Top-Up operation.

Before Top-Up could be implemented at Diamond, the risk of radiation doses being produced which could exceed the adopted dose limit of 1 mSv/year for staff, users and visitors, needed to be carefully assessed [11]. This included an extensive campaign of

numerical simulations to exclude the possibility for the electron beam to be channelled accidentally through the beamline apertures into the beamline hutches [12]. Numerous fault scenarios were investigated where the simultaneous occurrence of several errors in the setting of the magnetic elements and energy errors in the beam could conspire to create unacceptably high radiation doses. These studies showed the need for an additional beam interlock on the dipole currents in the booster-to-storage ring transfer line and storage ring to ensure that the injection energy in the storage ring is correct.

A significant effort was made in the equalisation of the four injector kicker pulses to minimise the residual oscillation of the stored beam during injection. Residual oscillation were reduced to less than 250 μm peak-to-peak and no users have yet reported problems in their data acquisition with such a level of beam perturbation during injection. Likewise the injection efficiency is continuously monitored and corrective actions are taken when the injection efficiency falls below 70%.
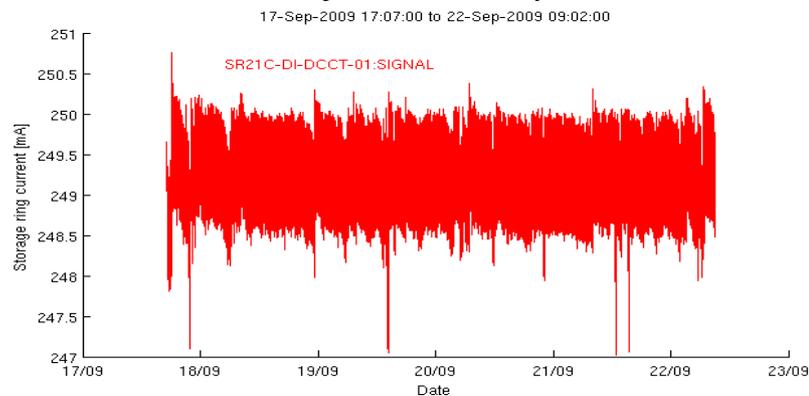
Figure 11: Continuous Top-Up operation at 250 mA for more than 4 days.

3.10.5 Low Alpha Operation

Diamond users have shown interest in the generation of short radiation pulses for pump-probe experiments. The natural bunch length provided by the Diamond storage ring is 10 ps rms. Since time-resolved experiments would benefit from shorter radiation pulses, a research programme was put in place to investigate the options for generating ultra-short pulses (1 ps rms) at the Diamond storage ring [13]. The simplest way to reduce the X-ray pulse length is to shorten the electron bunches in the so called low-alpha optics. Such optics also allow the generation of coherent THz radiation.

Extensive optics studies have led to the definition of a low-alpha lattice which allows reaching 1 ps rms bunch length while maintaining a very small emittance (4 nm) and good dynamic aperture for injection [14]. Streak camera measurements have confirmed that the low-alpha lattice produces shorter electron bunches as low as 1 ps rms at very low beam current. In practice 2-5 ps rms bunches can be served to users with an average current of 10-100 μA per bunch as shown in Figure 12.

The low alpha lattice is now served to the users in dedicated users' time for about a week per year. The analysis of THz radiation with this lattice is ongoing and the first indication show that Coherent THz radiation, with the correct quadratic dependence with the beam current, can be achieved and will be delivered to interested users in the near future.
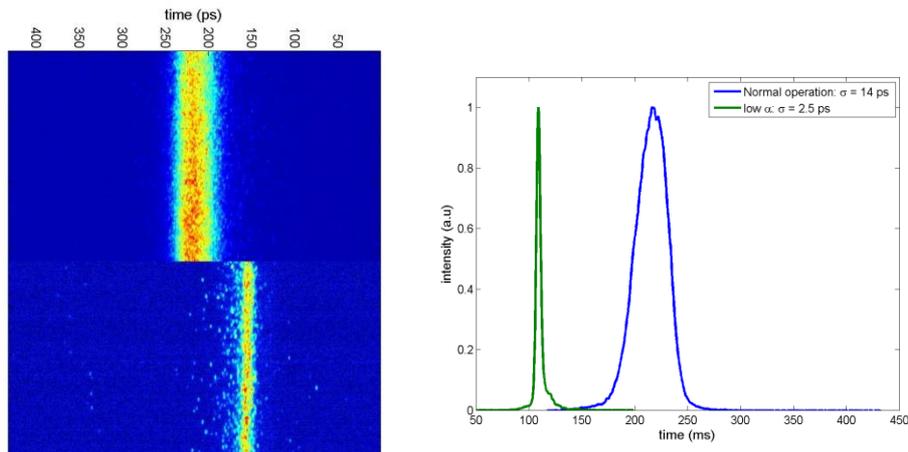
Figure 12: left: streak camera image of the electron bunch in normal operating mode (top) and low alpha mode (bottom); right: corresponding longitudinal profile.

3.10.6 Beam Stability

The stability requirements for third generation light sources are commonly defined in terms of beam dimensions, requiring that the position and angle stability of the beam orbit at the source point be less than 10% of the beam size and divergence respectively. These requirements have to be satisfied over widely different time scales, ranging from milliseconds to days.

Due to the excellent foundation stability, the target of 10% beam size and divergence has been achieved without the need of any orbit feedback in the range 1-100 Hz. Nevertheless a fast orbit feedback (FOFB) [15] was developed in order to control the orbit stability to well below 10% as well as to remove any effect due to ID gap changes At the same time a thorough analysis of the ground vibrations highlighted that most of the residual ground motion occurs in the frequency band 16-25 Hz. The causes of these vibrations were identified to be related to the operation of the water pumps of the cooling system, in conjunction with several structural resonances of the girder structure which occurred in the same frequency range [16]. Passive corrective actions were put in place to damp these vibrations by stiffening the supports of the pumps. The beneficial effect of these two measures are summarised in Figure 13 which show the integrated power spectral density (PSD) for the orbit motion with and without FOFB, before and after the passive measure describe earlier were put in place. It is clear that sub-μm stability is comfortably achieved both in horizontal and vertical planes of motion.

Concerning longer time scales, the introduction of Top-Up operation has substantially improved the long term stability as illustrated in Figure 14 which shows the angular stability of the beam as measured by an X-ray beam position monitor (XPBM) in a beamline for the case with (green) and without (blue) Top-Up operation. The red lines indicate the limits posed by the requirement of 10% beam size angular stability. The top graph refers to the horizontal plane, the middle graph to the vertical plane and the bottom graph shows the current variation with time.
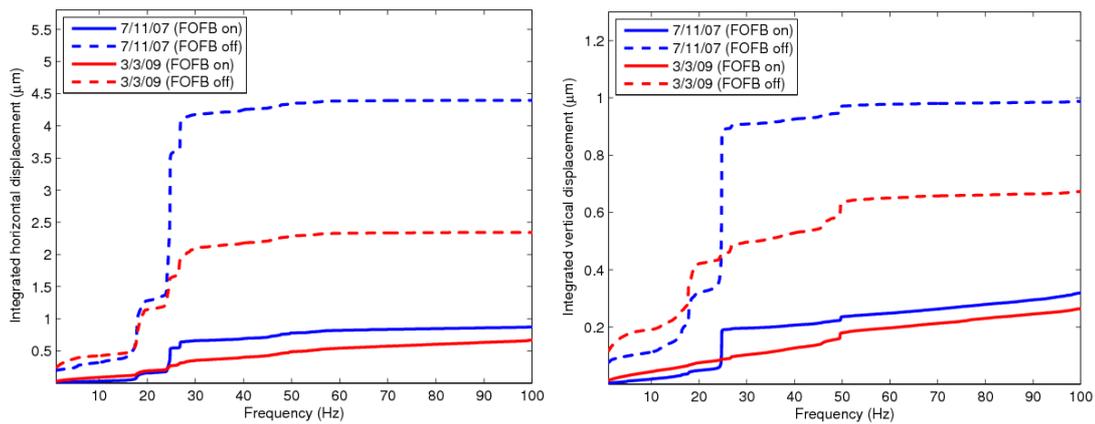
Figure 13: Integrated PSD with and without FOFB on, before and after passive damping measures described in text. Right is the horizontal motion left is the vertical motion
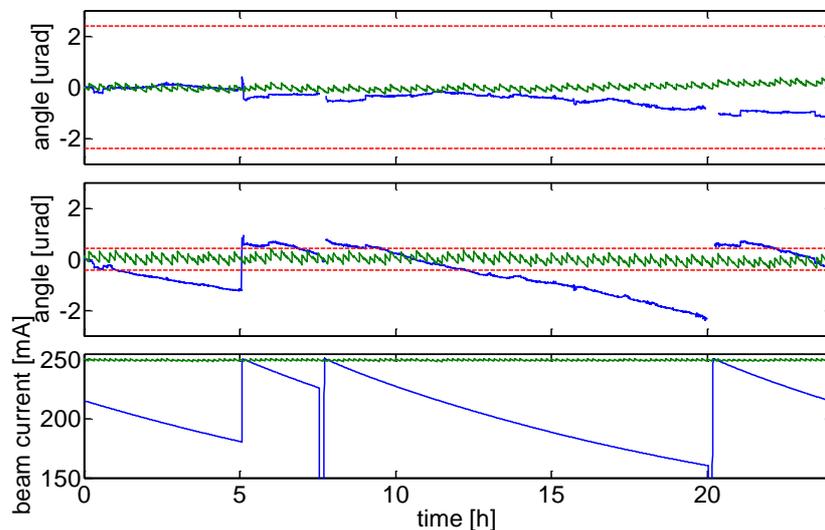
Figure 14: Improvement in beam stability in Top-Up mode (green lines) compared to the previous decay mode (blue lines), see text for details.

3.10.7 **Customised Optics**

A number of new requirements have arisen in connection with the later Phase II beamlines that have significant impact on the Diamond storage ring. For one beamline (I13) it is required to locate two in-vacuum undulators in one straight and in addition produce a horizontal focus of the photon beam at a given location. To achieve this the optics had to be redesigned to provide two minima of the β-functions in the vertical plane to accommodate two canted narrow gap IDs for each beamline branch. At the same time, the requirements for the control of the virtual horizontal focus in the two beamlines were satisfied by providing the horizontal β-functions with negative slope in both halves of the straight sections. This solution, shown in Figure 15, requires a new quadrupole doublet in the middle of the long straights as well as two additional quadrupoles at either end of the straight section. The effect on the nonlinear beam dynamics of these significant modifications of the linear optics were analysed with thorough tracking data and only minor detrimental effects on the lifetime and injection efficiency were found [17]. A similar arrangement will be employed for beamline I09,

studies having confirmed that two such optics modifications are acceptable from the beam dynamics point of view.
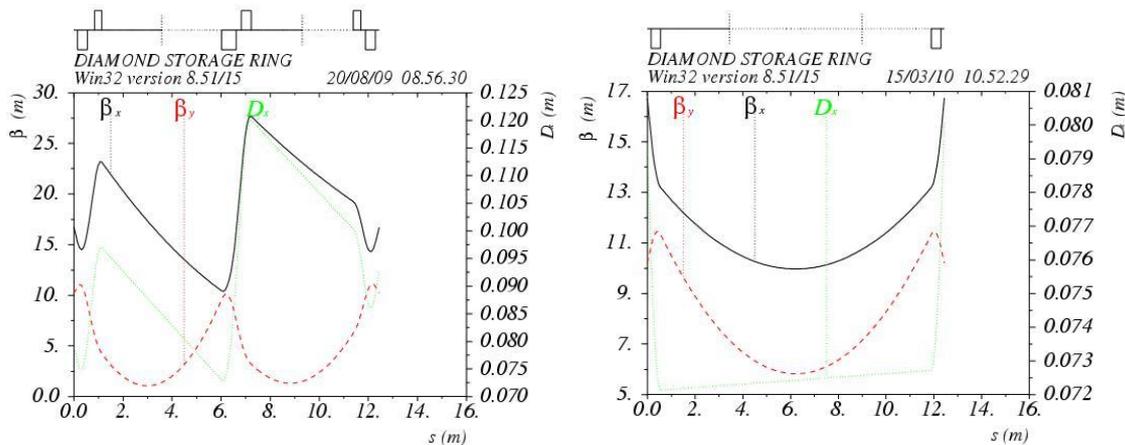
Figure 15: Optics functions in the long straight section 13, with (left) and without (right) the modification of the straight section. Straight 9 has a very similar design.

The layout of straight section 10 will be modified to satisfy the requirement for a rapid switching of the radiation polarization. In this case no modification of the optics is required, but the layout will be modified to include five kicker magnets which are capable of generating independent closed orbit bumps at each of the two APPLE-II undulators, as shown in Figure 16. The fast switch of the polarisation is achieved by rapidly selecting which photon beam is sent down the beamline. A sinusoidal variation of the orbit bump at 10 Hz will be used initially.
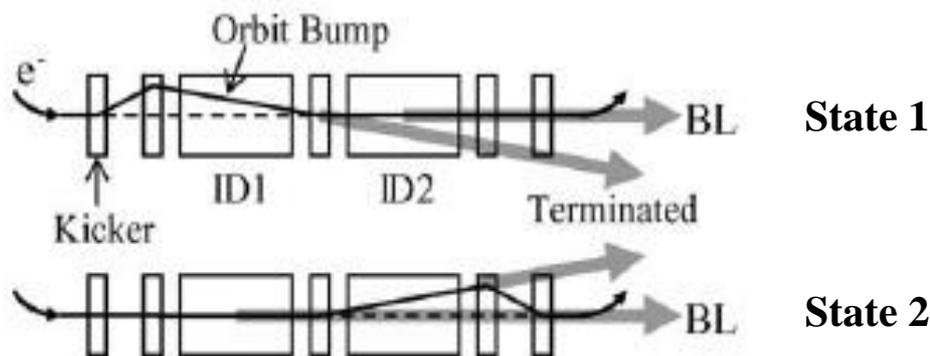
Figure 16: Schematics of the straight section 10 showing kicker magnets and the bump structure in state 1 (top part) and state 2 (bottom part) for fast polarisation switching [18].

3.10.8 **References**

1. R.P. Walker, "Commissioning and Status of the Diamond Storage Ring", pg. 66, Proceedings of the APAC07, Indore, India, (2007).
2. J. Safranek, "Experimental determination of storage ring optics using orbit response measurements", Nucl. Instrum. Methods Phys. Res. A **388**, 27 (1997)
3. C. Thomas, G. Rehm, I. Martin, R. Bartolini, "Xray pinhole camera and emittance measurements", PRSTAB, **13**, 022805, (2010).

4. M. Palmer in LER2010 close-out, Workshop on Low Emittance Ring 2010, CERN, Geneva, Switzerland, (2010), http://ler2010.web.cern.ch/LER2010/

5. I. Martin et al., "Further Advances in understanding and optimising beam dynamics in the Diamond storage ring", pg. 3032, Proceedings of the EPAC 2008, Genova, Italy, (2008).

6. R. Bartolini, I. Martin, J. Rowland, P. Kuske, F. Schmidt, "Correction of multipole nonlinear resonance in storage rings", PRSTAB, **11**, 104002, (2008).

7. R. Bartolini et al., "Analysis of collective effects at the Diamond storage ring", pg. 1574, Proceedings of the EPAC 2008, Genova, Italy, (2008).

8. A. Morgan, "Performance and features of the Diamond TMBF", pg. 3281, Proceedings of the EPAC 2008, Genova, Italy, (2008).

9. R. Nagaoka et al, "Studies of collective effects in Soleil and Diamond using the multiparticle tracking code sbtrack and mbtrack", Proceedings of the PAC 2009, Vancouver, Canada, (2009).

10. R. Bartolini et al, "Observation of longitudinal microbunching instability at the diamond storage ring", Proceedings of the PAC 2009, Vancouver, Canada, (2009).

11. R.P. Walker, "Preparation for Top-up Operation at Diamond", Proc. EPAC08, Genova (Italy), pg. 2121(2008)

12. I. Martin et al, "Top-Up safety simulations for the diamond storage ring", pg. 2085, Proceedings of the EPAC 2008, Genova, (Italy), (2008).

13. R. Bartolini et al., "Plans for the generation of short radiation pulses at the Diamond storage ring", pg. 160, Proceedings of the EPAC 2006, Edinburgh, UK, (2006).

14. I. Martin et al., "A low momentum compaction lattice for the Diamond storage ring", Proceedings of the PAC 2009, Vancouver, Canada, (2009).

15. G. Rehm et al., "Digital eBPM at Diamond and integration into a fast global orbit feedback", pg. 24, Proceedings of the DIPAC 2007, pg. 24, Venice, Italy, (2007).

16. R. Bartolini et al., "Analysis of Beam Orbit Stability and Ground Vibrations at the Diamond Storage Ring", pg. 1980, Proceedings of the EPAC 2008, Genova, Italy, (2008).

17. B. Singh, "Two mini-betay plus horizontal (virtual) focussing optic for I13 beamline for Diamond storage ring", Diamond Technical Note, AP-SR-REP-0170, (2009).

18. P. Steadman, private communication.

3.11 Progress on the Advanced Laser Plasma High-energy Accelerators towards X-rays (ALPHA-X) project and SCAPA

D.A. Jaroszynski
University of Strathclyde, Physics Department, Scottish Universities Physics Alliance, 107 Rottenrow, Glasgow G4 0NG, UK
Mail to: dino@phys.strath.ac.uk

3.11.1 Introduction

UK scientists have been active in the development of novel accelerators for several decades. In this newsletter article we will present the recent developments of laser-driven plasma wakefield accelerators in the UK and focus on the results of a Research Councils UK Basic Technology Programme supported project led by the University of Strathclyde, the Advanced Laser Plasma High-energy Accelerators towards X-rays (ALPHA-X) project that started in 2002. This project, which initially involved several UK Universities (Oxford, Strathclyde, Imperial College, St Andrews, Abertay Dundee

and Dundee) and two STFC laboratories (Daresbury and Rutherford Appleton Laboratories), and now also includes Lancaster University and support from the Cockcroft Institute and several international groups. Some aspects of ALPHA-X have also been supported by EU funds. By combining expertise in accelerator and plasma physics in the UK with the latest high power laser technology, rapid progress has been made in developing a reliable (dependent on the laser reliability) ultra-compact laser plasma wakefield accelerator with remarkable properties, notably a high peak current, femtosecond duration electron bunches, low energy spread, low emittance, and good shot to shot stability. Furthermore, excellent progress has also been made towards develop radiation sources based on wakefield accelerators. Apart from the pioneering achievements by the ALPHA-X teams in demonstrating controlled acceleration and applying the beams produced as a radiation source, one of the outcomes of the project has been the development of a state-of-the-art accelerator laboratory, as shown in Fig. 1.

Figure 1: The ALPHA-X beam-line and plasma wakefield accelerator.

The pioneering results from ALPHA-X are now the basis of a new centre of excellence, the Scottish Centre for the Application of Plasma-based Accelerators (SCAPA). This newsletter will present results from ALPHA-X project and briefly outline the objectives of SCAPA and the facilities that will be available.

3.11.2 Laser-Driven Plasma Wakefield Accelerators

Electron beam driven incoherent and coherent radiation sources have become indispensible tools for science and technology. The free-electron laser (FEL) requires a high brightness relativistic electron beam to produce brilliant coherent radiation over a wide spectral range from terahertz frequencies to X-rays [4-6]. They can be tuned over a large spectral range by varying the beam energy or the undulator parameters. They are used by an extensive user community probing the structure of matter and studying its evolution when subject to stimuli on ultra-fast time scales [5]. X-ray FELs are driven by large conventional accelerators based on microwave cavities limited to acceleration gradients of less than 100 MV/m. These limitations can be overcome using the huge electric fields available from charge separation in plasma, which provide the accelerating forces. The challenge is to create a travelling wave field matched to the particle velocities. Tajima and Dawson solved this by proposing using the ponderomotive force of intense laser pulses to drive plasma wakes, which in turn can rapidly accelerate particles to high energies [1], shown schematically in Figure 2.
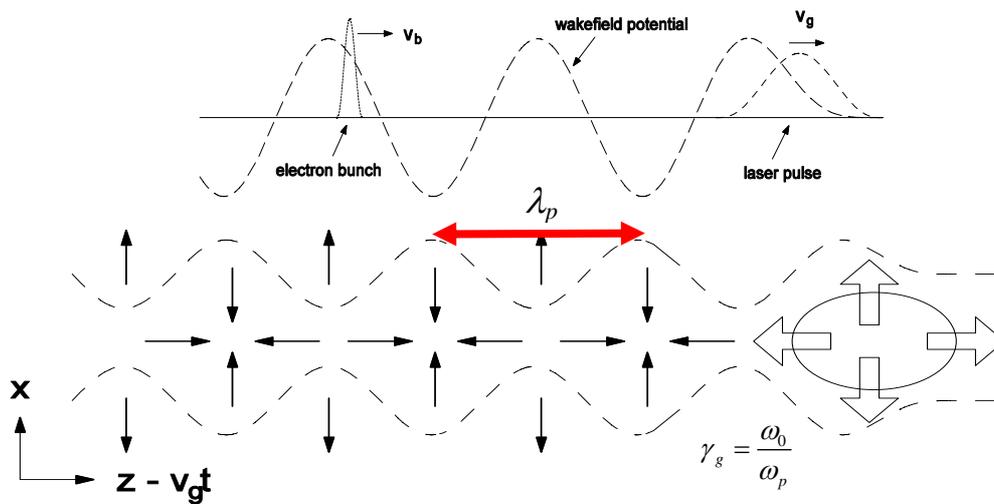
Figure 2: Schematic of the plasma wakefield accelerator showing the scale length of the accelerating structure $\delta_z \approx \lambda_p = c/\omega_p$, where ω_p is the plasma frequency.

A relativistic electron, positron or proton beam can be substituted for the laser pulse because the Coulomb field expels plasma in a similar way to the ponderomotive force. Initial experiments exploring wakefield acceleration produced electron beams with very broad energy spreads ($\approx 100\%$). However, over the last decade dramatic progress has been made in developing the laser wakefield accelerator (LWFA): millimetre-long 100 MeV [7-9] and centimetre-long GeV [10] accelerators have been demonstrated and an understanding of the properties and injection mechanisms of the LWFA is being built up. The main investigations are being directed towards understanding, characterising, controlling and scaling up the LWFA [2,3]. Serious efforts to develop the wakefield accelerator by many groups are being made because of its potential as a compact driver of FEL and synchrotron sources. Recent proof-of-principle demonstrations of undulator synchrotron radiation sources driven by LWFA have been carried out initially in the visible [11,13] and more recently extended to the VUV [12]. Measurement of the synchrotron spectrum in these experiments [13] indicates an electron beam relative energy spread of the order of 1%. VUV radiation from an undulator at Strathclyde (shown in Figure 3) has recently been measured.

Figure 3: The ALPHA-X undulator

To utilise the LWFA as a FEL driver it is necessary to produce a high brightness electron beam with a very low energy spread. FELs require beam r.m.s. energy spreads

less than the gain parameter ρ [14], which is of the order of 10^{-3} for the X-ray FEL. Energy spreads of 5 – 10% (1-10% when instrument resolution is accounted for) have been measured in LWFA experiments [14]. Recent results from the ALPHA-X beam line show that relative energy spreads of less than 0.5% can be obtained at ≈100 MeV [30,31]. It is generally accepted that a two-stage or a composite injector-accelerator LWFA will be needed to reach the several GeV energies with narrow energy spread required for an X-ray FEL[3]. Apart from requiring peak currents in excess of 1 kA for high gain, both σ_γ /γ and the normalised r.m.s. transverse emittance, ε_n, in a slice equal to the FEL cooperation length must be low. X-ray FELs require GeV accelerators with beam emittances and energy spreads of the order of 1 π mm mrad and 10^{-3}, respectively [5,6,15,20]. LWFAs have promising characteristics because of the size of their accelerating structures, which is of the order of the plasma wavelength. Recent measurements on the ALPHA-X beam line, (right hand side of Figure 3, which also shows a detail of the undulator) show that the normalised transverse emittance is of the order of 1 π mm mrad [32]. The electron bunch is constrained to a small fraction of λ_p, which restricts the duration to <<10 fs for plasma densities in the range of 10^{18} – 10^{19} cm^{-3} [17,90,20]. Ways of controlling the energy spread have been studied and beams with a measured r.m.s. energy spread of 3.1% have been produced using colliding laser pulses [18].

3.11.3 Pioneering Results

Further developments of wakefield accelerators were made possible by the rapid advances in high power lasers. The first experimental demonstration was carried out in 1995 by a group led by Imperial College using high power lasers at RAL, to demonstrated the existence of the plasma wake and inferred an accelerating gradient of more than 100 GV/m, and succeeded in producing electron beams with 100% energy spread characterised by a Maxwellian momentum spread.   For nearly a decade little progress was made to improve on this and the scientific community was sceptical about the viability of the plasma wakefield accelerator as a workable device. In the mean time, progress in the development of high power lasers resulted in the development of a new generation of table top terawatt lasers based on Ti:sapphire CPA amplifiers, which were capable of producing laser beams with intensities in excess of 10^{18} Wcm^{-3} and pulses as short as several 10s of femtosecond. This advance in laser technology was crucial for the next development of wakefield accelerators and several landmark experiments followed. These included the first demonstration of controlled acceleration in gas jets and the work was published in a trio of letters to Nature in 2004 by UK, US and French teams [7,8,9]. The pioneering UK experiments at RAL involving Imperial College, RAL and Strathclyde and were part of ALPHA-X [7]. These results completely transformed the landscape of laser-driven plasma wakefield accelerators. Initially, controlled acceleration to around 100 MeV was demonstrated but this was followed up in 2006 with extensions of the accelerator length using preformed plasma waveguides, which resulted in demonstration of   GeV beams in a collaboration between Berkeley and Oxford [10] (also part of the ALPHA-X project [20]). Around the same time, a group at UCLA used the SLAC accelerator to demonstrate the so called "afterburner" electron beam driven plasma wakefield accelerator, where a 42 GeV electron beam was used to accelerate trailing electrons to 85 GeV.
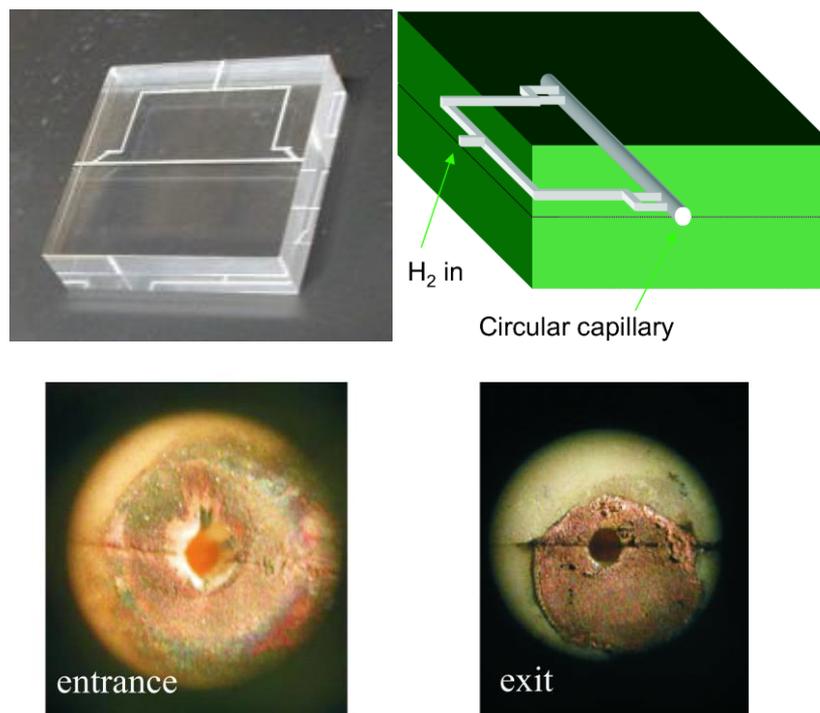
Figure 4: The ALPHA-X plasma waveguide capillary, after one year use in laboratory.

A very important part of the wakefield accelerator is the plasma media which support the plasma density waves and bubble structures. Depending on the application, plasma in the range of $10^{17} - 10^{19}$ cm^{-3} are required (i.e. for 0.3 GV/cm – 3 GV/cm). To achieve significant acceleration the laser pulse must be guided beyond its usual Rayleigh diffraction length. Two methods are used. The fist relies on relativistic self-focussing of the laser beam in the plasma. For sufficiently high laser intensities plasma electrons become relativistic which increases the permittivity and produces self-focussing which exactly compensates diffraction for matched laser beams. This has the advantage that no preformed plasma is required. The laser pulse ionises gas in a gas jet or cell and subsequently forms a relativistically self-guided channel while creating the plasma density wake and accelerating self injected particles. An alternative method is to use a preformed plasma channel waveguide or a gas filled hollow waveguide as a guiding structure. The preformed plasma channels provides an elegant method (developed by Oxford) to guide intense laser pulses over several centimetres without loss [33]. Furthermore, complex shapes of capillaries supporting the plasma waveguide can be manufactured using laser-micromachining methods (originally developed by Strathclyde) [20], which allows integration of injectors, modifying laser and/or plasma properties, curving plasma channel waveguides etc.. An example of a plasma waveguide is shown in Figure 4. This type of preformed plasma waveguide was used in the 1 GeV wakefield acceleration demonstration experiments at Berkeley in 2006 [10].
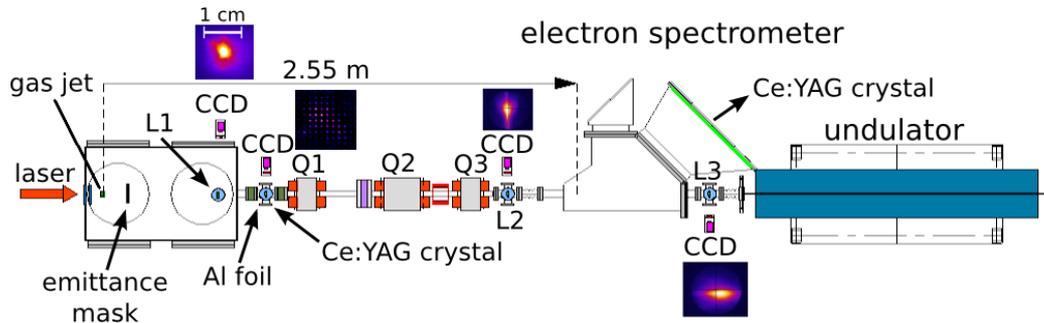
Figure 5: 135 MeV beam measured on the ALPHA-X beamline

The ALPHA-X beam line, shown in Figure 5, has been used to completely characterize the electron beam from a wakefield accelerator in the range of 50 – 200 MeV using 2 mm gas jet. Very low energy spread beams are obtained when the Coulomb field of bunch partially flattens out the acceleration potential. This beam loading effect has an optimum at low charge. Energy spreads <1% have been measured [8] when the electron beam is focused by a triplet set of quadrupoles, as shown in Figure 6. Focusing also improves the pointing stability of the accelerator [29].
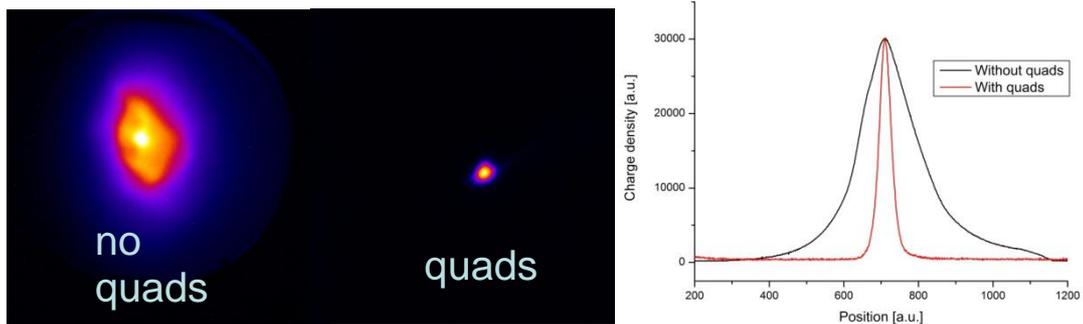
Figure 6: focussing of a 100 MeV beam using a PM triplet quadrupole magnets on the ALPHA-X beamline [26]

Direct energy spread measurements shown in Figure 7 have been confirmed by measurements of undulator spectrum, shown in Figure 8 [13]. Recent results from the ALPHA-X project are: quad focusing, emittance, beam stability, energy spread.
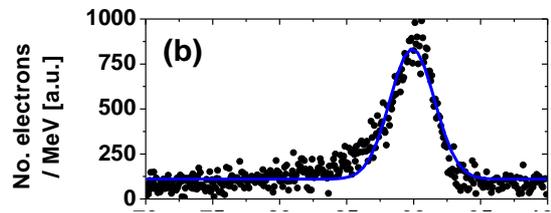
Figure 7: 90 MeV Electron beam spectrum measured on the ALPHA-X beamline [30,31].
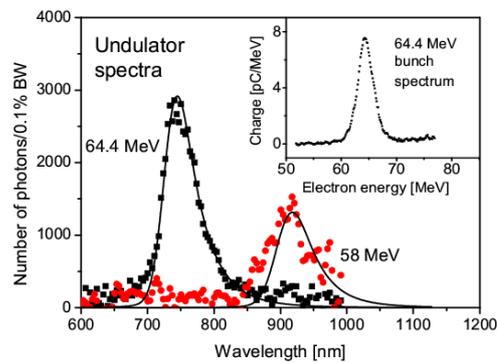
Figure 8: 1% energy spreads from a wakefield accelerator measured using an undulator as a spectrometer. Dots are measurements and line is the calculated optical spectrum using the measured electron beam energy spectrum [11.13].

Measurement of the energy spread, emittance, charge are consistent with a few femtosecond duration high brightness electron bunch with a peak current of the order of 1 kA. For a FEL using a LWFA beam to be useful for applications experiments it is also necessary to have a stable beam. The beams from the ALPHA-X beam line now regularly produce beams with an electron beam on every laser shot and with a beam energy that fluctuates in energy by about 5% at 100 MeV [31] and less than 2.5% (as shown in Figure 9) when the laser stability is optimized.
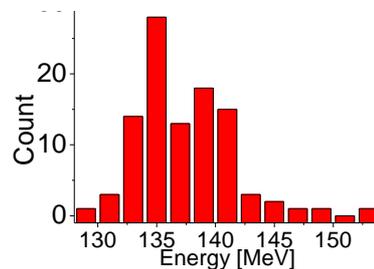
Figure 9: 135 MeV beam shot-to-shot measurement of mean energy: standard deviation 2.6%.

3.11.4 **The Scottish Universities Physics Alliance Centre of Excellence: SCAPA**

Scotland's new pooling efforts, which includes the Scottish Universities Physics Alliance (SUPA), are providing new opportunities to make coherence out of the

diversity of the 8 Scottish universities forming the alliance. With investment in SUPA from the Scottish Funding Council and major support from the Universities, there is now a realistic opportunity to create a very competitive research environment to harness some of Scotland leading intellectual effort on a scale sufficient to make a difference, where individual effort would otherwise not be competitive. One of the flag-ship projects is to set up a new centre for developing laser-plasma accelerators and applying them to a wide range of problems. This initiative, led by the University of Strathclyde, will provide unique and powerful tools in a state-of-the-art laboratory for SUPA scientists and their collaborators. The new centre, the Scottish Centre for the Application of Plasma-based Accelerators (SCAPA), will bring together a multidisciplinary team from the Universities of Strathclyde, Glasgow, West of Scotland, Herriot Watt, Edinburgh and Dundee, to harness the electrostatic forces of fully ionised gas, or plasma, using high power lasers, and accelerate charged particles to high energies. These high energy particles will then be used to produce electromagnetic radiation over a wide spectral region from terahertz frequencies to gamma rays, and particles such as electrons, ions, neutrons, etc., which can be used as powerful tools for the scientists. The feasibility of a LWFA driven free-electron laser, to generate femtosecond duration pulses of coherent X-ray radiation, will be investigated. Furthermore, the huge forces of the plasma will also allow very short pulses of gamma rays to be produced and high energy protons and heavier ions to be accelerated to high energy. These "tools for scientists" will be used to probe the structure of matter in many important areas of science and technology. Examples of these applications include the development of detectors for nuclear and particle physics and medical imaging, oncology, investigating medical radioisotope production, probing dense matter for nuclear fusion, probing nuclear reactions etc.
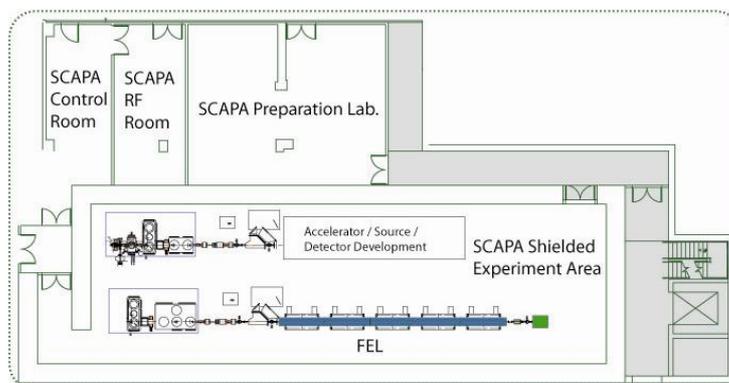
Figure 10: Layout of SCAPA showing ground floor plan. Lasers and ion labs on second floor (not shown).

To achieve this ambitious programme several new appointments will be made across SUPA and a new temperature controlled and shielded laboratory of about 900 m^2, layout shown in Figure 10, will be constructed at Strathclyde on an ultra-stable platform. This will include radiation shielded areas with three beam lines, a control room, areas for target preparation and several laser rooms and will coincide with refurbishment of the Department of Physics at Strathclyde.

Properties of the SCAPA synchronised electron, ion and photon sources:
- High quality, high current density electron bunches
- Incoherent X-rays

- Coherent IR to X-ray radiation
- High energy ions
- High power laser beams:
    - Wavelength: 800 nm
    - Duration: 20-30 fs
    - Peak power: 200 – 300 TW (possible extension to 1 PW in future)
    - 10 Hz repetition rate
    - 2 beams with adjustable power and polarisation
    - Contrast $>10^9$

Underlying all this is the compactness of the laser-plasma accelerator. Plasma can sustain much higher forces than any other medium and a large variety of particle and radiation sources can be developed with a much reduced infrastructure need ("under one roof"). The activities will include investigations of intense radiation field-matter interactions, probing hot dense matter, radiation and particle transport in matter, nuclear physics and development and characterization of particle detectors, health sciences and materials.

SCAPA will provide the infrastructure for challenging experiments and be well set up for long term projects.

3.11.5 **Acknowledgements**

3.11.6 **References**

1. Tajima, T. & Dawson, J. M. Laser electron accelerator. *Phys. Rev. Lett.* **43**, 267-270 (1979).
2. Malka, V. *et al.* Principles and applications of compact laser–plasma accelerators. *Nature Phys.* **4**, 447-453 (2008).
3. Esarey, E., Schroeder, C. B. & Leemans, W. P. Physics of laser-driven plasma-based electron accelerators. *Rev. Mod. Phys.* **81**, 1229-1285 (2009).
4. Bilderback, D. H., Elleaume, P. & Weckert, E. Review of third and next generation synchrotron light sources. *J. Phys. B: At. Mol. Opt. Phys.* **38**, S773-S797 (2005).
5. Feldhaus, J., Arthur, J., & Hastings, J. B. X-ray free-electron lasers. *J. Phys. B: At. Mol. Opt. Phys.* **38**, S799-S819 (2005).
6. McNeil, B. Free electron lasers: First light from hard X-ray laser. *Nature Photonics* **3**, 375-377 (2009).
7. Mangles, S. P. D. *et al.* Monoenergetic beams of relativistic electrons from intense laser–plasma interactions. *Nature* **431**, 535-538 (2004).
8. Geddes, C. G. R. *et al.* High-quality electron beams from a laser wakefield accelerator using plasma-channel guiding. *Nature* **431**, 538-541 (2004).
9. Faure, J. *et al.* A laser–plasma accelerator producing monoenergetic electron beams. *Nature* **431**, 541-544 (2004).
10. Leemans, W. P. *et al.* GeV electron beams from a centimetre-scale accelerator. *Nature Phys.* **2**, 696-699 (2006).

11. Schlenvoigt, H.-P. *et al.* A compact synchrotron radiation source driven by a laser-plasma wakefield accelerator. *Nature Phys.* **4**, 130-133 (2008).

12. Fuchs, M. *et al.* Laser-driven soft-X-ray undulator source. *Nature Phys.* **5**, 826-829 (2009).

13. Gallacher, J. G. *et al.* A method of determining narrow energy spread electron beams from a laser plasma wakefield accelerator using undulator radiation. *Phys. Plasmas* **16**, 093102 (2009).

14. Bonifacio, R., Pellegrini, C. & Narducci, L. M., Collective instabilities and high-gain regime in a free electron laser. *Opt. Commun.* **50**, 373-378 (1984).

15. Nakamura, K. *et al.* GeV electron beams from a centimeter-scale channel guided laser wakefield accelerator. *Phys. Plasmas* **14**, 056708 (2007).

16. Osterhoff, J. *et al.* Generation of stable, low-divergence electron beams by laser wakefield acceleration in a steady-state-flow gas cell. *Phys. Rev. Lett.* **101**, 085002 (2008).

17. Lu, W. et al. Generating multi-GeV electron bunches using single stage laser wakefield acceleration in a 3D nonlinear regime. Phys. Rev. ST Accel. Beams 10, 161301 (2007).

18. Rechatin, C. *et al.* Controlling the phase-space volume of injected electrons in a laser-plasma accelerator. *Phys. Rev. Lett.* **102**, 164801 (2009).

19. Pukhov, A., & Meyer-ter-Vehn, J. Laser wake field acceleration: The highly non-linear broken-wave regime. *Appl. Phys. B* **74**, 355-361 (2002).

20. Jaroszynski, D. A. *et al.* Radiation sources based on laser–plasma interactions. *Phil. Trans. R. Soc. A* **364**, 689-710 (2006).

21. Shanks, R. P. *et al.* Pepper-pot emittance measurement of laser-plasma wakefield accelerated electrons. *Proc. SPIE* **7359**, 735907 (2009).

22. Fonseca, R. A. *et al. Lecture Notes in Computer Science* (Springer, Heidelberg, 2002), Vol. 2331, p. 342.

23. Reitsma, A. J. W., Cairns, R. A., Bingham, R. & Jaroszynski, D. A. Efficiency and energy spread in laser-wakefield acceleration. *Phys. Rev. Lett.* **94**, 085004 (2005).

24. Katsouleas, T. *et al.* Beam loading in plasma accelerators. *Part. Accel.* **22**, 81-99 (1987).

25. Tzoufras, M. *et al.* Beam loading in the nonlinear regime of plasma-based acceleration. *Phys. Rev. Lett.* **101**, 145002 (2008).

26. Anania, M. P. *et al.* Transport of ultra-short electron bunches in a free-electron laser driven by a laser-plasma wakefield accelerator. *Proc. SPIE* **7359**, 735916 (2009).

27. F. Tsung et al Simulation of monoenergetic electron generation via laser wakefield accelerators for 5–25 TW lasers. *Physics of Plasmas* **13**, 056708 (2006))

28. Geddes, C. G. R. *et al.* Plasma-Density-Gradient Injection of Low Absolute-Momentum-Spread Electron Bunches. *Phys. Rev. Lett.* **100**, 215004 (2008).

29. Issac, R. C. *et al.* Electron beam pointing stability of a laser wakefield accelerator. *Proc. SPIE* **7359**, 735915 (2009).

30. Wiggins, S.M. et al., Progress towards a laser plasma wakefield driven compact X-ray free-electron laser, SPIE Newsroom DOI: 10.1117/2.1200903.1559 (2009)

31. Wiggins, S. M. et al., Towards a Compact XUV Free-Electron Laser: Characterising the Improving Beam Quality of Electron Beams Generated in a Laser Wakefield Accelerator, Particle Accelerator Conference'09, Vancouver, 2009. Proc. PAC'09 (2009)

32. Brunetti, E. et al., "Low emittance relativistic electron beams from a laser-plasma accelerator", *Proc. SPIE* **7359**, 735915 (2009).

33. Spence, D. J. and Hooker, S. M., Phys. Rev. E 6302, art. no.-015401 (2001).

3.12 The New Light Source Project

Richard P. Walker, on behalf of the NLS Source Design Team
Diamond Light Source, Harwell Science & Innovation Campus, Oxfordshire,
OX11 0DE, UK
Mail to: r.p.walker@diamond.ac.uk

3.12.1 Introduction and Current Status

The New Light Source (NLS) project [1] was launched in April 2008 by the UK Science and Technology Facilities Council (STFC) to consider the scientific case and develop a conceptual design for a possible next generation light source based on a combination of advanced conventional laser and free-electron laser sources. The design of the NLS facility has drawn on expertise from STFC Daresbury and Rutherford Laboratories - which includes the Accelerator Science and Technology Centre (ASTeC) and Photon Science Department (PSD) – as well as Diamond Light Source, the Cockcroft and John Adams Institutes, and other Universities.

The NLS project has been from its inception "science driven" i.e. the first step was to define the long-term key science drivers, the second step was to define the technical solution. A series of workshops and meetings were held in 2008 to define the main scientific themes that required a new light source capability in the UK and led to the publication of a Science Case in September 2008 which was subsequently approved by the relevant STFC Committees, giving the go-ahead to proceed to a conceptual design of the facility.

Further scientific consultation and design work then led to an updated Science Case and Outline Facility Design which was published in July 2009 [2]. The NLS project was then reviewed in detail as part of STFC's overall science prioritization exercise, involving extensive external peer review and international panel experts. The review concluded that "The NLS project would have very high impact. It would have a major lead in both a national and international context. It would be a unique, world leading facility in the area of biological imaging and would open up exciting new research areas and develop new communities." It also noted that "NLS could develop significant synergies with other national and international facilities." Unfortunately however, despite the extremely positive scientific outcome of the review, given the budget available, STFC decided that no further funding should be given for NLS development at this time. The review did however recommend that "STFC re-assess the NLS project in 3-5 years time in order to ensure that STFC considers future user needs."

Before drawing this initial phase to a close, work on the NLS project will continue over the next few months in order to complete the Conceptual Design Report (CDR) as originally planned, both as a starting point for any future design work as well as for the benefit of the wider accelerator community.

In this report we present an overview of the NLS design, referring the reader to various published reports and the forthcoming CDR for more details.

3.12.2 **Facility Overview**

3.12.2.1 *Required Source Properties and Main Parameters*

The NLS Science Case demands high repetition rate, ultrashort, high brightness, spatially and temporally coherent soft X-rays and a suite of light sources tightly synchronised to these spanning the THz to vacuum UV range. To realise this goal a unique facility has been designed which combines the following sources:

- Free-electron Lasers (FELs) will cover the range from 50 eV to 1 keV in the fundamental. Initially this will be covered by three FELs with overlapping tuning ranges as follows:

     FEL-1: 50-300 eV,   FEL-2: 250-850 eV,   FEL-3: 430-1000 eV.

   Harmonics will extend the range up to 5 keV.
- Conventional laser sources, tightly synchronized to the FEL sources, will cover the range from 60 meV (20 μm) to 50 eV.
- Coherent THz/IR radiation from 20–500 μm will be generated by the electron beams after passing through each FEL, for optimal synchronization between the FEL pulse envelope and THz/IR field for pump-probe experiments.

The required properties of the FEL sources are as follows:
- High brightness, $>10^{11}$ photons per pulse at 1 keV
- High degree of both temporal and transverse coherence
- High repetition rate of regularly spaced pulses, 1 kHz initially, increasing in future phases to 10 kHz, 100 kHz and eventually to 1 MHz
- Ultra-short pulses of 20 fs FWHM or less initially, with the possibility to reduce to the fs/sub-fs range at a later stage
- Variable polarization
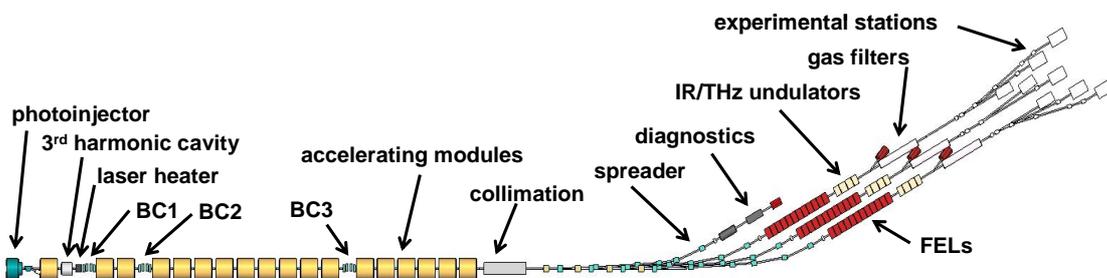
Figure 1: Schematic layout of the NLS.

Figure 1 shows a schematic layout of the proposed facility. The required high repetition rate of regularly spaced pulses demands a superconducting linac operating in continuous wave (CW). An energy of 2.25 GeV is required to obtain the required photon energies, with the selected undulator parameters. A common electron energy for all three FELs, together with variable gap undulators, assures the required independent operation and easy tunability of the three FELs. An alternative accelerator design based on a recirculating linac has also been studied with encouraging results [3], however the degree of optimisation is not yet at the level of the single-pass linac scheme.

The requirement for FEL pulses that are temporally coherent, close to Transform Limited, with smooth profiles reproducible from shot-to-shot demands that the FELs

operate in the seeded mode, rather than the more usual SASE mode. This also guarantees the best synchronization between the FEL pulses and conventional laser sources for pump-probe experiments.

A further requirement of the FEL sources is that they provide fully variable polarization. The current undulator design is based on the well developed APPLE-II scheme. An initial assessment of alternative schemes (APPLE-III, Delta and crossed-undulators) has been made [4], but further work would be required before definitely selecting one of these as part of the baseline design.

3.12.2.2 *Injector*
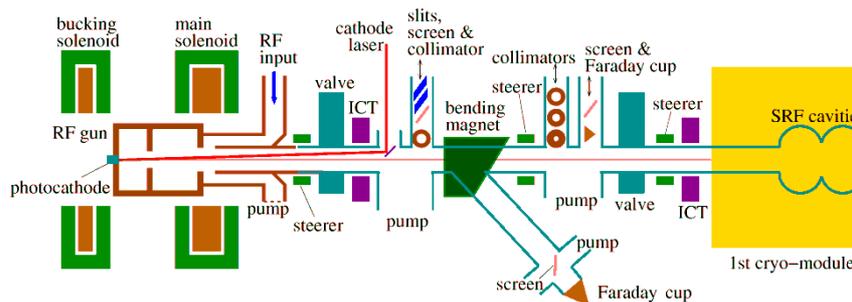
Figure 2: Schematic layout of the baseline injector.

Figure 2 shows a layout of the injector region, comprising the photocathode gun, diagnostics and 1st accelerating module. The baseline electron gun is a modified version of the successful DESY FLASH/XFEL gun, optimised for 1 kHz operation [5]. A detailed FEA study has been carried out to verify operation at 1 kHz using ANSYS [6]. The injector has been optimised using SUPERFISH [7] to calculate the gun cavity field, POISSON for the solenoid field, and ASTRA [8] for the beam dynamics simulation including space-charge. The parameters of the optimisation were the laser spot size, the length of the flat top pulse profile, the location and strength of the solenoids, and the location of the first accelerating module. The resulting performance after the first accelerating module (at ~110 MeV) is given in Table 1 for various operating modes and bunch charges.

Table 1: Optimised injector performance for various operating conditions.

	Short SASE FEL		SASE FEL	seeded FEL
Parameters	**2 pC**	**5 pC**	**50 pC**	**0.2 nC**
projected ε (mm mrad)	0.065	0.116	0.154	0.308
central slice ε (mm mrad)	0.058	0.097	0.143	0.305
length fwhm (ps)	3.5	4	12.5	14.5
central slice $\Delta E/E$	1.0E-6	1.1E-6	3.4E-6	6.2E-6
mean E (MeV)	106.2	106.2	110.2	112.6

A second-stage higher repetition rate gun is also under study. Both VHF normal conducting [9] and L-band superconducting options have been considered and appear suitable; the final choice will requiring further detailed study as well as R&D work.

3.12.2.3 *Linac*

Table 2: Linac accelerating module parameters.

	Optimum	Units
Bunch Charge	200	pC
Repetition Rate	1	MHz
Beam Current	0.2	uA
RF Frequency	1300	MHz
Gradient	15	MV/m
Qo	2.0E+10	
Cavity Length	1.038	m
R/Q	1036	Ohms
Number of Cryomodules	18	
Number of Cavities	144	
Qext	3.7E+07	
RF power per Cavity	4.6	kW
Total RF power	662	kW
1.8K Dynamic load per Cavity	11.7	W
Total 1.8K Dynamic Load	1.7	kW
1.8K Static Load per Cavity	2	W
Total 1.8K Static Load	0.288	kW
Total 1.8K Cryogenic Load	3.0	kW
RF AC Power	1.32	MW
Cryo AC Power	2.96	MW
Total AC Power	4.28	MW

A high repetition rate of equally spaced pulses, initially 1 kHz and increasing in subsequent phases up to 1 MHz, demands superconducting technology for the linear accelerator driver, operating in CW. The accelerating modules will be based on the well developed TESLA/XFEL design with appropriate modifications to accommodate the higher dynamic head load, higher power couplers and higher order mode absorbers demanded by CW operation. A detailed analysis has been carried out to optimise the accelerating gradient taking cost and other factors into account. A total capital + 10-year operating cost shows a broad minimum (within 5%) in the range 14.9-19.2 MV/m, however with electricity costs doubled this would move downwards to 13.3-17.5 MV/m. A nominal gradient of 15 MV/m has been selected which is towards the bottom of the range, not only to take into account likely future electricity cost increases, but also to increase cavity production yield, reduce risk of field-emission and poor cavity performance, and increase reliability and redundancy. This results in a requirement for 18 cryomodules to reach the required 2.25 GeV.

3.12.2.4 *Accelerator Optimisation*

The linac must not only accelerate the beam to the required energy but also create a beam that is suitable for driving a FEL by compressing it longitudinally in order to produce a high peak current (~ kA), while still preserving the high transverse beam quality (normalized emittance) produced by the injector. The operation of the FEL in a seeded scheme adds further constraints to the target beam quality. Not only do the electron beam slice beam parameters have to be constant along the length of the seed laser pulse in order to preserve temporal coherence, but this is required over a length that includes the relative timing jitter between the electron bunch and seed laser pulses.

The final linac configuration that was arrived at following extensive optimisation studies [10] is illustrated in Figure 1. Three bunch compressors (BC1-3) are located at optimised locations to compress the electron bunches while maintaining high beam quality. A 3rd harmonic cavity is included to optimise the beam dynamics by linearising the longitudinal phase space. A laser heater serves to introduce a controlled amount of energy spread in order to overcome the microbunching instability.

The code elegant [11] was used to optimise the linac parameters taking into account the non-linear terms in the RF and the bunch compressors, the effects of collective effects induced by Coherent Synchrotron Radiation (CSR), longitudinal space charge and cavity wakefields. An optimisation strategy for the linac working point (accelerating module gradient and phases, and bunch compressor strengths) was devised, which uses a fast evaluation of the FEL gain length and saturation power for each longitudinal slice of the electron beam using the Xie parameterization [12]. A multi-objective multi-parameter optimiser based on a genetic algorithm with a parallel search [13] was then used to produce an electron bunch with small gain length and high saturation power over as much of the electron bunch as possible. Many thousands of linac configurations were explored and the best solutions were used for further final optimisation. The electron beam properties for the final solution are shown in Figure 3. It can be seen that the bunch has a region of roughly constant FEL gain length of approx. 1.5 m (at 1 keV photon energy) covering more than 100 fs, with 1.2 kA peak current, normalized emittance of approx. 0.35 mm mrad and $< 2 \times 10^{-4}$ relative energy spread.
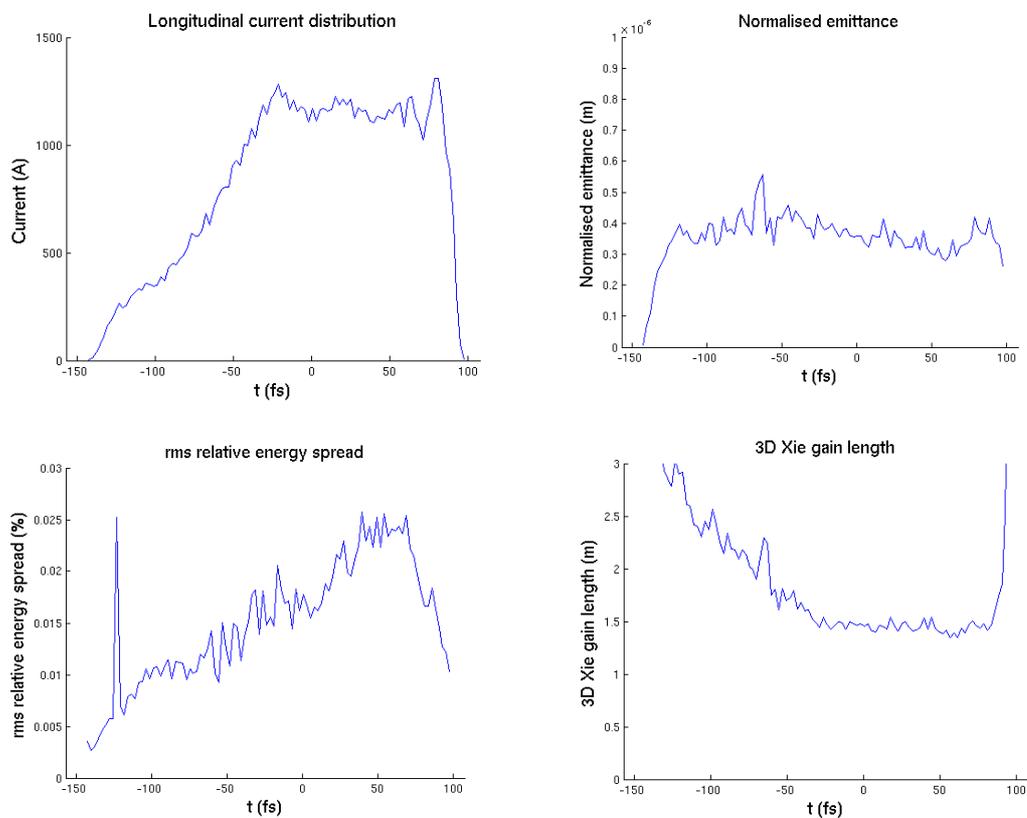
Figure 3: Optimised electron beam properties at the entrance of the FELs.

The final linac configuration was verified using full "start-to-end" simulations, tracking the electron bunch produced in the injector (calculated with ASTRA) through the linac and post-linac collimator and spreader (using elegant) and then importing this distribution into the FEL simulations (using Genesis[14]) to calculate the output radiation (see below). Furthermore, this process has been repeated for "jittered bunches" i.e. complete start-to-end simulations with randomly applied voltage, phase and bunch compressor errors in the injector and linac, to verify the stability of the FEL radiation pulses. The results of these ongoing simulations will be presented in the conceptual design report.

3.12.2.5 *Post-Linac Beam Transport and Collimation*

The linac is followed by a collimation section which is necessary to deal with the beam halo which may be generated by dark current in the injector and in the accelerating modules, scattering from residual gas particles, as well as off-energy beam tails caused by CSR in the bunch compressors [15]. If not collimated, this beam halo can demagnetize the undulator magnets and can activate the components of the facility. The collimation scheme devised for the BESSY FEL design [16] has been adopted for NLS. Transverse collimation is achieved using two betatron collimators separated by $\pi/2$ phase advance in each transverse plane. A dog-leg located after the betatron collimation section contains energy collimators at either or both high dispersion points.

Following the collimation section the beam enters the spreader which consists of a long FODO section with a series of extraction points to direct the individual electron bunches into the different FEL lines, or the diagnostics section. Each extraction section consists of two Triple Bend Achromat (TBA) arcs, in which a kicker and septum replace the first dipole of the first TBA arc. The spreader optics is similar to that of the LBNL design [17] with the addition of sextupoles for a better control of non-linear effects. Such a scheme was chosen for its flexibility to adjust repetition rates for the individual FEL beam lines as well as its adaptability for increasing the number of FEL beam lines in the future. One of the lines parallel to the FELs is a diagnostic section which incorporates a transverse deflection cavity for full slice analysis of the electron beam. With this arrangement sophisticated beam diagnostics can be carried out on-line, by occasionally deflecting bunches into the diagnostics line.

3.12.2.6 *Free-Electron Lasers*

HHG 75-100eV → **Modulator 1** $\lambda_w = 44$ mm   **Modulator 2** $\lambda_w = 44$ mm   **APPLE-II Radiator** $\lambda_w = 32.2$ mm   **FEL3**

e⁻ @ 2.25 GeV →

430 - 1000eV

HHG 75-100eV → **Modulator 1** $\lambda_w = 44$ mm   **Modulator 2** $\lambda_w = 44$ mm   **APPLE-II Radiator** $\lambda_w = 38.6$ mm   **FEL2**

e⁻ @ 2.25 GeV →

250-850eV

HHG 50-100eV → **Modulator** $\lambda_w = 49$ mm   **APPLE-II Radiator** $\lambda_w = 56.2$ mm   **FEL1**

e⁻ @ 2.25 GeV →

50-300eV
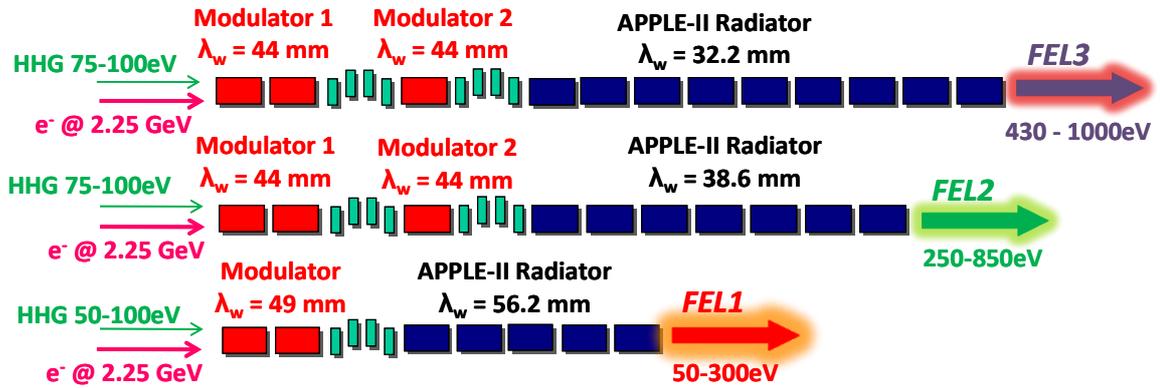
Figure 4: Schematic of the harmonic cascade FEL scheme. Red and blue blocks indicate individual undulator sections, each 2.5 m long.

To provide the required temporal coherence of the FEL radiation each FEL will be seeded with laser pulses, 20 fs long, obtained from High Harmonic Generation (HHG) in gases. Since HHG sources of the required intensity are not currently available above 100 eV, a one- or two-stage harmonic generation scheme is used to provide FEL radiation at up to 1 keV [18, 19], as shown schematically in Figure 4. Figure 5 shows the calculated FEL output from FEL-3 at 1 keV. It can be seen that the pulse is quite smooth, with a width of ~4.7 μm (16 fs) FWHM, a peak power of 2 GW and a linewidth of ~2.3 10^{-4} FWHM. The time-bandwidth product is therefore $\Delta t \Delta f \sim 0.9$, approaching the Fourier Transform limit (0.44). It is believed that this result can be improved with further optimisation of the scheme.
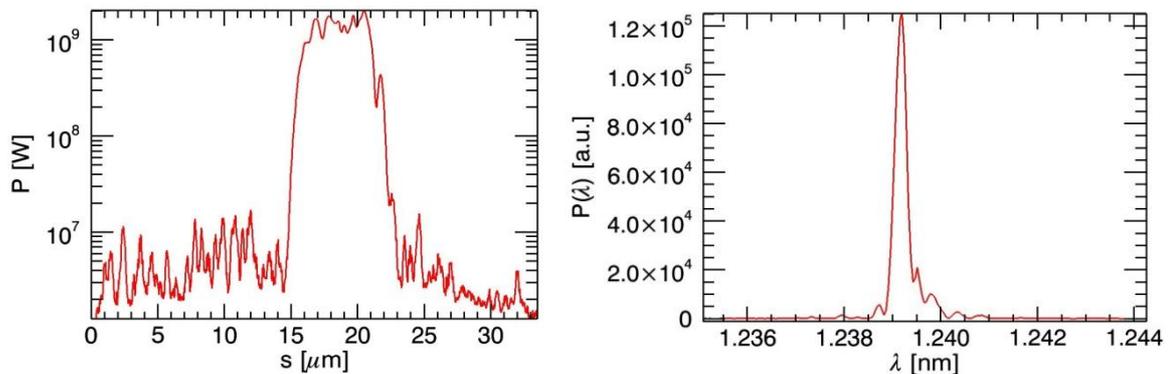
Figure 5: Calculated FEL output at 1 keV.

3.12.2.7 *Experimental Stations*

Eight initial experimental stations are currently planned. Each FEL will have one experimental station with directly focussed beam and one with a grating monochromator to improve spectral resolution and/or filter out unwanted spectral components [20]. In addition a time-preserving grating monochromator is foreseen on FEL-1, and a crystal monochromator on FEL-3 for accessing the harmonics in the range 2-5 keV. The photon beam transport region has been designed to avoid the optical components being damaged by the high peak power of the FEL radiation.

3.12.2.8 *Buildings & Services*

Figure 6 shows the overall layout of the facility. It can be seen that with this particular arrangement the "straight-ahead" direction is unobstructed, which allows the possibility of extending or building additional FEL and Experimental Halls at a later date, with the option also of extending the linac to higher energy.
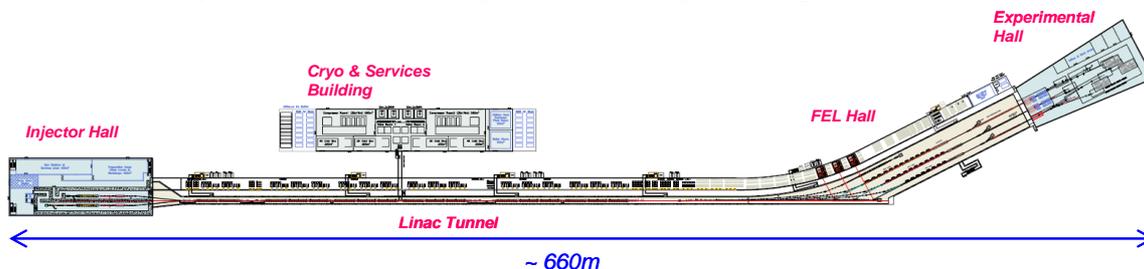
Figure 6: Layout of the NLS facility.

The favoured construction method is illustrated in Figure 7. The linac tunnel is built by shallow "cut & cover" with an earth mound on top. An earlier version saw the RF services building located on top of the earth mound directly above the linac tunnel, however for stability as well as cost reasons this has now been moved to the side, as shown in the figure.
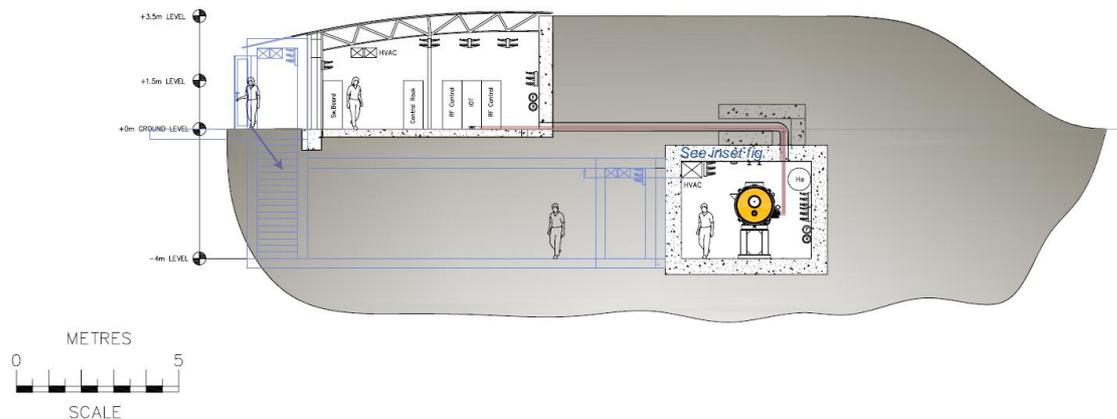
Figure 7: Cross-section of the linac tunnel and RF services building.

3.12.3 **References**

1. http://www.newlightsource.org/
2. NLS Project Science Case & Outline Facility Design, published by STFC, J. Marangos, R. Walker and G. Diakun eds., July 2009, available from [1].
3. P. H. Williams et al., Proc. FEL 2009, p. 336.
4. J. A. Clarke, Proc. FEL 2009, p. 722.
5. J.H. Han et al., Proc. FEL 2009, p. 340.
6. ANSYS v.11, ANSYS, Inc., http://www.ansys.com.
7. J.H. Billen and L.M. Young, "Poisson Superfish", LAUR-96-1834.
8. K. Floettmann, "ASTRA, A Space Charge Tracking Algorithm", http://www.desy.de/~mpyflo.
9. J. W. McKenzie and B. L. Militsyn, Proc. FEL 2009, p. 329.
10. R. Bartolini, Proc. FEL 2009, p. 480.

11. M. Borland, APS LS-287, (2000).
12. M. Xie, Proc. PAC 1995, p. 183.
13. E. Zitzler et al., ETH Technical Report 103, (2001).
14. S. Reiche, Nucl. Inst. And Meth. **A429**, 243, (1999) and http://pbpl.physics.ucla.edu/~reiche/
15. D. Angal-Kalinin, Proc. FEL 2009, p. 538.
16. T. Kamps, "Collimation System for the BESSY FEL", Proc. FEL 2004, p. 381.
17. A. A. Zholents et al "Design of the Electron Beam Switchyard for an array of Free Electron Lasers", CBP Tech Note 401, 2009
18. N. R. Thompson, Proc. FEL 2009, p. 694.
19. B. McNeil, "Novel FEL Schemes", *ibid.*
20. M. D. Roper, Proc. FEL 2009, p. 542.

3.13 Novel FEL Schemes

Brian McNeil
University of Strathclyde, Department of Physics, SUPA,
107 Rottenrow, Glasgow, G4 0NG, Scotland
Mail to: b.w.j.mcneil@strath.ac.uk

3.13.1 Introduction

The following describes some ideas for new types of FEL sources which have been studied by UK researchers over the past few years. The aims of many of the ideas are to improve the temporal coherence and shorten the duration of the light pulses generated. While some of the work was directed towards specific FEL projects (the now defunct 4GLS and NLS projects) other work is more general.

3.13.2 Regenerative Amplifier, Low-Q Cavity FELs

An interesting type of FEL that has yet to be demonstrated at photon energies in the VUV and beyond is the Regenerative Amplifier FEL (RAFEL). These sources have the potential to generate trains of pulses with high peak and average powers of very good temporal coherence with near Fourier transform limited pulses.

In essence the RAFEL is a high gain FEL amplifier, which is shorter than the high gain SASE saturation length, placed inside a low-Q cavity. The cavity provides sufficient feedback to dominate shot-noise at the beginning of the undulator and to allow the amplifier to saturate. For laboratory scale cavity lengths such a set-up requires electron bunches entering the cavity at frequencies in the MHz range such as those that can be provided by a super-conducting Energy Recovery Linac (ERL). Like cavity-based FELs in the IR, the design allows cavity length tuning of the radiation pulse length.

Such a RAFEL design was incorporated into the 4GLS project in the UK. This RAFEL was designed to generate radiation pulses in the 3-10eV photon energy range [1]. Because little was available in the literature on RAFEL design at shorter wavelengths, significant effort went into ensuring that, at least using full 3D FEL and cavity optics simulations [2], such a system would indeed work. The RAFEL design at these photon energies and with a cavity feedback factor of the output power to the

undulator entrance of only a few percent proved to be very robust with respect to cavity tolerances.

In order to investigate how small the cavity feedback factor could be reduced while retaining good temporal coherence, a generic RAFEL design, shown in Fig. 1, using scaled units was considered [3].
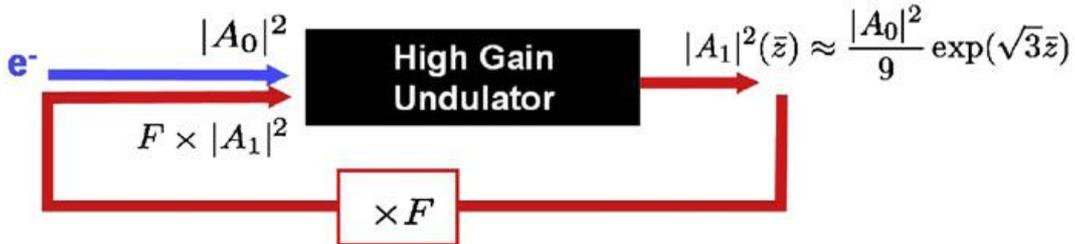
Figure 2: Schematic showing a generic high gain RAFEL system.

The feedback fraction F, required to optimise the temporal coherence and the output power $|A_1|^2$, was found to occur when the feedback power $F \times |A_1|^2$ is approximately double the shot noise power $|A_0|^2$. This may be achieved with cavity feedback factors as surprisingly low as $F \approx 5 \times 10^{-6}$.

Using the optimum feedback fraction, the average time bandwidth product is only double that of a Fourier transform limited Gaussian pulse. This is more than five times better than the equivalent SASE result. These results indicate that there is significant scope in extending the low feedback RAFEL concept to photon energies in the XUV and possibly further. The possibility of combining harmonic generation methods and RAFELs also exists and these exciting possibilities will be the subject of future research.

3.13.3 Near Fourier Transform Limited FEL at 1 keV Photon Energy

One of the main problems of an FEL high-gain amplifier that starts from the intrinsic spontaneous noise signal (Self Amplified Spontaneous Emission) is that the output consists of a series of chaotic spikes with poor temporal coherence [4]. (An exception occurs if the electron pulse is sufficiently short that it generates only one such spike, however the peak radiation power and pulse energy is lower.)

A method of improving the temporal coherence is to seed the FEL interaction with a coherent laser signal at the FEL resonant wavelength that dominates that of the spontaneous noise signal. The amplified seed retains its, assumed good, initial temporal coherence properties. This was the approach taken in the UK's 4GLS project which had an FEL amplifier designed to operate in the 10-100eV photon energy range and seeded by a 'conventional' High Harmonic Generation laser source [1, 5]. However, this approach does not work if no such seed exists at the fundamental FEL resonant wavelength!

This was the case for the design specification of the UK's New Light Source project [6] which aims to generate temporally coherent pulses of up to 1keV photon energy in pulse durations of ~20fs. Other FEL designs which attempt to generate such output e.g.

[7, 8] use the method of High Gain Harmonic Generation (HGHG) [9] to attain these temporally coherent photon energies.

A schematic of the scheme is shown at the top of Fig. 2. The high power seed laser ($\lambda \sim 250$nm) interacts with the electron beam within a short modulator undulator resonant with the laser seed. The interaction generates an energy modulation in the electron bunch of period equal to the seed laser wavelength. The electron bunch is then passed through a magnetic chicane to convert the energy modulation into a periodic density modulation, or bunching at the laser wavelength. There are also Fourier components of the bunching at higher harmonics of the seed laser wavelength. On passing into a radiator undulator tuned to one of these higher harmonics, the bunch radiates strongly and coherently at the harmonic wavelength. In principle, the process can now be repeated using this harmonic radiation to act as the new modulating seed. However, the process needs to be shifted to a 'fresh' part of the electron bunch, which has not undergone any previous energy modulation, to alleviate the effects of a deteriorating electron beam energy spread. This shifting is achieved by the 'Fresh Bunch Chicane'. If the 3rd or 5th harmonic is generated at each stage then 4 stages would be required to reach the target 1keV photon energy (1.24nm).
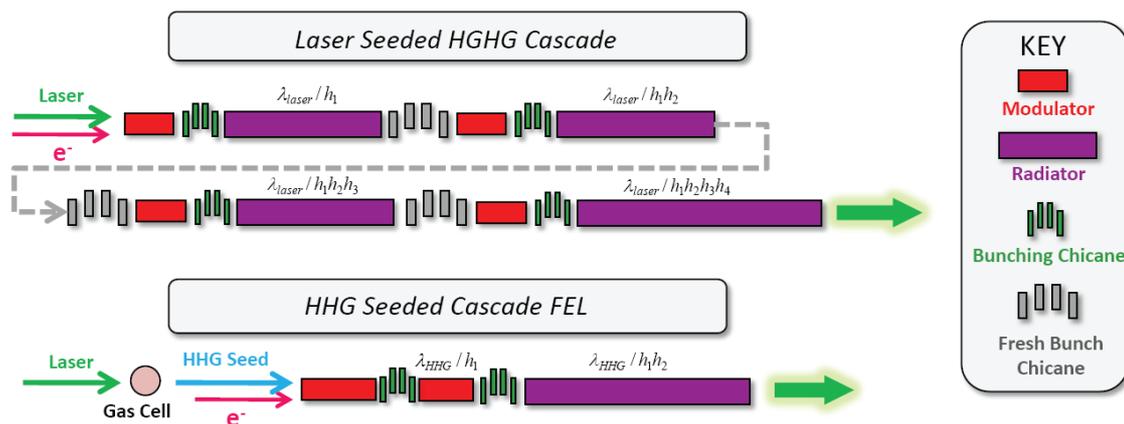
Figure 3: Schematic comparing the layout of two FEL schemes—the Laser Seeded HGHG Cascade FEL (top) and the HHG Seeded Cascade FEL (bottom).

In the scheme proposed for NLS [10] is shown in the bottom schematic of Fig. 2. (This scheme has similarities with the University of Wisconsin-Madison's WiFEL proposal for a XUV/soft x-ray FEL facility [11].) The first two stages of the HGHG scheme are effectively replaced by using an High Harmonic Generation laser system to generate radiation at ~12nm. Only two 3rd harmonic stages are then required to obtain the target ~1keV photon energy. For the first stage the power available from the 12.4 nm HHG seed is significantly lower than that available from the 250nm seed of the HGHG scheme. The first modulator undulator must therefore be longer to achieve the required energy modulation – the high-gain FEL interaction is used to amplify the seed and electron bunch energy modulation amplitude. Furthermore, the FEL interaction itself develops the required density modulation so that the chicane before the first harmonic radiator is used to simply enhance and/or optimize the bunching. As with the HGHG scheme this density modulation, or bunching, contains higher harmonic components, and after the first chicane the electron bunch enters an undulator tuned so that it's fundamental is resonant at one of these harmonics. Unlike HGHG this

undulator acts primarily as another modulator, not a radiator. The second chicane is then used to optimize the harmonic bunching of this interaction before the electron bunch enters the final radiator undulator tuned so that its fundamental is resonant at one of the harmonics of the second modulator. An initial strong coherent emission is generated in the final radiator and then amplified exponentially to saturation. Because the radiation power never approachs saturation value within the first and second modulators, the energy spread within the seeded part of the bunch is sufficiently small to allow exponential growth in the final radiator. Hence, the electrons are sufficiently 'fresh' to negate the need for the 'fresh bunch' bunch chicanes.

Results of a full 3D simulation [10] using a realistic electron bunch generated from a start-to-end simulation that has undergone laser heating [12] of the NLS design scheme operating at 1 keV photon energy are shown in Fig. 3. Both the temporal duration of ~11fs and the time-bandwidth product of $\Delta \nu\, \Delta t \approx 1$ demonstrate that good quality FEL output can be generated up to the ~1 keV photon energy level.
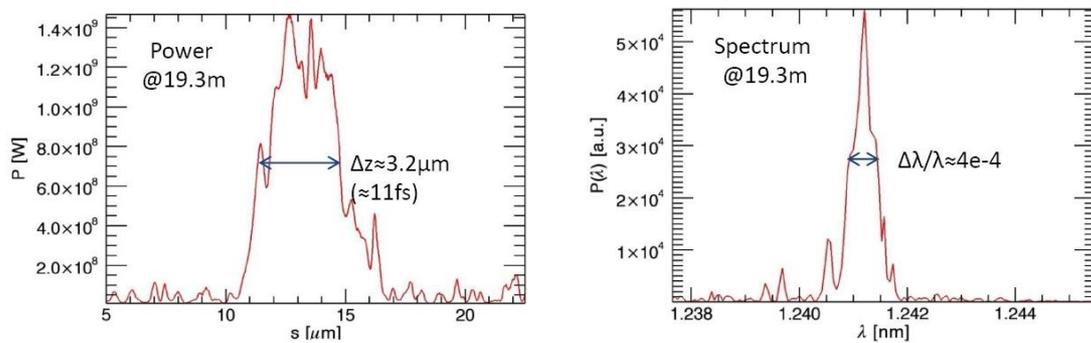
Figure 4: Genesis 1.3 simulation results of the NLS FEL-3 operating at 1 keV, using a realistic electron bunch with a laser heater. Left shows the output pulse temporal profile. Right shows the pulse spectrum.

3.13.4 Axial Mode Generation and Locking in a FEL Amplifier

With the advent of coherent x-rays at 1.5Å from LCLS [13, 14] and with several similar sources under construction or proposed, the ability to achieve bright spatial imaging of atomic processes is now possible. The next major milestone in light source development will be to achieve temporal resolution on the attosecond timescale which will then give science the ability to resolve atomic and molecular processes on the spatiotemporal scales at which they naturally occur.

It is no surprise, then, that there is significant effort pursuing this goal in FEL designs (see [15] and refs. therein.) Here, we focus on the ideas on the generation and locking of axial modes in an FEL amplifier presented in [16] and extended in [17, 18].

The concept of mode-locking in a FEL amplifier uses similar concepts borrowed from conventional cavity lasers where mode locking [19] is able to reduce pulse lengths down to a few femtoseconds. In these conventional lasers, the axial modes of the laser cavity have a frequency separation of $\Delta\omega = 2\pi c / s$, are usually uncoupled and have little or no relative phase relationship between them. This results in a c.w. output with a varying power envelope from the laser. By introducing a modulation in the lasing interaction at the cavity mode separation, each mode develops sidebands that overlay neighbouring modes and allow a coupled mode interaction. This can lock in a phase relationship between each mode. When this locking occurs, the wavefronts of each

mode constructively interfere only at certain periodic output times, spaced by the round trip-time of the cavity, $s/c = 2\pi/\Delta\omega$, to generate a train of short pulses.

In a FEL amplifier, the fact that the electrons and light are co-propagating at nearly the same velocity can be used to synthesis such a cavity-like interaction. This is achieved by introducing a periodic enhanced slippage of the light ahead of the electrons by means of magnetic chicanes that slow down the electrons. Fig. 4 shows a schematic of such an undulator/chicane lattice.
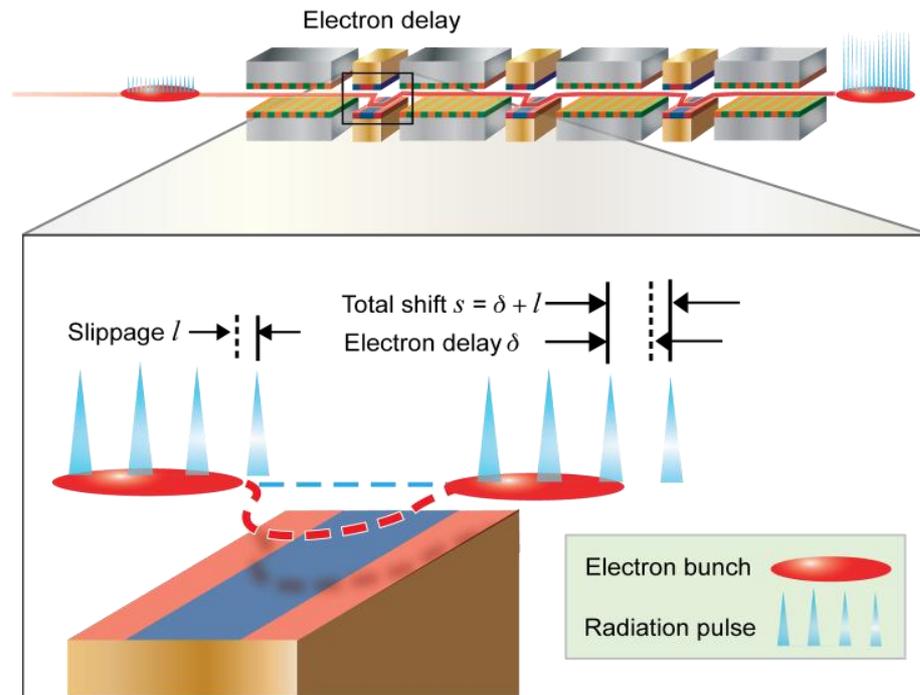
Figure 5: Schematic showing the undulator/chicane lattice for a mode-locking FEL scheme. The detailed inset shows the electron bunch slippage with respect to the light: l occurring in each undulator section and δ in each chicane.

Only those light frequencies that interfere constructively after successive chicane slippages with respect to the electron bunch will survive, giving rise to a set of modes with frequency separation of $\Delta\omega = 2\pi c/s$. These modes are analogous to those of a conventional cavity laser. Indeed a simple analysis in [16] demonstrates that the modal structure generated is formally identical with those of cavity.

Mode coupling may be achieved by simply modulating the electron beam energy at the mode spacing $\Delta\omega$. When this is done then 3D simulations predict that such a mode-locked FEL amplifier operating in the x-ray can generate a train of 23as pulses.
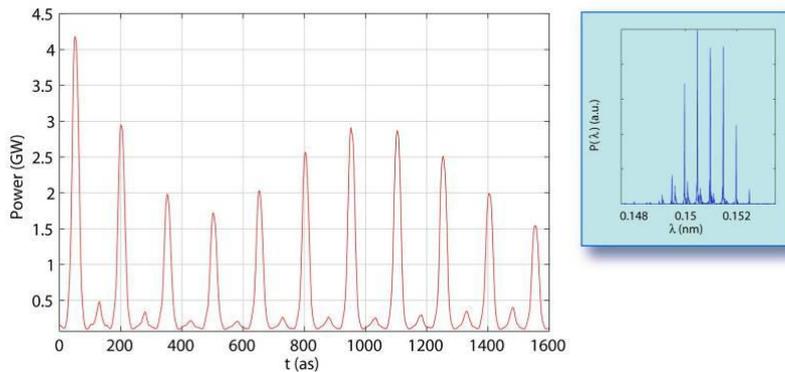
Figure 6: Simulation of a mode-locked FEL amplifier output at 0.15 nm showing a train of 23as pulses (left) and the corresponding power spectral density (right).

When realistic electron pulses generated from start-to-end simulations are used in 3D simulations, the mode-locking in the FEL appears to be robust with clean modes and well-formed attosecond pulse trains generated [18].

There is now significant interest in seeding FEL amplifiers with HHG seeds in the XUV and soft x-ray. Under normal FEL amplification the interesting attosecond pulse train structure of the HHG seed is 'washed out' by the FEL amplifier [5]. Simulations show, however, that by matching the HHG seed pulse train structure with a mode-locked FEL amplifier, the attosecond pulse train structure of the HHG seed may be retained during amplification [17, 18].

3.13.5 **The Quantum Free Electron Laser (QFEL)**

Several large international teams are constructing free electron lasers (FELs) to produce X-ray radiation via self amplified spontaneous emission (SASE) [13, 21, 22]. While the brightness of SASE-FELs far exceeds that of conventional synchrotron sources, the radiation produced by SASE-FELs is not ideal for many applications requiring a high degree of temporal coherence as the pulses produced contain many random superradiant spikes with a broad noisy spectrum [4].

A possible alternative to classical SASE-FEL emission for coherent short-wavelength generation arises from the fact that in quantum theory the radiation emission process is fundamentally discrete. When an electron emits a photon, the momentum recoil is ℏk, where k is the photon wavenumber. Hence, the electron momentum recoil is naturally quantized and can change in only discrete amounts. Including the effects of recoil in a quantum FEL (QFEL) theory, the number of photons emitted depends on the QFEL parameter, $\bar{\rho}$ [23] which is the ratio of the maximum classical momentum spread ($\sim \rho mc\gamma_r$) to the photon recoil momentum (ℏk) i.e. $\bar{\rho} = \rho \frac{\gamma_r mc}{\hbar k}$, where ρ is the classical FEL gain parameter [24] and γ_r is the Lorentz factor of a resonant electron. When $\bar{\rho} \gg 1$ many momentum levels are involved in the interaction, the discreteness of the momentum exchange becomes irrelevant and one recovers the classical behaviour characterised by a random series of superradiant spikes and a broad, chaotic spectrum. Conversely, when $\bar{\rho} \leq 1$ an electron emits a single photon and makes a single transition between momentum states, resulting in a single

128

narrow line. Hence, the QFEL appears promising as a quasi-monochromatic X-ray source (although at lower powers than in a classical SASE-FEL).

For an experimental realization of a QFEL it is necessary to use a laser wiggler in a Compton backscattered configuration instead of the magnetic wiggler usually used in classical SASE-FEL experiments [13, 21, 22]. In a laser wiggler configuration, a low-energy electron beam back-scatters a counter-propagating high power laser into photons frequency up-shifted by a factor $\approx 4\gamma_r^2$. Such a choice sets some stringent conditions on the electron and laser beam parameters [25]. One possibility being investigated involves the new generation of laser-driven wakefield accelerators [26]. Appealing features of this configuration are that both the electron beam and the laser wiggler are contained in a guiding structure and that the all-optical character of the configuration should allow it to be relatively compact.

3.13.6 The Light Well – A Step towards Nano-FELs?

The prospect of a nanoscale, continuously tunable light source is an enticing one for many applications requiring wavelength tunability with a high degree of spatial resolution. Such a source would allow mapping of various excitations in nanostructures over a range of energies and could be incorporated in nanophotonic circuits, displays or memories. Progress towards such a source, and perhaps a first step towards a nanoscale continuously tunable, coherent *laser* source, has been made through the generation of tunable light by a beam of electrons passing through a hole drilled in a nanostructure – a device termed a "light well"[27].

Free electrons generate light when passed through or close to a periodic structure. In free electron lasers, an electron beam is passed through a periodic, magnetostatic wiggler, whereas in Smith-Purcell radiation sources the electron beam passes close to a metal grating. In the light well [27] the periodic structure is a stack of alternating metal (Au) and dielectric (SiO_2) layers, each with a thickness of approximately 200nm. In this stack, a narrow (700nm diameter) hole was drilled and a narrow electron beam with a diameter of 30 nm from a scanning electron microscope was guided through it causing light to be emitted from the hole. Increasing the electron beam energy from around 20 keV to 40 keV, the wavelength of the light produced by the well was tuned from approximately 900nm down to 800nm. The emission mechanism appears related to Smith Purcell radiation from the periodic metal layers, but it is possible that other free electron emission mechanisms associated with the dielectric layers may also be present e.g. Cerenkov radiation and transition radiation [28].

In addition to wavelength tunability, it was demonstrated in [1] that emission from the light well was incoherent with power levels of around 0.1nW, so it is clear that the electrons passing through the light well are emitting spontaneously and the device is not yet operating as a laser. In order to move to a regime of coherent, stimulated emission and lasing it will be necessary to increase the length of the interaction region by the addition of more layers (11 layers were used in the experiments reported in [27]), control losses in the system e.g. surface plasmon generation, and increase the electron beam current while maintaining high beam quality. Whether the technical challenges associated with the higher beam currents and much higher radiation powers involved with a regime of coherent lasing (e.g. electron beam focussing and power dissipation) can be overcome remains to be seen.

3.13.7 **Simulation Code Development**

Finally, much of the work presented here relies upon the predictions of computational simulation codes. These codes are essential development tools that allow FEL scientists to explore new designs and ideas without the need for costly experiments. As FEL science develops, relying on more complex schemes and clever ideas, so the physics that is modelled and flexibility of these codes must develop. To this end, a parallel code has been under slow development over several years that can now model effects previously absent from simulations. In particular, modelling of electron/radiation interaction in 3D without constraints on the energy exchanged between electrons and light is now possible and is described in [20]. Furthermore, this code is able to model sub-wavelength effects that previous averaged codes cannot. It can also model FELs with variable polarisation undulators and include the effects of chicanes such as are required for HGHG [9], EEHG [15] and mode-locking [16-18] schemes. It is hoped that the code can be made available to the community in the not-to-distant future.

3.13.8 **References**

1. 4GLS Conceptual Design Report reference page: http://www.4gls.ac.uk/documents.htm
2. B.W.J. McNeil, N.R. Thompson, D.J. Dunning, J.G. Karssenberg, P.J.M. van der Slot and K.-J. Boller, New Journal of Physics 9, 239, 2007
3. D.J. Dunning, B.W.J. McNeil and N.R. Thompson, Nucl. Inst. Meth. Phys. Res. A593, 116, 2008
4. R. Bonifacio, L. De Salvo, P. Pierini, N. Piovella and C. Pellegrini, Phys. Rev. Lett. 73, 70, 1994
5. B.W.J. McNeil, J.A. Clarke, D.J. Dunning, G. J. Hirst, H.L. Owen, N.R. Thompson, B. Sheehy and P.H. Williams, New Journal of Physics 9, 82, 2007
6. Richard Walker, 'The New Light Source Project', ibid., and references therein.
7. D. Kramer et al., 'The BESSY Soft X-ray Free Electron Laser Technical Design Report', Berliner Elektronenspeicherring-Gesellschaft fur Synchrotronstrahlung m.b.H., 2004
8. FERMI@elettra Conceptual Design Report, Sincrotrone Trieste, 2007
9. L. H. Yu, Phys. Rev. E 44, 5178, 1991
10. N.R. Thompson, D.J. Dunning, B.W.J. McNeil and R. Bartolini, WEOD02, Proceedings of the 31st International FEL Conference, Liverpool, UK , 2009
11. J.J. Bisognano, Conceptual Design Study and R&D for a VUV/Soft X-ray Free Electron Laser User Facility, http://wifel.wisc.edu/, 2007
12. R. Bartolini, C. Christou, J.H. Han, I.P.S. Martin, J.H. Rowland, M.Venturini, D. Angal-Kalinin, F. Jackson, B. Muratori and P. Williams, WEOB02, Proceedings of the 31st International FEL Conference, Liverpool, UK , 2009
13. P. Emma et al., First Lasing of the LCLS X-Ray FEL at 1.5Å , Proceedings of PAC '09
14. D. Ratner et al., TUOA03, Proceedings of the 31st International FEL Conference, Liverpool, UK , 2009
15. D. Xiang, Z. Huang and G. Stupakov, MOPC80, Proceedings of the 31st International FEL Conference, Liverpool, UK , 2009 and refs. therein.
16. N.R. Thompson and B.W.J. McNeil, Phys. Rev. Lett. 100, 203901, 2008
17. B.W.J. McNeil, N.R. Thompson, D.J. Dunning and B. Sheehy, MOCAU04 Proceedings of the 30th International FEL Conference, Gyeongju, Korea, 2008
18. D.J. Dunning, N.R. Thompson, P.H. Williams and B.W.J. McNeil, MOPC69, Proceedings of the 31st International FEL Conference, Liverpool, UK , 2009

19. A. E. Siegman, Lasers (University Science Books, Sausalito, USA, 1986). See Chap. 27.
20. L.T. Campbell, R. Martin and B.W.J. McNeil, MOPC39, Proceedings of the 31st International FEL Conference, Liverpool, UK , 2009
21. F. Richard et al. (eds.), TESLA Technical Design Report,DESY2001-011, and http://tesla.desy.de.
22. T. Shintake, "Status of the SCSS Test Accelerator and XFEL Project in Japan" EPAC'06, Edinburgh 2006.
23. R. Bonifacio, N. Piovella, G.R.M. Robb, and A. Schiavi, Phys. Rev. ST Accel. Beams 9, 090701 (2006).
24. R. Bonifacio, C. Pellegrini and L. Narducci, Opt. Commun. 50, 373 (1984).
25. R. Bonifacio, N. Piovella, M.M. Cola, and L.Volpe, Nucl. Instrum. and Meth. in Phys. Res. A577, 745 (2007).
26. D.A. Jaroszynski et al., Phil. Trans. R. Soc. A 364, 689 (2006).
27. G. Adamo et al, Phys. Rev. Lett. 103, 113901 (2009).
28. C. Luo, M. Ibanescu, S.G. Johnson & J.D. Joannopoulos, Science 299, 368 (2003).

Neutron Science

3.14   ISIS – The World's Leading Spallation Neutron Source

D J S Findlay, A P Letchford, G H Rees, J W G Thomason, C M Warsop *et al.*
ISIS, Rutherford Appleton Laboratory, STFC, Oxon. OX11 0QX, UK
Mail to: david.findlay@stfc.ac.uk

3.14.1 Introduction

Under its director Andrew Taylor, ISIS has become the world's leading spallation neutron source in terms of science output. Other spallation neutron facilities may run at higher beam powers, but ISIS remains in leading place in terms of science output.

This section on ISIS is split into two parts: ISIS operations, and accelerator developments at ISIS. The accelerator development section is split two subsections: Front End Test Stand (FETS), and ISIS upgrades.

3.14.2 ISIS operations

ISIS is the world's leading spallation neutron source, and each year on average ~750 experiments on investigating the structure and dynamics of molecular matter are carried out involving ~1500 visitors who make a total of ~4500 visits (these numbers include roughly ~100 experiments and ~300 visits for muons). An 800 MeV proton synchrotron fed by a 70 MeV H⁻ injector linac (itself fed by a 665 keV RFQ) delivers beam powers of ~200 kW which can be split between two target stations. Typically ISIS runs for users for ~180 days a year (on a 24-hours-a-day basis); in addition some ~40–50 days a year are scheduled for running up equipment and for machine physics.

The original ISIS target station, now called TS-1, produced its first neutrons in December 1984, and is based on a fast-neutron-producing target configured as a series of water-cooled tantalum-clad tungsten plates. The second target station, TS-2,

produced its first neutrons in August 2008 and is optimised for the production of cold neutrons; it is based on a solid water-cooled cylinder of tantalum-clad tungsten (the target has been made as compact as possible to allow the moderators to intercept as much fast neutron flux as possible). Normally the synchrotron runs at 50 Hz, with 40 Hz and 10 Hz beams being delivered to TS-1 and TS-2 respectively. A muon-production target is incorporated in the proton transport beam line to TS-1. More information may be found at [1].

When TS-2 came into use, the repetition rate of the proton beam pulses to TS-1 was reduced from 50 to 40 Hz, but in order to maintain beam current to TS-1 the current delivered by the synchrotron has been increased by the addition of a second harmonic component to the synchrotron RF drivers [2]. Four second harmonic (2RF) ferrite-loaded cavities were added to the existing six fundamental RF (1RF) ferrite-loaded cavities. As well as enabling a ~30% increase in beam current from the synchrotron, the 2RF systems have also reduced beam losses around injection.

In order to offset the effect of ageing equipment (some of the equipment was already second-hand when ISIS was built), ISIS has been running a capital refurbishment programme for some years. Currently this programme is running at a level of ~5–10% of the operating costs.

3.14.3 Accelerator Developments at ISIS

3.14.3.1 *Front End Test Stand*

The Front End Test Stand (FETS) under construction at ISIS is the first stage of R&D towards a future H⁻ linac for ISIS upgrades. However, the design is completely generic, and so it addresses the requirements of a whole range of proposed future projects which will need a high-power injector linac including a neutrino factory, muon collider, accelerator driven sub-critical system, *etc.* The stated aim of FETS is to demonstrate the production of a high-current chopped H⁻ beam at 3 MeV of sufficient quality to meet the requirements of the next generation of high power linacs.

The work on FETS has been carried out through a series of fruitful collaborations between ISIS, STFC's Accelerator Science and Technology Centre (ASTeC), Imperial College in London, Warwick University, Royal Holloway University of London, and the University of the Basque Country and their commercial partners. These collaborations have been vital for making good progress on FETS, and have resulted in the training of young people new to the field as well as the exchange and sharing of ideas and hardware.

FETS will consist of an H⁻ ion source, magnetic low energy beam transport (LEBT), 3 MeV radio frequency quadrupole (RFQ), and medium energy beam transport (MEBT) containing a high speed beam chopper. In addition to conventional beam diagnostic devices, non-destructive laser diagnostics techniques are also being pursued.

The FETS ion source is a development of the highly successful ISIS H⁻ Penning-type surface plasma source. The generic beam performance specification for FETS calls for 60 mA of H⁻ ions at 65 keV in pulses of up to 2 ms at 50 pps with a normalised RMS emittance of 0.25-π mm-mrad, a considerable improvement over the standard ISIS operating parameters. An extensive programme of experimental and theoretical work has led to a far better understanding of the ISIS ion source and its performance limitations. This investigation has informed re-designs of the extraction electrode geometry, the 90° analysing magnet and the post-acceleration gap to remove beam

aberrations and reduce the beam size and emittance. The ion source has been routinely running on FETS producing >50 mA under optimum conditions. Pulses of 1.5 ms have been extracted, but power supply upgrades are necessary before the full 2 ms can be achieved at the maximum repetition rate. Other than the power supply limitation, no barriers to achieving the full duty factor are foreseen. As well as increasing the pulse length, a new extraction power supply being designed will allow the extraction voltage to be increased from 18 kV to 25 kV, further increasing beam current and improving beam quality. Since first operating the source on FETS a full parametric characterisation of the beam parameters has been carried out using a combination of scintillator profile measurements, slit-slit emittance measurements and full 4-D phase space measurements using a state-of-the-art pepper-pot scanner. This helps in understanding the source behaviour and provides realistic starting data for computer simulations of the subsequent stages of FETS.

A small-angle version of the FETS ion source, without the 90º magnet, has been given to our Spanish colleagues to investigate on the ESS Bilbao ITUR test stand. It is expected that data from these experiments will prove useful in further understanding the source performance as well as promoting progress on the Spanish accelerator R&D programme.

The beam from the ion source is transported and matched into the RFQ by a magnetic LEBT using solenoids. Based on the successful design of a similar LEBT for the ISIS RFQ upgrade, three solenoids have been chosen. Although in principle two solenoids may be sufficient, particularly for highly axi-symmetric beams, it is felt that three solenoids gives greater flexibility in the case of the non-symmetric beam from the slit extraction geometry of the Penning source, although a possible disadvantage is slightly greater stripping losses in the residual gas of the rather long LEBT. The LEBT is 1.7 m long and contains a pumping and diagnostic vessel between the second and third solenoids. This vessel houses two beam current transformers and a combined fast Faraday cup and beam stop. The solenoids are 30 cm long with a beam-pipe bore of 80 mm and were supplied by Tekniker through our collaboration with ESS Bilbao at the University of the Basque Country. Magnetic field measurements made at the Daresbury Laboratory were in very good agreement with computer models of the magnets produced during their design. The 27 V, 250 A solenoid power supplies were also supplied as part of our collaboration with ESS Bilbao and were manufactured by Jema. The LEBT is fully installed on FETS and is undergoing commissioning at this time. The first, very preliminary, beam measurements indicate an RMS emittance of ~0.3-π mm-mrad for a current of ~50 mA. Further optimisation of this is expected.

FETS will employ a 3 MeV, 4-vane RFQ operating at 324 MHz. The frequency choice was dictated by the ready availability of a suitable klystron developed by Toshiba for the J-PARC linac. Although designed for short-pulse high-peak-power operation it is capable of being operated in a low-power long-pulse mode as required by FETS. The beam dynamics design of the RFQ gives a structure 4.2 m long with beam transmission >95% and minimal emittance growth. Further slight optimisation of this design is expected before manufacturing commences. The current focus is on the mechanical design which it is hoped will overcome some shortcoming in previous RFQ designs of this type. The intention is to have three or four resonantly coupled sections to the RFQ, each section constructed from two major and two minor segments. The method to be used to join the segments together is still under investigation and is unlikely to involve vacuum brazing as is traditional. Electron beam and laser welding

are being looked into with assistance from The Welding Institute. A joining method which would allow disassembly at a future date is also being pursued, as repair of a fully welded or brazed structure is either very difficult or impossible, and some RFQs in operation have developed problems after commissioning. Various machining and joining test pieces will be manufactured soon to validate these ideas. Thermal modelling is progressing, aiming to achieve a cooling strategy which results in minimal resonant frequency drift under expansion. The structure will then be tuned by fixed and moveable slug tuners. A short cold model has been manufactured at Imperial College to test some machining and joining methods and to verify the integrity of the electromagnetic simulations; agreement between simulations and measurement were very good. An auto-tuner and digital I-Q RF control system has been developed at the University of the Basque Country and will be tested at low-power levels using the cold model. Because the cold model contains many of the features of a complete RFQ including vacuum pumping ports, it is hoped to mount it on the FETS beam line and transport a low energy beam through it at medium RF power levels as a first test of beam matching using the LEBT. Development of the FETS RFQ has used an integrated design method whereby the same model is used for mechanical, thermal, electromagnetic and beam dynamics simulations. Although this has required significant development effort it offers the advantage of not having to transfer designs and data between many different formats and codes, and allows for changes to be quickly propagated through the various design stages.

The 3 MeV beam from the RFQ will be transported through the MEBT which, in any complete linac, will match the beam into the following accelerating structure — most likely a drift tube linac (DTL). The MEBT also contains the very high speed beam chopper which will be essential for any linac that has to inject into a circular accelerator. Trapping the injected beam into the RF bucket in, for example, a synchrotron is a significant source of beam loss. As future high-power accelerators will be beam-loss-limited if hands-on maintenance is to be possible, controlling this loss is imperative. Very significant reductions in the trapping loss can be achieved by chopping the linac beam at the ring revolution frequency so as to inject a beam already bunched at the ring RF frequency rather than having to form the bunches after injection and incur inevitable beam loss. For a variety of technical and physical reasons the best place to achieve this linac beam chopping is at an energy of a few MeV just after the RFQ. Because the beam after the RFQ will be bunched at 324 MHz with a bunch-to-bunch spacing of ~3 ns, the chopper deflector must switch on and off in less than 2 ns if the chopping process is not to result in some partially chopped bunches. To achieve the required deflection of the chopped part of the beam so that it can be collected on beam dumps, a deflecting voltage of 1–2 kV is required. Achieving such high voltages with such short rise and fall times is a major challenge. The FETS chopper design utilises a two-stage chopping scheme whereby a very fast chopper creates short gaps in the bunch train which allows space for a slower, though still fast, chopper to turn on and chop the majority of the bunches to be removed. This novel approach overcomes the requirement for both very high bandwidth and relatively long flat tops to the chopper pulses. The electronic pulsers developed at ISIS have already achieved the specification in terms of voltage and rise and fall times. Several options for the chopper deflectors are under investigation and are being prototyped at the moment. Due to the requirement for preservation of the sharp pulse shape throughout the whole length of the chopper slow wave deflector, control of the bandwidth and pulse reflections is paramount. Utilising

the very high precision manufacturing facility used for millimetre wave technology at RAL, prototypes of the chopper components and currently being evaluated.

The design of the beam optics lattice into which the chopper deflectors and beam dumps have to be incorporated is very challenging. Due to the length of the chopper components the natural periodicity of the lattice is broken which has consequences for beam quality. To keep emittance growth low under such conditions a short MEBT is needed which conflicts with various engineering requirements. An alternative approach where the chopping is distributed along a longer but strictly periodic MEBT is also being investigated for FETS. Although inevitably much more expensive than the short MEBT designs, this offers the possibility of clean chopping and also minimal emittance growth together with more space for beam diagnostics. The computer modelling of the quadrupoles and re-bunching cavities for the MEBT has started, and the first cold models of the cavities will be produced through our Spanish collaboration later this year.

On any test stand, diagnostics are vitally important. FETS will use all the traditional beam measurement devices such as beam current transformers and intercepting profile and emittance measurement devices. However, due to the very high beam powers to be achieved, non-destructive methods are of great interest. In particular laser photo-detachment techniques are being pursued. Because the extra electron on the H^- ion is weakly bound it can be easily detached by a laser of a suitable wavelength. The resulting electrons or H^0 ions can then be collected for analysis. On FETS, laser photo-detachment will be used for both fully 2-D profile measurements and also emittance measurements. The first experiments used a small laser system to measure the beam profile immediately after the ion source and before the LEBT. Due to the relatively high pressure in this region so close to the source which leads to significant beam interactions with the residual gas and also a rather poor coupling of the available laser power into the particle beam, a very low signal-to-noise ratio was achieved with the photo-detached electron signal being swamped by electrons and ions reaching the detector from background gas ionisation. A recently initiated collaboration with the Laser Diagnostics Group at Royal Holloway University of London is leading to a better understanding of the laser optics to help couple more laser power into the beam as well as to greatly improved detector electronics to discriminate between the required signal and noise. FETS has also recently borrowed a higher power laser from colleagues at J W Goethe University in Frankfurt which will further improve the number of photo-detached electrons available for detection. With the combination of the more powerful laser, better optics and better electronics, it is hoped to demonstrate laser profile measurement within the next few months. For the later stages of an H^- linac where the vacuum is considerably better than in the ion source region, discrimination of photo-detachment and residual gas interaction signals should be much easier, so proof of principle at the source will prove viability at higher energies.

3.14.3.2 *ISIS Upgrades*

A detailed comparison of reasonable upgrade routes for ISIS that will provide a major boost in beam power has been carried out in order to identify optimal upgrades. Designs are to be developed primarily for an optimised neutron facility, and will include the provision of an appropriate proton beam to the existing TS-2 target station.

The recommended first stage of the upgrade path is to replace parts or all of the 70 MeV H^- injector. Replacement with a new or partly new linac of the same energy could

address obsolescence issues with the present linac, and ensure reliable operation for the foreseeable future. The more exciting but more challenging option is to install a higher energy linac (up to ~180 MeV), with a new optimised injection system into the present ring. This could give a substantial increase in beam power (factor ≤ 2), but there are numerous issues to be considered, and these are currently being worked on.

The next stage is a new ~3.2 GeV rapid cycling synchrotron (RCS) that can be employed to increase the energy of the existing ISIS beam to provide powers of ~1 MW. This new RCS would require a new building, along with a new ~1 MW target station. The new RCS could be built with minimal interruptions to ISIS operations, would give predictable increases in power at reasonable estimated costs, and would have well-defined upgrade routes. RCS designs will include features required for fast injection directly from ISIS, together with the option for optimised multi-turn injection from a new 800 MeV linac.

The final upgrade stage is to accumulate and accelerate beam in the ~3.2 GeV RCS from a new 800 MeV linac for 2–5 MW beams. It should be noted that a significant collimation section or "achromat" would be required after the linac to provide a suitably stable beam for injection into the RCS. The new RCS and 800 MeV linac would need to be located some distance from the present accelerators and also from the site for the new ~180 MeV linac. More details may be found in [3].

Studies and simulations will assess the key loss mechanisms that will impose intensity limitations. Important factors include injection, RF systems, instabilities and longitudinal and transverse space charge.

3.14.3.2.1 Linac and beam line studies

The 180 and 800 MeV linacs have a common initial 74.8 MeV design which is based around the 324 MHz frequency of available 2.5 MW Toshiba klystrons. The design includes an ion source, low energy beam transport (LEBT), 3 MeV RFQ, medium energy beam transport (MEBT), and a 74.8 MeV drift tube linac (DTL). In the case of the 800 MeV linac, an IEBT (intermediate energy beam transport) collimation section follows the DTL.

Three options have been considered for acceleration from 74.8 to 180 MeV and on to ~200 MeV. These include a room temperature coupled cavity linac (CCL) at 648 MHz, and superconducting cavity linacs at 648 MHz (ScL1) or 324 MHz (ScLa), both with geometric β_g values of 0.45. The first two options require a high power klystron development at 648 MHz but are preferred to the 324 MHz ScLa option for reasons of practicality and beam dynamics.

In the 800 MeV linac, after ~200 MeV is reached, new superconducting structures are used, with a β_g value of 0.62 at energies up to ~400 MeV and a β_g value of 0.76 for ~400 to 800 MeV. The two preferred options continue to use 648 MHz cavities, first in a ScL2 stage to ~400 MeV and then in a ScL3 to 800 MeV. The third option uses a 972 MHz third harmonic frequency for both an ScLb and ScLc stage (as a suitable Toshiba klystron is available).

Equipartition between longitudinal and transverse beam energies is established early in the first of four stages of the DTL and is maintained in the linacs up to their output energies. Longitudinal and transverse beam emittances are similar to those assumed in other high power linacs. Important features of the linacs are the MEBT and chopper designs and the matching between the various stages. Both the MEBT and the IEBT incorporate regions for beam collimation.

Beam transport lines between the linacs and rings need achromatic bending sections and also added cavities to ramp the output energy of the beam and to control the beam momentum spread. The new 800 MeV – ~3.2 GeV proton synchrotron requires long straight sections for the acceleration, extraction and beam collimation systems. The scheme for H$^-$ charge exchange injection into the synchrotron needs a linac beam current of 43 mA for 500 turns chopped at a 70% on-duty cycle over a pulse duration of ~0.75 ms.

Designs have followed those of the SNS and ESS linacs apart from the choices of the structure energies and frequencies and use of superconducting elliptic cavities at lower energies in two of the options considered. The use of spoke resonators down to 10 MeV, as proposed at FNAL, has not been adopted due to risk of a cavity failure at low energy. Initial stages employ the 324 MHz 2.5 MW peak power Toshiba klystron used in the J-PARC linac. A choice of 324 MHz instead of the 402 MHz used at SNS eases the design of the MEBT choppers.

Normalised RMS emittances assumed for the transverse and longitudinal planes at the MEBT input are 0.25 and 0.39 (π) mm-mrad respectively, values close to those achieved at SNS and J-PARC. Emittances obtained at RAL's Front End Test Stand need to be reduced to these values to allow use of current beam chopper designs, as plate separations and voltages have to scale with maximum transverse emittance values to avoid loss of un-chopped beam.

Two MEBTs have been studied — based on the chopper systems under design at RAL. Both exhibit halo and emittance growth; after matching into the first of four DTL tanks RMS emittances have increased to 0.30 (π) mm-mrad transversely and to 0.42 (π) mm-mrad longitudinally. The design preferred uses solenoids and triplets to provide long drifts and to allow 25% lower chopper voltages without any loss of the un-chopped beam and with less longitudinal halo.

Longitudinal inter-tank matching in the DTL is improved by the use of phase offsets in three of the four DTL tanks. An end cell is used together with a cell four or five periods upstream. Smooth transverse matching is obtained by adjusting six quadrupoles near the tank transitions. Apart from these adjustable elements, the DTL design assumes the use of permanent magnet quadrupoles. Equipartition between the longitudinal and transverse beam energies is obtained after matching into the first tank, and is maintained up to 800 MeV by appropriate quadrupole settings.

After the DTL, a three-doublet-cell collimator section (IEBT) is introduced into the 800 MeV linac. Its purpose is to remove halo, H^0, H$^+$ and far off-momentum beams and so prevent the type of low beam losses seen in the superconducting part of the SNS linac. In the first and the third cell there is a 648 MHz buncher cavity, and in the second a symmetrical dipole orbit bump (θ, -2θ, θ) which may be adjusted relative to collimator units by varying the common dipole currents over a range of values.

The 324 to 648 MHz frequency jump for two of the options requires the development of a high-power 648 MHz klystron. The third option of a 324 MHz ScLa after the IEBT followed by a 972 MHz ScLb and ScLc was prompted by availability of 3 MW 972 MHz Toshiba klystrons. However, a satisfactory design for the third option has not been found; the larger frequency jump leads to excessive emittance growth.

In the superconducting stages focusing is by doublet quadrupoles located in room-temperature regions for ease of alignment, although some designs economise with quadrupoles in the cryostats. Doublet quadrupoles are also used in the CCL for ease of the input and output matching, although 2.5 $\beta\lambda$ coupling cell lengths are needed and the

cell lengths for the ten-cell cavities proposed become 7.5 $\beta\lambda$ (βc is the beam velocity and λ is the free space wavelength at 648 MHz).

Six-parameter matching between high-energy stages is found by varying six quadrupole fields together with a ramp of cavity phases at the output of one stage and the input of the next. Large energy gains per cell lead to different matched parameters for adjacent cells, and so matching is not as exact as for a ring or high energy beam line. A range of matched parameters may be found, some better than others, and rapid change of focusing and beam size are best avoided. Beam tracking studies are used to check the results of the lattice-parameter-matching routines.

Superconducting linac design involves choosing β_g values, accelerating field gradients, peak fields, synchronous phase angles (φ_s), cavity geometry, numbers of cavities and cells per cavity, numbers of cavities per cryostat and per focusing period, and gradients for the doublet quadrupoles. The main aim is to minimise the numbers of cavities and cryostats without prejudicing issues of practicality and beam dynamics.

Factors affecting beam halo and RMS emittance growth include evolution of a non-stationary input distribution, the form of the distribution, the rates of change of beam amplitudes and aspect ratios, inter-stage matching, and resonance-induced effects due to space-charge tune spreads. Different distributions may have different growth rates and need modified matching. Cell tunes are chosen for energy equipartition and for limiting effects of machine errors and space-charge forces on coherent, longitudinal-transverse coupled envelope modes. The MEBT uses solenoids and triplets to limit beam aspect ratio changes which alter the ratios of linear to non-linear space charge forces.

As regards transporting the beam from the end of the linac(s) to the synchrotron(s), beam de-bunching under space charge forces and related changes of beam momentum spread may be approximated by a 1-D linear longitudinal envelope equation. More accuracy requires use of both an interactive 3-D linear beam envelope code for input matching, focusing and beam line design and a 2½- or 3-D code for tracking studies. The focusing used for the 800 MeV beam line is a continuation of the FoDO doublet focusing pattern of the linacs. For the new 180 MeV beam line to ISIS, however, a back-to-back doublet is first used, to allow a change to the DoFO pattern used in the ISIS ring superperiods.

Two beam lines are considered for ISIS, one for "inside" and one for "outside" ring injection. The latter is simpler but may lead to more complex injection. The outer line has two achromatic sections, one to orient the linac relative to ISIS, and one for bending the beam into the injection region. The solutions are linked to energy ramping, momentum spread control and the injection painting, and both are described in [3]. The 800 MeV line has only a final injection achromat.

3.14.3.3 *Ring Studies*

Present studies are concentrating on establishing the extent to which operation at higher beam powers may be possible by upgrading the ISIS linac and injecting a chopped beam into the existing ISIS RCS at higher energy. Injection at higher energies reduces the effects of space charge, and beam chopping improves trapping efficiencies. At present, effort is being concentrated in the following areas: design of a higher energy injection straight, control of beam losses and the increased activation at higher energies, beam dynamics and beam losses derived from increased space charge, and instabilities. Initial "study" parameters assume an injection energy of 180 MeV and beam powers of ~0.5 MW, but the practicality of these values is yet to be fully

established. The beam power resulting from the upgrade will be limited by beam losses together with the increased activation per proton because of the higher energy.

This study forms part of the on-going research programme into high intensity proton beams at ISIS [4], based on understanding, optimising and upgrading both the existing ISIS synchrotron and putative new upgrade synchrotrons at ISIS. Development and experimental testing of simulation codes is under way using the SNS code ORBIT [5] and also with the in-house code SET [6]. The latter is presently being expanded to cover 3-D particle motion, exploiting the parallel computing facilities available at RAL. The aim is to adapt models being verified on the present ISIS synchrotron to proposed new running régimes.

Beam dynamics studies for higher energy injection at higher power are covering a number of effects. Longitudinal dynamics are requiring careful simulation work to ensure appropriate evolution of bunch distributions to maintain stability and allow loss-less extraction with practical dual harmonic RF systems. Likewise, in the transverse planes, simulations are helping to assess the limits imposed by space charge, indicating how well transverse emittance and halo may be controlled, including effects like images. Optimising the 3-D injection painting is challenging; beam losses have to be minimised during injection, and particle distributions have to be produced that give rise to very small beam losses throughout the acceleration cycle.

Injecting at ~180 MeV into the existing long straight of ISIS is challenging, but magnet modelling and tracking studies (still under way) suggest it is probably practicable. Variations on the present injection scheme may need to be evaluated, depending on requirements dictated by beam dynamics and beam losses. Beam losses associated with the H^- stripping foil are another major concern, and foil parameters, expected efficiencies and distributions of losses associated with out-scattered protons and excited stripping states are all under study. Collimation and activation are also being looked at using the MARS code [7], again with experimental comparisons planned. Requirements for beam diagnostics at higher powers are also being evaluated. In particular, strip-line monitors are being developed that could form part of an active damping system (based on SNS ideas) to control transverse instabilities.

Until the study is complete, it will not be possible to confirm the viability of such an upgrade. However, the calculations, simulation models and experimental comparisons with the existing machine required in the course of the work will form an essential base-line for any further ISIS upgrades.

There are a number of possible candidates for the ~3.2 GeV, 50 Hz RCS, but studies are presently focused on a 3.2 GeV doublet-triplet design with five superperiods (5SP) outlined in [8] and a 3.2 GeV triplet design with four superperiods (4SP) outlined in [9]. The lattice for the 5SP design has been modified slightly to give the correct circumference for fast injection from the ISIS 800 MeV synchrotron which has a mean radius (R_0) of 26.0 m.

The 5SP ring has a mean radius (R) of 58.5 m ($R/R_0 = 9/4$) and RF cavities running at harmonic number h = 9, *i.e.* at nine times the ring revolution frequency (6.1–7.1 MHz). This ring is optimised to give small dipole apertures and therefore to minimise the magnet power supply requirements, but has RF buckets which are smaller than those for the ISIS synchrotron. Meanwhile, the 4SP ring has a mean radius of 65.0 m ($R/R_0 = 5/2$) and RF cavities running at harmonic number h = 5, *i.e.* at five times the ring revolution frequency (3.1–3.6 MHz). This ring gives RF buckets the same size as those for ISIS, making fast injection easier, but has larger apertures. Both of these

ring designs (and appropriate variations) will be studied in detail in order to assess their suitability for the recommended upgrades. Initial work, however, has concentrated mostly on the 5SP design.

Work is now under way to study the key issues for the ~3.2 GeV ring designs, underpinned by extensive development of the relevant codes and benchmarking during machine physics studies on ISIS. The main topics include space charge, injection, provision for RF, beam stability and the requirement to keep beam losses below about 0.01%.

3.14.4 **References**

1. http://www.isis.rl.ac.uk/.
2. A Seville *et al*., "Progress on Dual Harmonic Acceleration on the ISIS Synchrotron", proc. EPAC'08 (2008) p 349.
   Should be update of this for IPAC'10, but probably not in time for this paper
3. G H Rees, "Linac, Beam Line and Ring Studies for an Upgrading of ISIS, GHR1, ASTeC, 2009.
4. C M Warsop *et al.*, "Space Charge and High Intensity Studies on ISIS", 42nd ICFA Adv. Beam Dynamics Workshop on High-Intensity, High-Brightness Hadron Beams, Nashville, 25–29 August 2008.
5. http://neutrons.ornl.gov/APGroup/Codes/orbit.htm.
6. B G Pine and C M Warsop, "Image Simulations on the ISIS Synchrotron", proc. EPAC'08 (2008) p 3215. (See also B G Pine *et al.*, "Space Charge Simulations for ISIS", ICAP 2009, 31 August – 4 September 2009, San Francisco.)
7. http://www-ap.fnal.gov/MARS/.
8. G H Rees, "Note on an RCS for a 2 MW Spallation Source at RAL", private communication, 2007.
9. G H Rees, "Options for a 50 Hz, 10 MW, Short Pulse Spallation Source", FFAG Workshop, Grenoble, 12–17 April 2007.

Test Facilities and Accelerator Systems R&D

3.15 Recent Developments on ALICE (Accelerators and Lasers In Combined Experiments) at Daresbury Laboratory

Susan L Smith, on behalf of the ALICE Team,
ASTeC, STFC Daresbury Laboratory and Cockcroft Institute,
Daresbury Science and Innovation Campus, Warrington, WA5 2EE, UK
Mail to: susan.smith@stfc.ac.uk

3.15.1 **Introduction**

ALICE, formerly known as ERLP [1], is a new R&D facility currently being commissioned at Daresbury Laboratory. The accelerator is an energy recovery superconducting (SC) linac operating at the nominal beam energy of 35 MeV, see Figure 1. The high voltage DC photoelectron gun operates at nominal voltage of 350 kV and bunch charge of 80 pC. The bunch trains can be of variable length from a single

bunch regime to 100 μs with a bunch repetition frequency of 81.25 MHz within the train. The train repetition frequency can also be varied within the 1-20 Hz range.
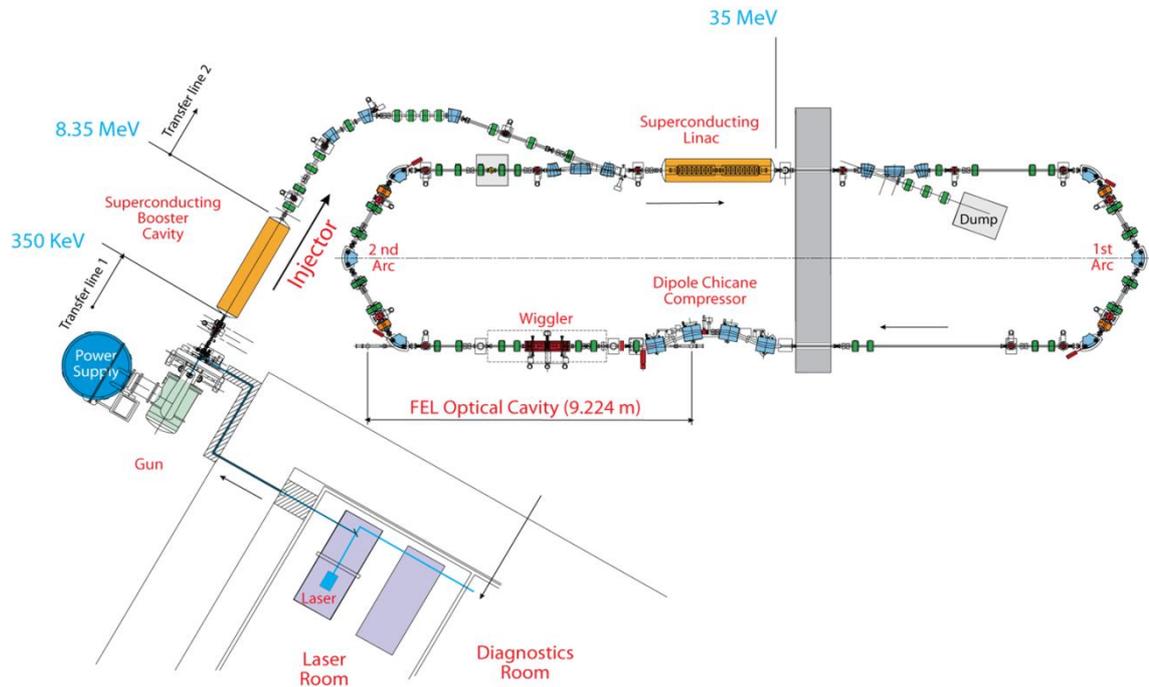
Figure 1: ALICE layout

In addition to the accelerator, several light sources are or will be available for conducting a variety of R&D projects, including pump-probe experiments. These are (i) an IR FEL with wavelength of ~4 μm; (ii) a THz source with coherent enhancement of the radiation intensity due to sub-picosecond bunch lengths generated by ALICE; (iii) a Compton Backscattering (CBS) X-ray source with photon energy of 15 or 30 keV depending on the collision angle between the photons and electrons. The CBS source is powered by a terawatt IR femtosecond laser that can also be used as a stand-alone light source for a variety of experiments.

3.15.2 **Present Status**

Full energy recovery and demonstration of the coherently enhanced THz radiation were successfully achieved on ALICE by the beginning of 2009. The injector can now reliably deliver beams with bunch charges well in excess of 80 pC and with the design bunch structure, i.e. 81.25 MHz bunches in trains up to 100 μs, repeating at 1-20 Hz. However, due to a number of mostly technical problems, some of the other ALICE design parameters have not been achieved at present.

The gun operating voltage of 350 kV was initially used for gun commissioning [2] but, after several failures of the high voltage insulating ceramics [3], it was necessary to install a more robust but smaller inner diameter ceramic that reduced the maximum gun operating voltage to ~250 kV. Furthermore, a field emitter on the GaAs cathode wafer located close to its centre necessitated a reduction of the gun voltage down to 230 kV. This field emitter is likely to be responsible for a hole in the quantum efficiency map of the cathode. This hole becomes more pronounced towards the end of the cathode

activation cycle but virtually disappears after the cathode re-caesiation (Fig.2). An improved 500 kV ceramic insulator is currently being developed and manufactured in collaboration with Jefferson Laboratory and Cornell University that will restore the ALICE gun nominal voltage to 350 kV.
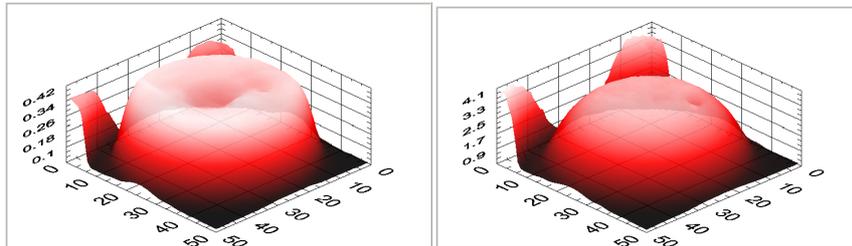
Figure 2: Typical QE maps at the end of the activation cycle before the re-caesiation (left) and after a full cathode activation including a heat cleaning treatment of the wafer (right).

The photocathode can now be routinely activated and re-Caesiated to quantum efficiencies of 2.5-3.0% with the dark 1/e lifetime of the cathode exceeding 1000 hours. The operational cathode lifetime is however limited to several hundreds of hours due to excessive outgassing in the gun beamline when the machine is operated at long train lengths of 50-100 μs and bunch charges above ~40 pC. The cathode quantum efficiency is regularly restored by a quick and simple re-caesiation procedure.

We presently run the machine at the bunch charge of 40 pC. This is dictated mostly by the inability of the analogue LLRF system to cope efficiently with beam loading effects in the injector SC booster. We plan to replace the existing LLRF system with the digital version. The prototype has been developed and first tests appear to be promising for increasing the operational bunch charge above 40 pC.

Due to excessive field emission from the main linac module, designed to bring the beam energy to 35 MeV [3], the beam energy was reduced to 21 MeV for the initial machine commissioning. The corresponding beam energy after the injector was 4.8 MeV to allow injection and extraction chicanes to operate correctly. From September 2009, after extensive work on SC linac cavities conditioning, improvements in the cryogenic system and optimisation of the linacs operating parameters allowed ALICE to operate at higher beam energy of ~30 MeV.

3.15.3 **Energy Recovery and Beam Characterisation**

The gun was commissioned and the 350 keV electron beam was fully characterised at a range of different bunch charges of up to 80 pC. The results are reported in [2,4].

Initially, full energy recovery was established at 21 MeV beam energy and several bunch charges up to 20 pC. This is illustrated by the RF power demand signals from the two superconductive cavities of the main linac (Fig.3). At the time, higher bunch charges were not possible to achieve because of the beam loading effects in the injector SC booster cavities.
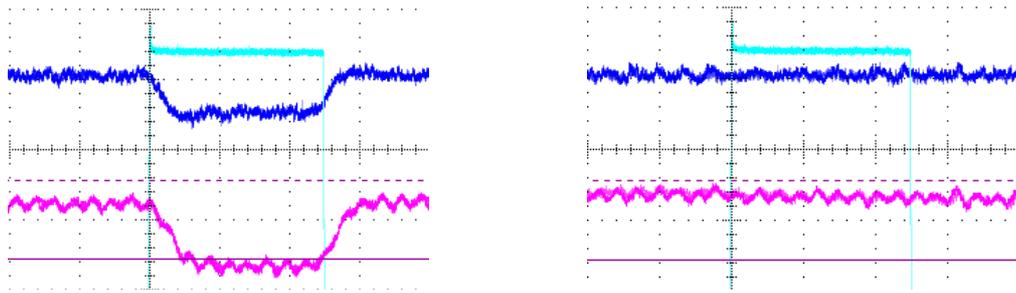
Figure 3: Main linac RF power demand signals: without (left) and with (right) energy recovery.

Beam loading in the booster cavities was clearly visible on the LLRF signals at train lengths of a few tens of microseconds and bunch charges above 10 pC. The major impact of this on the beam was that the beam energy towards the end of the macropulse was lower than at the beginning by a few percent. The effect of beam loading was also observed on the Faraday cup located in a dispersive section of the injector beam line. In the presence of the beam loading, the current measured by the Faraday cup is not constant because the beam sweeps across the cup aperture due to change in the beam mean energy during the train length. Extensive work on optimisation of the LLRF system and the external quality factors of the booster cavities allowed to extend operation of the machine to ~40 pC bunch charge and up to 100μs train lengths in an energy recovery regime.

The field emitter on the cathode wafer remains a serious problem especially at levels of quantum efficiency above 3% when the flow of field emission electrons becomes too intense after acceleration in the booster. Replacing the wafer in the current gun design is a complicated and time consuming procedure and, based on experience, may lead to vacuum, HV and cathode problems. Increase of the field of the first solenoid, next to the gun, disperses the field emission electrons within the gun beamline and only a smaller fraction is picked up by the booster cavities and accelerated further. At lower bunch charges, this increased solenoid field is too high, leading to a transverse cross-over and correspondingly larger beam emittance. It is close to the optimal setting for higher bunch charges of ~80 pC.

Beam characterisation and optimisation was not a priority during latest commissioning periods. Only a limited number of emittance measurements were made in the injector beamline using quadrupole and slit scans. Provisional results show that the normalized emittance is at or below ~10 mm-mrad. It has to be noted that no attempts were made to minimise the emittance for each bunch charge. This and the existence of the field emission current probably accounts for the somewhat larger emittance values compared to that expected from the ASTRA model (~3 μm at 80 pC). A systematic optimisation of the injector settings is planned and a significant improvement in overall beam quality including the transverse emittance is expected.

3.15.4 THz Generation Studies

Coherent enhancement in the synchrotron radiation from short electron bunches produces high power THz radiation at high repetition rates. This radiation provides a useful diagnostics tool for the accelerator, but will also allow new photon science developments.

The final dipole in the compression chicane is the source of THz radiation. A plane mirror within this vessel deflects radiation through a 38 mm aperture CVD wedged diamond window. The overall acceptance of the beamline is 70×70 mrad. The window separates the accelerator vacuum from the THz beamline which transports the radiation to a diagnostics laboratory. The beamline was optimised by extensive modeling with the wavefront propagation code SRW [5]. There are two intermediate foci in the 17 m optical path to the diagnostics laboratory. The beam can then be directed into a nitrogen purged diagnostics enclosure which includes a custom high-aperture step-scan Martin-Puplett interferometer, or further transported on to a suite of THz exploitation laboratories including a tissue culture facility (TCF), see Fig. 4. Here the beam is condensed by a Winston cone through a TPX exit window where live human tissue cells can be irradiated.

Figure 4: Tissue culture laboratory where THz radiation can be condensed into living human tissue cells

Monitoring the intensity of the radiation at the diagnostics enclosure allowed the accelerator RF system to be tuned to put the optimum energy chirp onto the electron bunch to give maximum compression in the chicane.

Under these conditions a linear dependence on THz detector signal on the bunch train length was observed at constant bunch charge, and a clear quadratic dependence on bunch charge was observed at constant train length, as shown by the fitted line in Fig. 5. This is indicative of coherent emission.
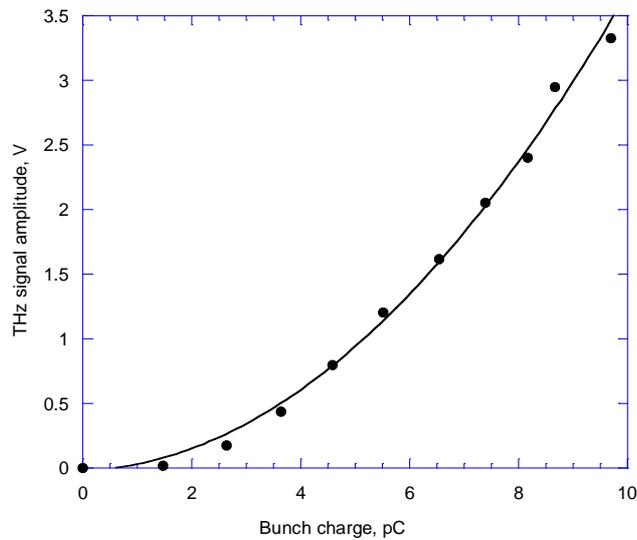
Figure 5: Dependence of the THz signal amplitude on the bunch charge

The latest observations of the THz intensity at the bunch charge of up to 40 pC indicate that the THz pulse energy can reach several tens of µJ with some preliminary measurements suggesting around 150 µJ may be achievable. These measurements were made however in the vicinity of the compression chicane and showed a very large divergence of the THz radiation in the horizontal plane. Experimental evidence suggests that not only the last dipole of the chicane contributes to the overall output. A significant fraction may come from the upstream dipole as well. The radiation transport along the THz beamline was found to be very poor as a result of, most likely, non-optimal electron bunch compression. We have planned a set of specific experiments that will allow efficient THz generation and transport through the THz beamline over tens of meters to the diagnostic room and to the tissue culture laboratory.

3.15.5 **Compton Backscattering Experiment**

The Compton backscattering experiment in a 180 degrees (head-on) configuration was successfully demonstrated in November 2009, see Fig. 6. The multi-TW Ti:sapphire laser (800 nm, 70 fs, 500 mJ per pulse, 10 Hz) and 40 pC, 29.6 MeV electron beam were used for the demonstration. The electron beam could be focused to ~35 µm RMS but, in these CBS experiments, both laser and electron beams were focused to ~100 µm FWHM. Due to a necessity to start installation of the IR FEL on ALICE, virtually no time was allowed for x-ray characterisation and optimisation. The next phase of the CBS experiment in the 90 degrees configuration is however planned that will make possible operation of both IR FEL and the CBS x-ray source.
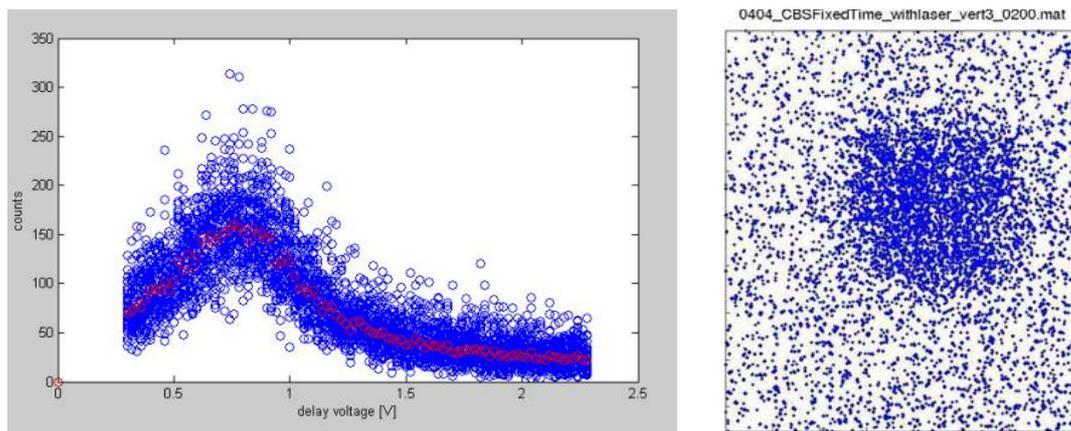
Figure 6. Scan of the laser pulse arrival time with respect to the electron bunch arrival time (left) and the CBS x-ray signal.

3.15.6 Future Developments

The ALICE R&D facility faces several exciting developments and challenges in 2010-11.

Commissioning of the IR FEL has been started and we expect it to become operational in the nearest future. As part of the FEL programme, the electro-optic diagnostic for measuring longitudinal profiles of short, ~1 ps, electron bunches will be also commissioned.

In the middle of 2010, the commissioning of the first non-scaling FFAG accelerator EMMA will commence [6] and continue throughout 2010 and, hopefully, beyond.

Three major upgrades are also expected including installation of the load-lock system on the photogun, extension of the gun beamline to include diagnostics for full beam characterisation before the booster, and installation of the new improved SC linac module that is currently being constructed and is a result of a multinational collaboration. The present LLRF system will be replaced with the digital version being currently developed in-house.

The helium processing of the main linac cavities will be conducted in the second half of March 2010 with the help of JLab personnel. This will potentially alleviate field emission problems in the linac and will pave the way for reaching the nominal beam energy of 35 MeV on ALICE.

A programme of THz studies is planned including the first experiments at the TCL to determine the safe limits of human exposure to THz radiation. In view of the present problems with transporting the THz beam to TCL and for the sake of obtaining first preliminary results, initial experiments will be conducted in the accelerator hall in the shielded enclosure with the use of miniature cell incubators.

In conclusion, ALICE commissioning has reached the point when it is now becoming a true R&D facility capable of accommodating and testing novel ideas, and conducting proof-of-principle experiments.

3.15.7 References

1. S. L. Smith et al, "The Status of the Daresbury Energy Recovery Linac Prototype", PAC'07, Albuquerque, 2007, TUPMN084, p. 1106 (2007).
2. Y. M. Saveliev et al, "Results from ALICE (ERLP) DC photoinjector gun

commissioning", EPAC'08, Genoa, MOPC062, p. 208 (2008).

3. D. J. Holder et al, "The status of ALICE, the Daresbury energy recovery linac prototype", EPAC'08, Genoa, 2008, TUOAM02, p. 1001 (2008).
4. Y. M. Saveliev et al., "Characterisation of electron bunches from ALICE (ERLP) DC photoinjector gun at two different laser pulse lengths", EPAC'08, Genoa, 2008, MOPC063, p. 211 (2008).
5. O. Chubar and P. Elleaume, EPAC-98, 1998, pp1177-1179.
6. R. Edgecock et al., "EMMA-the world's first non-scaling FFAG", EPAC'08, Genoa, 2008, THPP004, p. 3380 (2008).

3.16   The EMMA FFAG

Rob Edgecock

STFC Rutherford Appleton Laboratory, Chilton, Didcot, Oxon, OX11 0QX
Mail to: rob.edgecock@rl.ac.uk

3.16.1 Introduction

As described previously [1], non-scaling Fixed Field Alternating Gradient (ns-FFAG) accelerators have a significant potential for future applications, potentially replacing the currently used cyclotrons and synchrotrons. However, they, in particular linear ns-FFAGs, have a number of unique features and characteristics [2], including:

- Very large momentum compaction (Livingood definition [3])
- Large betatron tune variations and multiple resonance crossings
- Serpentine (bucketless) acceleration
- The requirement for purpose-built tracking codes
- The need for a highly symmetric lattice

Due to these features and the need to benchmark the tracking codes employed with this type of accelerator, it was concluded that a proof-of-principle ns-FFAG needed to be built before this technology could be further developed for real applications. This machine is called EMMA (the Electron Model for Many Applications) and is currently (March 2010) under construction at the STFC Daresbury Laboratory. EMMA forms one of the biggest accelerator R&D projects underway in the UK at this time.

The following sections will describe the EMMA parameters and the resulting layout of the accelerator, the main components of the machine and the plans for commissioning and the experimental programme.

3.16.2 EMMA Specifications

To prove the principle of ns-FFAGs and investigate the features listed above, it has been decided to design and build a linear machine, employing fixed frequency RF acceleration. To minimize cost, EMMA will accelerate electrons from 10 to 20 MeV and will use a beam provided by the existing ALICE accelerator [4] at Daresbury. The parameters of the machine have largely been determined by scaling down those for a muon FFAG in the Neutrino Factory [5] and are listed in Table 1. A doublet lattice has been chosen, to minimise cost, and there will be 42 cells.

To deliver the aims of the project, 8 different lattice configurations have been designed [6], which probe the longitudinal and transverse dynamics of the machine and different regions of the tune diagram. The specifications for EMMA have been determined by these lattices and the resulting machine layout is shown in Figure 1. The ring itself is built on 7 girders, with 6 cells per girder. Figure 2 shows a single cell, consisting of a magnet doublet and an RF cavity, and 4 of the girders in place next to the injection line from ALICE.

Table 1: EMMA Parameters

Parameter	Value
Kinetic energy range	10 to 20 MeV
Cell	Doublet
Number of cells	42
RF	19 cavities; 1.3 GHz
Cell length	394.481 mm
Ring circumference	16.57 m
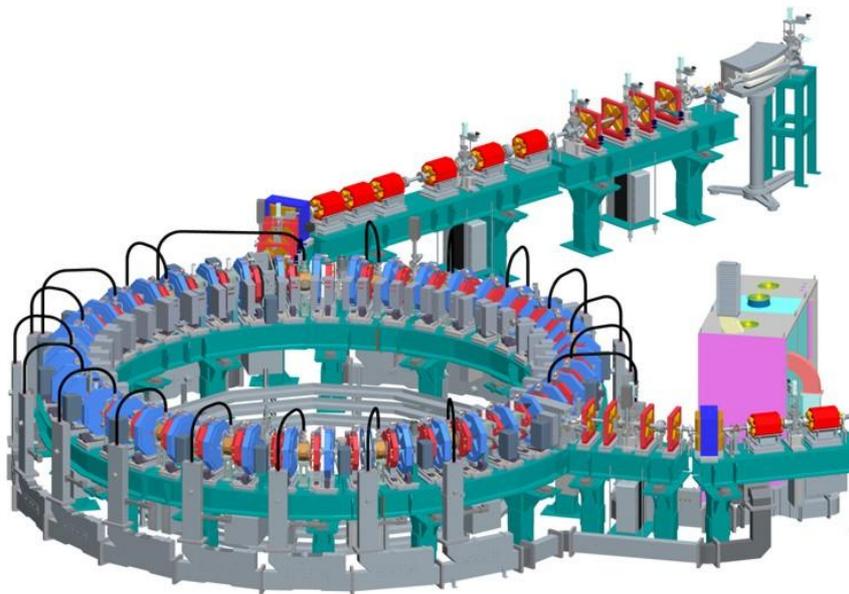
Figure 1: Layout of EMMA, showing the last part of the injection line from ALICE (to the right), the EMMA ring and the extraction line, holding the destructive diagnostic devices.

3.16.3 EMMA Hardware

The design and construction of the hardware for EMMA has been challenging for a number of different reasons. As this the first machine of its type, many problems have arisen that have required novel solutions. Further, the flexibility needed to provide the proof-of-principle for non-scaling optics and meet the requirements of the 8 lattices has created significant difficulties. Finally, as shown in figure 1, the lattice is very compact and fitting everything into the machine has been a huge problem. The following subsections will outline the design of the three main components of the accelerator: the magnets, the RF and the diagnostics. All other parts are described elsewhere [7].

3.16.3.1 *Magnets*

A number of different magnet types are required for EMMA and these are summarised in Table 2. The 84 main ring DC magnets require independently variable dipole and quadrupole components. They are implemented as quadrupoles and the dipole component is obtained by using them off-axis. This component is adjusted by mounting the magnets on precise, computer controlled sliders. As shown in Figure 2, each doublet is surrounded by clamp plates. These are to prevent field leakage into the iron of the kicker magnets, but are mounted on each doublet to minimise orbit errors from asymmetry. Almost all of the magnets will be powered from two power supplies, one for the Fs and one for the Ds. Two of each type of magnet will be powered using individual supplies, to allow the field strengths to be changed compared to the others to introduce artificial errors for resonance studies.

Figure 2: An EMMA cell with a royal visitor (left) and 4 EMMA girders in place (right), with the end of the injection line at the bottom right of the photograph.

The pulsed magnets, the kicker magnets and septa, have proved to be the most difficult to design. The selected scheme is to use a septum and two kickers in adjacent cells for both injection and extraction. To avoid passing through the magnets in the neighbouring cell, the entrance and exit angles are 65° and 71°, respectively. Further, the space available is limited to about 20 cm for each magnet and the fall (rise) time of the injection (extraction) kicker must be less than the revolution period of 55 ns. To be able to inject and extract and to probe the full acceptance of the ring at all energies, it is also necessary to be able to move and rotate both septa. Examples of these magnets are shown in Figure 3.

Vertical steering and combined vertical and horizontal steering magnets are required in the injection line, the main ring and the diagnostics beam line. The combined steerers are used for orbit correction in the external lines, while the vertical steerers will be used to scan the full vertical acceptance of the ring. Horizontal scanning will be performed by the kicker magnets. The vertical steerers in the ring will be used for vertical orbit correction.

3.16.3.2 *RF System*

Rapid acceleration is obtained by placing accelerating cavities in every other cell around the EMMA ring, with two cavities omitted for injection and extraction of the electron beams. The RF system consists of 4 major sub-systems: a high power RF amplifier system, a RF distribution system, a low level RF (LLRF) control system and finally RF cavities that transfer energy to the beam. All 19 RF cavities are driven from

the same RF source, with a complex distribution scheme providing equal power to each cavity. Synchronisation of the electron bunches to the RF cavity is also required to tight tolerances, to ensure that the accelerating field is present as the electron bunches pass each RF cavity. The RF operating parameters can be found in Table 3.
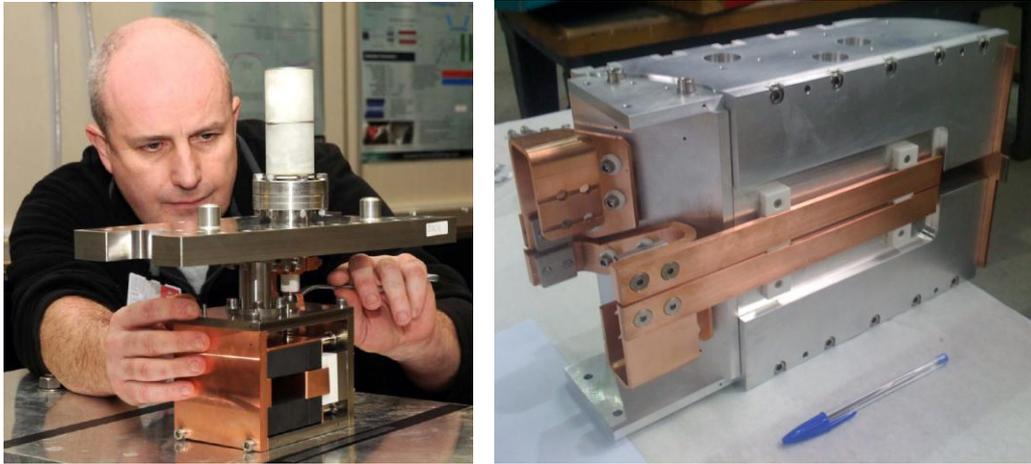
Figure 3: EMMA kicker (left) and septum (right) magnets.

The high power RF amplifier system consists of a high voltage power supply, a 1 kW solid state amplifier and an Inductive Output tube (IOT). This system will provide 90 kW of pulsed RF power at 1.3 GHz. The pulse length for the RF is 1.6 ms, with a pulse repetition frequency of up to 20 Hz required. Due to the R&D requirements for EMMA, a 5.5 MHz operational tuning range is specified. This puts additional strain on achieving stable operation as the master oscillator clock, which also synchronises the RF to the ALICE RF, will be fixed at 1.3 GHz. For this reason, a full 360 degree phase shifter is required prior to each cavity to allow local phasing of the RF.

Table 2: EMMA magnets

Location	Type	Number
Injection line	Quadrupole	18
	Dipole	4
	Vertical steerer	2
	Combined steerer	4
Injection system	Septum	1
	Kicker	2
EMMA ring	Quadrupole – F	42
	Quadrupole – D	42
	Vertical steerer	16
Extraction system	Septum	1
	Kicker	2
Diagnostics line	Quadrupole	14
	Dipole	2
	Vertical steerers	2
	Combined steerers	4

The EMMA RF system is unique in that the 19 cavities are all fed from the same RF source distributed around a compact ring. A bespoke waveguide section that includes circulator, load, phase shifter, directional coupler and waveguide to coaxial transformer has been designed and built to achieve this.

Table 3: Specifications for the EMMA RF system.

Machine Parameters	Values	Units
Frequency	1.3	GHz
Frequency range	-4.0 to 1.5	MHz
Number of straights	21	
Number of cavities	19	
Total voltage per turn	2.3	MV
Upgrade voltage per turn	3.4	MV
Beam aperture	40	mm
RF pulse length	1.6	ms
RF repetition rate	1 to 20	Hz
Amplitude control	0.3	%
Phase control	0.3	°

As it is essential that the RF is synchronised with the beam in order to place the beam at the correct place in longitudinal phase space, a LLRF system is required to monitor signals from each cavity and provide the necessary phase or voltage adjustment to ensure the optimum RF settings are maintained. In order to maintain this stability during operation, feedback signals from the cavity fields are monitored in the LLRF system.

Figure 4: Design of an EMMA RF cavity (left) and a cavity under test (right).

The ultimate performance on the accelerator will be the ability of the cavities to efficiently transfer energy to the beam. For EMMA, a normal conducting single cell re-entrant RF cavity design has been optimised for high shunt impedance, working within geometrical constraints of ø40 mm beam aperture and 110mm flange to flange length

availability. The custom in-house design shown in figure 4 meets the operation specification.

3.16.3.3 *Diagnostics*

As EMMA is a purely experimental machine, it is very important that it has sufficient diagnostic devices to make detailed measurements of the beam throughout the acceleration cycle. These are located in the injection line, to measure beam properties on injection into EMMA, and the ring itself. Destructive devices are located in an external diagnostics beamline. The extraction system into this is designed to allow extraction at all energies, so that measurements can be made at any energy. The devices employed are summarised in table 4 and their locations in the machine are shown in Figures 5 and 6.
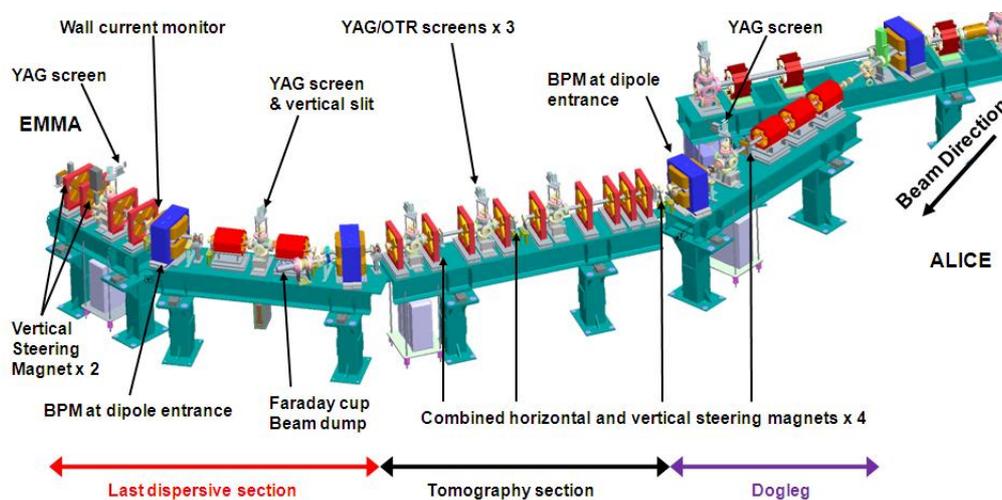
Figure 5: EMMA injection line, showing the locations of the diagnostic devices

3.16.4 **Experimental programme and commissioning**

An extensive experimental programme is planned with EMMA. This will include, for each lattice:

- Demonstrating serpentine acceleration (see figure 7)
- Demonstrating beam acceleration with multiple resonance crossings
- Measuring the variation of the horizontal and vertical tune with energy
- Measuring the variation of the time of flight with energy (see figure 7)
- Scanning longitudinal phase space, including the variation of serpentine acceleration and beam emittance with the longitudinal parameters
- Scanning the transverse phase space, including the variation of the dynamic aperture with energy and the time of flight and acceleration with beam amplitude.
- Studying resonance crossings with low acceleration

These measurements will need to be repeated with each lattice and all the measurements made compared with the expectations from the tracking codes.
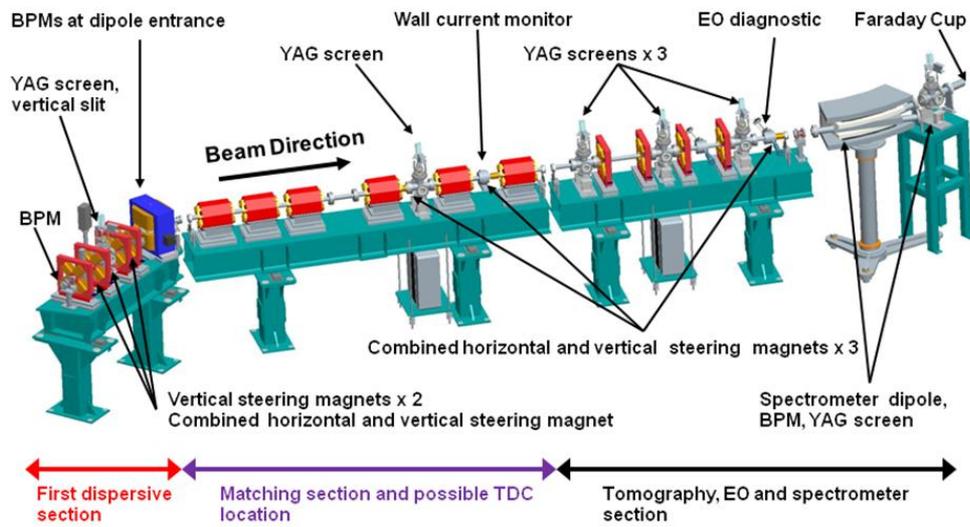
Figure 6: EMMA diagnostics beam line, showing the locations of the diagnostic devices.
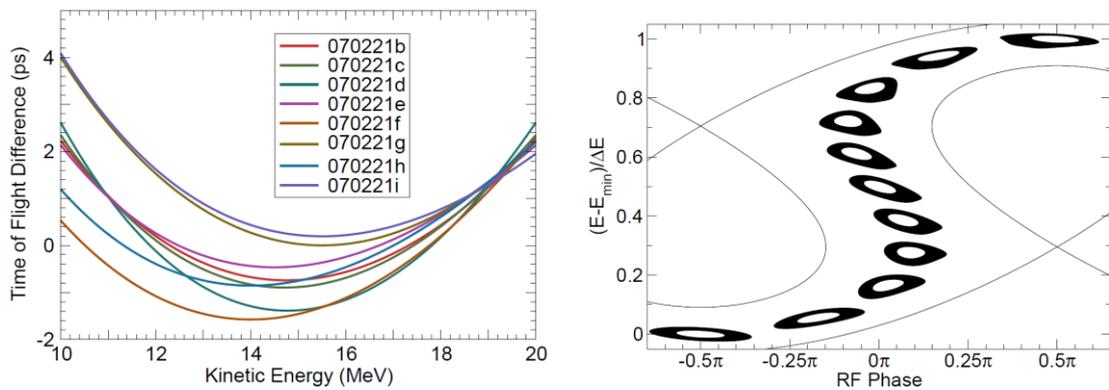
Figure 7: Time of flight curves for the 8 EMMA lattices (left) and serpentine acceleration (right)

The commissioning phase of EMMA is being designed to make these measurements possible. It will include making beam measurements in ALICE, commissioning the injection line and injection system, placing the beam on the correct orbit, commissioning the diagnostic devices with beam, testing the extraction system and verifying the proposed methods for making the measurements listed above. The accelerator control system has been designed to allow a set of machine parameters to be tried out with an online model before and in conjunction with using them on the real machine, to enhance debugging and understanding the machine operation. It is expected that first results from EMMA will be available during the summer of 2010.

Table 4: The diagnostics devices to be used on EMMA. The location of the devices is shown in bold in the first column

Measurement	Device	Number
Beam position **Ring**	4 button BPM	82
Beam position **Injection**	4 button BPM	7
Beam position **Extraction**	4 button BPM	5
Beam profile **Ring**	Screens	4
Beam profile **Injection**	Screens	5
Beam profile **Extraction**	Screens	6
Beam charge **All**	Wall current monitor	3
Phase wrt RF **All**	Wall current monitor	3
Transmission **All**	Wall current monitor	3
Transmission **Extraction**	Faraday cup	1
Beam loss **Ring**	Beam loss monitor	4
Emittance **Inj/Ext**	Screens	3
Momentum **Ring**	BPMs	
Momentum **Extraction**	Spectrometer	1
Long. Profile **Extraction**	Electro-optic monitor	1

3.16.5 **References**

1. C.R. Prior (ed), ICFA Beam Dynamics Newsletter #43, August 2007.
2. F. Mills, Proc. 4th Int. Conf. Physics Potential and Development of μ+ μ- Colliders, San Francisco, 1997, 693-696; C. Johnstone, ibid., 696-698 (1998); A. Garren, C. Johnstone and W. Wan, in proceedings of the 1999 Particle Accelerator Conference, New York, 1999, pp 3068-3070.
3. J.J. Livingood, Principles of Cyclic Particle Accelerators, D. Van Nostrand, New York, 1961.
4. D.J. Holder et al, in proceedings of the 11th European Particle Accelerator Conference, Genoa, Italy, 23 - 27 Jun 2008, pp 1001-1003.
5. S. Machida, in proceedings of the 22nd Particle Accelerator Conference, Albuquerque, New Mexico, USA, 25-29 June 2007, pp.2614-2618.
6. J.S. Berg, "The EMMA Main Ring Lattice," Nucl. Instrum. Methods A 596 (2008) 276–284.

7. C. Beard et al, "EMMA – The World's First Non-Scaling FFAG", to be submitted to Nucl. Instrum. Methods A.

3.17   FFAG Accelerator Study at Rutherford Appleton Laboratory

Shinji Machida and David J. Kelliher
STFC Rutherford Appleton Laboratory, Didcot, Oxfordshire, OX11 0QX, UK
Mail to: shinji.machida@stfc.ac.uk

Abstract:
Fixed Field Alternating Gradient (FFAG) accelerator has the potential for variety of applications from particle physics by means of a muon accelerator for a muon collider and a neutrino factory, a proton and ion accelerator for a particle therapy facility and a high power proton driver for an accelerator driven subcritical reactor (ADSR). In this report, we will describe the research activities in the FFAG accelerator field at STFC Rutherford Appleton Laboratory in UK. A related construction project of a nonscaling FFAG called EMMA is discussed in a separate article [1].

3.17.1 Introduction

Developments of particle accelerators have been mainly motivated by particle physics since they were invented. The primary goal of a particle accelerator is to have the highest energy beams on Earth – so called energy frontier research. When it was realized that high precision physics and physics with secondary particles can be done if the intensity of an accelerated beam is high, another direction of accelerator development was initiated. This opens a new field of an accelerator of intense beams. A facility which accommodates a high intensity accelerator is called a particle factory.

For energy frontier research, a synchrotron was the only option until recently because of its compact magnets and efficient use of rf acceleration. To realise a high intensity accelerator, on the other hand, there have been a variety of options. A meson factory was constructed with a cyclotron at TRIUMF and with a linac at LANL. For a neutron source, ISIS uses a synchrotron and PSR relies on a full energy linac and accumulates protons in a storage ring. More recently, SNS follows a similar scheme to PSR while J-PARC has two synchrotrons for neutron as well as neutrino and secondary particle users.

Despite the invention and development of an FFAG in the 1950s, no physics project to date has made use of this type of accelerator. It is understandable considering the fact that an FFAG was competing with a synchrotron as an energy frontier machine when it was first developed. The relatively complicated magnets and large nonlinearity made the design of hardware as well as optics difficult. As the demands on high intensity beams increased, however, it was realised that an FFAG has some advantages over other types of accelerators for these uses. The original paper in the 1950s already mentioned the possibility of high repetition operation to increase the average current [2]. Another use of an FFAG, which was probably not obvious when it was invented, is the acceleration of a beam of particles with short life such as muons and unstable nuclei. Lattice magnets with constant field can give the high acceleration rate which is only limited by the available rf voltage.

In this paper, we will discuss the recent development of optics and beam dynamics in an FFAG accelerator carried out at the Rutherford Appleton Laboratory.

3.17.2 Muon FFAG

The baseline design of a neutrino factory assumes a muon FFAG as the final accelerator from 12.6 GeV to 25 GeV [3]. This is a so-called nonscaling type of FFAG with linear magnets and a highly symmetric lattice structure. An FFAG is believed to be a cheaper option than a Recirculating Linear Accelerator (RLA). Demonstration of the feasibility of a linear nonscaling FFAG was planned and is now a construction project EMMA about to deliver the first beam at the Daresbury Laboratory [1].

A study during the International Scoping Study (ISS) collaboration period, however, revealed some issues that affect the use of an FFAG as a muon accelerator. First, the straight sections are too short to accommodate the injection and extraction systems for a huge muon beam. The septum and kicker strengths become beyond the engineering limit. This is due to the highly symmetric structure and the requirement to reduce the dispersion function as small as possible so that the beam orbit shift over the whole energy range can be minimised.

Secondly, we found that the muon beam emittance is so large that the time of flight difference between small and large transverse amplitude particles cannot be neglected [4]. The natural chromaticity does not help to eliminate the effects. Even worse, in the so-called serpentine acceleration scheme, small differences in the time of flight end up as a sizable momentum spread at the end of acceleration. This makes it hard to design more than one FFAG in a cascade, which we originally planned as a future Neutrino Factory upgrade.

3.17.2.1 *Injection and Extraction*

Based on a newly revised main lattice optics [5], the design of injection and extraction with hardware feasible from engineering point of view is underway. The short straight sections necessitate the use of distributed kickers. A superconducting septum may also be required. After studying three different types of lattices, it was decided that the triplet lattice with 3m drift is the most feasible from the point of view of injection and extraction. Injection in the horizontal plane can be achieved using three kickers in consecutive straights, each with a peak field of 0.09 T. The extraction system, this time in the vertical plane (due to the relatively high vertical betatron function in the straight at 25 GeV), consists of four kickers in consecutive straights with a peak field of 0.08 T. In each case, a 2T septum is assumed, though this field requirement may rise depending on the clearance required.

The injection and extraction systems are mirror-symmetric so that the same set of kickers is used by both muon signs. Special large aperture magnets will be needed to accommodate the excitation of the kicked beam. Previous simulations suggest that the symmetry breaking effects of these magnets will not be too severe [6]. The design of the kicker and septum magnets is ongoing.
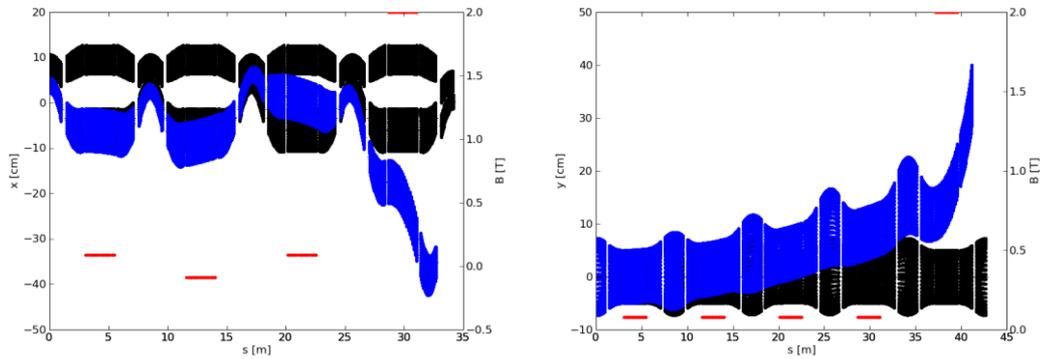
Figure 1: Injection (left) and extraction (right) in the muon FFAG. The 30π mm acceptance of the kicked (blue) and circulating (black) beam is shown. The peak field in the kicker magnets and septum is also shown (red dash, scale on right).

3.17.2.2 *Chromaticity Correction*

One of the ways to mitigate the time of flight problem depending on transverse amplitude is to correct chromaticity. It is possible to introduce nonlinearity in the main magnets and make the tune variation as a function of momentum almost flat. On the other hand, reduction of dynamic aperture becomes a main concern. Although a muon beam circulates only 10 to 20 turns, a small reduction may conflict with the aperture requirement for a muon beam of 30 π mm-rad normalized emittance.

Figure 2 shows the cell tune as a function of momentum before and after chromaticity correction using some multipoles. It shows that the fairly flat tune is obtained only with sextupole component.
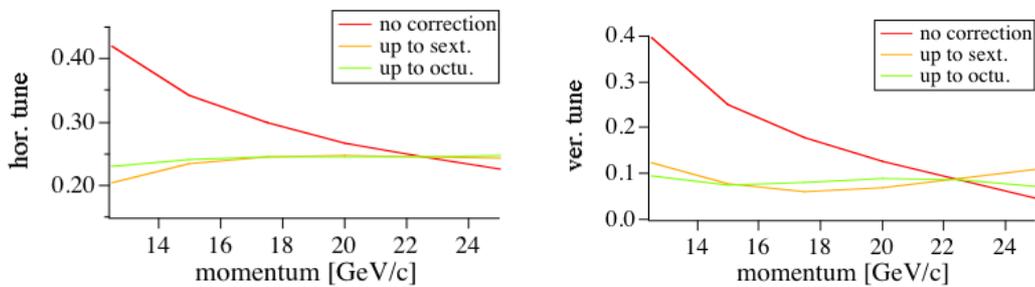
Figure 2: Tune as a function of momentum. Horizontal (left) and vertical (right) tune with and without multipole.

Dynamic aperture, on the other hand, deteriorates and the design acceptance is not satisfied when the full chromaticity correction is applied as shown in Fig. 3. In the figure, sextupole strength is normalized so that 100% correction gives the flat tune of Fig. 2. A dip around the sextupole strength of 40% corresponds to a single cell resonance where a cell tune is 1/3. A compromise between chromaticity correction and dynamic aperture can be found by the chromaticity correction with about 70% sextupole strength.
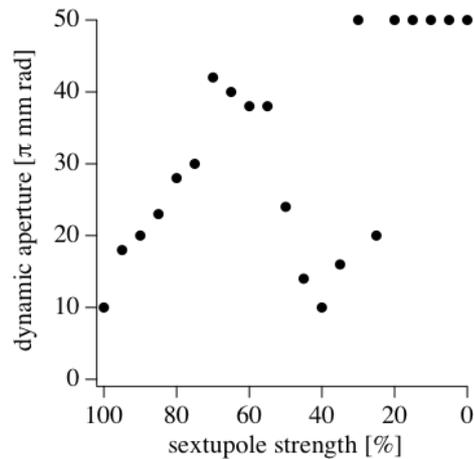
Figure 3: Dynamic aperture with sextupole correction. 0% means natural chromaticity and 100% sextupole strength makes the tune flat as in Fig. 2.

3.17.2.3 *Insertion*

Although the original idea of a nonscaling FFAG is to have high symmetry so that resonance crossing will not become an issue [7, 8], it is not clear if breaking symmetry really affects dynamic aperture. On the other hand, breaking symmetry of the lattice and having insertions with long straight section eases the injection and extraction.

It is possible to design a long triplet cell and install it every 11 cells, which makes a five fold superperiod lattice. Two long cells with 5 m drift space create one 7 m drift space and two 5 m drift spaces every 11 cells. The lattice functions are no longer identical for the operational momentum range, but the distortion is acceptable as shown in Fig. 4. With sextupole components to correct the chromaticity, dynamic aperture with and without insertion is almost the same.
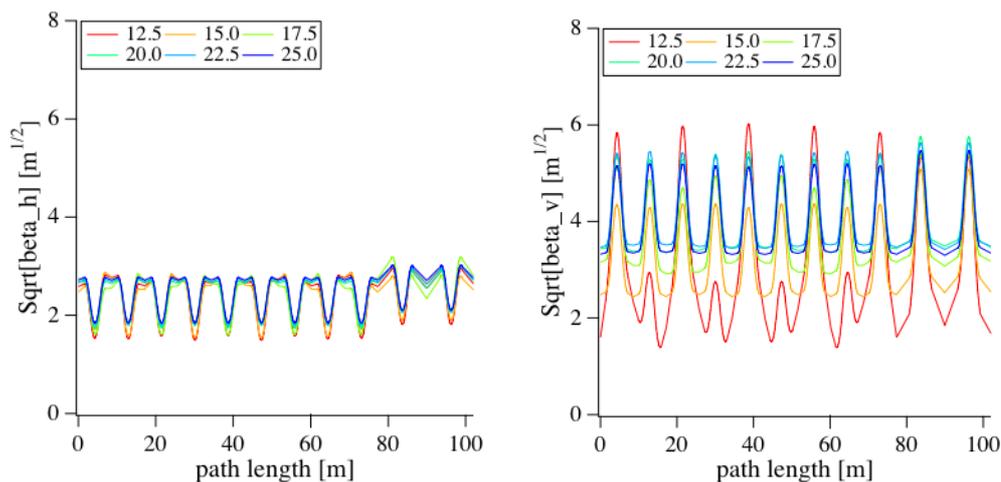
Figure 4: Horizontal (left) and vertical (right) beta functions of one superperiod. There are two long cells at the right end. The legend shows the beam momentum in GeV.

3.17.3 **FFAG for Proton Therapy**

3.17.3.1 *Requirement*

In order to use an accelerator in the fields where physicists are not the end users, considerations such as ease of operation, short times for maintenance and reliability become more important. This is especially the case when an accelerator is used as a charged particle therapy machine. Since it uses DC magnets and relatively simple rf systems, an FFAG is considered to be an ideal accelerator for such application with advantage over cyclotrons and synchrotrons. The potential of very high repetition rates of operation of the order of 1 kHz makes a spot scanning technique possible. One big problem is, however, that there is no experience of FFAG operation. Demonstration of such a machine is needed and the PAMELA project launched at the John Adams Institute of Accelerator Science at Oxford University is described in a separate paper [9].

3.17.3.2 *Optics*

FFAG accelerators were originally designed in order to keep the tune constant during acceleration. This can be done by introducing nonlinearity in the magnets. This type of FFAG is called a scaling FFAG. A muon FFAG on the other hand uses linear magnets and the tune moves during acceleration unless chromaticity correction is applied. It is called a linear nonscaling FFAG. For medical applications, both the advantage of a scaling FFAG that is free from resonance crossing and the compactness of a linear nonscaling FFAG are required. The design we made is a variety of a linear nonscaling FFAG based on a scaling FFAG, which becomes a nonlinear nonscaling FFAG.

The magnets of a scaling FFAG have a field profile of r^k to make the tune constant independent of momentum, where r is the radial coordinate and k is called the field index. In our design, we first expand the field into multipoles and take low order terms only. Secondly, we take a rectangular magnet instead of a scaling FFAG magnet which has a wedged shape. Thirdly, three magnets, which make triplet focusing, are aligned along a straight line so that alignment tolerance is improved. We found that a nonlinear nonscaling FFAG following this procedures still gives a fairly flat tune over the momentum range of a factor three [10].

Another novel feature of the design is to use the second stability region of Hill's equation [11]. Since the alternating gradient focusing was invented, accelerators have always relied on the first stability region of Hill's equation because the sensitivity to errors is large and beam envelope becomes enormous in the second stability region. In addition, there was no obvious advantage to operate an accelerator in the second instead of in the first region.

In our design of the nonlinear nonscaling FFAG, we use the second stability region to make the orbit shift smaller. For example, in the machine for particle therapy, the orbit shift is reduced by a factor of five. The sensitivity and beam size increase as one expects. However, it is controllable by choosing lattice parameters carefully.
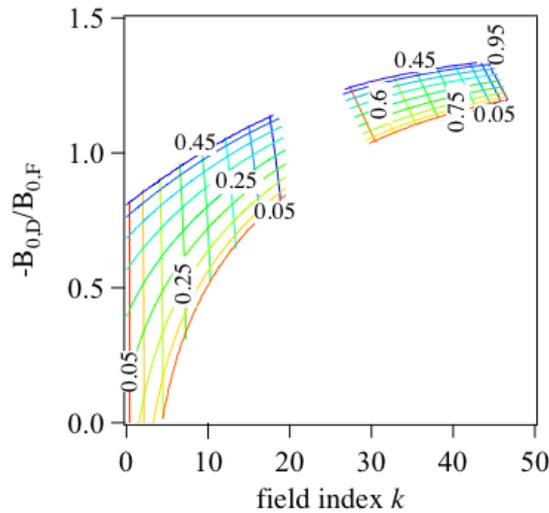
Figure 5: Stability diagram with practical lattice configuration. Upright numbers indicate vertical cell tune and vertically aligned numbers indicate horizontal cell tune. Lines are drawn in steps of 0.05.

3.17.3.3 *Beam Transport Idea and Gantry*

Although an accelerator and gantry is now ready to deliver a beam with different momenta at a rate of 1 kHz, the beam transport line in between are not ready for a beam for wide momentum range. It is natural to apply FFAG optics to transport a beam with wide momentum range. A straight beam transport line with a scaling FFAG field profile has designed. Figure 6 shows the orbit and optics of the design [12].
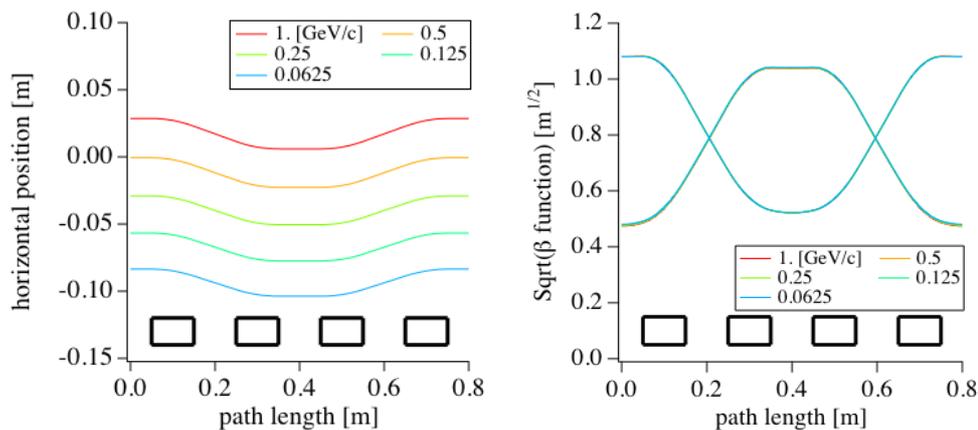
Figure 6: Different momentum orbits (left) and optics (right) in a unit cell which satisfies the periodic boundary condition. The rectangles at the bottom show the position of the FDDF magnets.

3.17.4 **FFAG as a High Intensity Proton Driver**

The potential for high repetition rate in FFAG operation makes it easy to deliver high average current keeping the bunch charge at a reasonable level. The conventional issues related to high intensity accelerators, such as space charge effects and collective instabilities, can be avoided.

One application of a high average current accelerator is a proton driver for accelerator driven subcritical reactor (ADSR). An ADSR must have almost CW beams from the proton driver and the beam time structure from an FFAG, of about 1 kHz repetition, matches the requirement. It is considered to be easier to increase the proton energy to more than 1 GeV than in the case of cyclotron. Based on the same design principle developed for a particle therapy accelerator, a design study of a proton driver for ADSR is underway. Figure 7 shows one example of the accelerator complex.
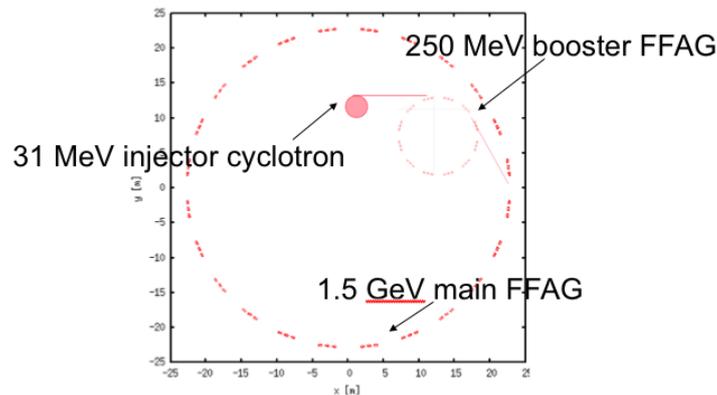
Figure 7: FFAG accelerator complex to deliver 1.5 GeV high intensity protons for ADSR.

3.17.5 **Summary**

Since the rebirth of an FFAG accelerator in Japan about ten years ago, intensive study on its optics, hardware development and construction of novel variations of this type of accelerator have been carried out all over the world. The Rutherford Appleton Laboratory has been at the centre of these activities and expects to continue to be so in future.

3.17.6 **Acknowledgment**

We would like to thank all those people collaborating with us under the UK Neutrino Factory, EMMA, PAMELA and ThorEA projects.

3.17.7 **References**

1. R. Edgecock, "The EMMA FFAG", in this issue.
2. K. R. Symon, D. W. Kerst, L. W. Jones L. J. Laslett, and K. M. Terwilliger, "Fixed-Field Alternating-Gradient Particle Accelerators", Phys. Rev. **103**, No. 6, 1956.
3. C. R. Prior, "Neutrino Factory Studies", in this issue.
4. S. Machida, "Longitudinal emittance blowup in fixed field alternating gradient muon accelerators", Phys. Rev. ST Accel. Beams **9**, 104002 (2006).
5. J. S. Berg, private communications.
6. J. Pasternak, M. Aslaninejad, J. S. Berg, D. J. Kelliher, S. Machida, "Feasibility of injection/extraction systems for muon ffag rings in the neutrino factory", Proceedings of PAC 09 (2009).
7. S. Machida and D. J. Kelliher, "Orbit and optics distortion in fixed field alternating gradient muon accelerators", Phys. Rev. ST Accel. Beams **10**, 114001 (2007).

8. S. Machida, "Resonance crossing and dynamic aperture in nonscaling fixed field alternating gradient accelerators", Phys. Rev. ST Accel. Beams **11**, 094003 (2008).
9. K. Peach, "Hadron Therapy in the UK", in this issue.
10. S. L. Sheehy, K. J. Peach, H. Witte, D. J. Kelliher, and S. Machida, "Fixed field alternating gradient accelerators with small orbit shift and tune excursion", submitted to Phys. Rev. ST Accel. Beams.
11. S. Machida, "Scaling Fixed-field alternating gradient accelerators with a small orbit excursion", Phys. Rev. Lett. **103**, 164801 (2009).
12. S. Machida, "Beam transport line with scaling fixed field alternating gradient type magnets", submitted to Phys. Rev. ST Accel. Beams.

3.18 High Voltage DC Photoinjector Development at Daresbury Laboratory

B.L. Militsyn[1], I. Burrows[1], R.J. Cash[1], B.D. Fell[1], L.B. Jones[1], J.W. McKenzie[1], K.J. Middleman[1], H.E. Scheibler[2] and A.S. Terekhov[2]

[1]STFC Daresbury Laboratory and Cockcroft Institute, Warrington, WA4 4AD, UK
[2]Institute of Semiconductor Physics SB RAS, Novosibirsk, 630090, Russia
Mail to: boris.militsyn@stfc.ac.uk

Abstract:

STFC Daresbury Laboratory currently operates a 350 kV DC electron gun using caesiated GaAs photocathodes to provide bunches up to a nominal 80 pC up to an average current of 6.5 mA. This serves as the injector for ALICE (Accelerators and Lasers In Combined Experiments) - a 35 MeV energy recovery linac based on 1.3 GHz superconducting RF technology. An upgrade to the electron gun is under way to incorporate a three-chamber photocathode preparation facility forming a load-lock with the gun chamber. This will allow rapid changeover of photocathodes without breaking the gun vacuum and improve photocathode activation procedure. Initial results of the activation in the commissioned preparation facility have produced quantum efficiencies of up to 15 % at 635 nm. The status of the project and ongoing research and development is presented here.

3.18.1 Introduction

GaAs photocathode based high voltage DC electron guns are operational at a number of different laboratories worldwide as injectors for energy recovery linacs and free electron lasers due to their potential to deliver beams of high average current (up to 100 mA in CW mode) with a relatively low normalized emittance of a few mm·mrads. DC guns with GaAs and other III-V family semiconductor photocathodes have typically being used as a source of polarized electrons at energies around 100 keV. Since the minimum emittance, ε_{min}, of the produced electron beam is related to the electric field strength on the cathode surface, E_c, as [1]

$$\varepsilon_{min} = \sqrt{\frac{q}{4\pi\varepsilon_0 E_c}\frac{k_B T_\perp}{m_e c^2}} \tag{1}$$

there is a drive towards higher voltage. GaAs based DC guns have been employed at TJNAF [2], Daresbury Laboratory [3] and JAEA/KEK [4] with power supplies rated to 500 kV and at Cornell University [5] with a 750 kV power supply.

3.18.2 **ALICE Gun**

The electron gun, shown in Figure 1, at Daresbury Laboratory is a modified version of the gun developed for the TJNAF Infra-Red FEL [2]. This operates at a nominal 350 kV with the standard ceramic insulator. The GaAs photocathodes are currently activated in-situ in the gun chamber with Cs and O_2 or NF_3 in a "yo-yo" procedure. The photocathodes are illuminated by a mode-locked Nd:YVO_4 laser, frequency doubled to 532 nm [6]. This provides 7 ps FWHM pulses at a repetition rate of 81.25 MHz. A pulse stacker is used to generate either 14 or 28 ps pulses. The pulse train length can be varied from a single bunch up to 100 μs with a train repetition rate of up to 20 Hz. The nominal bunch charge is 80 pC with a corresponding average train current of 6.5 mA. The maximum achieved quantum efficiency (QE) of the photocathodes has been 3.7 % and a maximum bunch charge of ~ 150 pC has been measured from the cathode. Typical operational photocathode 1/e lifetime is 100-250 hours with a dark lifetime measured at over 900 hours. A typical lifetime plot is shown in Figure 2.
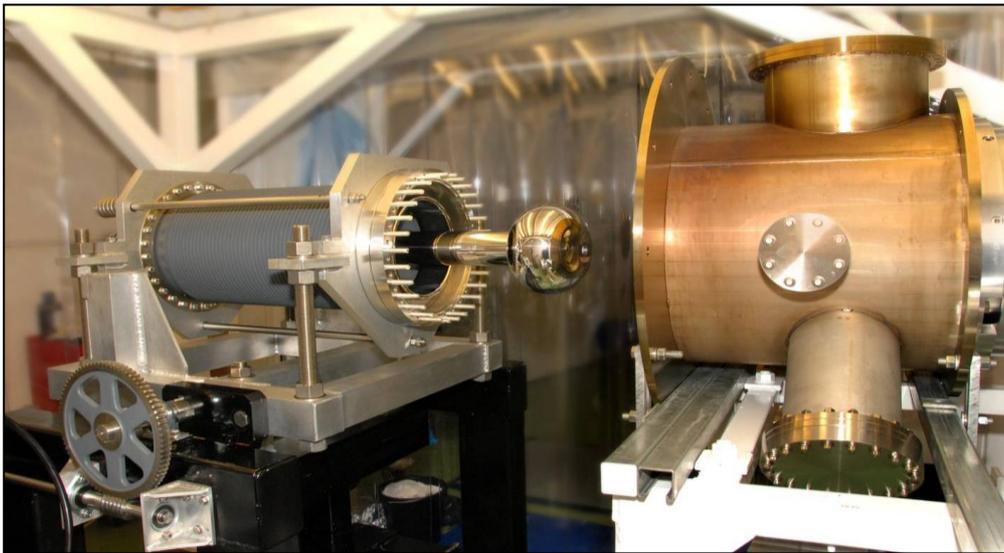
Figure 1: The ALICE electron gun before final assembly, showing ceramic and cathode ball.

The main modification to the TJNAF gun design is the use of a single large ceramic with bulk-doped controlled resistivity as the high voltage insulator. Whilst initially successful, with routine conditioning to 450 kV (up to a maximum of 485 kV), the long-term reliability of the brazing joints under load due to thermal cycling during baking has been poor. A collaboration between Daresbury Laboratory, TJNAF and Cornell University has resulted in design and delivery of an insulator with a modified taper near the brazing. In the interim period, ALICE has been operating with a smaller, two-piece insulator, limiting the operating voltage to ~250 kV. Field emitters on the current photocathode have further reduced operational voltage to 230 kV. A reduced bunch charge between 20 and 60 pC has been using whilst commissioning ALICE to minimize

downtime due to photocathode re-activation and to minimize beam loading effects in the superconducting RF booster.

Figure 3 shows QE maps of the current ALICE photocathode at the end of an operational cycle, and just after heat cleaning and re-activation. At the end of operations, the whole photocathode surface is reduced in QE. The large hole in the centre of the QE map is due to ion back-bombardment but is fully recovered after the heat cleaning and re-activation procedure. The smaller hole in the QE maps is a likely field emission point.
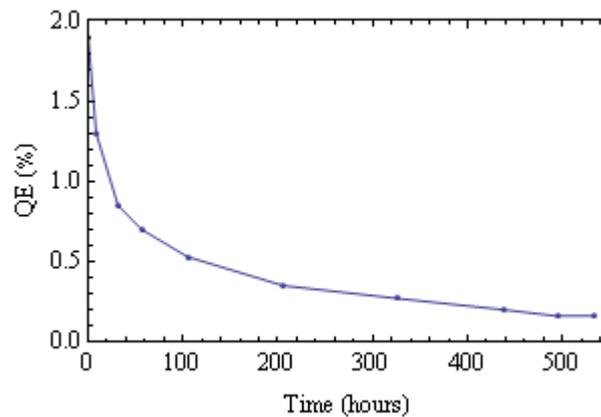
Figure 2: Example QE lifetime plot for photocathode during ALICE commissioning showing 1/e lifetime ~ 250 hours.
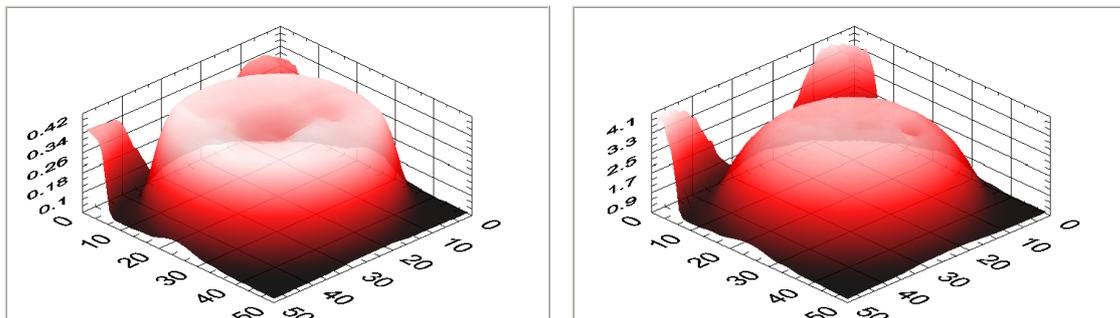
Figure 3: Typical QE maps at the end of the operational cycle (left) and after a full cathode re-activation including heat cleaning (right).

3.18.3 **ALICE Gun Upgrade**

An upgrade to the ALICE gun is currently underway, for installation in 2011, involving development of new photocathodes, a "load-lock" photocathode preparation facility (shown in Figure 4), and a side loading transport mechanism of the photocathode into the gun. These elements are described below. An extended gun beamline incorporating a suite of diagnostics useful for ALICE operations as well as testing different photocathodes is also being considered and is described in [7].
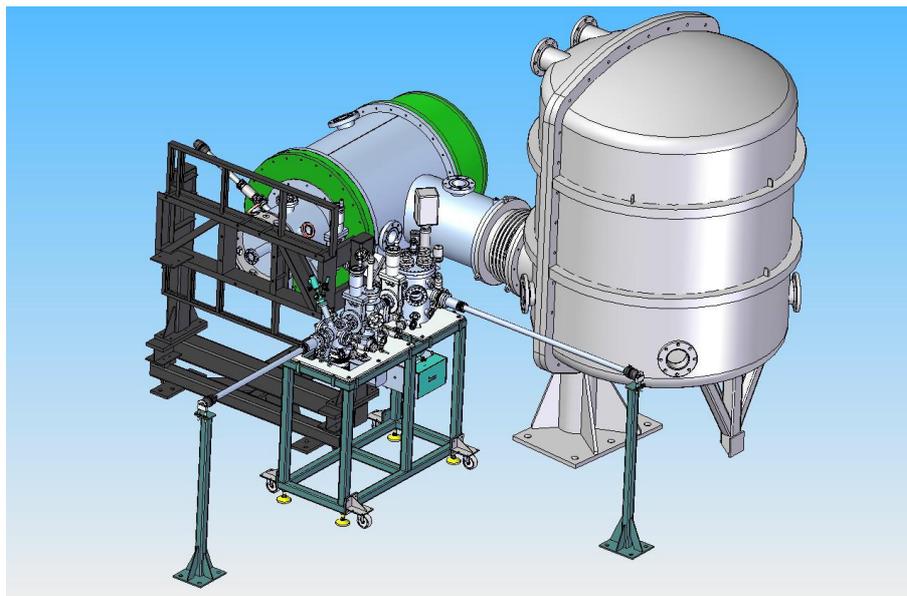
Figure 4: General view of the ALICE gun equipped with the photocathode preparation facility.

3.18.3.1 *Photocathode Development*

Originally III-V family photocathodes such as GaAs, GaAsP, InGaAsP were mainly used in DC guns for production of polarised electrons. As grown, these materials have a positive electron affinity (PEA), which for GaAs is 4 eV. In order to make GaAs photocathodes able to emit electrons when illuminated by 532 nm light, the electron affinity should be reduced to less than 1 eV - or even brought to a negative value. This activation process basically comprises deposition on the atomically-clean photocathode surface of a thin layer of Cs and an oxidant, typically O_2 or NF_3. Before the activation, the surface of the photocathode is chemically etched and heat cleaned in order to remove As and Ga oxides.

GaAs photocathodes place extremely high demands to operational vacuum conditions as they are very sensitive to the presence of oxidants in the residual atmosphere. For example the 1/e lifetime of GaAs does not exceed $2 \cdot 10^{-8}$ mbar·s of oxygen exposition [8]. The pressure in typical GaAs guns is of the level of 10^{-11} mbar. Low operational life time is also an issue. The dominant mode of GaAs degradation is bombardment of its surface by back streaming ions.

ALICE currently uses GaAs photocathodes with a diameter of 25 mm. The new cathode assembly of the gun, however, has been designed to accommodate photocathodes with an emission surface diameter of 10 mm, as shown in Figure 5. This is because the laser only illuminates an area ~ 4 mm in diameter and a smaller active area could help reduce the beam halo. The preparation facility allows a variety of III-V photocathodes to be tested in the ALICE photoinjector, with varying active layer composition, thickness, and electron affinity.

Figure 5: GaAs photocathodes on molybdenum substrate

Recent measurements of the QE spectra indicate that GaAs activated to PEA, where it is capable of picosecond level response times, has a QE of a few per cent [9]. This is enough to deliver bunches with a charge of several dozen pC. Figure 6 shows QE spectra for PEA GaAs photocathodes activated with Cs only to different levels of Cs coverage. The position of low energy threshold corresponds to the energy gap Eg for GaAs, and the position of I_{hot} corresponds to the vacuum level. The energy difference between these two thresholds is equal to the effective electron affinity. Figure 6 also shows measured longitudinal energy distribution of electrons emitted from a PEA GaAs photocathode, indicating that the trade-off for a fast response time is that the energy spread is relatively large.
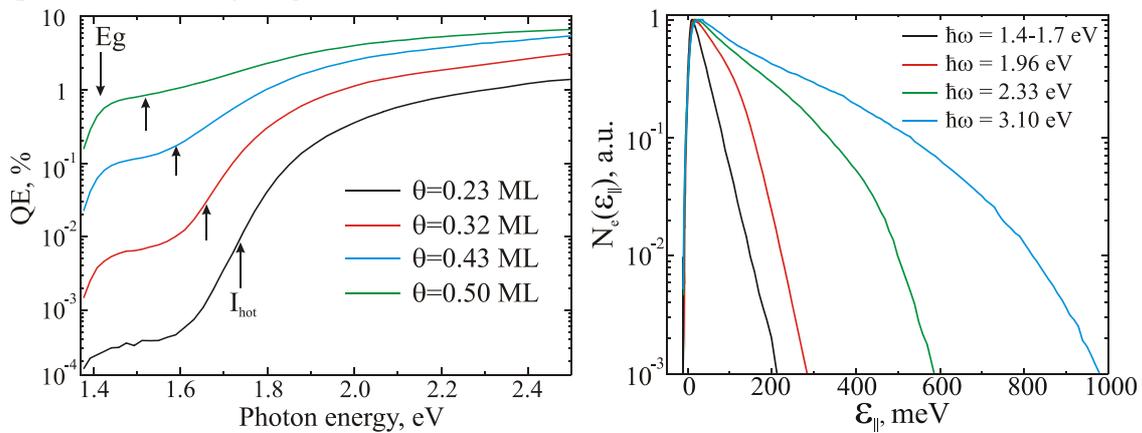
Figure 6: QE spectra of p-GaAs(Cs) –photocathode for different Cs coverage θ (left),and longitudinal energy distribution curves at different photon wavelengths for a PEA GaAs photocathode (right).

3.18.3.2 *Photocathode Preparation Facility*

As the photocathodes are currently activated in situ in the ALICE gun chamber, the process of photocathode changeover takes weeks due to the need to break and restore the vacuum to 10^{-11} mbar whilst replacing the photocathode, including an extensive bakeout at 250°C. A load-lock system will allow photocathode replacement to be made without breaking the vacuum thus reducing the time taken to a matter of hours. A separate preparation facility also removes the activation process of the GaAs photocathodes outside of the gun, thus reducing the introduction of contaminants into

the gun vacuum system and eliminating the risk of spreading Cs onto other parts of the cathode ball - which causes undesired field emission, and on the high voltage insulator - which reduces maximum achievable voltage. Such a facility has currently been built and commissioned at Daresbury Laboratory with plans for later installation onto the ALICE electron gun.

Figure 7: The assembled photocathode preparation facility.

The preparation facility, shown in Figure 7, consists of three chambers: a loading chamber where photocathodes are introduced to the system, a hydrogen-cleaning chamber to remove contaminants from the photocathode surface and a preparation chamber where photocathodes are activated. A magnetic manipulator is used to transport the photocathode between the three chambers. Before assembly, the components of facility were vacuum fired at a temperature of 950ºC for five hours to deplete the 316LN stainless steel of hydrogen.

Photocathodes are introduced into the loading chamber, as shown in Figure 8, by a z-translation stage containing a magazine holder capable of accommodating four photocathodes. To load new photocathodes, the magazine holder is removed from the loading chamber and transported under dry nitrogen to a nitrogen-purged glove box where new photocathodes are chemically etched. The etched photocathodes are inserted into the magazine holder, and the z-stage is closed such that the 'O' ring seals. The photocathodes are thus stored in a leak tight nitrogen environment. The z-stage is then re-inserted in to the loading chamber, the 'O' ring seal opened and the chamber evacuated to ensure the photocathodes are not exposed to any contaminants from the atmosphere. The pumping system of the loading chamber includes an ion pump and an oil-free preliminary pumping station. After the photocathode is placed into the loading chamber, it is pumped down to a pressure of 10^{-9} mbar.
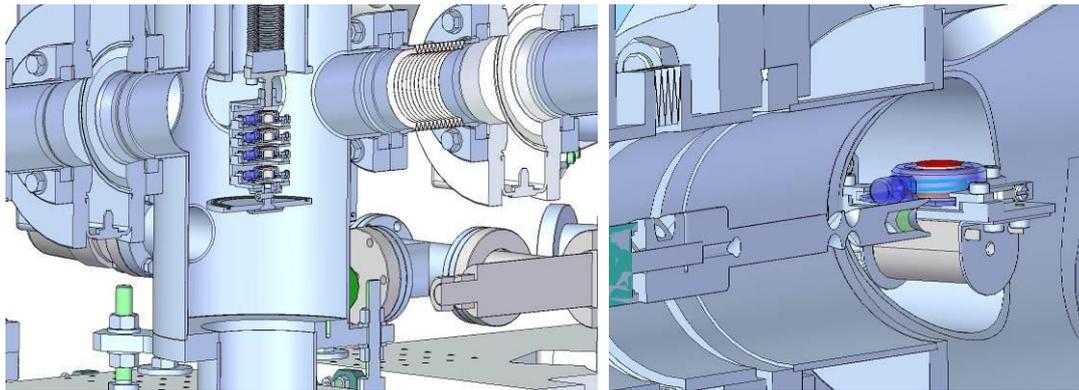
Figure 8: Section views of (left) the loading chamber, and (right) the hydrogen cleaning chamber.

The hydrogen cleaning chamber, shown in Figure 8, is used to initially process photocathodes before activation, and to process used photocathodes before re-activation. The photocathode is heated to ~300 ºC via the use of a halogen bulb. The bulb is shielded by tantalum screen to avoid any radiative heating of other components whilst focusing the heat onto the photocathode, thus minimising the power requirements. The hydrogen cleaning process makes use of a thermal gas cracker that uses electron bombardment of a tungsten capillary to thermally dissociate the gas passing through it. Given the right conditions the thermal cracking efficiency of hydrogen is very high and this is important in order to minimise the number of H^+/H^- ions in the cleaning process.
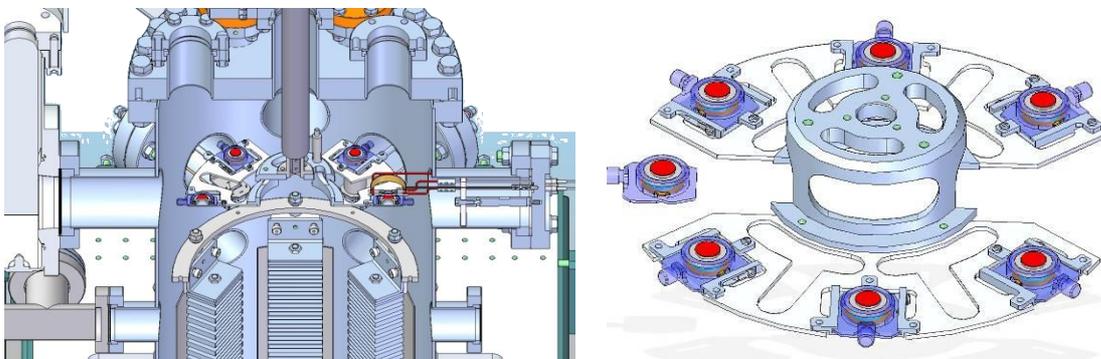
Figure 9: Section view of the activation chamber (left), the photocathode carousel (right).

Figure 9 shows the activation chamber - which contains a carousel capable of holding six photocathodes. A photocathode, transferred from the hydrogen cleaning chamber, is first heat cleaned. There are two heating positions in the chamber, each using the same halogen bulbs as in the hydrogen cleaning chamber. Finite element analysis shows that the temperature of the neighbouring photocathodes should remain less than 100°C during the heat cleaning process. Once cooled, the heat cleaned photocathode is rotated into the single activation position. Cs dispensers are positioned within 10 mm of the photocathode surface, as is the charge collector used to measure the photocurrent. The O_2/NF_3 is injected into the system via a piezo-electric fine leak valve which is positioned on the conflat flange that sits directly above the photocathode. XHV conditions are maintained in the activation chamber by means of ion pumps and

168

six non-evaporable getter strips. The typical pressure is less than 10^{-11} mbar, with partial pressures of oxygen, water vapour and CO_2 less than 10^{-14} mbar.

The photocathode preparation facility was successfully commissioned in spring 2009, with a maximum achieved quantum efficiency of 15% at a wavelength of 635 nm. Figure 10 shows the "yo-yo" procedure used.
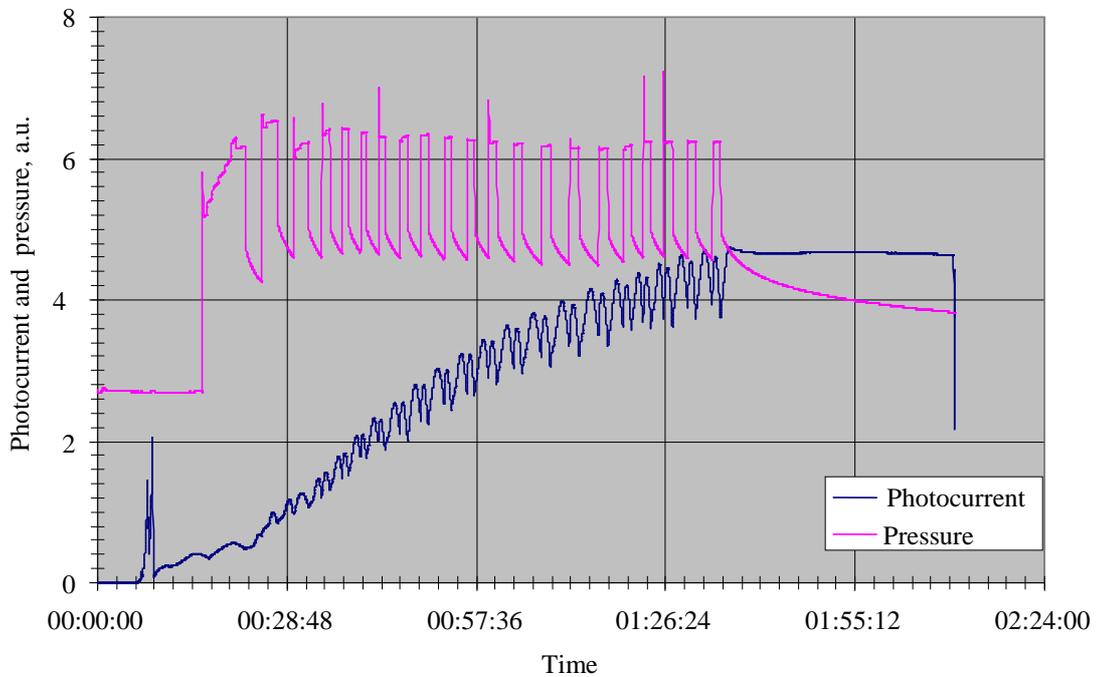
Figure 10: Cs-O activation of a GaAs photocathode using the "yo-yo" procedure.

3.18.3.3 *Cathode Ball Design*

It is proposed that the photocathodes are loaded from the preparation chamber into the side of the gun, in order to avoid disruption to the existing ALICE infrastructure. This involves a re-design of the cathode ball from the present rear-loading mechanism. The ball requires a slot in the side for loading of the photocathode. This has been positioned on the cylindrical part of the ball surface to keep the field distortion low. The photocathode then has to be moved forward into position, requiring a second slot further back in the cathode ball for insertion of a magnetic screwdriver to drive the winding mechanism. A third slot, perpendicular to the loading slot, is required as a viewport to ensure the photocathode is loaded properly. Figure 11 shows the electric fields at 350 kV on the cathode ball surface, as modelled in CST Studio [10]. The electric field has been kept lower than 10 MV/m on the curved surface of the ball and also around the edges of the slots. A focussing electrode has been added and optimised by performing beam dynamic simulations in ASTRA [11]. Figure 12 shows that the transverse beam properties for the new gun design compared to the existing gun which lacks the focussing electrode.
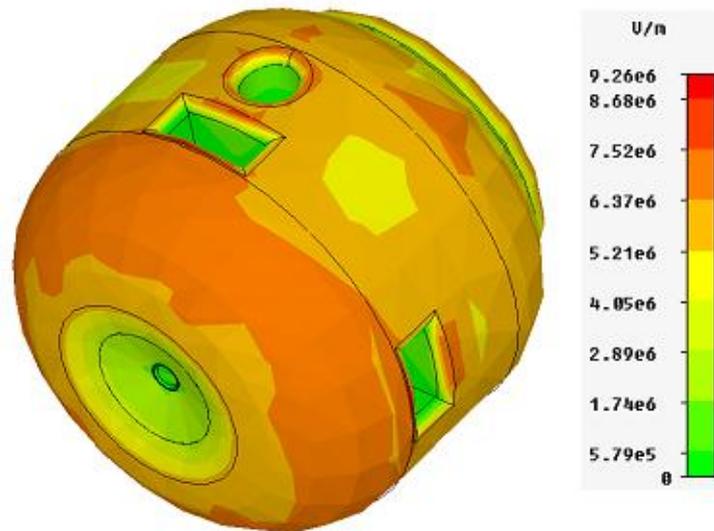
Figure 11: The cathode ball with slots and focusing electrode showing electric fields.
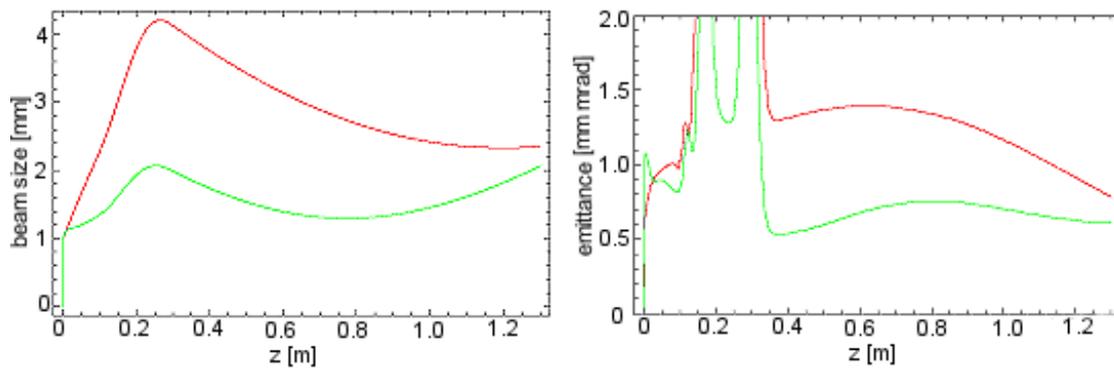
Figure 12: RMS beam size (left) and transverse emittance (right) for the new gun design (green) compared to the current gun (red) including a 330 G solenoid at 0.25 m.

3.18.4 **Summary**

The GaAs based 350 kV DC gun for ALICE has been operational since August 2006 – with a maximum QE of 3.7 % achieved and dark lifetime in excess of 900 hours. Following development of III-V photocathodes on different substrates and activated to differing levels of electron affinity, a three-chamber photocathode preparation facility has been constructed at Daresbury Laboratory. This has successfully been commissioned and GaAs photocathodes have been activated with a maximum QE of 15% measured at 635 nm. This facility will be installed on the ALICE gun in 2011, enabling faster photocathode changeover and better vacuum conditions in the gun. The design of the photocathode preparation facility means that in future additional chambers can be added, allowing testing of multi-alkali photocathode materials, such as K_2CsSb, in the ALICE electron gun. These should offer high QE (up to 20 %) at the 532 nm wavelength of the current ALICE photoinjector laser and have a fast response time. They could also offer a longer lifetime than GaAs photocathodes since they have shown a much higher robustness under exposition to oxygen [12]. However, their stability to ion back-bombardment is unknown and has to be investigated.

3.18.5 **References**

1. I.V. Bazarov et al., "Thermal Emittance and Response Time Measurements of Negative Electron Affinity Photocathodes", J. App. Phys. 103, 054901 (2008)
2. T. Siggins et al., "Performance of a DC GaAs photocathode gun for the Jefferson lab FEL", NIM A475 (2001) 549-553.
3. Y.M. Saveliev et al., "Results from ALICE (ERLP) DC Photoinjector Gun Commissioning, proceedings of EPAC 2008.
4. N. Nishimori et al., "Development of a 500-kV Photo-cathode DC Gun for the ERL Light Sources in Japan", proceedings of FEL 2009.
5. B.M. Dunham et al., "Performance of a Very High Voltage Photoemission Electron Gun for a High Brightness, High Average Current ERL Injector, proceedings of PAC 2007.
6. L.B. Jones, "Status of the ERLP photoinjector drive laser", proceedings of ERL 2007.
7. J.W. McKenzie, B.D Muratori, Y.M. Saveliev, "Extended ALICE Injector", proceedings of PAC 2009.
8. S. Pastuszka, A.S. Terekhov, A. Wolf, "'Stable to unstable' transition in the (Cs, O) activation layer on GaAs (100) surfaces with negative electron affinity in extremely high vacuum", Applied Surface Science 99, (1996) 361
9. B.L. Militsyn et al., "Design of an upgrade to the ALICE photocathode electron gun", proceedings of EPAC 2008.
10. CST Studio Suite, http://www.cst.de
11. K. Flöttmann, ASTRA, http://www.desy.de/~mpyflo
12. P. Michelato et al., "R & D activity on high QE alkali photocathodes for RF guns", proceedings of PAC 1995.

3.19 **Cryomodule Development at Daresbury Laboratory**

P. A. McIntosh, R. Bate, C. D. Beard, M. A. Cordwell, D. M. Dykes, S. M. Pattalwar and J. Strachan, STFC Daresbury Laboratory and Cockcroft Institute, Keckwick Lane, Warrington, WA4 4AD, UK

S. Belomestnykh, E. Chojnacki, Z. Conway, G. Hoffstaetter, M. Liepe, H. Padamsee, P. Quigley, J. Sears, V. Shemelin and V. Veshcherevich
Cornell University, Ithaca, NY, 14853, USA

D. Proch and J. Sekutowicz, DESY, Hamburg, Germany

A. Büchner, F. Gabriel and P. Michel
FZR Rossendorf, Strahlungsquelle ELBE, PF 510119, D-01314 Dresden, Germany

J. N. Corlett, D. Li and S. Lidia, LBNL, Berkeley, CA 94720, USA

T. Kimura and T. I. Smith, HEPL Stanford University, Stanford, CA, 94305, USA

S. Koscielniak and R. Laxdal, TRIUMF, 4004 Wesbrook Mall, Vancouver, Canada

3.19.1 **Introduction**

Preparations for the assembly of a new Superconducting RF (SRF) cryomodule, which has been developed for long-term high Q_{ext} and CW operation for application on

Energy Recovery Linac (ERL) accelerators, is well underway at Daresbury Laboratory [1].

Table 1: Cryomodule Design Parameters

Parameter	Value
Frequency (GHz)	1.3
Number of Cavities	2
Number of Cells per Cavity	7
Cryomodule Length (m)	3.6
R/Q (Ω)	762
E_{acc} (MV/m)	> 20
E_{pk}/E_{acc}	2.23
H_{pk}/E_{acc} (Oe/MV/m)	46.9
Cryomodule Energy Gain (MeV)	> 32
Q_o	>1 x 10^{10}
Q_{ext}	4 x 10^6 - 10^8
Maximum Beam Current	100 mA
Max. Cavity Forward Power (kW)	25 SW

To date, the international partners who have participated in this collaborative development (Cornell and Stanford Universities, Daresbury Laboratory, DESY, FZD-Rossendorf, Lawrence Berkeley Laboratory, and more latterly TRIUMF) have identified appropriate sub-system solutions to achieve the fundamental requirements for this new cryomodule, which have been reported previously elsewhere [2]. Stanford University have provided a cryomodule which has an identical layout to that of the modules available on the ALICE facility at Daresbury, such that the completed module can be incorporated onto ALICE and its associated support services. Cornell University will provide the HOM absorber design to be incorporated into the cryomodule and DESY will provide 7-cell TESLA/TTF cavities [3] (previously used for the superstructure) that will be modified by Cornell and integrated by Daresbury. LBNL, FZR Rossendorf and Daresbury are providing engineering resources to facilitate the integration process, in particular with regards to the mechanical and RF optimisation. This includes opening up the beam pipe diameter to conduct all HOMs out to the ferrite beam pipe loads.

Table 1 highlights the primary cryomodule design parameters, which will be installed on the ALICE ERL accelerator at Daresbury Laboratory and validated with beam in 2010.

3.19.2 Cavity Design and Fabrication

The cavity optimisation process has used as a baseline the TESLA 7-cell superstructure geometry developed at DESY and our design utilises the same 5 centre cells as the TESLA superstructure cavity, with optimisation of the end cells and enlargement of the beam pipes (see Figure 1) to match to beam-pipe HOM absorbers as developed by Cornell.

To reach the required Q_{ext} tuning range ($10^7 - 10^8$), the position of the input coupler with respect to the cavity end cell has been analysed. Due to the physical size of the coupler employed (see later), its location is restricted to 113.1 - 133.1 mm measured from the coupler axis to the equator of the end-cell.
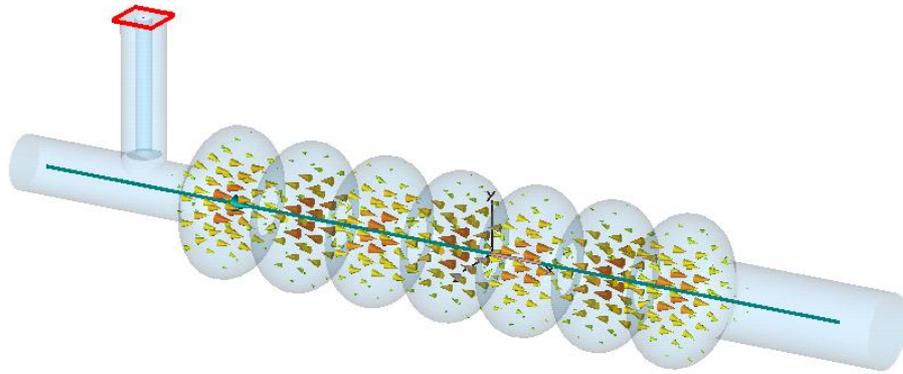
Figure 1: Plot of the E-Field inside the ERL 7-Cell cavity

The coupler antenna has a penetration adjustment of up to 15 mm and a full parametrisation of coupler distance from the end cell and its penetration has been assessed. The required range of Q_{ext} as a function of antenna penetration was achieved with the coupler located 123.1 mm from the end cell (see Figure 2). At a 123.1mm offset, the required Q_{ext} range is nearly obtained with a 15 mm variation in antenna penetration. The addition of a triple-stub tuner can be used to extend the upper range of the operational Q_{ext} to beyond 10^8 if required.
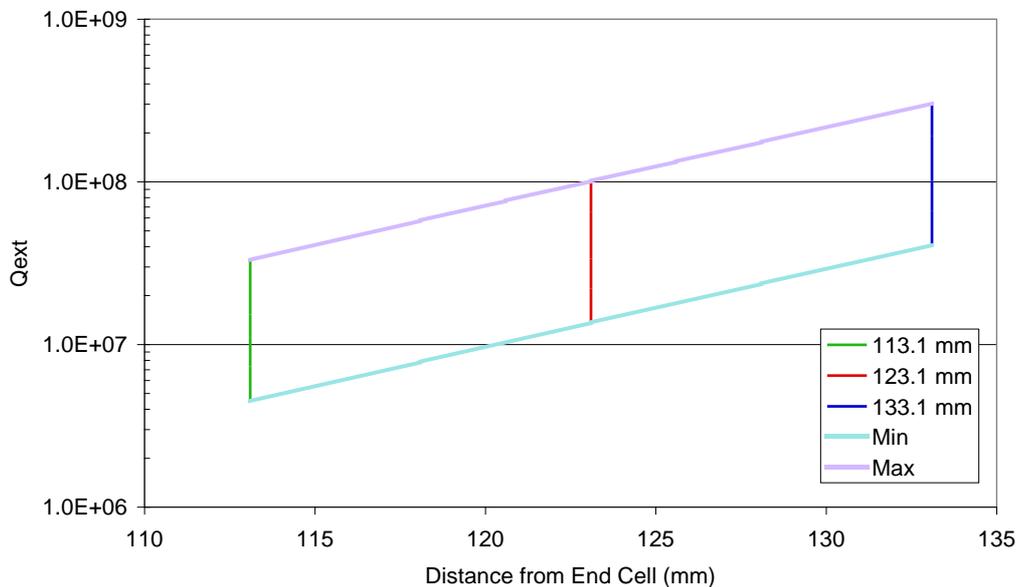
Figure 2: Variation of Q_{ext} with antenna extension and position

Two seven-cell niobium cavities have been fabricated (Figure 3). The section from the first to the last equator was cut from two seven-cell superstructure cavities provided by DESY. The outer half-cells and associated beam pipes (end groups) are of a new design developed by LBNL, Daresbury and Cornell. Their geometries were optimized

to facilitate the propagation of higher order mode power to ferrite-lined beam-pipe loads.

Figure 3: 7-cell cavity after final electron-beam welding.

Figure 4 shows a schematic of the end cell geometries and integrated cavity string assembly. After fabrication, the cavities have been tuned for field flatness of the π-mode. As the gradient will be 20 MV/m or less in operation, only BCP treatment is used for the final stage of cavity preparation (see Figure 5). So far, one of the two cavities was tested twice in a vertical cryostat. The first test was performed after light BCP (10 to 15 microns of surface material removal) and HPR. A low field Q of the π-mode was measured to be 2.2×10^9 at 1.8 K. In this test we were not able to couple to all modes of the fundamental pass-band, hence we could not localize the cells responsible for the low Q. Also, the coupling was too weak to perform reliable RF field calibration and Q vs E measurement.
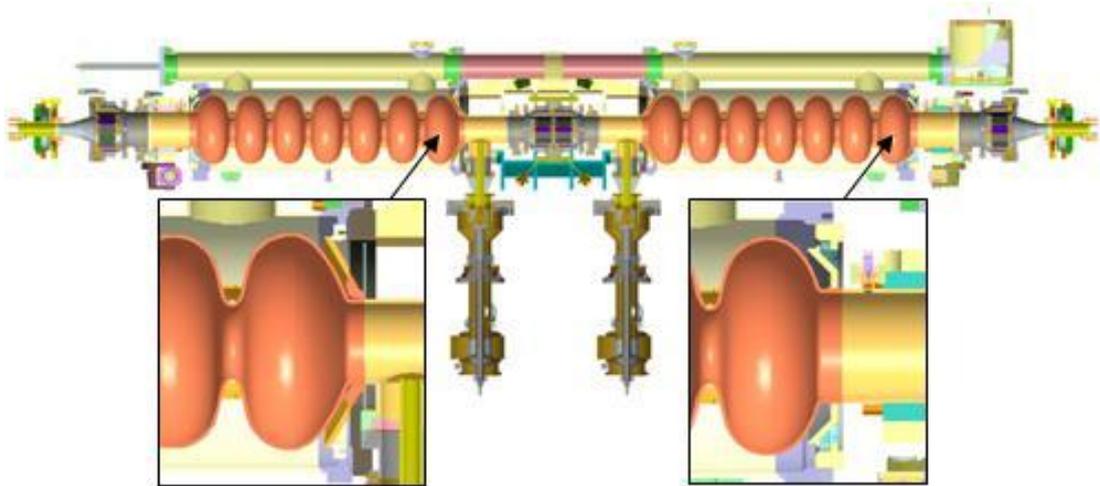
Figure 4: ERL cavity string assembly

After an additional light BCP (about 20 microns) and HPR, the cavity was re-tested. Again, a low Q (1.5×10^9 at 2 K) was measured for the π-mode. This time however, we were able to measure low field Q's of all seven fundamental pass-band modes. These measurements indicate that excessive losses in the end cell(s) are responsible for the low quality factor of modes with high fields in those regions. The $\pi/7$ mode, which has very low fields in the end cells, has a rather decent Q of 1.1×10^{10}.
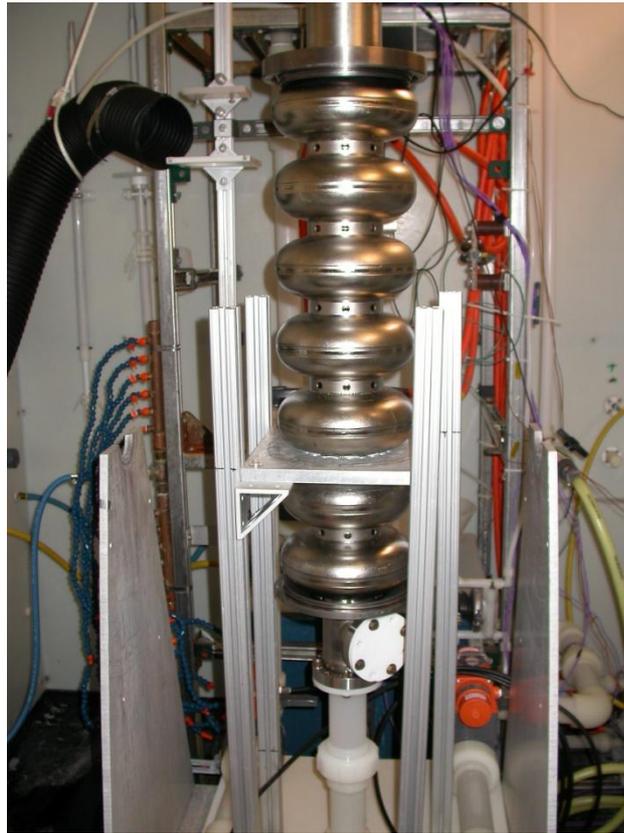
Figure 5: First cavity prepared for BCP processing

The second cavity is in the final stage of preparation for a vertical test. The results of which, along with close examination of the first cavity's end groups will guide further decisions for repeated tests. All flange designs have been changed to knife-edge conflat interconnections, with brazing to Nb beam tubes similar to that used for the Cornell Injector cryomodule [3]. The Ti-helium vessel and gas return pipe designs are modified to conform to the FZD Rossendorf cryomodule discussed below. The blade tuner used for the TTF superstructure test was changed to a modified Saclay II tuner design so that it would fit in the chosen cryomodule envelope. The input couplers and HOM loads have been chosen to be identical to the ones used in the Cornell Injector module [4]. The design of the cavity string is carefully laid out to fit inside the module.

3.19.3 **Tuner Development**
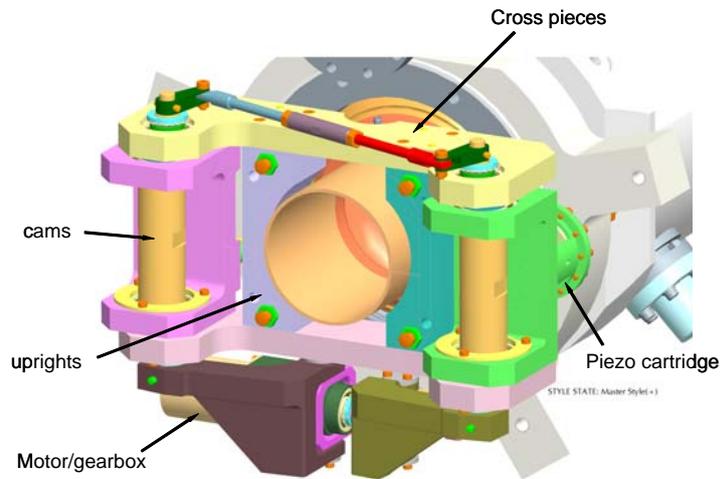
Figure 6: Adaptation of the Saclay II tuner to the 7-cell cavity.

After examining different tuner alternatives it was decided to adopt a design based on the Saclay II tuner which was developed as part of the CARE project by CEA Saclay (see Figure 6) [5]. This design was chosen due to its compact size, its adaptability to the large beam pipe diameter of the 7-cell cavity and the promising test results observed when utilised to compensate for Lorenz force and microphonics detuning on a 9-cell cavity on CryHoLab at Saclay [6] and on HoBiCaT at BESSY [7].

Figure 7: Modified Saclay-II tuner assembly.

The Saclay II tuner design must fit over the larger diameter beam tube (106 mm) of the 7-cell cavity (see Figure 7). The piezo cartridge design of the tuner is being modified to allow the piezos to be pre-compressed without relying on the forces generated through tuning of the cavity string. Furthermore, we are replacing the low voltage piezo stack with a high voltage stack to achieve a higher degree of stiffness.

3.19.4 **INPUT Coupler Preparations**

The chosen solution for a suitable input coupler, capable of delivering 20 kW CW in standing wave, whilst also providing adjustability in terms of its Q_{ext} setting, is the Cornell ERL injector coupler (see Figure 8) [8]. CPI have successfully fabricated a number of these couplers and the power handling capability has been proven up to 50 kW CW in travelling wave.
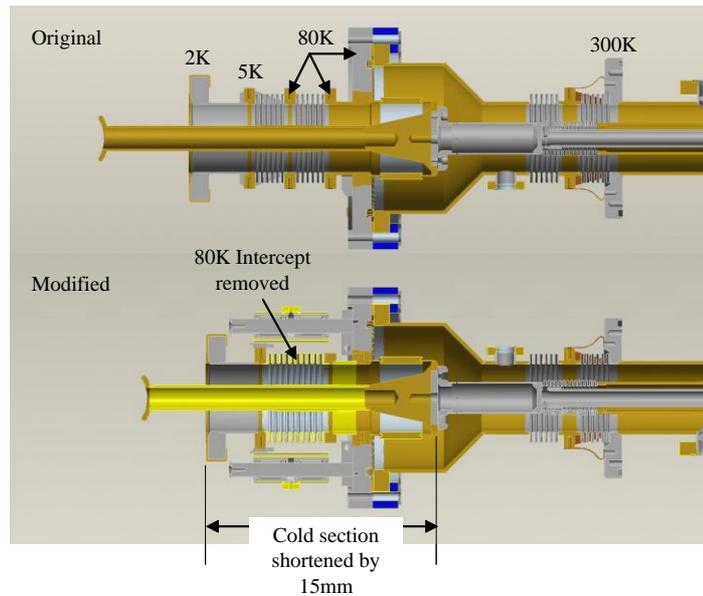
Figure 8: Original and modified Cornell ERL injector coupler.

To allow for the insertion of the cold part of the coupler and the modified cavity string into the cryomodule, its total length has been shortened by removal of the secondary 80 K thermal intercept which was fundamentally required for 50 kW operation. This enables the cavity string to be inserted into the cryomodule without interfering with the cryomodule vessel. The modified coupler heat loads due to these modifications are shown in Table 2.

Table 2: Modified Cornell Coupler Heat Loads

Parameter	Original	Modified
Max Power (kW)	50 TW	20 SW
Antenna Stroke (mm)	>15	<15
Heat Leak to 2K (W)	0.23	0.13
Heat Leak to 5K (W)	1.7	2.5
Heat Leak to 80K (W)	43	34

Prior to assembly of the couplers into the cavity string, they must be rigorously cleaned and inspected, before being baked and high power RF processed. Both couplers have been assembled onto their respective cold and warm baking stations (see Figure 9 a) and b)) and baked at 150 C for 24 hours.
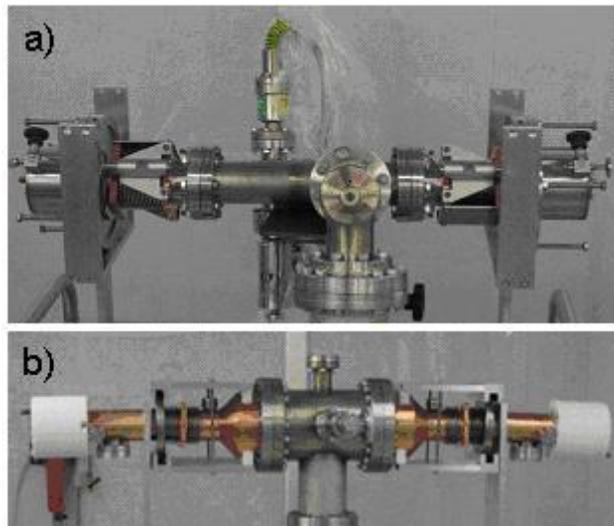
Figure 9: a) Cold and b) Warm coupler bake assemblies at Daresbury.

The couplers have now been assembled in a back-to-back configuration, onto a high power coupling box to allow for high power conditioning (see Figure 10).
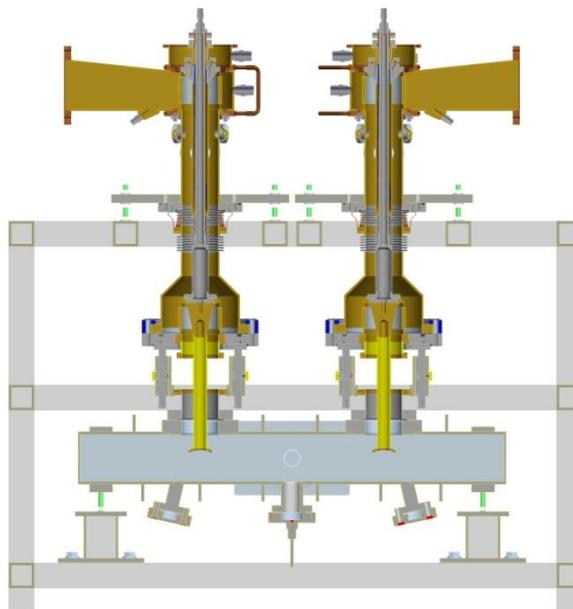
Figure 10: Input coupler RF conditioning assembly.

RF power will be limited to ~10 kW CW during conditioning, as gaseous helium (GHe) cooling will not be available. Pulsed conditioning will then be performed up to the 30 kW limit of the IOT test stand at Daresbury (see Figure 11).
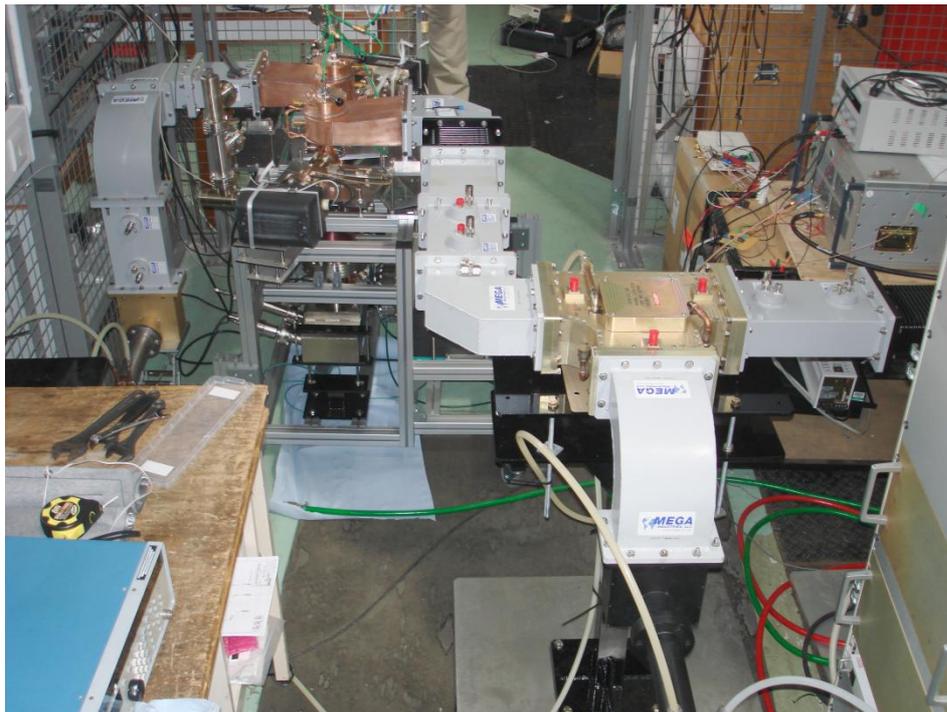
Figure 11: High power couplers assembled on IOT test stand.

3.19.5 **Cryomodule Assembly Process**

Wherever possible, existing assembly procedures and tooling fixtures have been employed from the original ALICE cryomodule, fabricated by ACCEL GmbH (now Reaserch Instruments GmbH) under license from FZD Rossendorf [9]. All of the major internal cryomodule components have however been modified including; cavities, input couplers, tuners, HOM absorbers, magnetic shields and cryogenic cooling circuits.
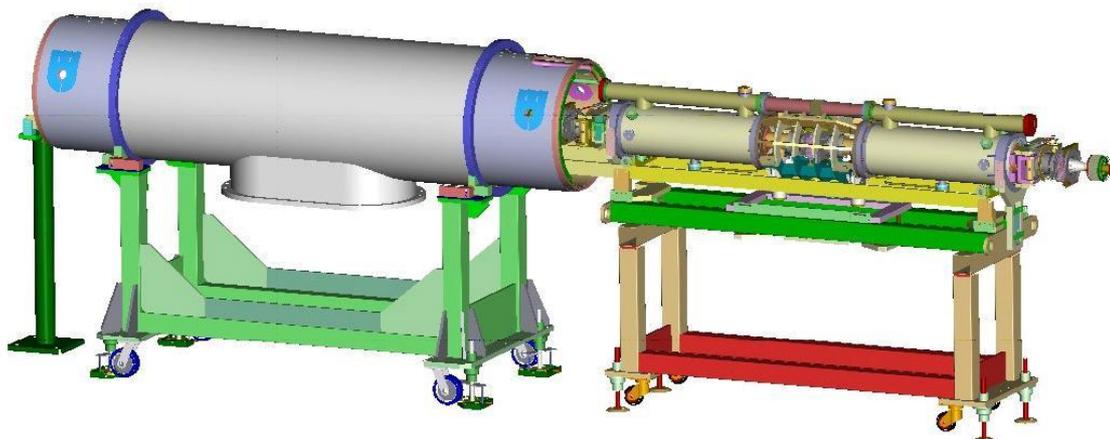
Figure 12: Cavity string assembly into outer cryomodule.

By utilisation of a cantilevered rail system, the sealed cavity string assembly can be rolled into the outer cryomodule vessel (see Figure 12). Once positioned, the cavity string is then locked in place by a single titanium locking fixture, which then provides a longitudinal constraint on the mechanical component contraction when the cryomodule

is cooled to cryogenic temperatures (see Figure 13). In this way, the contraction occurs from both ends of the cryomodule towards this central, locked position. This ensures that the input couplers (which are positioned very close to the central locked reference position) do not get exposed to excessive lateral stresses during cool-down.

The cryomodule incorporates three layers of magnetic shielding in order to try and maximise the achievable Q_o and thereby minimise the cavity dynamic heat load; two mu-metal magnetic shields are attached to the outer 80 K skeleton and a third cryoperm magnetic shield covers each cavity helium vessel.
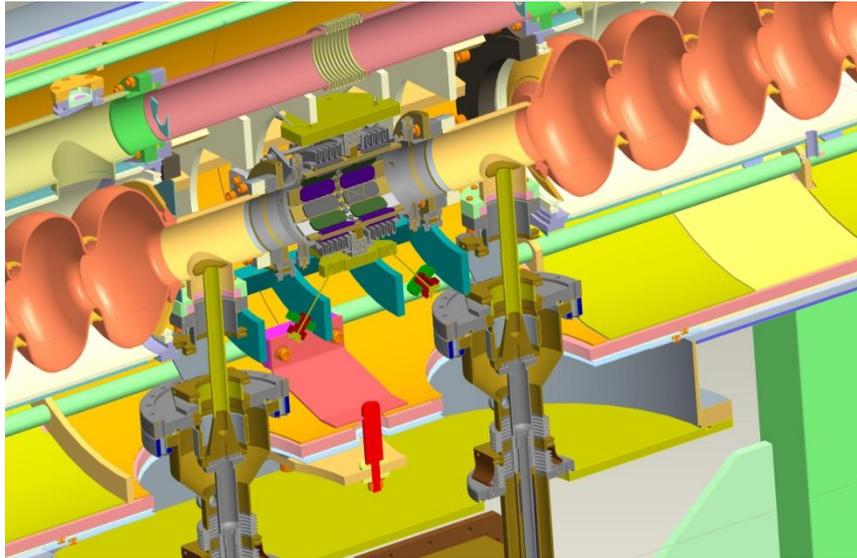
Figure 13: Central cavity string locking position.

3.19.6 **ALICE Cryoplant Modifications**

Presently on ALICE, the cryomodule 80 K skeleton is cooled using liquid nitrogen (LN2), however for this new cryomodule GHe will be used, which will have the anticipated benefit of reducing turbulent pressure fluctuations, leading to a lower cryomodule microphonics sensitivity. In addition, both the input couplers and all three beam-pipe HOM absorbers have 5 K cooling intercepts, which the existing ALICE cryogenics system does not currently provide (see Figure 14).

180
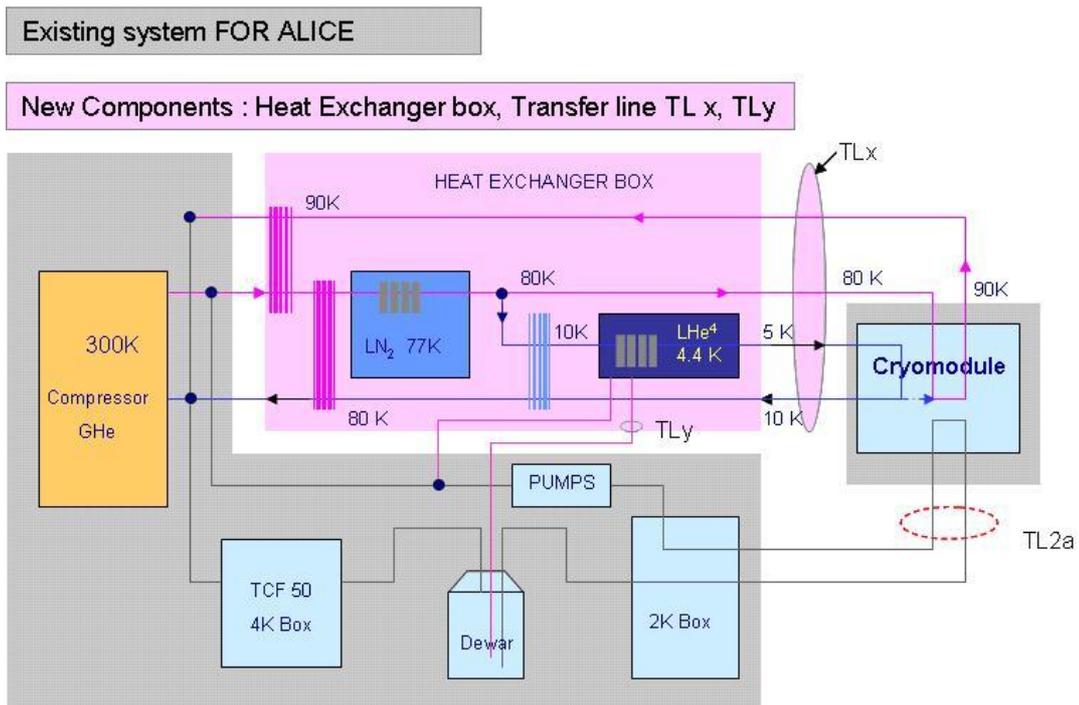
Figure 14: ALICE cryoplant modifications.

A secondary heat exchanger system (designated COOL-IT; COOLing to Intermediate Temperatures) [10] has therefore been developed which taps off available 300 K, high pressure GHe from the main compressor, plus an additional LHe feed from the 4 K reservoir dewar. The high pressure GHe circuits at 80 K and 5 K are then generated via the heat exchanger box, which will be located close to the ALICE ERL cryomodule as shown in Figure 15.
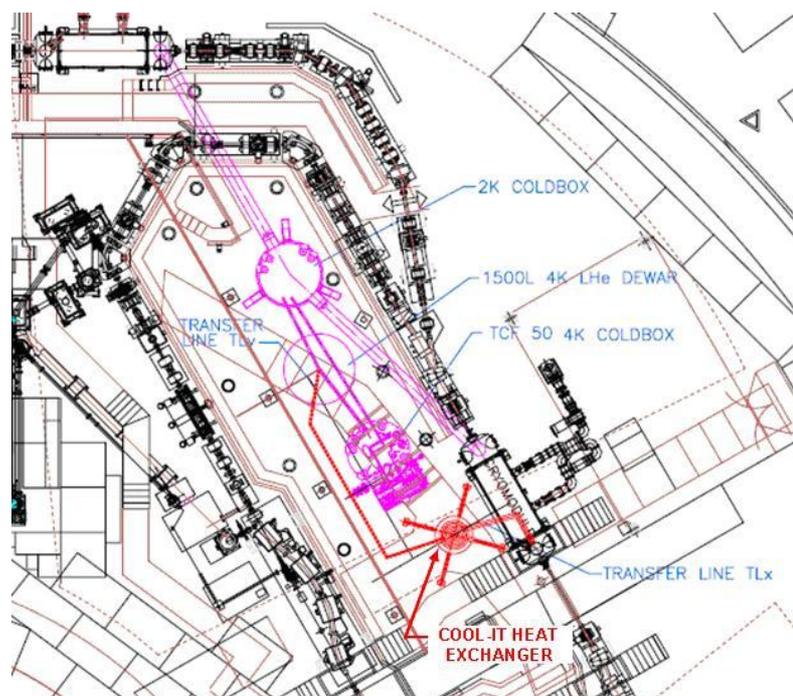
Figure 15: COOL-IT system installation on ALICE.

The COOL-IT heat exchanger system is currently being fabricated by AS Scientific in the UK and first acceptance tests have been completed to ensure vacuum integrity of all components (see Figure 16). Final stability checks were performed in preparation for delivery at Daresbury in October 2009. COOL-IT is now installed on ALICE, with all interfacing and instrumentation testing underway.

Figure 16: COOL-IT heat exchanger at AS Scientific.

3.19.7 **Summary and Outlook**

The vast majority of the cryomodule hardware is now either available or under fabrication. We anticipate having both couplers RF conditioned and cavities available at Daresbury by mid 2010. All tooling and fixtures required for the cryomodule assembly are complete and cleanroom assembly of the cavity string is expected to start later this year. The COOL-IT system is now installed on ALICE in readiness for connection to the new cryomodule when installed in early 2011.

3.19.8 **References**

1. M.W. Poole et al, "4GLS and the Energy Recovery Linac Prototype Project at Daresbury Laboratory", PAC'05, Knoxville, USA, 2005, pp. 431-433.
2. P. A. McIntosh et al, "Realisation of a Prototype Superconducting CW Cavity and Cryomodule for Energy Recovery", SRF2007, Beijing, Oct 2007.
3. J. Sekutowicz et al., "Superconducting Superstructure for the TESLA Collider; A Concept", PR-ST AB, 1999.
4. M. Liepe et al, "SRF Experience with the Cornell High-Current ERL Injector Prototype", PAC09, Vancouver, 2009..
5. "TESLA Test Facility Linac – Design Report", TESLA-Collaboration, DESY, March

1995, TESLA 95-01.

6. G Devanz et al, "Compensation of Lorenz Force Detuning of a TTF 9-cell Cavity with a New Integrated Piezo Tuner", EPAC'06, Edinburgh, June 2006, pp. 378–380.

7. O. Kugeler, "Measurement and Compensation of Microphonics in CW Operated TESLA-type Cavities, ERL'07, Daresbury Laboratory, UK, May 2007.

8. V. Veshcherevich, "Input Coupler for ERL Injector Cavities", PAC'03, Portland, USA, May 2003, pp. 1201–1203.

9. Peter vom Stein et al, "Fabrication and Installation of Superconducting Accelerator Modules for the ERL Prototype (ERLP) at Daresbury", EPAC'06, Edinburgh, 2006, pp. 178–180.

10. R. Bate and S. Pattalwar, "Instrumentation and Control System for the International ERL Cryomodule", Submitted SRF09, Berlin, 2009.

3.20 SCRF Third Harmonic Cavity HOM Diagnostics and the Quest for High Gradient Cavities for XFEL and ILC

Roger M. Jones, on behalf of the MEW group
Cockcroft Institute, Daresbury, Warrington, Cheshire WA4 4AD, UK
University of Manchester, Oxford Road, Manchester, M13 9PL, UK
Mail to: roger.jones@manchester.ac.uk

3.20.1 Introduction

In the area of SCRF, our work is focused on two main areas: optimization of fields in 1.3 GHz cavities, with a view to facilitating a ~50 MV/m accelerating electric field gradient and, on instrumenting and studying, higher order modes in the 3rd harmonic cavities recently installed in the FLASH facility at DESY. The latter entails a close collaboration with colleagues at both DESY laboratory and with colleagues at the Universität of Rostock. In both areas of work, we capitalize on our past experience in both modeling electromagnetic fields in multi-cavity structures [1-2] and in the latter area, we profit from our past work on HOM diagnostics made in the main accelerating cavities at FLASH [3].

3.20.2 Third Harmonic SCRF Cavity HOM Diagnostics

In order to produce SASE-FEL radiation at the FLASH facility and in the future XFEL, compressed electron bunches are required. This is achieved by accelerating the beam off-crest. This results in an energy spread along the bunches within the beam, which increases towards the tail. The beam is then sent through a magnetic chicane, where the tail catches up with the head of the bunch. This results in a compressed bunch profile. The cosine-like energy spread however deteriorates the bunch properties. It is desirable to reduce this energy spread by flattening the overall field and this can be achieved by including harmonics of the fundamental frequency of the linac. A single frequency operating at the nth harmonic can be used flatten out the dependence of the energy gain verses phase, by cancelling the second derivative of the fundamental at its peak.

In practice, the first component in a Fourier expansion is used, namely the 3rd harmonic. This minimises the effect of transverse wakefields. It is also important to note that flattening the field also reduces the growth of transverse phase space. The

transverse magnetic fields arise from the rate of change of the longitudinal electric field. Thus, flattening the electric field will also result in a reduced magnetic field. Hence the use of a cryo-module of third harmonic cavities will reduce the dilution of both longitudinal and transverse phase space. FNAL have designed and fabricated such a cryo-module, which has recently been installed in the FLASH facility at DESY.

Figure 1: Schematic of a FNAL cryo-module [4] consisting of four 3.9 GHz cavities.

These cavities are expected to improve the longitudinal beam profile considerably. However, as the transverse momentum kick of higher order modes (HOMs) scales with the third power of the fundamental frequency (3.9 GHz), these cavities are capable of giving rise to a significantly larger emittance dilution of the beam than that imparted to the beam due to the main accelerating cavities (with a fundamental frequency of 1.3 GHz). The focus of our work is to ensure these HOMs are well-characterised and their effect on the beam is mitigated for with HOM diagnostics, which will allow the alignment of the electron beam and the monitoring of the beam position. A series of transmission measurements, have recently been conducted at DESY, on the properties of these HOMs. We have also conducted an analysis of the band structure of the monopole modes [5] and this has entailed a study of the influence of fabrication errors on the field flatness in these cavities. In addition, the dipole HOMs have been simulated in detail. The sensitivity of trapped modes in these cavities to fabrication errors has also been investigated.

The overall goal of our work is to instrument the cavities with diagnostics to ensure the effects of the HOMs are mitigated for with beam position diagnostics. In this manner, the beam position will be precisely determined with HOM-based beam position monitors. This work is pursued in close collaboration with DESY laboratory and the Universität of Rostock.

3.20.3 High Gradient SCRF Cavity Design

The ILC [6] design aims at colliding leptons at an initial center of mass energy of 500 GeV with a proposed later upgrade to 1 TeV. The superconducting cavities in the main accelerating linacs of the ILC are based on the TESLA [7] design. The baseline design aims at an average accelerating gradient of 31.5 MV/m. However, other designs exist with the potential for higher accelerating gradients. Increasing the accelerating gradient is desirable, as it raises the overall efficiency of the machine. Re-entrant (RE) [8], Low-loss (LL) [9] and Ichiro (IR) [10] are candidates for higher gradient cavities. These designs aim at producing accelerating gradients of ~50 MV/m within 9-cell cavities. Single cells have achieved gradients in excess of 50 MV/m. Indeed at Cornell,

a RE cell achieved 52 MV/m [11] and Low Loss (LL) cells at KEK have obtained between 45 to 51 MV/m [12]. These designs are focussed on minimising the ratio of the surface e.m. fields to the accelerating gradient. In particular, the ratio of the surface magnetic field to accelerating gradient (Bs/Ea) has been minimised by suitably shaping the walls of the cavity. The critical surface magnetic field is in the range 180 -230mT [13]. Another recent design incorporates minimising an additional quantity, the ratio of the surface electric field to surface accelerating field (Es/Ea) and this is the Low Surface Field design (LSF) [14]. However, the bandwidth of accelerating mode in LSF design is reduced by ~18% compared to the LL cavity. This reduces the overall stability of the cavity as the frequency separation of modes is proportional to the bandwidth [15-16].
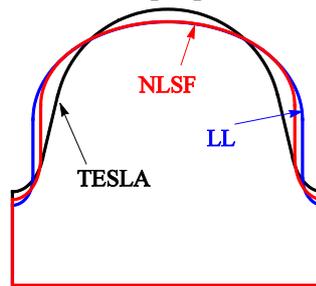
Figure 2: NLSF optimized cavity geometry compared to alternative designs.

We have studied means to increase the bandwidth increase the bandwidth of the fundamenral mode whilst minimising two additional quantities: of Es/Ea and Bs/Ea. This has resulted in a new design, which we refer to as the New Low Surface Field (NLSF) [15-16] cavity, based on LL and LSF geometries. Detailed simulations on the e.m. fields for the middle cells of NLSF were reported in [16]. The NLSF shape has comparable surface e.m. fields ratio to that in the LSF cavity, but with an enhanced fractional bandwidth. The main inner cell is illustrated in Fig. 2, in comparison with other current cell shapes. The overall design is almost complete, all cells have been designed including ends cell, but the couplers remain to be finalised. This work has included an analysis of the dipole modes, which provide a transverse kick to the beam. The mode distribution is a little different from those in TESLA, but not substantially different and hence appropriate modification of the HOM couplers is anticipated to allow all modes to be efficiently damped.

3.20.4 Summary

We are making substantial progress on two main tasks: firstly on optimisation of the 1.3 GHz cavity for the ILC, and secondly on instrumenting diagnostics for the third harmonic cavities at FLASH. In the latter area, initial measurements on the properties of the HOMS in the 3.9 GHz cavities at DESY have been completed, prior to installation in FLASH. Over the course of this year, tests of the HOM diagnostics of the cavities subsequently installed in FLASH will be completed. This research has received funding from the European Commission under the FP7 Research Infrastructures grant agreement no.227579.

3.20.5 References

1. I.R.R. Shinton, R.M. Jones, *Rapid cavity prototyping using mode matching and*

globalised scattering matrix, Proceedings of 44th ICFA Advanced Beam Dynamics Workshop: X-Band RF Structure and Beam Dynamics, Warrington, United Kingdom, 1-4 Dec 2008.

2. I.R.R. Shinton, R.M. Jones, *Scattering matrix simulations of fields and dispersion relations in superconducting cavities for XFEL and ILC,* Proceedings of 24th International Linear Accelerator Conference (LINAC08), Victoria, British Columbia, Canada, 29 Sep - 3 Oct 2008.

3. M. Ross, J. Frisch, K.E. Hacker, R.M. Jones, D. McCormick, C.L. O'Connell, T. Smith, *Cavity Alignment Using Beam Induced Higher Order Modes Signals in the TTF Linac*, Proceedings of Particle Accelerator Conference (PAC 05), Knoxville, Tennessee, 16-20 May 2005.

4. T. Khanibouline, N. Solyak, R. Wanzenberg, FERMILAB-TM-2210, 2003.

5. B. Szczesny, I.R.R. Shinton, R.M. Jones, *Third Harmonic Cavity Modal Analysis,* proceedings of 14th International Conference on RF Superconductivity, Berlin, Germany, 20-25 Sep 2009.

6. *The International Linear Collider Reference Design Report, 2007.*

7. *R. Brinkman et al. (eds.), The TESLA Technical Design Report, March 2001, DESY Report 2001-33.*

8. V. Shemelin*, PAC05, TPPT068, 2005.*

9. J. Sekutowicz *et al., PAC05, TPPT056, 2005.*

10. T. Saeki *et al., EPAC06, MOPLS087, 2006.*

11. T. Saeki*, SMTF Collaboration meeting, 2005.*

12. R.L. Geng*, Physica C 441, 145-150, 2006.*

13. K. Saito*, Pushing the Limits of RF Superconductivity workshop, 2004.*

14. Z. Li and C. Adolphsen*, LINAC08, THP038, 2008.*

15. N. Juntong, R.M. Jones, I.R.R. Shinton, *SRF cavity geometry optimization for the ILC with minimized surface e.m. fields and superior bandwidth,* Proceedings of Particle Accelerator Conference (PAC 09), Vancouver, BC, Canada, 4-8 May 2009.

16. N. Juntong, and R.M. Jones, *High-gradient SRF Cavity with Minimized Surface E.M. Fields and Superior Bandwidth for the ILC,* Proceedings of 14th International Conference on RF Superconductivity, Berlin, Germany, 20-25 Sep 2009.

Advanced Accelerator R&D and New Initiatives

3.21 Laser-Driven Accelerators

Simon Hooker

Dept of Physics, U. of Oxford, Clarendon Laboratory, Parks Road, Oxford, UK
Mail to: simon.hooker@physics.ox.ac.uk

Zulfikar Najmudin

Blackett Laboratory, Imperial College London, Prince Consort Road, London SW7
Mail to: z.najmudin@imperial.ac.uk

3.21.1 Introduction

Plasma-based accelerators are of great interest because they can accelerate particles many orders of magnitude faster than conventional accelerators, and because the beams

they generate have unique properties, such as high peak current and femtosecond bunch duration. They therefore offer the prospect of a new generation of very compact accelerators with several potential near-term applications, such as driving next generation light sources or creating ion beams for cancer therapy; in the longer term they offer a route to the beam energies required for future particle colliders.

Rapid progress, partly as a result of advancing laser technology, has been made in laser-driven acceleration in recent years. Highlights include: generation of quasi-monoenergetic electron beams; the generation of high-charge proton and heavy ion beams with energies greater than 10 MeV per nucleon; GeV level laser-accelerated electron beams; and the use of the compact accelerators in light-source applications.

The UK has several internationally leading groups, most university-based, working on different aspects of plasma accelerators. These groups have played a leading role in this field for more than 20 years. Some of their key contributions are summarised in Table 1. To date most experimental work by the UK groups has been performed at the Central Laser Facility at the Rutherford Appleton Laboratory (RAL), or at facilities outside the UK. However, it is expected that new medium-sized laser systems – such as those based at Strathclyde and Queen's University Belfast (QUB) – will play an important role in the future. In this report we summarise briefly recent results obtained by groups in the UK working on laser-driven accelerators.

Table 1: Summary of recent achievements by UK groups in laser-driven accelerators

Year	Result	Group	Ref.
2000	Generation of $E > 30$ MeV protons, and heavy ions with $E > 10$ MeV per nucleon	IC-RAL	[1, 2]
2003	Use of laser generated heavy ions for isotope production	Strathclyde-IC-RAL	[3]
2004	First generation of quasi-monoenergetic electron beams. Beam energy approximately 100 MeV.	IC-Strathclyde-RAL	[4]
2006	Quasimonoenergetic proton beams from microdot targets	Jena-Strathclyde	[5]
2006	First generation of quasi-monoenergetic electron beams with energies of 1 GeV.	Oxford-LBNL	[6]
2006	Ultrafast switching of laser generated proton beams to generate narrow energy spread.	QUB, LULI, Düsseldorf	[7]
2008	Generation of visible radiation from laser-accelerated electron beams.	Strathclyde-Jena	[8]
2008	Near-GeV electron beams produced by self-guided laser pulses.	IC-RAL	[9]
2008	Synchrotron radiation from laser undulated electrons in direct laser accelerated regime.	IC-LOA-LULI-UM	[10]
2008	Synchrotron radiation with brightness $> 10^{22}$ W photon s^{-1} mm^{-2} mrad^{-2} 0.1%BW^{-1} at 5 keV	IC-Michigan	[11]
2009	Generation of soft x-ray undulator radiation from laser-accelerated beams.	Oxford-MPQ	[12]
2009	Light-sail acceleration due to radiation-pressure.	LIBRA	[13]
2010	Quasi-monoenergetic proton beams from shock acceleration	IC-BNL-Stonybrook	[14]

3.21.2 **Electron Acceleration**

An intense laser or particle beam propagating through a plasma expels plasma electrons away from the beam, which return after passage of the driver, thus setting up a plasma wave in its wake. The intense electric fields present within the wakefield can accelerate charged particles at an unprecedented rate [15]. These fields, which propagate at close to the speed of light, can be of the order of the wave-breaking field $E_{wb} = m_e c \omega_p / e$, where $\omega_p = \sqrt{ne^2/\varepsilon_0 m_e}$ is the plasma frequency, and n_e is the plasma electron density. For example, for a plasma of $n_e = 1 \times 10^{18}$ cm^{-3}, $\omega_p = 5.6 \times 10^{13}$ rads^{-1} and $E_{wb} \approx 100$ GV m^{-1} – more than three orders of magnitude greater than the accelerating field achieved in conventional radio-frequency accelerators (for a recent review of laser-driven plasma accelerators, see [16]).

For the case of a particle beam driver the expulsion of the plasma electrons is due to the Coulomb force, whilst for an intense laser pulse it is the ponderomotive force. Particle-beam-driven plasma accelerators have accelerated electrons by up to 42 GeV in a plasma only 0.85 m long using a 3 km long conventional accelerator to generate the driving beam [17]. In the USA, both laser and particle driven wakefield research have recently received significant funding, through the FACET programme at SLAC [18] – which will extend the capabilities of beam-driven plasma accelerators – and the BELLA programme at LBNL – which aims to demonstrate laser-driven acceleration to 10 GeV energies. This report will concentrate on laser-driven accelerators.

Most present-day experiments take advantage of developments in high-power femtosecond laser systems and utilise the "bubble" or "blow-out" regime [19] – often after the laser pulse has been steepened by optical compression and relativistic self-focusing as it propagates through the plasma. The bubble regime is reached when the peak intensity of the laser pulse is sufficiently high to expel most of the ambient electrons, forming a "bubble" or electron density cavity immediately behind it. The electric field of this cavity can be large enough to trap and accelerate some of the background plasma electrons within the bubble.

In early work the generated electron beams had a relative energy spread of essentially 100%. A milestone in the field, then, was the observation in 2004 of nearly-monoenergetic electron beams by groups at Imperial College, Lawrence Berkeley National Laboratory (LBNL), and Laboratoire d'Optique Appliquée [4, 20, 21]. In those three experiments electron beams were generated with energies of 80 – 170 MeV, a relative energy spread down to a few percent, and a bunch charge of ≈ 100 pC.

3.21.2.1 *Plasma Accelerators Driven over Extended Lengths*

The energy gain of a plasma accelerator varies approximately as $1/n_e$, provided that acceleration is maintained over the dephasing length $L_d = \lambda_p^3/\lambda^2$, where λ is the laser wavelength. The dephasing length is the distance over which the electrons outrun the plasma wave. The first monoenergetic electron beam experiments were performed at $n_e \approx 10^{19}$ cm^{-3}, corresponding to $L_d \approx 2$ mm, which was the interaction distance used in all of these early experiments. Increasing the electron energy by an order of magnitude requires operation at correspondingly lower plasma densities and acceleration over a distance $10^{3/2} \approx 30$ times longer which - unless diffraction is reduced by increasing the size of the laser focus and hence its intensity - requires that the laser pulse is guided in

some way. UK groups have investigated two approaches for achieving this: relativistic guiding, and guiding in pre-formed plasma channels.

The refractive index of a plasma is given by $\eta = \sqrt{1 - \dfrac{n_e(r)e^2}{\gamma(r)m_e\varepsilon_0\omega^2}}$, where $\omega = 2\pi c/\lambda$ and γ is the relativistic factor associated with the electron quiver motion in the laser field. Both n_e and γ may depend on the radial distance r from the axis of propagation. Relativistic self-focusing (RSF) arises because γ increases with the laser intensity: it is larger near the axis, where the intensity is high. This causes the refractive index to decrease with r, leading to continual focusing of the propagating laser pulse.

The threshold for RSF can be shown to be power dependent, $P > P_c = 17.4 \, (\omega_0/\omega_p)^2$ GW. However, at high laser intensities, the laser pulse "snow-ploughs" plasma in front of the laser pulse, which tends to counteract RSF. As a consequence, in this regime, the front of the laser pulse diffracts away, and relativistic guiding can only be said to be effective when the rate of diffraction of the front of the laser pulse is slow compared to the rate at which the front of the pulse is etched by transferring energy to the plasma wave. Lu et al. have considered this regime and showed that this requirement increases the required power for RSF to $P_c^{diff} = (1/8)(\omega_0/\omega_p)^{6/5} P_c$ [22, 23]. A plasma channel can ease this requirement by preventing, or slowing, the diffraction of the front of the laser pulse. In a preformed plasma channel, a radially increasing electron density causes the refractive index of the plasma to decrease with r, leading to continual focusing of the laser pulse, just as in a gradient refractive index fibre.

3.21.2.2 *Electron Acceleration by Self-Guided Laser Pulses*

The Astra Gemini laser, commissioned in 2008 at RAL, was a major advance for laser driven particle acceleration in the UK. This is not only because it features an ultrashort high-intensity pulse, which is ideal for laser wakefield acceleration, but also because it is designed to operate at relatively high-repetition rate (1 shot every 20 seconds) as compared to previous petawatt-scale laser facilities. Gemini increased by a factor of 10 the laser energy available on the Astra facility (as had been used for the first monoenergetic self-injected beam experiments in 2003 [4]). This allows a laser wakefield to be driven to close to wavebreaking at lower density. This is advantageous since at lower density the accelerator has a higher (phase) velocity, and so electrons can reach a higher energy before being dephased. Of course, to obtain maximum energy gain this must be coupled with longer interaction length.
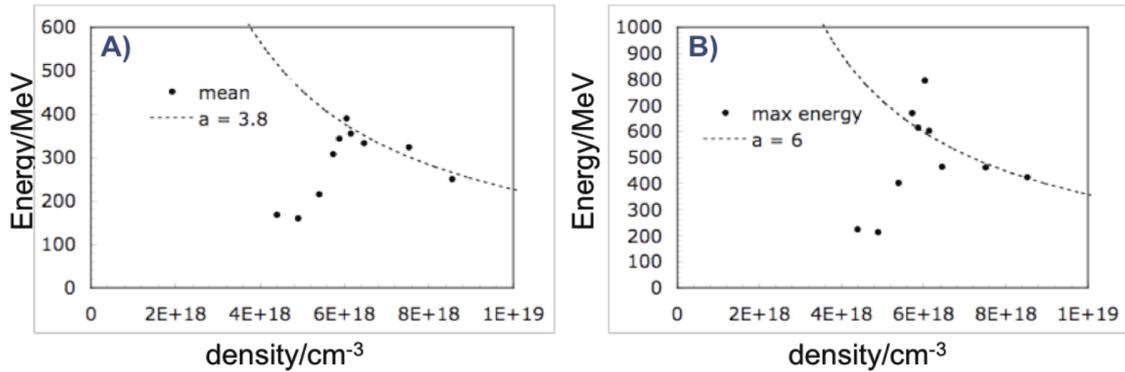
Figure 1: Maximum and mean energy of shots produced from a 1 cm nozzle irradiated with a_0 ≈ 3.8 Gemini pulse. (Note, for linearly polarised laser pulses $a_0 = 0.86 \, (I_0 \, [10^{18} \, \text{Wcm}^{-2}] \, \lambda^2 \, [\mu\text{m}])^{1/2}$, where I_0 is the peak laser intensity). Mean energies show close to expected density scaling down to a threshold density ≈ 5×10^{18} cm^{-3}. However maximum energies can be in excess of that (by ≈ 2.25 ×) to a maximum of ≈ 800 MeV.

Figure 1 shows the scaling of maximum observed beam energy, as a function of density, on the first user experiment on the Gemini laser performed by the Imperial College group. Due to the increasing group velocity of the laser in lower density plasma, the wakefield can accelerate to a higher energy (up to a maximum of 800 MeV) with decreasing density, down to an optimum of n_e ≈ 5.5×10^{18} cm^{-3}. At this density, electron beams were produced on every shot. Simultaneous imaging of the exit of the target showed that in these shots the laser pulse is maintained at close to its focal spot size even though it is many Rayleigh lengths away from best focus. This is due to RSF and shows that the high intensity beam can self-guide the sufficiently long distances required to trap and accelerate electrons from the background plasma [9]. Also the higher than expected maximum final energies implies that under ideal conditions, the laser can be "intensity-amplified" and thus drive a higher amplitude plasma wave. Intensity amplification occurs through a combination of RSF and also temporal compression of the laser pulse, which was measured simultaneously on the same experiment. Below the threshold, the electron beams produced become less intense and more sporadic in appearance, in part due to the decreasing effectiveness of RSF at these densities. At optimum conditions it is noted that as much as 500 pC of charge can be accelerated to relativistic energies (>100 MeV), though usually in multiple bunches of varying energies. This high beam-loaded charge has implications on applications such as radiation generation, which will be expanded upon later.

3.21.2.3   *Electron Acceleration in Plasma Channels*

The Oxford group has led the development of the gas-filled capillary discharge waveguide [24], and its application to laser-driven plasma accelerators. As illustrated in Figure 2(i), in this device a capillary with a diameter of typically 200 μm, and a length of several tens of millimetres, is filled with hydrogen gas to an initial pressure of ≈ 100 mbar. A current pulse, with a peak of typically 500 A and a duration of 200 ns, is driven through the capillary, ionising the hydrogen gas to form a plasma. Thermal conduction to the capillary wall causes the plasma temperature to decrease with radial distance from the capillary axis r, and hence – since pressure is rapidly equilibrated – the plasma density increases with r and a plasma channel is formed. This channel has been shown

to guide laser pulses with peak intensities above 10^{17} Wcm^{-2}, over distances up to 50 mm, with very low losses [24].
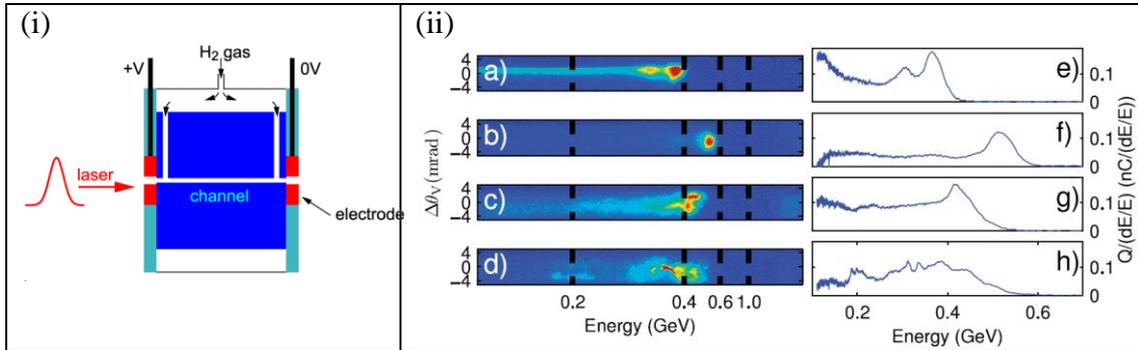
Figure 2: (i) Schematic of a gas-filled capillary discharge waveguide (ii) Raw electron energy spectra (a–d) and spectra in units of charge per relative energy spread (e–h) for: (a, e) initial hydrogen pressures P = 50 mbar, discharge delay td = 147 ns; (b, f) P = 80 mbar, td = 189 ns; (c, g) P = 110 mbar, td = 181 ns; (d, h) P = 200 mbar, td = 150 ns.

Previous experiments with capillary guided laser wakefields performed at LBNL, have demonstrated energy gain in excess of 1 GeV from a laser accelerator for the first time [6]. The role of the plasma channel was investigated in more detail in recent experiments performed with Astra Gemini. In these, 80 fs laser pulses with energy up to 5 J were focused at the entrance of the plasma channel formed in a 33 mm long, 200 μm diameter capillary. The size of laser focal spot was 22 μm (FWHM); however, by introducing a soft aperture in the unfocused laser beam it was possible to increase the size of the focal spot to 35 μm (FWHM) whilst also improving the focal spot quality. The best electron beams were obtained for a corresponding initial axial electron density ne ≈ 1.8×1018 cm-3, with a laser energy of 2.5 J and with the aperture in place. As shown in Figure 2, for these conditions electron beams of energy 540 MeV were generated, with divergence in the horizontal and vertical directions of approximately 4 and 5 mrad (1/e full-width) respectively [22, 25].

Without the aperture the threshold laser energy for generating electron beams was approximately 3.5 J, but with the aperture in place electron beams were produced with input laser energies as low as 2 J. Simulations show that the reduced threshold achieved by introduction of the soft aperture arises from removal of laser energy in higher-order transverse modes [22]. This illustrates that attention to the quality of the laser beam is important for the optimisation of laser-driven plasma accelerators.

Simulations performed using the 3D axi-symmetric PIC code WAKE [26] show that in these experiments the plasma channel is important in maintaining the laser intensity as it propagates through the plasma (Figure 3). The propagation of the laser is compared in two cases: (i) a uniform fully ionised plasma of $n_e = 1.8 \times 10^{18}$ cm^{-3} and (ii) a fully ionised plasma channel of axial density $n_e = 1.8 \times 10^{18}$ cm^{-3} and a lowest-order mode of 41 μm FWHM. In both cases the peak input power of the laser pulses was 22 TW and P_c^{diff} = 131 TW. The simulations show that without external guiding the laser pulse initially self-focuses relativistically, but then diffracts away as expected for $P < P_c^{diff}$. However, in a plasma channel, the pulse maintains a small spot size over many Rayleigh ranges through a combination of channel guiding of the front of the laser pulse and relativistic guiding of the back. The plasma guide allows the normalised vector potential a_0 to increase through temporal compression. This allows a_0 to evolve

sufficiently to reach the threshold for self-injection of electrons into the wake, which occurs at $a_0 \approx 3$–4 [23]. For a given electron density this combination of relativistic and channel guiding enables injection to occur at lower laser powers than RSF alone.
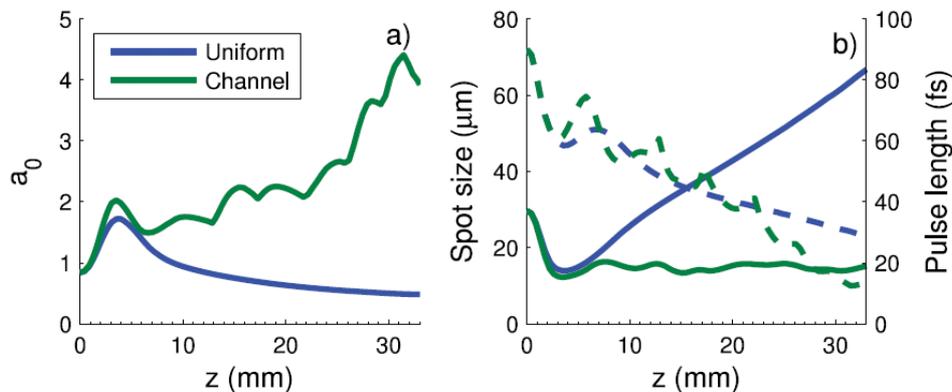
Figure 3: Variation of (a) the peak a_0, (b) the mean spot size (solid) and duration (dashed) of pulses propagating through a gas-cell (blue) and plasma channel (green). Temporal and transverse spatial profiles of the input pulses were gaussian, with initial FWHM duration of 90 fs and focal spots of 35 μm. Laser energy was 2 J, so $P = 22$TW.

In addition to self-injection at high intensity, electron beams have been observed in capillary experiments for even lower initial a_0 [27]. By comparing the electron density measured interferometrically with that determined from the Raman shift of a probe laser, it was determined that electron beams were generated when the plasma channel was not fully ionised. This indicates that injection in these experiments can in part be explained by the birth of ionised electrons within the laser pulse, and hence dephased from the coherent motion of the remaining plasma wave electrons. This also demonstrates that capillaries could be of importance for plasma accelerators working in the linear regime, provided an alternative method of injection, such as ionisation-induced injection (III), can be utilised. III has recently been demonstrated to work in gas jets by introducing controlled amounts of impurities [28, 29].

3.21.3 Ion Acceleration

Ion beams can be generated by the enormous near-stationary electric fields generated when an intense laser beam strikes an opaque target such as a solid foil. Again energetic electrons are produced by the intense laser-matter interaction, and as they exit into vacuum away from the target, they generate a large space-charge field between themselves and plasma ions. This space-charge field rapidly accelerates the ions. At very high intensities, since the electrons are mostly pushed forward by the light pressure of the laser, the acceleration can also be strongly directed, making this process more efficient. Recent theoretical work suggests that for low mass targets in this radiation-pressure regime all of the target electrons can be forced out of the target causing the following ions to be accelerated rapidly and with a near uniform force over the focal volume, leading to narrow energy spread [30].

The UK has been at the forefront of studies into laser driven high-energy ion sources, beginning with the pioneering work done at RAL in the early 1990s. These

experiments were the first to be able to demonstrate the acceleration of ions to multi-MeV energies using high-intensity CPA lasers [1, 2]. A major new development has been the creation of a consortium of UK groups working in this area by a new RCUK funded Basic Technology grant called Libra. Libra brings together the leading groups working on laser plasma ion acceleration (QUB, RAL, Strathclyde, Imperial). In addition, groups (RAL, Southampton) are working on advanced targetry and target injection, whilst others (Surrey, Birmingham and NPL) are applying this new breed of accelerator to applications. Libra has already resulted in a number of new and exciting advances. In the following sections, we expand on some of the key acceleration studies.

3.21.3.1 *Sheath Acceleration*

This is the most studied mechanism for ion beam generation by high-intensity lasers. The hot electrons generated by absorbed laser light expand from a both front and rear surfaces of a solid, and in the process pull surface ions along with them. The sheath potential and thus the maximum energy that ions can gain are comparable to the hot electron temperature. Since this temperature depends on intensity and is usually of the order of the ponderomotive potential, this means that for lasers with intensity in excess of 10^{18} Wcm^{-2} the energy of these ions can easily exceed several MeV [31].

A number of methods are being investigated in the Libra program to optimise sheath acceleration. Reduced mass targets are being implemented to maximise the mean temperature of electrons by limiting their number. Also both varying surface finish and using structured targets are being investigated to see if electric field enhancement on the target surface can increase absorption and so enhance efficiency. Finally, the influence of laser parameters on the acceleration process is being studied. The parameters to be investigated include; improving laser contrast to improve absorption and prevent degradation of the sheath, varying laser angle of incidence and polarisation to maximise hot electron temperature, and controlling electron divergence through resistivity changes in the targets. One interesting discovery recently made is that at high intensity ($a_0 > 10$), ion production is not optimised at glancing incidence, which would increase the electric field component into the target. This is due to relativistic effects where electrons are driven strongly into the target even for near-normal incidence [32].

As part of the Libra programme, sheath accelerated ions are being assessed for ion beam applications. In particular, a set of experiments initiated at a QUB using the new Taranis laser will investigate the irradiation of biological samples with this ion source, to determine its suitability for cell irradiation, in particular for treating tumours.

3.21.3.2 *Radiation Pressure Acceleration*

An interesting new avenue of exploration for ion acceleration has been schemes that rely on the radiation pressure of the new generation of highest intensity lasers, such as the Astra Gemini and Vulcan Petawatt (VPW) lasers at RAL. The radiation pressure $P_R = 2I/c$ can be $\approx 10^{12}$ bar for these lasers. This means that for sufficiently light targets, this pressure is sufficient to drive the foils to relativistic energies in the duration of the laser pulse. But perhaps more interesting, is that the foil is driven as one body, and so radiation pressure acceleration can result in inherently small energy spreads. This is of particular interest for applications of laser-generated ion beams such as injectors for ion accelerators. Recently, major advances have been made by the Libra collaboration on both Gemini and VPW lasers investigating RPA. On Gemini, at close to best focus,

carbon foils of thicknesses down to tens of nanometres have been accelerated to energies in excess of 200 MeV for C^{6+} ions, and $\approx$ 20 MeV for protons, but with significantly reduced energy spread. Such high energies, and their non-linear scaling with intensity, imply the first evidence of RPA in the light-sail regime [13].

Experiments performed on VPW with ultrathin foils have demonstrated the importance of having uniform foils and laser beam profile for RPA. In particularly, for the thinnest foil it has been demonstrated that that ion beam profile produced is strongly modulated spatially, with extremely high contrast between filaments and voids. The voids are spatially correlated with the transmitted laser profile after it has burned through the foil. This suggests interplay between the acceleration of the foil and directing of laser energy, in other words a photon-fluid driven Rayleigh-Taylor instability [33]. The study of this modulation is clearly of importance in the study of the stability of ultrathin foils to these enormous accelerations.

3.21.3.3 *Shock Acceleration*

In the initial stage of RPA, since the skin-depth of the plasma is usually thicker than the target thickness, not all of the plasma is accelerated immediately. Instead a ponderomotively-driven sheath is formed near the front surface of the interaction. The sheath is driven forward by the light pressure, but is balanced by the inflow of material into this electrostatic shock front. Hence the shock quickly reaches a steady velocity v_{hb} = $(2I/\rho c)^{1/2}$. For solid targets, this hole-boring phase does not really produce interesting ion energies (even for Gemini and VPW $E_p < 1$ MeV), however this would change if the density of the target can be significantly reduced. But for the radiation pressure to be applicable the target must be opaque, which means that its density must be greater than the critical density, $n_e > n_{cr} = \varepsilon_0 m_e \omega_0 / e^2$.
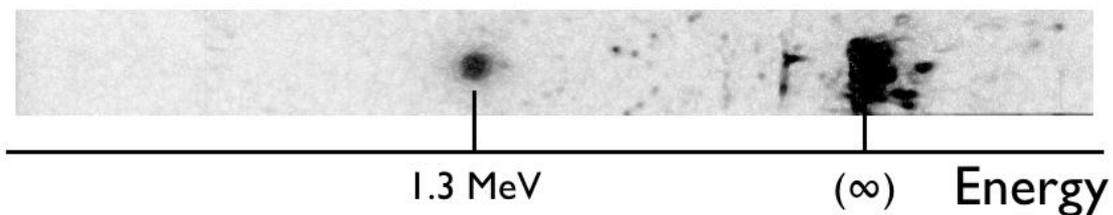
Figure 4: Example of a shock accelerated ion beam from incidence of $\lambda = 10$ μm, I = 5 × 1015 Wcm-2 laser on a gas-jet target at peak density around 5 × 1019 cm-3. The ion peaks at Ep $\approx$ 1.3 MeV and shows remarkably small energy spread (< 4% rms) and background ion level. (The mark at E = ∞ is due to scattered light and neutrals).

For $\lambda = 1$ μm lasers, $n_{cr} \approx 10^{21}$ cm^{-3}, which is difficult to attain since it is somewhere between solid and gas densities. Some experiments have been performed with foam targets, but it is difficult to produce foams with the required level of uniformity. However for a $\lambda = 10$ μm lasers (such as a CO_2 laser), $n_{cr} \approx 10^{19}$ cm^{-3}, which is easily obtainable with gas targets. Of course the fact that the critical density is reduced also decreases the mass density further, which is of benefit to shock acceleration. In experiments performed with the ATF laser at the Brookhaven National Laboratory, an Imperial College led team has demonstrated the use of gas-jet irradiation to drive a shock into a low mass target, which has produced quasi-monoenergetic proton beams on the MeV energy scale [14] (e.g. figure 4). Since a hydrogen jet was used, these beams are relatively free from impurity (which is not the case if a solid was used). The

narrow energy spread beams produced in both this and the Gemini are amongst the first clear indications that RPA can help control the energy spread of laser accelerated ion beams, and vindicates the importance given to these studies by the Libra project.

3.21.4 **Radiation Generation**

An exciting application of laser-driven electron beams is the generation of pulses of tunable, femtosecond-duration radiation in the extreme ultraviolet (30 nm–100 nm) and soft x-ray (1 nm–30 nm) spectral regions. As is routinely done at synchrotron facilities around the world, radiation can be generated from an electron beam by passing it through a magnetic undulator. The wavelength of the radiation generated is given by

$$\lambda = \frac{\lambda_u}{2\gamma^2}\left(1 + \frac{K^2}{2}\right)$$

(1)

where λ_u is the undulator period, and the undulator parameter $K = eB_0\lambda_u/2\pi m_e c$, in which B_0 is the peak magnetic field. For example, 1 GeV electrons passing through an undulator with $\lambda_u = 10$ mm generates soft x-rays with a wavelength of about 1 nm (i.e. a photon energy of 1 keV).

Although this spontaneously emitted radiation is incoherent, the favourable characteristics of laser-accelerated electron bunches – notably the high peak current ($\approx$ 10 kA) and the short bunch length ($\approx$ 10 fs) – allow the generation of ultra-short soft x-ray pulses which could be used for time-resolved experiments. Radiation sources with similar characteristics, driven by larger conventional accelerators, have been operated for several years. Replacing the conventional accelerator with a laser-driven plasma accelerator could bring radiation sources of this type into university-sized laboratories, potentially transforming many branches of the biological and physical sciences.

3.21.4.1 *External Undulator*

The first steps in this direction were taken in experiments by work by a Strathclyde / Jena collaboration. In that work 55–75 MeV electron beams, generated by a plasma accelerator driven in a gas jet, were directed through a 1 m long undulator of period $\lambda_u = 2$ cm and $K = 0.6$. Radiation with wavelengths in the range 675 nm to 925 nm was generated, depending on the energy of the electron beam, with an estimated 3×10^5 photons per pulse in a bandwidth of $\approx$ 50 nm. The peak brilliance of the undulator radiation was estimated to be 6.5×10^{16} photons/second/mrad^2/mm^2/0.1% bandwidth [8]. These results were recently extended to the soft x-ray spectral region by a MPQ / Oxford collaboration. In this case, 210 MeV electron beams from a laser wakefield were passed through a 30 cm undulator with $\lambda u = 15$ mm to generate radiation at 18 nm (fundamental) and 9 nm (second harmonic). The peak brilliance of the soft x-ray pulses was estimated to be 1.3×1017 photons/second/mrad2/mm2 /0.1% bandwidth [12].

A remaining question, and one of current interest, is whether the quality of the laser-driven electron beams is high enough to drive compact free-electron lasers (FELs) [34]. This exciting possibility is being investigated by several groups in the UK.

3.21.4.2 *Betatron Radiation*

Extending light sources to operate in the x-ray region is of major importance due to their shorter wavelength and extended penetration, which thus improves their imaging properties. A recent advance has been the operation of the LCLS at SLAC to operate in the x-ray region, which has extended the usability of this light source to the point where it becomes possible, for example, to fully image a virus in a single shot. Clearly it would be desirable to extend plasma accelerator based light sources to the x-ray region if they are to offer the same level of performance as conventional ones. However for the currently available 100 MeV-GeV level plasma accelerators, this would require a shrinking of the undulator size to less than a millimetre.

Luckily due to the intense fields within a plasma wave, this is an inherent feature of wakefield accelerators. A wakefield has transverse, as well as longitudinal electric fields, which are vital to prevent accelerating electrons from being lost transversally from the wakefield. Due to these fields, any electron born away from axis or with some small transverse momentum will be directed back to axis, where it will overshoot and begin a transverse oscillation. This is the betatron motion and has a frequency (in the bubble regime) of

$$\omega_\beta = \omega_p / 2\sqrt{\gamma} \qquad (2)$$

The betatron motion is identical to that of an electron inside an undulator, and will thus cause radiation to be emitted at $\omega = \gamma 2\omega_\beta$. For a wakefield operating at density ne $\approx$ mid-1018 cm-3 producing electron beams > 200 MeV, it can be seen that this radiation is comfortably in the x-ray region (Ephoton > keV).

First measurements of betatron radiation in the bubble regime were performed in the experiment on Gemini by the Imperial College group, which demonstrated that betatron radiation can produce an extremely bright x-ray source. Furthermore, due to the small spatial scales of the combined accelerator / undulator, the x-ray emission has an unmatched small source size. Later studies (performed at U. Michigan) have shown that this source size can be w0 < 2 μm, which coupled with the high photon number (> 108), implies an x-ray brightness, which is unprecedented from a laser-generated source: > 1022 photons/second/mrad2/mm2/0.1% bandwidth [11]. Indeed this figure can only be matched by 3rd and 4th generation light sources.
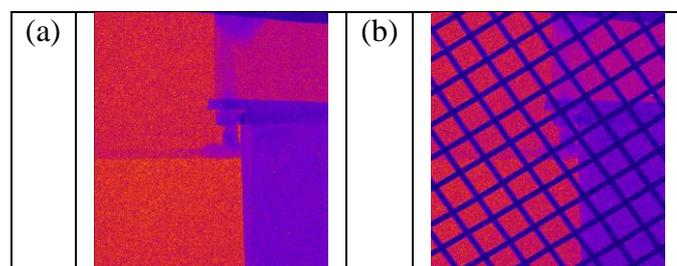
Figure 5: X-ray generated by 400 MeV beam from self-guided accelerator on Gemini as seen on an x-ray CCD camera: (a) differentially filtered beam profile showing x-rays are generated in the range 1-10 keV and beyond. (b) Radiograph of a grid made of 100 μm Cu wires placed between wakefield and CCD detector. Electrons have been deflected out of detector by bending magnet. The edge contrast of the radiograph suggests a source size < 5 μm.

3.21.5 **Summary**

As can be seen from this report, UK groups continue to make world-leading contributions in the field of laser-driven accelerators; including the production of quasi-monoenergetic electron beams at near GeV energies with and without plasma guiding structures, the use of these beams in the generation of short-pulse duration radiation, and now the first indications of ion beam generation due to radiation-pressure.

Future work on laser-accelerated beams will centre on: increased control of electron injection and improved shot-to-shot stability, increasing output electron beam energy, staging plasma accelerators, and developing their applications, such as radiation generation, and ion beam radiography and medical treatment.

3.21.6 **References**

1. E.L. Clark*, et al.*, "Energetic heavy-Ion and proton generation from ultraintense laser-plasma interactions with solids." *Physical Review Letters* **85** 1654-7 (2000).
2. E.L. Clark*, et al.*, "Measurements of Energetic Proton Transport through Magnetized Plasma from Intense Laser Interactions with Solids." *Physical Review Letters* **84** 670-673 (2000).
3. P. McKenna*, et al.*, "Demonstration of fusion-evaporation and direct-interaction nuclear reactions using high-intensity laser-plasma-accelerated ion beams." *Physical Review Letters* **91** 075006 (2003).
4. S.P.D. Mangles*, et al.*, "Monoenergetic beams of relativistic electrons from intense laser-plasma interactions." *Nature* **431** 535-538 (2004).
5. H. Schwoerer*, et al.*, "Laser-plasma acceleration of quasi-monoenergetic protons from microstructured targets." *Nature* **439** 445 (2006).
6. W.P. Leemans*, et al.*, "GeV electron beams from a centimetre-scale accelerator." *Nature Physics* **2** 696-699 (2006).
7. T. Toncian*, et al.*, "Ultrafast laser-driven microlens to focus and energy-select mega-electron volt protons." *Science* **312** 410-3 (2006).
8. H.P. Schlenvoigt*, et al.*, "A compact synchrotron radiation source driven by a laser-plasma wakefield accelerator." *Nature Physics* **4** 130-133 (2008).
9. S. Kneip*, et al.*, "Near-GeV Acceleration of Electrons by a Nonlinear Plasma Wave Driven by a Self-Guided Laser Pulse." *Physical Review Letters* **103** 105006 (2009).
10. S. Kneip*, et al.*, "Observation of synchrotron radiation from electrons accelerated in a petawatt-laser-generated plasma cavity." *Physical Review Letters* **100** 105006 (2008).
11. S. Kneip*, et al.*, "Bright Spatially-Coherent Synchrotron X-rays From a Tabletop Source ". *Submitted* (2010).
12. M. Fuchs*, et al.*, "Laser-driven soft-X-ray undulator source." *Nature Physics* **5** 826-829 (2009).
13. M. Zepf*, et al.*, "Radiation Pressure Acceleration of Ions with Ultraintense Lasers: The Light-Sail Regime." *In preparation* (2010).
14. C.A.J. Palmer*, et al.*, "Pure monoenergetic proton beams accelerated by the radiation pressured hole-boring of an intense 10μm laser ". *Submitted* (2010).
15. T. Tajima and J.M. Dawson, "Laser Electron-Accelerator." *Physical Review Letters* **43** 267-270 (1979).
16. E. Esarey, C.B. Schroeder, and W.P. Leemans, "Physics of laser-driven plasma-based electron accelerators." *Reviews of Modern Physics* **81** 1229-1285 (2009).
17. I. Blumenfeld*, et al.*, "Energy doubling of 42 GeV electrons in a metre-scale plasma wakefield accelerator." *Nature* **445** 741-744 (2007).

18. J. Amann*, et al. Facility for Advanced Accelerator Experimental Tests at SLAC (FACET). Conceptual Design Report*. 2009 Available from: http://www-public.slac.stanford.edu/sciDoc/docMeta.aspx?slacPubNumber=SLAC-R-930.

19. A. Pukhov and J. Meyer-ter-Vehn, "Laser wake field acceleration: the highly non-linear broken-wave regime." *Applied Physics B-Lasers and Optics* **74** 355-361 (2002).

20. C.G.R. Geddes*, et al.*, "High-quality electron beams from a laser wakefield accelerator using plasma-channel guiding." *Nature* **431** 538-541 (2004).

21. J. Faure*, et al.*, "A laser-plasma accelerator producing monoenergetic electron beams." *Nature* **431** 541-544 (2004).

22. T.P.A. Ibbotson*, et al.*, "Investigation of the role of plasma channels as waveguides for laser-wakefield accelerators." *New Journal of Physics* **12** (2010).

23. W. Lu*, et al.*, "Generating multi-GeV electron bunches using single stage laser wakefield acceleration in a 3D nonlinear regime." *Physical Review Special Topics-Accelerators and Beams* **10** 061301 (2007).

24. A. Butler, D.J. Spence, and S.M. Hooker, "Guiding of high-intensity laser pulses with a hydrogen-filled capillary discharge waveguide." *Physical Review Letters* **89** 185003 (2002).

25. T.P.A. Ibbotson*, et al.*, "Laser-wakefield acceleration of electron beams in a low density plasma channel." *Physical Review Special Topics-Accelerators and Beams* Accepted for publication (2010).

26. P. Mora and T.M. Antonsen, "Kinetic modeling of intense, short laser pulses propagating in tenuous plasmas." *Physics of Plasmas* **4** 217-229 (1997).

27. T.P. Rowlands-Rees*, et al.*, "Laser-driven acceleration of electrons in a partially ionized plasma channel." *Physical Review Letters* **100** 105005 (2008).

28. C. McGuffey*, et al.*, "Ionization Induced Trapping in a Laser Wakefield Accelerator." *Physical Review Letters* **104** 025004 (2010).

29. A. Pak*, et al.*, "Injection and Trapping of Tunnel-Ionized Electrons into Laser-Produced Wakes." *Physical Review Letters* **104** 025003 (2010).

30. A.P.L. Robinson*, et al.*, "Radiation pressure acceleration of thin foils with circularly polarized laser pulses." *New Journal of Physics* **10** 013021 (2008).

31. S.C. Wilks*, et al.*, "Energetic proton generation in ultra-intense laser-solid interactions." *Physics of Plasmas* **8** 542 (2001).

32. D.C. Carroll*, et al.*, "Carbon ion acceleration from thin foil targets irradiated by ultrahigh contrast (1010), ultraintense (7×1020 Wcm-2) laser pulses." *New Journal of Physics* Accepted for publication (2010).

33. J. Schreiber*, et al.*, "Rayleigh-Taylor Instability of an Ultrathin Foil Accelerated by the Radiation Pressure of an Intense Laser." *In preparation* (2010).

34. F.J. Gruner*, et al.*, "Design considerations for table-top, laser-based VUV and X-ray free electron lasers." *Applied Physics B-Lasers and Optics* **86** 431-435 (2007).

3.22 The LIBRA Project: Laser-Driven Beam of Ions and Their Applications

M. Borghesi

Centre for Plasma Physics, The Queen's U. of Belfast, Belfast BT7 1NN, UK

Mail to: m.borghesi@qub.ac.uk

3.22.1 Introduction

LIBRA (Laser Induced Beams of Radiation and Applications) [1] is a consortium funded by the Engineering and Phsyical Sciences Research Council (EPSRC) under the

Basic Technology programme. The consortium includes several UK institutions and aims to develop laser-driven ion sources as a reliable, generic technology for a broad range of applications. The institutions parts of the consortium are: The Queen's University of Belfast, The Rutherford Appleton Laboratory (RAL) of the Science and Technology Facility Council, Imperial College London, The Universities of Strathclyde, Surrey, Birmingham and Southampton, with the National Physical Laboratory (NPL) as an external partner. Further details on the project and on participants can be found on the project website [1]. The consortium builds on pre-existing collaborations between several of the member institutions, which have often collaborated in the past in experiments carried out at the Central Laser Facility of the Rutherford Appleton Laboratory. This article will describe briefly the background, structure and progress of the project, which has recently passed its mid-term).

3.22.2 **Background**

Energetic beams of ions can be produced from thin metallic foils, as a result of their irradiation with relativistically intense, short laser pulses [2]. These beams have unique characteristics, which differ greatly under several aspects from beams of comparable energy obtained from conventional accelerators.

Mechanisms leading to forward-accelerated, high-quality ion beams, operating at currently accessible intensities in laser-matter interactions are mainly associated to large electric fields set by laser-accelerated electrons at target interfaces. In particular, the fast electrons that are electrostatically confined on the target rear-surface set up a charge separation field over a Debye length λ_D, typically of the order of a micron, inducing strong (~TV/m) electric fields [3]. Such fields can ionize atoms and rapidly accelerates ions normal to the initially unperturbed surface. The accelerated ions form a dense bunch of short duration that is charge neutralized by co-moving electrons. The extremely short duration of the acceleration and the fact that, at the target rear, it starts from an initially cold surface are essential facts that result in excellent emission properties. After this initial phase, ions stream into vacuum with electrons, preceded by a Debye sheath of hot electrons. This acceleration from the target rear has been described as an extension of the classical case of a plasma expanding into vacuum, driven by the ambipolar electric field generated in a narrow layer at the front of the plasma cloud. This mechanism for ion acceleration from the target rear is usually referred to as Target Normal Sheath Acceleration (TNSA) [3]. Due to the presence of contaminant layers on target surfaces, protons and Carbon ions are always found as the main components of accelerated ion beams unless the target is treated just prior to the irradiation.

An alternative acceleration mechanism, which has been studied extensively in theory and simulations over the past few years is based on the radiation pressure of intense laser pulses [4]. Predictions suggest that for laser intensities in excess of 10^{22} Wcm^{-2} the radiation pressure (>1000 Gbar) exerted by the electromagnetic wave of the laser is so extreme that all the irradiated particles in a thin foil can be accelerated to peak velocities approaching the speed of light, on length scales of only a few micrometers [5]. This mechanism is sometimes referred to as *light sail*, and is predicted to have a much faster scaling with laser intensity than TNSA. Some indications of this mechanism have started to emerge in experiments.
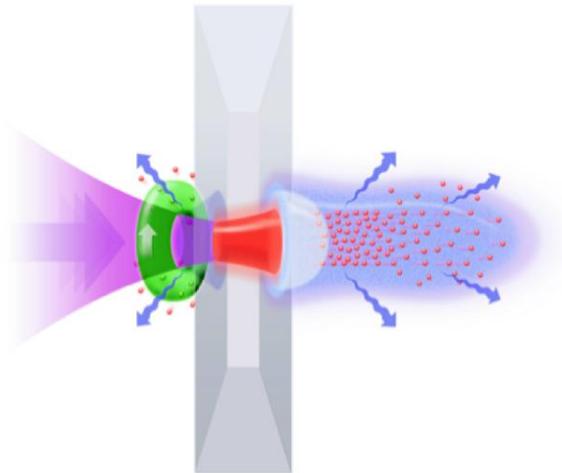
Figure 1: Schematic of accelerator based on the TNSA mechanism. An intense laser pulse (left) is focused on the surface of a thin foil. A fraction of the laser energy is converted into relativistic electrons, which propagate through the target. The sheath field created by the electron at the rear accelerates away from the target the ions present on the surface.

The current interest in laser-driven ion sources arises from a number of factors, including ease of beam production and synchronization in scientific experiments, and some unique features of their emission properties, opening up ample opportunities for applications [2]. The ions are accelerated in ultrashort bursts of ps duration at the source, opening up the possibility of employing them in innovative pump-probe experiments. Furthermore, it has been shown that for the higher energy end of the proton spectrum, the transverse emittance is extremely low. Emittances as low as 0.004 mm.mrad have been reported, i.e. 100-fold better than typical RF accelerators and at a substantially higher ion current (kA range) [6].

Among the applications proposed for these beams, their use in plasma radiography for density and field detection has already been demonstrated successfully [2,7]. Other proposed applications include the production of high energy density matter of interest for astrophysics, high-brightness injectors for accelerators, use in cancer therapy or radioisotope production, or as a fast trigger for Inertial Confinement Fusion pellets. Some of these will require highly improved beam specifications compared to current performances. For example, proton therapy for cancer treatment of deep-seated tumors requires beams with energies in the range 50-250 MeV, and a bandwidth of a few % of the central energy [8]. While 60 MeV proton production has been demonstrated [3], energies in excess of 200 MeV are still beyond current capabilities. In addition, TNSA beams currently produced have broad energy spectra and are divergent, therefore there is a requirement to develop methods to reduce the energy spread to acceptable values and to control the beam divergence. On the other hand, Radiation Pressure Acceleration (RPA) appears promising for this purpose as it should lead to intrinsically narrow band and quasi-collimated beams [5].

3.22.3 The LIBRA Project

The LIBRA project aims to address the current limitations of laser-driven ion sources by improving their characteristics, with the final aim to provide a generic

technology applicable in a number of different contexts. In addition to improving the energy spectrum of the beams, a necessary requirement is to provide energetic ions at high repetition rate. So far, acceleration to high energies (several tens of MeV/nucleons) has been possible only on large Nd:glass systems, such as the VULCAN laser at RAL, which typically provide significant laser energy (up to 100s J) in ps pulses, and operate on a single shot basis (i.e. a laser shot every 20 minutes or so). The most interesting drivers in view of applications are systems based on Ti:Sa technology, which reach high powers by providing smaller amounts of energy (up to a few joules) in pulses of duration of a few tens of femtoseconds, and can operate at higher repetition rate. For example, the GEMINI system currently operational at RAL delivers laser pulses at 20 seconds intervals, but emerging laser technologies based on diode pumping of the amplifier media have the potential to deliver within a few years high power pulses with much higher repetition.

Besides understanding, controlling and optimizing the acceleration mechanisms, a crucial aim of the project is to develop targetry, diagnostics and interaction environment enabling ion source operation at high repetition (e.g. > 10 Hz). Plans and progress in each of these areas will be briefly discussed in the following.

3.22.3.1 *Targetry*

Ions are routinely accelerated from thin foils with μm scale thickness. However, recent results have highlighted the possibility of enhancing the ion beam properties by reducing the target thickness and transverse dimensions. Target miniaturization (down to thicknesses of nm scale and μm transverse dimensions) is seen as a way to increase the electron density at the target rear surface and consequently the strength of the accelerating field. LIBRA aims to develop techniques for delivering at high repetition rates in the interaction volume small, thin disks. We plan to achieve this by a combination of various techniques: silicon etching manufacturing of microdisk targets, target delivery via an electrostatic or electromagnetic injector, and use of optical levitation techniques for control and positioning of the targets. There is significant progress in each of these areas and integration of these technologies in a demonstrator is planned over the next two years.
Alternative approaches investigated include the use of rasters of targets etched in silicon wafers, in particular *spok*e targets, where extreme miniaturization has been demonstrated (Si disks with 30 nm thickness and 1 μm radius).

3.22.3.2 *Diagnostics and Interaction Environment*

While passive detectors such as RCF, CR39 or image plates (requiring post-irradiation retrieval or processing) are routinely used for detection of laser-driven ions, the development of high-repetition diagnostics with real-time response is crucial in view of the development of high repetition sources. LIBRA has investigated the use of fast-response detectors able to operate on a repetitive basis. In particular we have developed a multichannel system for energy-resolved monitoring of the proton beam footprint. This is based on the use of a number of consecutive fast response scintillators which are imaged optically onto CCD cameras. This diagnostic has been used to monitor the divergence of the proton beams in an experiment carried out on the GEMINI laser [9]. In parallel, LIBRA has developed a suite of Thomson parabola

spectrometers, based on Micro-Channel Plate detectors, which have been fully calibrated for proton and Carbon ion response [10].

An issue associated with high-repetition operation is the production of debris, which can lead to degradation of the interaction environment and transport and focusing optics. A workpackage within LIBRA is charged with monitoring and controlling debris production. The use of limited mass targets as discussed in the previous paragraph is advantageous also to this respect as debris is in this case virtually suppressed.

3.22.3.3 *Source Development and Acceleration Mechanisms*

The consortium has been active in extensive experimental activity aimed to progress source development, explore ways to optimize the source characteristics and investigate novel acceleration mechanisms. Significant achievements have been:

- The demonstration, in experiment carried out at LULI with limited mass targets, that the reduction of target transverse size leads to an increase of ion energy and conversion efficiency in TNSA accelerators, due to enhanced electron density and electron recirculation effects.
- The first ion acceleration experiments on the GEMINI laser at RAL, carried out by the consortium, have shown the production of 20 MeV protons and >200 MeV Carbon ions, with laser pulses containing 5 J. These energies are the highest obtained so far with ultrashort (50 fs) pulses, and higher than what obtained with longer laser pulses of similar energy. These results are promising as further increase with optimized laser pulses appears possible.
- Most remarkably, the GEMINI experiment has highlighted the emergence of Radiation pressure acceleration, as predicted by simulations for this interaction regime [11]. Non-thermal spectra with clear high-energy peaks in the proton spectrum and a clear Carbon ion- proton correlation have been measured, when circularly polarized laser pulses were used at normal incidence on target. Indication of a transition to a fast energy scaling with laser intensity, which is typical of the light-sail mode of Radiation pressure, has also been obtained.
- Finally, experiments have been carried out with innovative targets, which are intrinsically capable of high-repetition operation, e.g. water spray targets or high density gas jets. In particular the interaction with water sprays has highlighted the possibility of producing, besides positively charged ions, bright sources of MeV O$^-$ ions, which opens up new applicative opportunities for laser-driven ion sources.

3.22.3.4 *Dosimetry and Radiobiology*

A part of the project is devoted to the development of techniques for precise dosimetry of laser-driven ion beams, particularly in view of future applications in the medical area. Dosimetry approaches developed aim to cope with the intense pulse nature of a laser-induced ion beam, and yield a reduced overall uncertainty, especially at the end of the proton range in the Bragg peak. The approaches investigated by the Birmigham group, in collaboration with the National Physical Laboratory, include Gafchromic film dosimetry, nuclear activation techniques and the development of a portable graphite calorimeter for high-flux proton beams.

Also in view of medical applications, the project aims to assess the biological effectiveness of laser-driven ions. The main motivation for this work lies in the

ultrashort nature of laser-driven ion bursts, which allow ion irradiation at extremely high dose rates (several orders of magnitude higher than tested so far). This is a completely unexplored area of radiobiology, which is currently under the attention of several projects worldwide.

3.22.4 **References**

1. http://www.qub.ac.uk/sites/LIBRA
2. M.Borghesi et al., "Fast ion generation by high intensity laser-irradiation of foils and applications", Fusion Science and Technology, 49, 412 (2006) and references within
3. R. Snavely et al, "Intense High-Energy Proton Beams from Petawatt-Laser Irradiation of Solids", Phys. Rev. Lett., 85, 2945 (2000)
4. T. Esirkepov, M. Borghesi, S.V. Bulanov, G. Mourou and T. Tajima, "Highly Efficient Relativistic-Ion Generation in the Laser-Piston Regime" Phys. Rev. Lett. 92, 175003 (2004)
5. B.Qiao, M. Zepf, M.Borghesi and M.Geissler, "Stable GeV Ion Beam Acceleration from Thin Foils by Circularly Polarized Laser Pulses", Phys. Rev. Lett., 102, 145002 (2009)
6. T.E. Cowan et al, "Ultralow Emittance, Multi-MeV Proton Beams from a Laser Virtual-Cathode Plasma Accelerator", 92, 204801 (2004)
7. K.Quinn et al, "Laser-Driven Ultrafast Field Propagation on Solid Surfaces", Phys. Rev. Lett., 102, 194801 (2009).
8. U.Amaldi, " Cancer therapy with particle accelerators", Nuclear Phys., 654, C375 (1999).
9. J.S. Green et al, "Multi-channel system for imaging laser accelerated proton beams" in Central Laser Facility Annual Report 2008-2009, STFC, p. 311
10. R.Prasad,et al.," Calibration of Thomson parabola—MCP assembly for multi-MeV ion spectroscopy, Nucl. Instr. And Meth. A (2010), doi:10.1016/j.nima.2010.02.078
11. N.Dover et al, "Accessing the RPA regime – target thickness effects on ion acceleration mechanisms", in Central Laser Facility Annual Report 2008-2009, STFC, p. 79

3.23   **DITANET - A European Training Network on Beam Diagnostics for Particle Accelerators**

Carsten P. Welsch, on behalf of the DITANET Consortium
Cockcroft Institute and the University of Liverpool, UK
Mail to: carsten.welsch@quasar-group.org

3.23.1 **Introduction**

Beam diagnostics is a rich field in which a great variety of physical effects are made use of and consequently provides a wide and solid base for the training of young researchers. Moreover, the principles that are used in any beam monitor or detector enter readily into industrial applications or the medical sector which guarantees that training of young researchers in this field is of relevance far beyond the pure field of particle accelerators.

DITANET – "DIagnostic Techniques for particle Accelerators – a Marie Curie Initial Training NETwork" - covers the development of advanced beam diagnostic methods for a wide range of existing or future accelerators, both for electrons and ions. The network is the largest ever EU education action for PhD students and Postdocs in

the field of beam diagnostic techniques for future particle accelerators with a total budget of more than 4 M€. The network is coordinated by the University of Liverpool.

3.23.2 **Introduction**

DITANET covers the development of advanced beam diagnostic methods for a wide range of existing or future accelerators, both for electrons and ions. DITANET consists of the following network participants:

University of Liverpool (coordinator, UK), CEA (France), CERN (Switzerland), DESY (Germany), GSI (Germany), HIT GmbH (Germany), IFIN-HH (Romania), Stockholm University (Sweden), Royal Holloway University of London (UK), and the University of Seville/Centro Nacional de Aceleradores (Spain).

This consortium is complemented by seventeen associated and adjunct partners from all over the world:

Diamond detectors Ltd (UK), ESRF (France), idQuantique (Switzerland), INFN-LNF (Italy), Instrumentation Technologies (Slovenia), Lawrence Berkeley National Laboratory (USA), MPI for Nuclear Physics (MPI-K), PSI (Switzerland), THALES (France), Thermo Fisher Scientific (USA), TMD Technologies Limited (UK), TU Prague (Czech Republic), University of Dundee (UK), University of Maryland (USA), University of Uppsala (Sweden), ViALUX (Germany), and WZW Optics (Switzerland).

Once all positions are filled, the network will train 18 Early Stage Researchers (PhD candidates) and 3 Experienced Researchers (normally Postdocs) within its four year duration.

A core idea of DITANET is that all network members interact and collaborate closely, promote the exchange of trainees and staff within the network, and jointly organize training events, such as workshops and conferences that are open also to external participants.

The participation of industry is an integral part of the training within DITANET and all partners from industry are included as members of the supervisory board to ensure that industry-relevant aspects are covered in the different projects carried out within the network and to enhance knowledge transfer. In addition, they offer internships to the students from the network to complement the scientific training and thus actively contribute to building the bridge between the academic and the industrial sector.

3.23.3 **Research**

DITANET covers very different kinds of particle accelerators from very low energies to present and future high energy colliders, diagnostics for electron as well as for ion beams [1]. In addition to the laser wire developments for the ILC/CLIC as reported in Section 3.4.3 in this newsletter, some examples from the present R&D program of the UK DITANET partners are summarized in this section. More information on the research program can be found in [2,3].

3.23.3.1 *Simulation of Coherent Diffraction Radiation Process*

Any method for diagnostics of a charged particle beam is based on interaction of the particles or fields generated by the particles with surrounding media loosing a small fraction of their energy. A part of the lost energy is transformed into electromagnetic

(EM) radiation which characteristics depend on different particle beam parameters. Measuring the EM radiation characteristics, or, to be more precise, their distortion, one can measure such particle beam parameters as transverse size and divergence, position, bunch length and chromaticity. In most cases the ideal EM radiation characteristics must be predictable either for diagnostics itself or for optimization of the device performance before manufacturing it.

One of such methods developed for longitudinal particle beam profile diagnostics through the analysis of a Coherent Diffraction Radiation (CDR) generated when a charged particle (electron) moves in the vicinity of a conducting screen (target). The beauty of the phenomena is that the particle beam does not directly interact with the screen that excludes a possibility to deform the beam parameters by the screen itself. In order to derive the longitudinal profile of the bunch from a measured spectrum one must know the spectrum generated by a single electron. Because of that the configuration of the screen is usually chosen to be as simple as possible in order to predict the spectrum using the existing approximated theory. However, a simple target does not mean an optimal. There are so many phenomena which are a lot more attractive from experimental point of view such as Smith-Purcell Radiation (SPR) appearing when an electron moves parallel to a conducting grating; however, it is very difficult to predict its characteristics with an appropriate accuracy.

In this project a computer code is being developed for simulating the CDR generated by a single electron. It is a staged approach that combines both numerical and experimental studies. A computer code for simulating the CDR process for a single target configuration was developed and compared with existing models. Single target configuration was used at CTF3 bunch profile monitor before upgrade in 2010, which included installation of a second target. Simulations were done for one single half target, Fig.1. [4].
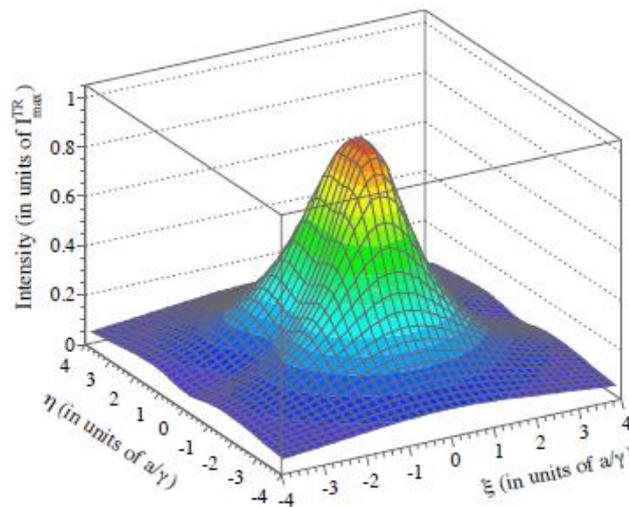
Figure 1: CDR emitted from half target.

The following parameters for the setup at CTF3 are used: target dimensions 40x60 mm, beam energy $\gamma = 235$, distance from target to detector $a \approx 2m$, wavelength λ depending on the detector. Experimental results show good agreement with expectations, but there is some distortion that can be explained by background caused upstream through wake-fields, CSR, etc., see Fig. 2.
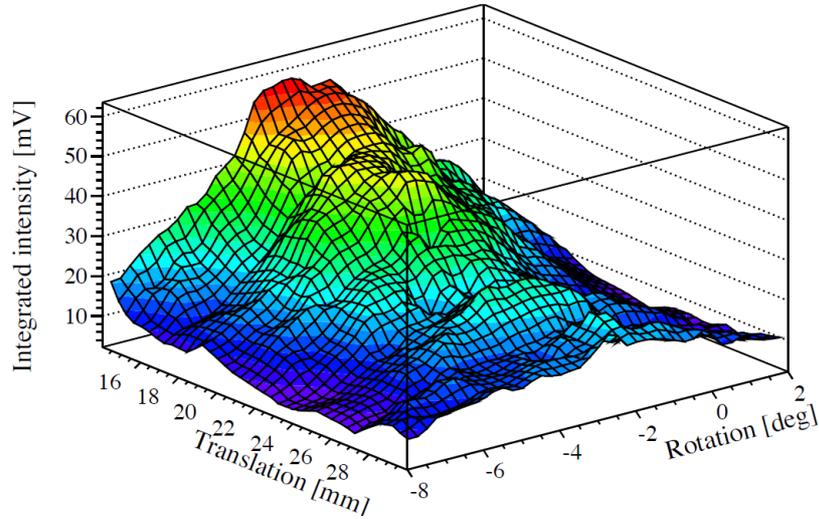
Figure 2: Results from measurements at CTF3.

As a next step, the computer code will be extended to allow for simulating more complicated phenomena such as CDR from two targets, Fig. 3 and Smith-Purcell radiation (SPR) from targets with more complicated shapes.
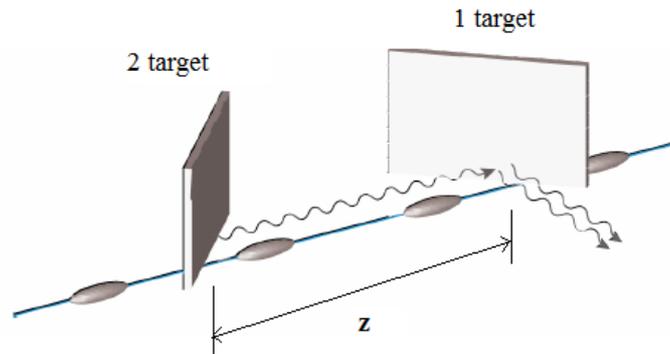
Figure 3: Illustration of CDR measurement from two targets.

The diffraction radiation spatial distribution from two targets can be written as:

$$\frac{d^2W^{DR}}{d\omega d\Omega} = 4\pi^2 k^2 a^2 \left[\left| E_1^{BDR} - E_2^{FDR} \exp\left[-\frac{ikz}{\beta}\right] \right|^2 \right]$$

(1)

where E_1^{BDR} is a backward diffraction radiation from the first target, E_2^{FDR} is a forward diffraction radiation from the second target, z is a distance between targets, k is a wave number and $\beta = v/c \approx 1$. In this analysis a classical theory of BDR based on a Huygen's principle of a plane wave diffraction will be involved. Simulations for two

targets configuration that currently is used at the CTF3 bunch profile monitor is a part of ongoing work.

3.23.3.2 *Development of Beam Position and Tilt Monitors for ITB, CTF3 and CLIC*

Beam position monitors (BPM) are essential diagnostics devices for monitoring the beam relative to magnetic devices and extracting important properties of magnetic lattices. In addition, position and angle feedback signals from BPMs can be used as a signal for closed loop feedback applications, where the response of the BPM is used directly after some processing to modify the beam control, such as kickers, steering magnets and quadrupoles.

The main aim of this project is the development of beam position monitors for electron accelerator facilities such as ILC and CTF3/CLIC in CERN. Particular emphasis will be placed on the electromagnetic design, ease of fabrication and analogue signal processing.

In collaboration with DITANET partner CERN and collaborators in KEK and SLAC, the next generation of beam position monitors is being developed. An integral part of the project is to understand with industry the most cost effective, yet high performance beam position monitor design.

There exists space at the CLEX area of the CTF3 facility to build a new Instrumentation Test Beam (ITB). Beam position monitor test systems will be installed in this area, including the local RF infrastructure for example master oscillator phase locked local oscillator sources.

3.23.3.3 *Beam Diagnostics for the Ultra-low Energy Antiproton Storage Ring (USR)*

In the future Facility for Low-energy Antiproton and Ion Research (FLAIR) at GSI [5,6], the Ultra-low energy electrostatic Storage Ring (USR) [7,8] will provide cooled beams of antiprotons down to energies of 20 keV. The storage ring is developed by the QUASAR Group [9] and described in detail in Refs. 7 and 19.

Table 1 summarizes the USR parameters that are most relevant from a beam diagnostics point of view. Antiprotons will be injected into the storage ring at an energy of 300 keV at intensities of up to $2 \cdot 10^7$ particles. With a ring circumference of 42.6 m, the revolution time of this beam equals to 5.6 µs. The ring's split achromat lattice [10] allows for varying the beam width in the center of the straight sections between a few millimeters during internal collision experiments and up to 20 mm before electron cooling. Depending on whether slow or fast extraction will be applied, the beam intensity and its time structure of the extracted beam will vary in a wide range [11,12].

Table 1: Summary of USR parameters at 20 keV that are relevant for the beam diagnostics system.

Parameter	Value
Energy	300 keV → 20 keV
Relativistic $\beta=v/c$	0.025 → 0.006
Revolution frequency	177 kHz → 46 kHz
Revolution time	5.6 μs → 32.8 μs
Number of particles	$\leq 2 \cdot 10^7$
Bunch length	1 ns - DC beam
Effective in-ring pbar rates	10^{10} pps - 10^{12} pps
Average rates of ectracted pbars	$5 \cdot 10^5$ pps - 10^6 pps

Current Measurement

An electrostatic Faraday cup will be used as a simple destructive monitor for absolute beam current measurements. The mechanical design of the Faraday cup has been optimized for the USR, i.e., the aperture has been prepared for the beams of diameter up to 2 cm and the suppressing electrode length has been adjusted to increase the electron collection efficiency.

Fig. 4 shows the simulation of secondary electrons emitted from the inner surfaces due to proton impact. For the intensity measurements, a sensitive amplifier needs to be applied because the expected average beam currents in the transfer lines will be as low as »100 fA. For the injection and fast extraction stages, the problem can be resolved by taking the advantage of the bunched beam delivery and measuring the peak current with a fast currentto-voltage converter working in the required bandwidth.
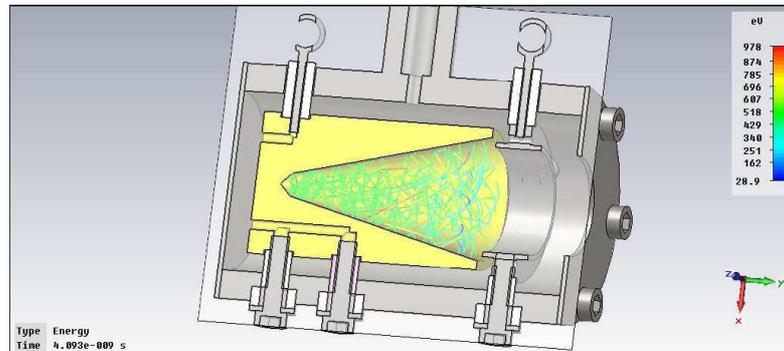
Figure 4: CST Studio simulation of the imported model of the Faraday cup: Suppression of secondary electrons.

A limitation of this solution is, however, that antiprotons will generate not only secondary electrons but also MeV-scale charged pions and recoil ions. Such particles cannot be captured within the cup. Therefore, the main use of the cup will be during the commissioning stage with protons or H⁻ ions.

Position Measurement

For the non-destructive beam position determination, up to 8 capacitive pick-ups (PUs) will be installed at the USR. Their design is shown in Fig. 5. In order to avoid

beam instabilities due to beam-to-ground impedance jumps, the PU should have the same diameter as the beam pipe. To increase the signal amplitude, the pipe diameter has been reduced from 250 mm to 100 mm.
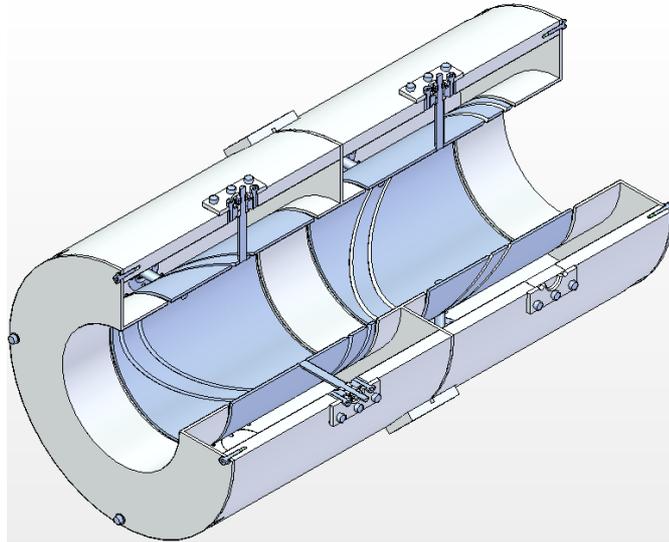
Figure 5: Design drawing of the USR diagonal-cut capacitive pick-up.

The coupling capacitance between opposite PU plates and adjacent PU units can be minimized by introducing separating rings at ground potential. With the proposed diagonal-cut design a high linearity is achieved. Adjacent plates are separated by grounded rings which allow for a higher sensitivity to the beam displacement.

Beam Profile Measurement

A scintillator-based monitor will deliver information on the transversal beam profile. However, limited sensitivity and light yield decrease due to surface sputtering have been reported [12,13]; it is not clear if these results can be applied to the USR case for two reasons. First, the tests were mainly limited to plastic scintillators and other materials have not been fully investigated under different irradiation conditions. Second, the thickness and other parameters of the screens were not optimized for the lowest possible beam currents. Therefore, further studies on scintillator-based monitors were undertaken using different types of screens.

Experiments at the Nuclear Physics Laboratory INFN-LNS in Catania, Italy were carried out with the invaluable help of Paolo Finocchiaro, Luigi Cosentino and Alfio Pappalardo. The tests were based on irradiation of the screens with a continuous beam of protons in the keV range with intensities down to a few fA. The scintillating materials used during the investigations included CsI:Tl, YAG:Ce and a Tb-glass-based Scintillating Fibre Optic Plate (SFOP). In order to reduce the initial beam currents of a few pA to only a few fA, pepper-pot-like attenuators were used, which produced multi-peak images. This allowed resolution testing of the screens at the same time.

Preliminary results indicate a high sensitivity to low intensity, low energy beams such as those expected from FLAIR. For 200 keV protons, the beam was still visible at approx. 10 fA and only a few seconds of averaging with a resolution better than 0.5 mm.

In addition to the above monitor, an ionization beam profile monitor relying on a supersonic gas-jet shaped into an extended thin curtain will be used [14,15]. Existing in-ring monitoring techniques, such as residual gas monitors, can take up to about 100 ms [16] to make meaningful measurements due to the low residual gas pressure. The curtain jet monitor allows for varying the gas density and thus the event rate and for a two dimensional transverse profile measurement as well as beam imaging [17].

This monitor relies on a neutral gas-jet, shaped into a thin curtain crossing the beam. In its simplest configuration, the gas curtain crosses the stored ion beam under an angle of 45°. While the stored beam crosses the jet, ionization occurs. These ions are then accelerated by an electric extraction field towards an amplification stage with an MCP and detected via a phosphor screen and a CCD camera. The nozzle-skimmer system that shapes the gas jet was optimized in simulations with the Gas Dynamics Tool (GDT) [18] which formed the basis for the mechanical design. Most components of the monitor are already manufactured and the system is presently mounted at the Cockcroft Institute.

3.23.4 Training

Training within DITANET is composed of training through research, local training by the individual institutions, often in close collaboration with partners, and network-wide events, such as school, topical workshops, or conferences. Partners offer for examples lecture programs, seminar courses, and language classes to their trainees. Some international events were already organized by the network and are summarized in this section. Detailed information on all events can be found on the DITANET homepage.

3.23.4.1 *First DITANET School on Beam Diagnostics*

From March, 30th - April, 3rd 2009 the first DITANET School on Beam Diagnostics took place at Royal Holloway, University of London. The School was combined with the first DITANET annual meeting and brought together more than 70 researchers from major Research Centers, Universities and private industry from all over the world, see Fig. 6.

Figure 6: Participants of the first DITANET School on beam diagnostics.

The School started with an introduction to accelerator physics and the definition of particle beams, before basic beam instrumentation such as beam energy, beam current or transverse beam profile measurement were covered. Later in the week more advanced topics, e.g. monitoring of the machine tune or electron cloud diagnostics were presented. An excursion to Rutherford Appleton Laboratory including visits to ISIS and DIAMOND on Wednesday, April 1st in addition to two tutorials and one poster session complemented the broad program.

A particular highlight was a dedicated industry session on the last day where lecturers from Thermo Fisher Scientific, TMD, Thales, ViALUX, and Instrumentation Technologies gave an insight into cutting edge R&D activities in the industry sector with a focus on differences as compared to research in academia.

3.23.4.2 *First DITANET Topical Workshop on the Diagnostics of Low Energy and Low Intensity Ion Beams*

The first DITANET topical workshop took place on November, 24th and 25th in Hirschberg-Großsachsen near Heidelberg in Germany. It focused on the diagnostics of low energy and low intensity ion beams and brought together around 40 scientists and engineers from all over the world. Its particular aim was to join early stage researchers both from within the network and from the wider community with renowned experts to allow for establishing important contacts for their careers and for reviewing the status of the different R&D activities.

The first day started with an introduction to the future Facility of Antiproton and Ion Research, where many of the monitors presently under development in different groups will be used to monitor all beam characteristics with a high precession. It then stretched to the beam instrumentation used at different storage ring and cyclotron facilities around the world.

The second day concentrated on electrostatic storage rings which are the ideal tool for lowest beam energies down to a few tens of keV and intensities as low as 10^4 pps. Presentations were given on the ELISA (ISA, Arhus), DESIREE (MSL, Stockholm), CSR (MPI-K, Heidelberg), and USR (FAIR, Darmstadt) facilities and triggered interesting discussions on these challenging developments.

3.23.4.3 *Second DITANET School on Complementary Skills*

All DITANET Trainees will attend a Complementary Skills School at the University of Liverpool 15th-19th March 2010. Participants will arrive in Liverpool on the morning of Monday 15th March with sessions commencing that afternoon. Day one will include full introductions and an opportunity for trainees to get to know each other followed by a skills session on presentations. Professional trainers will cover many aspects providing insight into skills to enhance PhD study and research. Working days will provide a wide variety of practical skills including problem solving techniques; scientific writing; intellectual property rights and building the bridge from academia to industry. In addition to working sessions there will be an opportunity to tour the Daresbury Laboratory and the Cockcroft Institute. This School is also seen as an important means for Trainees to network with each other and the management team.

3.23.4.4 *Second DITANET Topical Workshop on Longitudinal Beam Profile Measurements at High Energy Accelerators and Light Sources*

The University of Liverpool is presently in the process of organizing the second DITANET Topical Workshop. This will be held at the Cockcroft Institute, Daresbury, UK on the 12th and 13th July 2010. Although this is still very much in the planning stage, expert speakers have been confirmed from partner institutions and industry; there will be topical talks and discussion sessions where future projects and collaboration can be explored. The workshop is for researchers at PhD and Postdoc level in addition to more advanced colleagues.

3.23.5 **Summary**

DITANET quickly established itself as a frame for international collaboration and training in beam diagnostics. Almost all position vacancies have been filled with highly qualified early stage and experienced researchers from all over the world. The network's research projects are making remarkable progress and this brief overview can only summarize a few developments.

The joint organization of international training events, such as the first school on beam diagnostics and the network's first topical workshop, showed that DITANET has already become a real network where close collaboration between partners is one of the core ideas.

The network will organize further topical workshops and schools, as well as an international conference in 2011. Institutions and researchers that share the network's ideas and ambitious are invited to contact the coordinator about opportunities.

This work is supported by the EU under contract PITN-GA-2008-215080.

3.23.6 **References**

1. http://www.liv.ac.uk/ditanet
2. C.P. Welsch, "DITANET: A European Initiative in the Development of Beam Instrumentation for Future Particle Accelerators", Proc. XXIV International LINAC Conf., Victoria, BC, Canada (2008)
3. C.P. Welsch, "DITANET – An Overview of the First Year Achievements", Proc. Part. Acc. Conf., Vancouver, Canada (2009)
4. M. Micheler, R. Ainsworth, G. Blair, G. Boorman, R. Corsini, P. Karataev, T. Lefevre and K. Lekomtsev, "Longitudinal beam profile monitor at CTF3 based on Coherent Diffraction Radiation", Proc. VIII International symposium RREPS-09, Sep 7-11, Zvenigorod, Russia (2009)
5. http://www.oeaw.ac.at/smi/flair/LOI.html
6. http://www.oeaw.ac.at/smi/flair/TP.html
7. C.P. Welsch, et al., "An ultra-low-energy storage ring at FLAIR", NIM A 546 (2005) 405–417
8. C.P. Welsch, M. Grieser, A. Dorn, R. Moshammer, J. Ullrich,"Exploring Sub-Femtosecond Correlated Dynamics with an Ultra-low Energy Electrostatic Storage Ring", AIP Conf. Proc. 796 (2005) p. 266-271
9. http://www.quasar-group.org
10. A. Papash, C.P. Welsch, "An Update of the USR Lattice: Towards a true multi-user experimental facility", Proc. Part. Acc. Conf., Vancouver, Canada (2009)
11. J. Harasimowicz, C.P. Welsch, "Beam Instrumentation for the Future Ultra-low Energy

Storage Ring at FLAIR", Hyperfine Interact. 194 1-3 p. 177-181 (2009)

12. J. Harasimowicz, et al, "Beam diagnostics for the USR", Proc. Part. Acc. Conf., Vancouver, Canada (2009)
13. T. Sieber et al., "A Beam Diagnostics System for the Heidelberg Cryogenic Storage Ring CSR", Proc. Europ. Part. Acc. Conf., Edinburgh, Scotland (2006)
14. M. Vogel et al., "Scintillation Light Produced by Low-energy Beams of Highly-charged Ions", Nucl. Instrum. Meth. B 263(2), 518-522 (2007)
15. K.-U. Kühnel, et al., "Putignano, C.D. Schröter, J. Ullrich, C.P. Welsch, "A Novel Beam Profile Monitor Based on a Supersonic Gas Jet", Proc. Europ. Part. Acc. Conf., Genoa, Italy (2008)
16. M. Putignano, et al., "A fast, low perturbation ionization beam profile monitor based on a gas-jet curtain for the ultra low energy storage ring ", Hyperfine Interact. 194 1-3 p. 189-193 (2009)
17. T. Honma et al., "Design and Performance of a Nondestructive Beam-profile Monitor Utilizing Charge-division Method at HIMAC", Nucl. Instr. Meth. A 490(3), 435-443 (2002)
18. M. Putignano, K.-U. Kühnel, C.P. Welsch, "Design of a Nozzle-Skimmer System for a Low Perturbation Ionization Beam Profile Monitor", Proc. DIPAC Workshop, Basel, Switzerland (2009)
19. A. Papash and C.P. Welsch, "Realization of Nanosecond Antiproton Pulses in the Ultra-low Energy Storage Ring", NIM A (2010), accepted for publication.

3.24 Beam Halo Monitoring

Sayyora Artikova and Jan Egberts, MPI for Nuclear Physics, Heidelberg, Germany

R. Fiorito, S. Bernal, I. Haber, R. Kishek, P. G. O'Shea, A. Shkvarunets, H. Zhang
University of Maryland, USA

Carsten P. Welsch, Cockcroft Institute and the University of Liverpool, UK
Mail to: carsten.welsch@quasar-group.org

3.24.1 Introduction

A primary concern of modern high intensity, high energy accelerators is potential damage and radio activation of accelerator components resulting from uncontrolled beam losses. Beam losses must be monitored all along the machine in order to keep the radiation level and the activation as low as possible. A major source of loss is the formation and evolution of beam halos at the periphery of the beam requiring high dynamic range beam profile measurements and thus putting high demands on the beam diagnostic system. As a consequence, halo and tail studies are needed in order to minimize any potential performance limitations of future accelerators from this source. It is imperative to have a clear understanding of the mechanisms that can lead to halo formation and to have the possibility to test available theoretical models with an adequate experimental setup. Measurements exploiting radiation in the visible spectrum such as optical transition radiation, diffraction radiation or synchrotron radiation provide interesting opportunities for high resolution measurements of the beam profiles and are under investigation for the purpose of halo monitoring.

3.24.2 **Flexible Core Masking Technique**

The flexible core masking technique is based on the core masking technique which is well established in astronomy to observe for example the corona of the sun [1]. For an accurate image acquisition of the corona, an exposure time is required at which a normal camera overexposes due to the bright central region. The resulting blooming effects will superimpose the corona light and make an accurate image acquisition impossible. Therefore, the central bright region region of the sun is masked out to allow for a corona measurement without any negative blooming effects. Measurements with fixed masks are often used for the observation of astronomical objects [2, 3].

However, in contrast to astronomical objects, the core of a particle beam is not of constant shape and varies with time. Initial experiments with fixed masks were already done at CERN [4] where the beam was adjusted to match a predefined mask. For time-dependant particle beams, however, it is important that the mask can be adjusted to the beam shape on a short time scale. Unlike astronomical objects, a particle beam profile is typically variable in shape which is why an acquisition technique based no a fixed mask is no longer sufficient. Therefore it was decided to design a novel monitor based on a Micro Mirror Arrays (MMA).

(a) Laser profile measurement   (b) display beam core on MMA
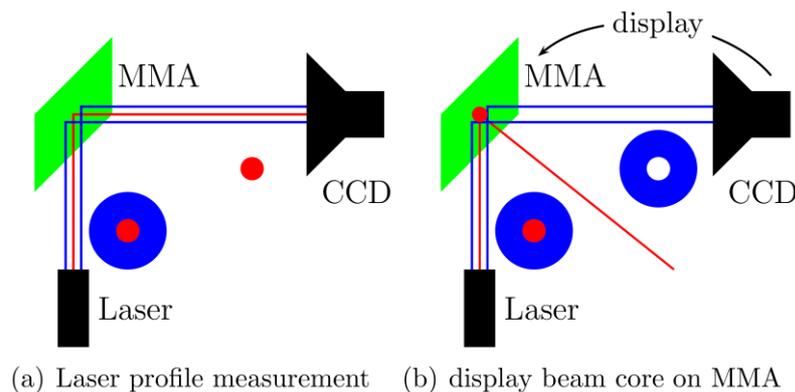
Figure 1: Principle of MMA-based beam profile measurements.

The laser beam is reflected by an MMA into a camera that measures the two dimensional beam profiles, as illustrated in Fig. 1. If the mask is displayed on the MMA, the central beam core (red) will be deflected, while the halo (blue) is still reflected into the CCD-camera. The challenge of measuring a high dynamic range is reduced to the problem of measuring a low intensity. This can be realized by increasing the exposure time of the camera or adjusting the light level with different neutral density filters in case of a bright initial source.

First results were obtained in lab measurements, where the light generated by a particle beam was simulated by a small laser. The opening angle of a tenth of a degree corresponds to typical values of OTR or SR from a 150 MeV electron beam as it is used in CTF3. These measurements indicated a dynamic range of up to 10^5 with a conventional 8-bit camera system [5-8].
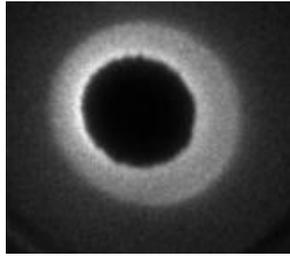
Figure 2: Halo image measured at UMER [9]. The beam core was deflected by the MMA.

Further studies with beam were then realized at the University of Maryland Electron Ring (UMER) with measurement data shown in Fig. 2.

3.24.3 Summary and Outlook

Beam halo monitoring based on a flexible mask generated by a micro mirror array has demonstrated a high potential in lab measurements, where dynamic ranges of up to 10^5 were reached even with a simple 8-bit camera system. In first measurements with beam at UMER, a mask was generated with the MMA as a function of the actual beam profile and with adjustable threshold levels. Data analysis is presently being done and this technique shall ultimately help improving the understanding of beam halo formation and propagation, as well as phase space tomography.

3.24.4 References

1. F. Martinache, O. Guyon, A. Pluzhnik, R. Galicher, and S.T. Ridgway, "Exoplanet imaging with a phase-induced amplitude apodization coronograph". The Astrophysical Journal, 639, 1129-1137, 2006
2. G. Guerri, et al., "Apodized lyot coronagraph for vlt-sphere: Laboratory tests and performances of a first prototype in the visible". Instr. Meth. for Astrophys., 2009
3. T. Lefevre, E. Braun, R. Corsini, D. Schulte, and A.L. Perrot. Beam halo monitoring at CTF3. Proc. Europ. Part. Acc. Conf., Lucerne, Switzerland, 2004
4. B.R. Oppenheimer et al, "The Lyot Project: Status and Deployment Plans", AMOS Technical Conference, 2003
5. C.P. Welsch, E. Bravin, and T. Lefevre, "A beam halo monitor based on adaptive optics" Proc. of SPIE 6616:9, 2007
6. C.P. Welsch, E. Bravin, B.Burel, T.Chapman, T. Lefevre, M.J. Pilon, "Alternative Techniques for Beam Halo Measurements", Meas. Sci. Technol. 17, 2035c, 2009
7. J. Egberts, S.Artikova, C.P. Welsch, "Flexible Core Masking Technique for Beam Halo Measurements with High Dynamic Range"', Proc. DIPAC, Basel, Switzerland, 2009
8. J. Egberts, C.P. Welsch, "Flexible Core Masking Technique for Beam Halo Measurements with High Dynamic Range", JINST, *submitted* (2010)
9. R. Fiorito et al., "Beam Halo Imaging with an Adaptive Optical Mask", Proc. BIW, Santa Fe, USA (2010)

3.25   Optical Fiber Beam Loss Monitoring

Angela Intermite, Massimiliano Putignano and Carsten P. Welsch
Cockcroft Institute and the University of Liverpool, UK
Mail to: Angela.Intermite@quasar-group.org

3.25.1 Introduction

Beam loss monitors are one of the key components of any machine protection system as they help preventing beam induced damages. They should detect particle losses, identify their location and provide an input signal that, if necessary, triggers an interlocking system.

It will be of high importance for all future high current accelerators to minimize particle losses and thus avoid activation of the installation. In the particular case of CTF3, with its 4kW average beam power, a final machine protection system will have to provide loss measurements at sensitivities of $10^{-4} - 10^{-5}$ with respect to the nominal in-tensity and a time resolution of better than 10 ns.

The design of a monitor based on the exploitation of the Cherenkov Effect in optical fibers is presently being worked out. For the last four decades, it has been known that optical fibers show a tremendous increase of their attenuation when exposed to ionizing radiation [1,2]. In the last decade, fiber optic radiation monitoring systems for accelerators based on the generation of Cherenkov light by relativistic charged particles were integrated in different accelerators, see e.g. [3-5]. Such fast systems can be used for rapid accelerator switch off during unacceptable high beam losses and their localization, but they are not well suited for accurate radiation dose measurements. A particular difficulty at CTF3/CLIC comes from the fact that its two beam lines are very close to each other and the beam losses need to be monitored with a good spatial and angular resolution for both simultaneously, but independently.

3.25.2 Detector Characterization

Optimization of the signal level requires detailed investigation into all system components, in particular the optical fibers and the photon detectors. In this context, the introduction of Silicon Photomultipliers (SiPM) as single photon sensitive detectors represents a promising alternative to traditional photomultiplier tubes. They promise distinct advantages especially in applications in which it is compulsory to attain magnetic field insensitivity, low photon flux detection, quantum efficiency in the blue region that is comparable to standard photomultipliers, high timing resolution, dimensions comparable to the dimensions of an optical fiber diameters, and low costs.

The structure of the SiPM is based on an array of independent avalanche photodiodes (APDs) working in Geiger-mode at a low bias voltage with a high gain. The output signal is proportional to the number of pixels "fired" by impacting photons. The detection efficiency for state-of-the-art devices is in the order of 20% at 500 nm.

The intrinsic noise of a number of SiPMs was characterized in the Cockcroft Institute's optical lab, see Fig. 1. The more precise this noise is known, the better it can be filtering from the signal generated from the Cerenkov Effect which will then allow for a cleaner signal to estimate the losses.

In addition, knowledge of the noise characteristics allows for an in-detail characterization of the performances of alternative detectors and for determining their real applicability to loss monitoring. Finally, the knowledge of the noise rate will allow for calibrating these devices in different operating scenarios.
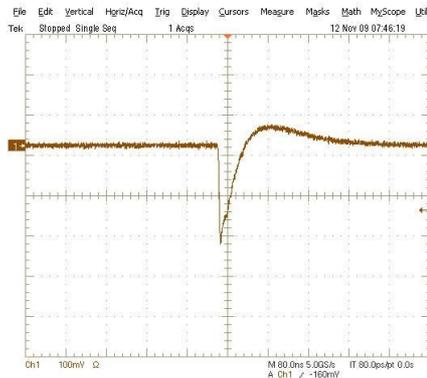
Figure 1: Example signal from one of the SiPMTs under investigation.

These tests allowed for a selection of the best performing PMTs. As a next step, the coupling efficiency of the SiPMTs to different optical fibers will be analyed, and measurements with beam will be carried out at CTF3.

3.25.3 **References**

1. R.D. Maurer, E.J. Schiel, S. Kronenberg, R.A. Lux, "Effect of neutron- and gamma-radiation on glass optical waveguides", Appl. Opt. 12 (9) (1973) 2024
2. B.D. Evans, G.H. Sigel, "Permanent and transient radiation induced losses in optical fibers", IEEE Trans. Nucl. Sci. NS-21 (6) (1974) 113
3. G. Schmidt, E. Kasel, K. Wille, M. K. orfer, H. Henschel, J. Kuhnhenn, "Optical fibre beam loss monitors for storage rings at DELTA", Proc. 9th European Part. Acc. Conf., Paris, France (2002)
4. R. Nishiura, N. Izumi, "Radiation sensing system using an optical fiber", Mitsubishi Elec-tronic ADVANCE, (2001) pp. 25–28
5. H. Henschel, M. Körfer, J. Kuhnhenn, U. Weinand, F. Wulf, "Fibre optic radiation sensor systems for particle accelerators", Nucl. Instr. and Meth. A 526 (2004) 537–550

3.26   Mathematical Physics Activities at the Cockcroft Institute

DA Burton, J Gratus, V Perlick, RW Tucker, DC Christie[1], S Goto, AC Hale,
A Noble[2], T Walton, CES Canovan, M Ferris, R Gallego Torrome,
JDA Smith and H Wen
Department of Physics, Lancaster University, Lancaster, UK
Cockcroft Institute of Accelerator Science & Technology, Daresbury, UK
Mail to: d.burton@lancaster.ac.uk

3.26.1   Introduction

The intense international activity involved in probing the structure of matter on all scales, with particle beams and radiation, owes much to recent advances in accelerator science and technology. Developments in the production of high power laser radiation also offer new avenues for accelerator design and new diagnostic tools of relevance to medical science, engineering and the communications industry [1]. Contemporary issues in novel accelerator development have motivated considerable interest in the interaction between charged particles and the electromagnetic field in domains where relativistic effects cannot be ignored. Our recent research spans numerous topics ranging from fundamental issues associated with radiation reaction, to the development of efficient analytical methods for obtaining electromagnetic fields driven by relativistic particle beams. A recurring theme in our work is the examination of effective theories of large collections of electrically charged relativistic particles and their electromagnetic couplings.

The following is a brief account of recent work emphasising certain challenges associated with the interaction between matter and electromagnetic fields. The background literature associated this subject is vast and no attempt is made here to provide a complete list of references.

Any self-consistent theory describing a large collection of charged particles must include all electromagnetic forces between the particles. However, the notorious problem of determining the classical force on a single accelerating point charge due to its own electromagnetic field has stimulated research for over a century and remains unresolved (see [2, 3] for recent reviews). The structure of an isolated single electron is currently beyond observation and one often proceeds classically by associating the electron with a singularity in the electromagnetic field described by Maxwell's equations in vacuo. Following Dirac [4], an equation of motion for the charged particle may be obtained by appealing to conservation of the total energy-momentum of the particle and its electromagnetic field. In order to remove singularities in the equation of motion Dirac made "natural assumptions" about the origin of the electron mass. The resulting Lorentz-Dirac equation of motion contains the acceleration of the particle and its proper time derivative and possesses solutions that violate intuition. In particular, unless special conditions are adopted for the final state of the electron, it predicts that a free electron in vacuo can self-accelerate; furthermore the equations predict solutions where the electron may experience a sudden acceleration before it enters a region of space containing a non-vanishing external electrostatic field.

---

[1] Current address : Greenspace Research, Lews Castle College UHI, Stornoway, Isle of Lewis, Scotland.
[2] Current address : Department of Physics, SUPA, University of Strathclyde, Glasgow, Scotland.

Although one can employ approximation schemes that circumvent some of the above difficulties [5], it is not clear that such methods are applicable to distributions of relativistic particles with sufficiently high proper number density. As schemes for accelerating charged particles become more complex and ambitious in their aims such approaches may be inadequate for a proper understanding of new challenges.

If one forgoes the use of point particle methods in favour of self-consistent effective theories based on classical continuum methods [2, 6], the existence of non-linearities in the governing partial differential transport equations gives rise to other challenges. In particular, the matter density in relativistic simple (single-component) fluid models of a beam of charged particles may exhibit singular behaviour [6] due to the evolution of shocks. This situation is analogous to shock formation in fluid and gas dynamics. Similarly, the electron velocity field of a cold plasma undergoing sufficiently large amplitude electrostatic oscillations may become multi-valued [6]. However, the dominant inter-particle forces in a cold collisionless plasma are long-range and multiple streams can form dynamically; in particular, particles may become trapped in an electrostatic wave and fine-scale mixing may destroy the wave. The evolution of an electrically charged continuum with a dynamical number of components was studied in [6].

Alternatively, one may describe such continua using the velocity moments of a one-particle distribution function. For modelling warm plasmas or warm particle beams, it is common to assume that the infinite hierarchy of field equations, obtained from velocity moments of the Vlasov equation, may be truncated to yield a closed set of field equations. A novel geometric averaging procedure for constructing velocity moments was recently developed [7-9] and used to establish rigorous conditions for the validity of the truncation in the ultra-relativistic regime. Geometrical constructions of distributional solutions to the Maxwell-Vlasov system were explored in [10].

The maximum sustainable amplitude (the "wave-breaking limit") of non-linear electrostatic oscillations has been a subject of considerable interest for over half a century [11–17]. Recent years have seen a resurgence of interest in the wave-breaking limit of warm plasma oscillations based on macroscopic fluid (hydrodynamic) models of plasmas. Wave-breaking limits were first calculated for cold plasmas undergoing nonlinear longitudinal electrostatic oscillations, and thermal effects were later included in non-relativistic and relativistic contexts [12, 13]. The results for the cold plasma are uncontroversial, but recent discussion has uncovered difficulties establishing an agreed analytical description of longitudinal wave-breaking in warm plasmas; in particular, it has been noted that different plasma models based on different assumptions yield different results [14]. Models of nonlinear plasma waves near breaking are approaching the limits of their domain of applicability, and different models exhibit different wave-breaking limits. Although recent experiments operate in the three-dimensional "bubble" (or "blow-out") regime, and exploit transverse wave-breaking, recent work has rekindled interest in the theory of longitudinal wave-breaking.

In an attempt to address issues raised in [14], we recently developed [15, 16] a geometric reduction of the Vlasov equation using a self-consistent 3-dimensional generalization of the 1-dimensional relativistic waterbag concept introduced by Katsouleas and Mori [12]. Furthermore, we showed [17] that the maximum amplitude of nonlinear longitudinal electric waves for a particular class of 3-dimensional waterbags converges as the phase velocity of the wave tends to the speed of light, whereas the maximum amplitude in the 1-dimensional Katsouleas-Mori model diverges

in this limit. The results in [17] bear some resemblance to the behaviour of fluid models such as [13], and we conclude that the dimensionality of the waterbag plays an important role in the behaviour of the electrostatic field. Work is currently underway to include the effects of trapped particles in the formalism.

In the high energy regime in which relativistic effects dominate – such as laboratory based laser-plasma acceleration – plasmas are commonly described by the collisionless Vlasov equation. This approximation is often justified as the timescales governing relativistic processes in an underdense plasma are typically much shorter than the average time between collisions. However, recent advances in high energy density science have increased the demand for efficient descriptions of plasma dynamics fully incorporating both relativistic and collisional effects.

Although the relativistic Fokker-Planck equation describes collisional plasmas in the relativistic regime, it contains a non-linear integral operator and is cumbersome to work with in many cases of interest. Furthermore, it does not easily lend itself to the generation of succinct fluid models. To address this issue, we recently developed [18] a relativistically covariant extension of the non-relativistic Lenard-Bernstein equation and used it to generate a new relativistic plasma fluid model that includes dissipative effects. Our induced fluid model contains new terms that arise from the non-trivial geometry of the unit hyperboloid in 4-dimensional (Lorentzian) phase space, and was used in [18] to investigate electric waves.

For small amplitude classical electromagnetic fields recourse is often made to a linear approximation scheme in which the appropriate constitutive relations arising from the coupled matter-field equations are linearized. If the medium is uniform in space Fourier techniques are adequate since (if gravity is ignorable) the coupled system can be projected into plane-wave eigen-solutions of the Helmholtz equation. Such an approach leads to the concept of classical dispersion in which the parameters describing such eigen-solutions are required to satisfy constraints involving properties of the medium. However if the medium is inhomogeneous, exhibits relaxation or memory properties, or gravitational fields are present such Fourier methods no longer diagonalize the system and prove impractical. We have developed new approaches to circumvent these difficulties [19] and obtained integral equations that supercede classical dispersion relations in homogeneous media permitting investigation of Landau damping in non-stationary and inhomogeneous relativistic plasmas.

Macroscopic fluid models are particular examples of theories based on the relativistic continuum paradigm. The vanishing of the space-time divergence of the total stress-energy-momentum tensor (describing matter and electromagnetic fields) leads to relativistic equations of motion and continuity equations for the material continuum. A specification of the total stress-energy-momentum tensor defines the (constitutive) model of the fully interacting continuum including fields and matter. Macroscopic descriptions of continua may involve effective theories demanding substantial input from experiment. Before the advent of precision experimentation and modern gauge descriptions of the the interaction of light with matter, stress-energy-momentum tensors associated with electromagnetic fields in a classical medium were guessed on the basis of relativistic covariance. A long running dispute based on alternative proposals by Minkowski [20] and Abraham [21] about one hundred years ago has yet to be settled by experiment. Our research has shown [22] how the choice made by Abraham follows naturally from a variational principal involving gravitation and the motion of the medium, and that the symmetrized version of the choice made by Minkowski follows

by alternative gravitational interactions [22, 23]. Although recent experiments employing sophisticated methods based on cold atom optics seem to favour Minkowski's choice other experiments seem to prefer the Abraham tensor and a final consensus is still to be achieved [24]. These issues have led us to develop a new approach to the calculation of electromagnetic forces and torques on magneto-electric media using the concept of a drive form [25].

We are exploring constitutive relations for uniformly rotating media [26] and how forces and torques can be defined covariantly and calculated for arbitrarily moving media. In particular, for a class of media with simple electromagnetic constitutive properties we show that, under the influence of an incident monochromatic, circularly polarized, plane electromagnetic wave, the Abraham and symmetrized Minkowski tensors induce different time-averaged torques on a uniformly rotating materially inhomogeneous dielectric cylinder and suggest that this observation may offer new avenues to explore experimentally the covariant electrodynamics of more general accelerating media. This work may have relevance to the development of new accelerating structures based on materials with novel constitutive properties (meta-materials).

Beam pipes that spatially curve and taper through magnet arrays in small-gap undulators feature in the designs of advanced machines for producing pulsed sources of intense focused electromagnetic radiation. The production of femto-second radiation pulses requires high peak electric currents and the maintenance of low emittance electron beams. Extreme design criteria are required to sustain beam stability in the presence of radiation backreaction on accelerated sources in SASE X-ray sources. A direct analytic approach to this electrodynamic problem via the coupled system of Maxwell's field equations and the equations of motion for the particle beams encounters difficult problems due to nonlinearities and retardation effects. Furthermore, the geometry of the beam pipe may be such that direct numerical solution of Maxwell's equations is too inefficient, especially when sweeping across a wide range of design parameters. Such considerations motivated the development of perturbative methods for calculating the electromagnetic fields inside curved [27] and tapered [28] beam pipes. In [27] a perturbative expansion in a small parameter characterising the curvature of the beam pipe is used to determine the longitudinal wake potential inside the pipe. Longitudinal wake potentials and impedance formulae are developed in [28] for a beam pipe whose circular cross-section slowly varies with radius; there, an asymptotic approximation is developed for the electromagnetic field based on a parameter that characterizes the slow variation of the cross-section's radius. Agreement with direct numerical solution of Maxwell's equations is impressive for tapers whose geometries are representative of the next generation of lepton colliders, with narrow bunches whose lengths are a couple of millimetres. The difficult challenge remains to develop analytical methods for tackling considerably shorter bunches.

We also demonstrated [29] how interference effects in the electromagnetic field of an ultra-relativistic bunch in a straight beam-pipe shows a striking resemblance to that occuring due to CSR in cyclic machines, despite the fact that in the ultra-relativistic limit the source is no longer accelerating. We analysed how such enhanced spectral behaviour depends on the geometry of the source and the details of the stochastic distribution of structure within the source [29].

In a further attempt to address the radiation reaction problem and the breakdown of traditional Maxwellian electrodynamics in the context of high-field laser interactions

with matter, attention is currently focussed on high-field nonlinear vacuum electrodynamics. One expects classical vacuum Maxwellian electrodynamics to break down near critical electric field strengths of 1.3×10^{16} V/cm or magnetic field strengths of 4.4×10^{13} G, where electron-positron pair creation becomes possible. Such fields might be reached in a future laser with peak intensity 2.3×10^{29} W/cm^2. However there may be a classical breakdown of Maxwell equations well before one needs quantum-electrodynamics. A classical fluid model of non-linear electrodynamic interaction with matter in vacuo based on the vanishing of the divergence of the total stress-energy-momentum tensor has been developed [30] that reduces to Maxwellian electrodynamics for suitably low-field strengths. In particular, the remarkable properties of the Born-Infeld theory offer a promising constitutive model since this preserves electromagnetic duality and possesses singular charged (Bionic) vacuum solutions with finite field-strengths at the location of the singularity.

An exploration of the consequences of non-linear electrodynamics was recently initiated in [30]. Since the effects of the non-linearity are most marked for very high fields, it might be expected that astrophysical phenomena (such as magnetars, quasars and gamma-ray bursts) are the most likely candidates for exploring the ramifications of such theories. However, for Born-Infeld theory, we showed in [30] that a plane electromagnetic wave in a constant magnetic field propagates with a phase speed less than the speed of light in the vacuum and that this might be detectable in a terrestrial experiment.

In summary, although Maxwell's equations have been known for over a century and a quarter, a number of intriguing theoretical challenges are revealed when one attempts to develop effective theories and approximations inspired by the on-going advances in plasma physics, laser technology and particle accelerator science.

3.26.2 **Acknowledgements**

3.26.3 **References**

1. H.-P. Schlenvoigt, K. Haupt, A. Debus, F. Budde, O. Jäckel, S. Pfotenhauer, H. Schwoerer, E. Rohwer, J. G. Gallacher, E. Brunetti, R. P. Shanks, S. M. Wiggins and D. A. Jaroszynski, Nature Phys. 4, 130 (2008).
2. D.A. Burton, J. Gratus and R.W. Tucker, "Asymptotic analysis of ultra-relativistic charge", Ann. Phys. 322 (3) 599 (2007). arXiv:physics/0512218.
3. E. Poisson, arXiv:gr-qc/9912045.
4. P.A.M. Dirac, Proc. R. Soc. Lond. A 167 148 (1938).
5. L.D. Landau and E.M. Lifshitz, The Classical Theory of Fields, (Oxford: Pergamon, 1962).
6. D.A. Burton, J. Gratus and R.W. Tucker, "Multiple currents in charged continua", J. Phys. A: Math. Theor. 40 811 (2007). arXiv:physics/0609089.
7. R. Gallego Torrome, "Averaged dynamics associated with the Lorentz force equation", arXiv:0905.2060.
8. R. Gallego Torrome, "Averaged Lorentz dynamics and an application in plasma dynamics", arXiv:0912.0183.

---

9. R. Gallego Torrome, "Fluid models from kinetic models using a geometric averaging procedure", arXiv:0912.2767.

10. J. Gratus, "Distributional solutions to the Maxwell-Vlasov equations", arXiv:0809.2944.

11. J.M. Dawson, Phys. Rev. 113 383 (1959).

12. T. Katsouleas and W.B. Mori, Phys. Rev. Lett. 61 90 (1988).

13. C.B. Schroeder, E. Esarey and B.A. Shadwick, Phys. Rev. E 72, 055401 (2005).

14. R.M.G.M. Trines and P.A. Norreys, Phys. Plasmas 13 123102 (2006).

15. D.A Burton and A. Noble, "Geometry of thermal plasma oscillations", AIP Conf. Proc. 1086 252 (2009).

16. D.A. Burton, A. Noble and H. Wen, "Discontinuous distributions in thermal plasmas", Il Nuovo Cim. C 32 1 1 (2009). arXiv:0906.1096.

17. D.A. Burton and A. Noble, "Longitudinal wave-breaking limits in a unified geometric model of relativistic warm plasmas", J. Phys. A: Math. Theor. 43 075502 (2010). arXiv:0908.4498.

18. A. Noble and D.A. Burton, "Modelling collisions in a relativistic plasma", arXiv:0910.4368.

19. J. Gratus and R.W. Tucker, "Covariant constitutive relations, Landau damping and non-stationary inhomogeneous plasmas", arXiv:1003.2062

20. H. Minkowski, Nachr. Ges. Wiss. Göttn. Math. -Phys. KI. 53 (1908).

21. M. Abraham, Rend. Circ. Matem. 30 33 (1910).

22. T. Dereli, J. Gratus and R.W. Tucker, "The Covariant Description of Electromagnetically Polarizable Media". Phys. Lett. A 361 190 (2007). arXiv:math-ph/0610078.

23. T. Dereli, J. Gratus and R.W. Tucker, "New perspectives on the relevance of gravitation for the covariant description of electromagnetically polarizable media ", J. Phys. A: Math. Theor. 40 5695 (2007). arxiv:math-ph/0610082

24. U. Leonhardt, Nature 444 823 (2006).

25. R.W. Tucker and T. Walton, "An intrinsic approach to forces in magnetoelectric media", Il Nuovo Cim. C 32 1 205 (2009). arXiv:0811.4394.

26. C.E.S. Canovan and R.W. Tucker, "Maxwell's equations in a uniformly rotating dielectric medium and the Wilson-Wilson experiment", Am. J. Phys. (accepted) .

27. S. Goto and R.W. Tucker, "The electrodynamics of inhomogeneous rotating media and the Abraham and Minkowski tensors", J. Math. Phys. 50 063510 (2009). arXiv:0808.1670.

28. D.A. Burton, D.C. Christie, J.D.A. Smith and R.W. Tucker, "Wake potentials and impedances of charged beams in gradually tapering structures", arXiv:0906.0948.

29. A.C. Hale and R.W. Tucker, "Energy spectra from electromagnetic fields generated by ultra-relativistic charged bunches in a perfectly conducting cylindrical beam pipe", J. Phys. A: Math. Theor. 43 025402 (2010). arXiv: 0908.3839.

30. R.W. Tucker and T. Dereli, "Charged relativistic fluids and non-linear electrodynamics", Euro. Phys. Lett. 89 20009 (2010). arXiv:1001.1282.

Applications to Energy, Health and Security

3.27 ADSR Activities in the UK

Roger Barlow

School of Physics and Astronomy, U. of Manchester, Manchester M13 9PL and
Cockcroft Institute, Keckwick Lane, Daresbury Science and Innovation Campus,
Warrington WA4 4AD

Mail to: Roger.Barlow@manchester.ac.uk

3.27.1 Introduction

The UK currently emits approximately 10 tons of CO_2 equivalent per person per year, which is broadly in line with the European average.[1] The government has set ambitious targets to improve this, including the cutting of CO_2 emissions by 80% by 2050 from the 1990 baseline[2], but there is no firm plan as to how such goals will be met. There is some scope for development of wave and tidal power and for offshore wind farms, less for onshore wind and solar power, however it appears virtually impossible to meet such targets without the use of nuclear power.

Although the UK currently obtains about 20% of its electricity from nuclear power, the reactors are old and are all but one due to be out of service by 2023. Steps are being taken to replace and even expand these plants, though progress is slow as there is still considerable public opposition.

The Thorium ADSR (accelerator-driven subcritical reactor) system is well placed as a match between the pragmatic need and the distrustful public: it is manifestly safe, as switching off the accelerator switches off the reactor, it produces no (or almost no) long lived waste, and it is highly proliferation resistant. Although there has been little UK activity in this area until recently, this is changing rapidly and the number of groups and people interested in, and working on, the topic has grown greatly in recent years.

3.27.2 ThorEA

ThorEA (Thorium Research for the Energy Amplifier) is a not-for-profit organisation and learned society. It aims to promote thorium-fuelled energy amplifier systems as a safe, sustainable and publicly-acceptable form of nuclear power. Its goal is the construction of a thorium-fuelled ADSR in the United Kingdom. It provides a framework within which individuals and organisations can co-operate in pursuit of this.

There are over 80 individuals on the mailing list, and some 40 names appear (with permission) as members on the organisation website. They cover a very broad range of disciplines: Accelerator Scientists, Particle Physicists, Nuclear Physicists, Nuclear Engineers, and Economists. They also come from many different institutes: the UK Accelerator Institutes, Cockcroft and John Adams, are well represented, as are the Rutherford Appleton and Daresbury Laboratories. There are members of 10 different universities, and several from industry. Although most are UK based there are several from continental Europe, the US and elsewhere that use this as a way of keeping in touch, and they are very welcome – we are aware that we are behind in many areas. (Anyone who wishes to join should contact the author.)

ThorEA maintains a website http://www.thorea.org as a central point of information and contact, which includes details of the organisation, a news feed of relevant stories, links to other sites, and details of meetings. These open and informal workshops take place 3-4 times a year, and normally get around 30 participants and about 10 talks, covering all aspects of ADSR systems from the accelerator to the economics.

ThorEA also acts as a forum for partnerships to respond to funding opportunities. There have been several small successful bids: further ones are in progress. It seeks out and exploits opportunities to publicise Thorium and ADSRs, through the web, in the press, by public talks and private lobbying.

3.27.3 Design Choices

In order to focus ideas one has to propose a particular system. In doing so we are aware that choices may need to be reconsidered as circumstances change and more knowledge is obtained.

- We propose a Thorium fuelled fast reactor. Uranium ADSRs do not solve the waste or proliferation problems, and thermal Thorium reactors do not produce the fast neutrons needed for transmutation.
- We emphasize energy production, with transmutation as an extra benefit, as we think this will have a stronger political appeal (in the UK situation) than a system purely for waste disposal.
- We propose a 1 GW Thermal power station, large enough to make an appreciable contribution to the electricity generation capacity.
- We propose a production reactor as the first system, rather than a prototype, which would be expensive with no return on investment.
- We operate at a criticality k of 0.985. We believe that this is low enough to be safe.
- For this we require an accelerator (or multiple accelerators) delivering approximately 30 mA at 1 GeV
- This would be achieved by a 3 stage process, with a conventional cyclotron to 35 MeV, a ring accelerating protons to 400 MeV, and another for the final acceleration to 1 GeV.
- We use lead as target, coolant and moderator, and operate at a high temperature for high Carnot efficiency.
- We have benchmarked different simulation codes (MCNPX, FLUKA, GEANT4 and models within these) for the spallation process, and shown how target optimisation can increase the neutron yield [3].
- Fuel must be recycled. ^{233}U must be reclaimed not only as fuel but also as it will be a proliferation hazard after a few hundred years, when the ^{232}U has decayed. There is also a long term waste problem from the ^{233}U decays. The design of fuel elements to survive in high temperature lead is a challenge, but should be possible.

The FFAG is our preferred accelerator [3]. Its DC magnets are cheaper and more reliable than those of a synchrotron. The acceleration rate is limited by the RF rather than the magnets, and we envisage acceleration up to 1 GeV in around 1000 turns, which would take 1 ms for a 50 m ring. The beam energy of 1 GeV is very hard to

attain using a cyclotron, and 10 mA is very hard to attain using a synchrotron. A Linac can achieve both, but its capital cost is inevitably large due to its length.

We are currently engaged in construction of EMMA, first nsFFAG, at Daresbury, which will start operating in 2010 [4,5] and hopefully this low energy electron accelerator will show the viability a high current proton machine.

At 1 KHz, if an FFAG is run with a 'synchrotron style' duty cycle, in which individual pulses are injected, accelerated, and extracted, then a 10 mA current requires $\sim 6 \times 10^{13}$ protons/bunch. This is well over typical space charge limits, which are of order 10^{13}. A large harmonic factor (several bunches per turn) can only help slightly. However if it can be run 'cyclotron style' with a 100% duty cycle the bunch is only $\sim 6 \times 10^{10}$ particles which presents no space charge challenge, however the sweeping of the RF frequency (in itself an unsolved problem) limits the duty cycle.

3.27.4 Reliability: the Next Accelerator Frontier

The accelerator for an ADSR must attain levels of reliability far beyond those of present accelerators. Requirements stated in the literature vary between 3 and 1000 trips per year, with varying definitions of a 'trip'. Thermal stresses in the window and target are directly beam-related, thermal stresses in the core and its components are moderated by the time constant of the reactor and cooling, and there are also limits from economics: a 1 GW plant cannot just drop out of the Grid with impunity. We urgently need more investigation to harden up the actual requirements, but even the less rigorous limits quoted are far beyond current experience with accelerators.

Reliability is a science: it can be achieved by redundancy, robustness, graceful failure, under-rating and planned maintenance. These have a cost penalty, and the design must include them only where necessary. Ion Sources are known to be fallible and two or more should be used. The DC magnets will probably be sufficiently reliable. RF components will fail, and the design must cope with this: this probably rules out clever designs such as the Separated-Orbit Cyclotron, Recirculating Linear Accelerators, and harmonic number jumping, as these require the bunch to have a specified energy at a specified point in the cycle. There are also mundane components such as vacuum and power. Multiple accelerators may be needed to provide adequate reliability.

3.27.5 Conclusions

ADSR involvement in the UK is increasing rapidly. We have a wide range of specialists working together across discipline boundaries. Activities are increasing in many areas, and those interested are welcome to browse the ThorEA website and help us towards the goal of establishing Thorium powered ADSRs as the sustainable carbon-free energy source of the future.

3.27.6 References

1. D. Mackay: *Sustainable Energy -- without the hot air*, UIT Cambridge Ltd, (2009).
2. Climate Change Act 2008 UK, Government Office of Public Sector Information, (2008)
3. C Bungau, R Barlow, R Cywinski and S Tygier, *Accelerator driven systems for energy production and waste transmutation* Proc. European Particle Accelerator Conference,

Genoa, (2008).

4. R Barlow, J. Pozimski, K. Peach, N. Bliss, N. Marks, H. Owen, M.Poole and T.R. Edgecock, *The CONFORM project: construction of a nonscaling FFAG and its applications* Proc. Particle Accelerator Conference, Albuquerque, (2007).

5. T. R. Edgecock, this publication

3.28 Hadron Therapy in the UK

Ken Peach

John Adams Institute for Accelerator Science,
University of Oxford and Royal Holloway University of London
Mail to: Ken.Peach@adams-institute.ac.uk

3.28.1 Introduction

Hadron Therapy, or Proton Therapy, or Light Ion Therapy, or Particle Beam Therapy was first proposed by Wilson [1] in 1946 in a paper modestly entitled "Radiological use of fast protons". The potential advantages of protons over MV photons are clear from Figure 1.
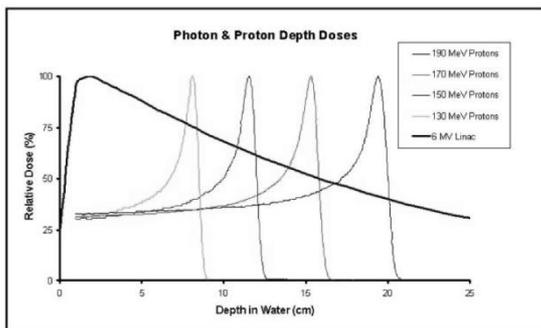
Figure 1: The energy deposition in tissue (water equivalent) for protons and photons, showing clearly the "Bragg peak" at the end of the proton range compared with the near-exponential decay of the photon energy deposition. Note that there is no energy deposition beyond the distal edge of the tumour, and that there is a small *excess dose* in the first few mm below the skin. (Diagram from the Francis H Burr Proton Therapy Center, Massachusetts General Hospital, Boston)
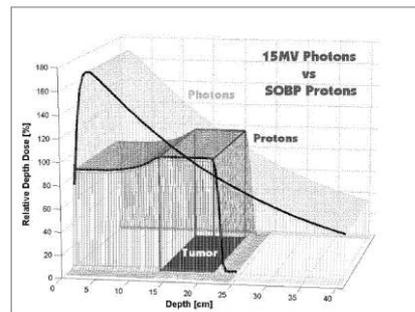
Figure 2: The "Spread-Out Bragg Peak" (SOBP) demonstrating how the tumour volume can be covered with a uniform dose by superimposing many Bragg peaks. (Diagram from the Francis H Burr Proton Therapy Center, Massachusetts General Hospital, Boston)

The power of the technique is illustrated in Figure 2, which compares the "Spread Out Bragg Peak" (SOBP) with the equivalent dose distribution from MV X-rays for a large volume tumour. In conventional radiotherapy, with Intensity Modulated Radio Therapy (IMRT), it is possible to obtain excellent high dose distributions, which conform well to the tumour geometry by combining many beam directions, but at the cost of subjecting a large volume of healthy tissue and other organs to a significant

dose. With protons and other light ions, it is possible to achieve the same dose distributions in the tumour while irradiating a much smaller volume of healthy tissue and sparing vital organs using beams from a small number (two or three) of directions. Light ions have a higher Relative Biological Effectiveness (RBE) − for carbon this is typically 3-5 − in the Bragg peak due to the increase in ionisation density on a microscopic scale. This couples with the dose advantage to provide a greater difference in bio-effectiveness between the tumour and most healthy tissues already traversed by the beam. Beyond the Bragg peaks there is only a small fragmentation dose beyond the tumour. For these reasons, there are now about 30 centres operating around the world, with 2/3rd of them in hospitals, and a further 20 facilities are under construction or in the planning stage. A complete list of facilities in operation and under construction can be found on the Particle Therapy Co-Operative Group (PTCOG) website [3].

The UK has lagged behind many other countries in developing this therapy and making it available, despite having the world's first hospital-based service at the Clatterbridge Centre for Oncology near Liverpool, which opened in 1989, about a year before Loma Linda in California. The Douglas Cyclotron has proton energy of only 62 MeV, and was initially intended for trials of neutron therapy. However, when the clinical trials produced disappointing results [3], the cyclotron was converted to treat tumours of the eye, and has treated more than 2000 patients in the past 20 years, with a very high success rate. In 1995, there were studies [4] of the possible use of the ISIS accelerator at the Rutherford Appleton Laboratory, which could have treated one patient per hour with protons using a PSI-like gantry and fast (50 Hz) variable energy extraction. However, this option was not pursued.

In 2007, the UK Research Council's Basic Technology Fund supported two new programmes in accelerator R&D with potential application for hadron therapy. The first of these (CONFORM − the Construction of a Non-scaling FFAG for Oncology, Research and Medicine) uses conventional accelerator technology, whereas the LIBRA (Laser Induced Beams or Radiation and their Application) uses high-power lasers to generate ion-beams from specially designed targets ranging from small plastic films to water droplets.

In August 2009, the UK Department of Health announced that it had asked the National Specialised Commissioning Team to identify possible providers of proton therapy to treat up to 1600 patients with rare cancers, especially children, per year. A procurement process is under way.

3.28.2 **Clinical Requirements**

Table 1: A summary of the main clinical requirements on the accelerator for a Charged Particle Therapy centre with both protons and carbon ions.

Parameter			Value	
Extraction energy (proton) [Min, Max]		[MeV]	60, 250	
Extraction energy (carbon) [Min, Max]		[MeV/u]	110, 450	
Energy step (proton)	[@Min, @Max]	[MeV]	5, 1	
Energy step (carbon)	[@Min, @Max]	[MeV/u]	15, 6	
Energy resolution (FWHM) [@Min, @Max]		[%]	3.5, 1.8	
Voxel Size	[Min, Max]	[mm]	4×4×4, 10×10×10	
Uncollimated field size	[Min, Max]	[mm]	100×100, 250×250	
Average tumour dose rate (proton)	[Min, Max]	[Gy/min]	2, >10	
Average tumour dose rate (carbon)	[Min, Max]	[Gy/min]	2, >10	

A partial set of requirements on the accelerator capabilities for a clinical therapy system is shown in Table 1. The potential advantages of FFAG accelerators over cyclotrons and synchrotrons are that in principle they should be able to extract the beam at variable energy and at a high (~kHz) repetition rate, with the ability to change between protons and light ions relatively quickly, and to be able to match cyclotrons and synchrotrons in terms of dose rate, dose stability and dose precision

3.28.3 **The PAMELA Project**

The PAMELA Project stands for Particle Accelerator with Medical Application.

While present day technology for proton and light ion therapy is adequate, both cyclotrons and synchrotrons have limitations. In principle, Fixed Field Alternating Gradient (FFAG) accelerators can address these limitations – being fixed field, the accelerator can be rapid-cycling (~kHz) and because the orbit-excursion is limited, variable energy extraction is possible. However, in the original FFAG configuration (now known as a *scaling* FFAG), the orbit excursion is still quite large (~1m). It was realised [5] in 1999 that if the scaling assumption was relaxed, the orbit excursion could be constrained still further, at the cost of having to deal with resonance crossing. In the original model, the magnetic design was arranged to compress the range of orbit radii and thus the magnet aperture, while maintaining a linear magnetic field, leading to expectations of smaller apertures, and thus significant cost reduction when compared with scaling machines. EMMA, the Electron Model with Many Applications will demonstrate the feasibility of this technology, and is described elsewhere [6]. Briefly, EMMA is a 42-cell, densely-packed ring, with the linear magnetic fields provided by displaced quadrupoles, and achieving rapid acceleration by using 19 1.3GHz cavities, each with an accelerating voltage of 20-120kV, giving an energy gain per turn of between 0.38 MeV and 1.28 MeV.

While this lattice is a natural starting point for PAMELA, there are features that make it unsuitable for protons and light ions. Studies with a 48-cell densely packed

linear lattice showed that it was difficult to achieve the high packing fraction with a realistic magnet design, and there was insufficient space in the short straight sections for the variable frequency RF cavities needed for the non-relativistic acceleration. It was also shown that the requirements on the field accuracy and alignment precision were severe.

An alternative is to study a less dense lattice with longer straight sections, which means departing from simple linear magnetic fields. An advantage of this approach is that it is then possible to stabilise the horizontal and vertical tune (to avoid resonance crossing) and to limit the orbit excursion. There are several ways to achieve this. One approach [7] uses both edge and alternating gradient focussing to stabilise the tune. An alternative approach [8,9] is to stabilise the tunes through the addition of higher-order multipoles.

In order to avoid resonance crossing it is necessary to constrain the total betatron tune to within an integer throughout acceleration. In other types of accelerators two methods are used which can achieve this. The first, employed in synchrotrons, is chromatic correction, adding higher order multipoles to achieve a constant tune. The second, used in a scaling FFAG, employs a magnetic guide field which follows the scaling law $B = B_0(r/r_0)^k$, where r is the radial co-ordinate, k is the field index defined as $k = (r/B_y)(dB_y/dr)$ and y is the vertical direction. This results in a constant tune throughout acceleration. The PAMELA lattice design employs a combination of these two methods. Starting with the concept of a radial-sector F-D-F triplet scaling FFAG, a number of changes and simplifications are made. Firstly, the magnetic field becomes non-scaling, by expanding the scaling field profile and retaining only the dipole and first few multipoles. This significantly changes the magnet design, removing the need for iron-cored magnets with complicated pole shaping used in a scaling FFAG. To ease cost, construction and alignment issues, the magnets are made rectangular rather than sector-shaped and are aligned along a straight line in each cell rather than along an arc, further violating the scaling law. One such lattice is shown in Figure 3. The lattice has 12 triplet (FDF) cells, with a median radius of 6.25m and 1.95m long straight sections (about 1.7m of useful length) see Table 2.
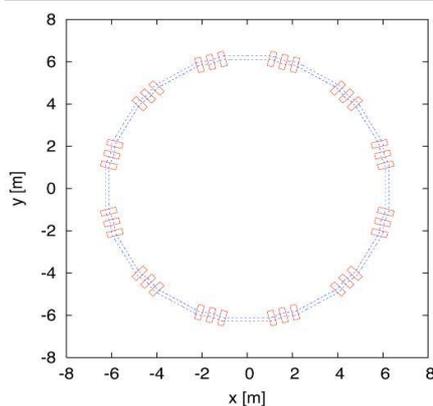
Figure 3: A tune-stabilized non-linear non-scaling FFAG lattice for protons 31 MeV to 250 MeV. The blue lines represent the orbits at injection (inner lines) and extraction at full energy (outer line).
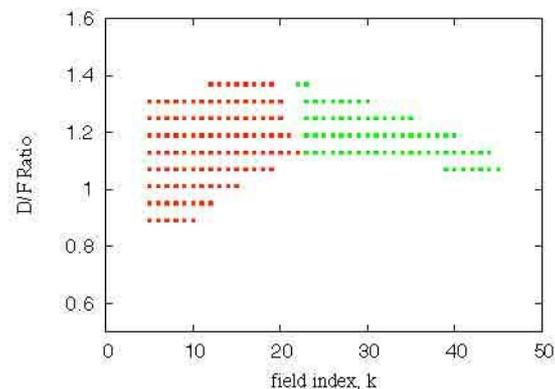
Figure 4: Available working points for the PAMELA lattice at reference energy (118 MeV protons). The 2nd stable region with $\upsilon_x > 0.5$ is shown to the right.

Table 2: Lattice Parameters

	Injection	Reference	Extraction
Proton K.E.　　[MeV]	31	118	250
C6+ K.E　　[MeV/u]	7.8	31	68.4
Bρ　　　　[Tm]	0.81	1.62	2.43
# Cells, R_0　　[m]	12, 6.25		
K value, D/F ratio	38, 1.35		
B^D_0, B^F_0　　　[T]	2.25, 1.67		
Packing factor	0.48		
Long, Short drift [m]	1.7, 0.31		
Magnet length　　[m]	0.31		
Orbit excursion　[m]	0.17		

A number of parameters can be used to further describe the PAMELA lattice design, including the field index, k and geometrical factors including the lattice packing factor, magnet length and average radius. The field index (k) influences both the magnetic focusing strength and the orbit excursion, that is, the difference in radial position of the maximum and minimum energy orbits, as shown by the two lines in Figure 3. A large field index results in a small orbit excursion, which is advantageous as it reduces the bore of the magnets, the beam pipe aperture and the RF aperture. However, the field index is limited when using the first stable region of Hill's equation, where the phase advance per cell is less than 180 degrees. In this design the second stable region of Hill's equation is used, with a horizontal phase advance per cell greater than 180 degrees. This allows for a larger field index to be used, resulting in a smaller orbit excursion. The available working points as a function of field index and D/F magnet strength ratio are shown in Figure 4. By carefully choosing the field index to be as large as possible, a D/F ratio si selected to give cell tunes around $\upsilon_x = 0.75$, $\upsilon_y = 0.25$.

The performance of the PAMELA lattice was studied using the ray-tracing code ZGOUBI [10] for tracking studies and S-Code [11] for the variation of basic lattice parameters. The beta functions in one cell, as calculated with S-Code, are shown in Figure 5. The variation of betatron cell tunes throughout acceleration is shown in Figure 6. The variation of the total horizontal tune is 0.054 and the total vertical tune is 0.067, both of which are well within half an integer, as indicated by the dotted lines. These results illustrate that the design method for constraining betatron tunes is successful. A typical tracking example using ZGOUBI including acceleration is shown in Figure 7, clearly showing the small natural orbit excursion which is 17.6cm in total.
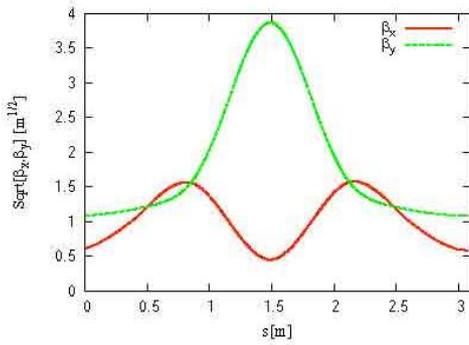
Figure 5: Beta-functions in one cell of the PAMELA lattice.
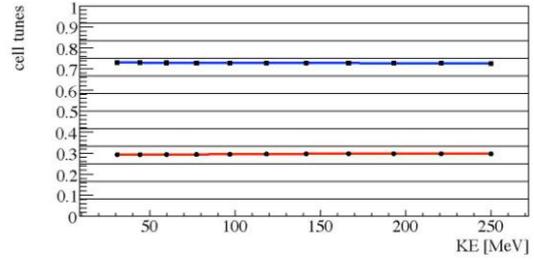
Figure 6: Variation of horizontal (upper) and vertical (lower) cell tunes.
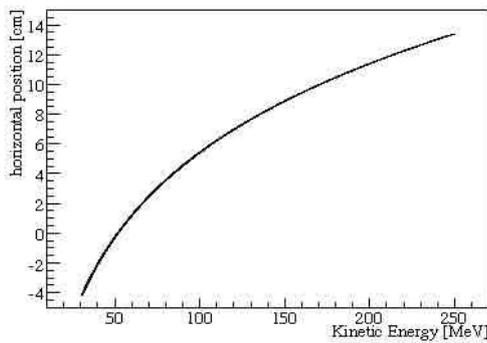
Figure 7: Horizontal particle position vs. proton kinetic energy through acceleration at centre of long straight section.
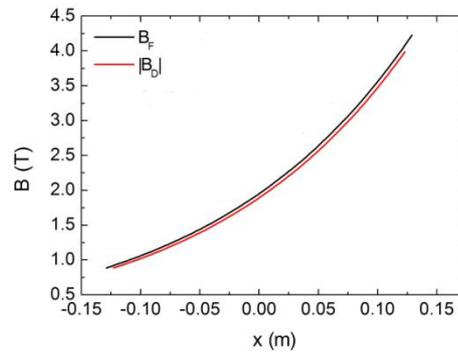
Figure 8: Magnetic field as a function of radius for the F and D magnets

Preliminary ideas for the design of the magnets [12] and the RF [13] have been developed. The field shapes for the main ring magnets are shown in Figure 8. An outline of the RF cavity from reference [13] is shown in Figure 9, with the principal parameters in Table 3.
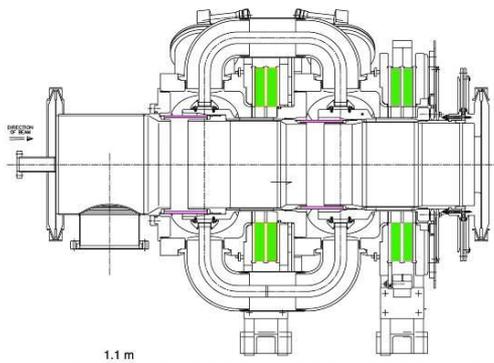
Figure 9: PAMELA RF cavity
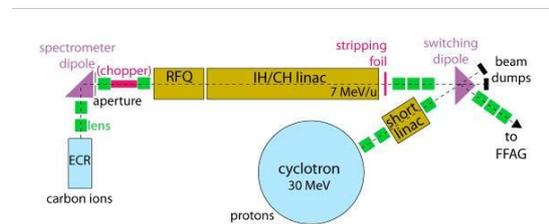
Figure 10: Schematic of proposed injector assembly, including ion sources, LEBT, pre-accelerators and MEBT. The proton source is contained within the cyclotron.

Table 3: RF Cavity Parameters

Frequency [h=10] injection	[MHz]	19.4
Frequency [h=10] extraction (max)	[MHz]	46.2
Repetition Rate	[kHz]	1
Energy gain/turn	[keV]	100
Number of cavities		≤ 8
Length	[mm]	1100
Aperture	[mm]	230

There are also preliminary ideas [14-15] for the injection chain (see Figure 10). The protons and carbon ions will be produced in separate sources, allowing faster switching between ion species in a clinical situation, improving the productivity of the facility. A Low Energy Beam Transport line (LEBT) will transport the particles from the sources into a pre-accelerator, and another beam transport section (MEBT) will inject the particles into PAMELA. A standard 30MeV proton cyclotron can be used for the proton beam injection, and a radio frequency quadrupole (RFQ) and linac can be designed for the carbon injection.

Finally, in order to achieve the performance requirements in the treatment room, it is necessary to use an achromatic beam transport and gantry. Studies are under way [16] to design an FFAG-like beam transport system.

3.28.4 **Laser-Driven Ion Acceleration**

High power lasers can be used to generate accelerated beams of ions (see for example [17]). The beams have interesting properties, for example they are intrinsically low emittance and different ion species can be readily accelerated. However, so far the energies are achieved are in the tens of MeV range, and the energy spread is generally large. Nevertheless, there has been significant progress over recent years, as shown in figure 11, where the maximum achievable proton energy tracks the available laser power.

The LIBRA (Laser Induced Beams or Radiation and their Application) consortium (see [18]) is investigating the generation of protons and ions from laser-induced interactions with thin films. One mechanism is Target Normal Sheath Acceleration (TNSA), illustrated schematically in figure 12, first observed in 2000 [19,20]; the proton energy spectrum obtained in [20] is shown in figure 13. More recently, a new acceleration regime has been proposed [21-23] – Radiation Pressure Acceleration (RPA) – which uses circularly polarised high power laser pulses incident on thin films to achieve efficient acceleration at moderate intensities – the maximum proton energy scales as the laser intensity in RPA, to be compared with scaling as the square root of the intensity for TNSA. Testing RPA is currently under investigation. A simulated proton energy spectrum from [21] is shown in Figure 14. There remain limitations in terms of laser repetition rates, but optimisation of target composition, shape and means

of their delivery into the laser beam are being addressed along with accuracy and reproducibility of dose profiles. The wider energy spectrum may be usefully employed to cover most of a tumour, while using narrower ranges of energies for its periphery. Also the production of gamma rays along the beam direction may allow useful simultaneous imaging.
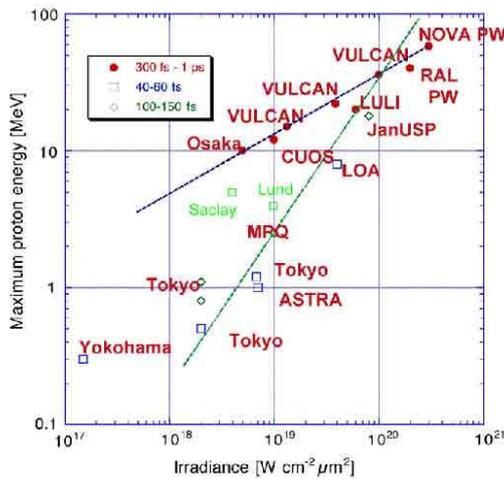
Figure 11: Maximum proton energy from laser-irradiated metal foils for experiments on different laser systems as a function of the laser pulse irradiance, grouped in three different ranges of pulse durations [18].
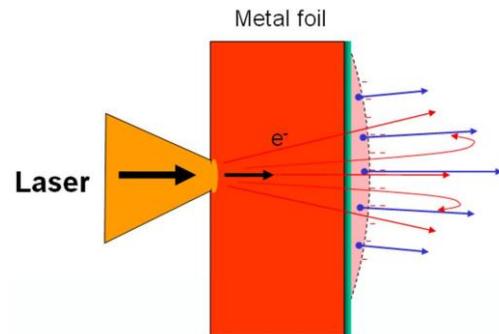
Figure 12: Sketch of Target Normal Sheath Acceleration (TNSA) (after Borghesi).
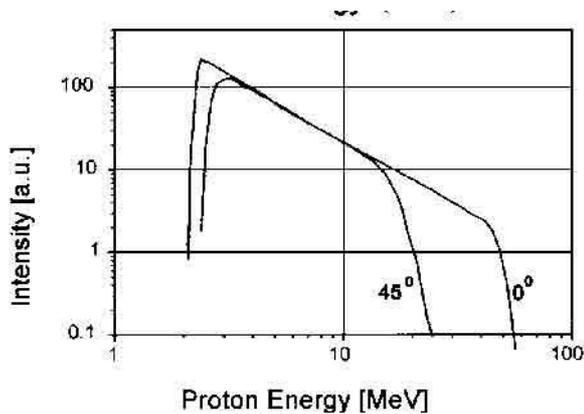
Figure 13: The proton energy spectrum from [20].
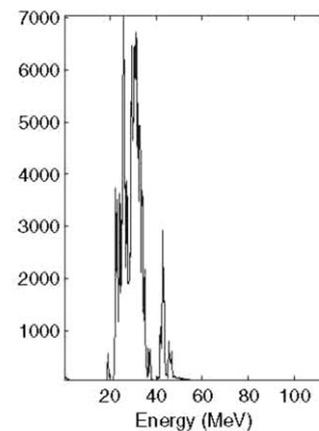
Figure 14: Simulated proton energy spectrum from [21].

In the medium term, laser-plasma ion acceleration could provide a compact and flexible ion source, allowing conventional acceleration of a range of ion species (helium, carbon, oxygen …) for therapy, and in the longer term could provide beams of ions with the required energy and intensity.

3.28.5 **Summary**

Hadron therapy (the use of beam of energetic protons and light ions such as carbon) for the treatment and local control of tumours is an established modality in the management of cancer, particularly well adapted to a range of tumours and some paediatric cases. Existing technology is adequate but is capable of improvement. There is an established programme of innovative research in the UK aimed at addressing some of these limitations.

3.28.6 **References**

1. R.R. Wilson, "Radiological use of fast protons", Radiology 47, 487 (1946)
2. http://ptcog.web.psi.ch/
3. B. Jones, "The neutron therapy saga: a cautionary tale", MedicalPhysics web http://medicalphysicsweb.org/cws/article/opinion/32466 (2008). See also B Jones, R. G. Dale and A. Cárabe-Fernández, "Charged particle therapy for cancer: The inheritance of the Cavendish scientists?" Applied Radiation and Isotopes 67 (2009) 371–377
4. D.J. Adams, C.M. Warsop, M.R. Harold, I.S.K. Gardner, "The Use of ISIS as a Proton Therapy Facility", 5th European Particle Accelerator Conference (EPAC 96), Sitges, Spain, 10-14 Jun 1996
5. C. Johnstone et al, "Fixed Field Circular Accelerator Designs", PAC'99, New York, March 1999, p. 3068.
6. S.L. Smith, "EMMA, the World's First Non-Scaling FFAG Accelerator", WE4PBI01, PAC09, Vancouver.
7. C. Johnstone and S. Koscielniak, "Tune-Stabilized Linear-Field FFAG for Carbon Therapy", Proceedings of EPAC Edinburgh (2006), 2290
8. S. Machida, "Scaling fixed field alternating gradient accelerators with small orbit excursion", Phys. Rev. Lett. 103, 164801 (2009)
9. S. Sheehy et al, "PAMELA Lattice Design and Performance", FR5PFP001, PAC09, Vancouver.
10. F. Meot, Nucl. Instr. Meth. A, 427, p. 353 (1999)
11. ICFA Beam Dynamics Newsletter No. 43, ed. by C. R. Prior, p. 54 (2007).
12. H. Witte et al, "PAMELA Magnets - Design and Performance", MO6PFP073, PAC09, Vancouver
13. T. Yokoi et al, "PAMELA: Development of the RF System for a Non-Relativistic Non-Scaling FFAG", WE5PFP011, PAC09, Vancouver
14. M. Aslaninejad et al, "Injection Layout for PAMELA", MO6RFP029, PAC09, Vancouver
15. M. Easton et al, "RFQ Design Optimisation for PAMELA Injector", FR5REP066, PAC09, Vancouver
16. R. Fenning et al, "An FFAG Transport Line for the PAMELA Project", TH6PFP022, PAC09, Vancouver.
17. M. Borghesi at al, "Laser-driven proton acceleration: source optimization and radiographic applications", Plasma Phys. Control. Fusion 50 (2008) 124040
18. See http://www.qub.ac.uk/sites/LIBRA/News/
19. E.L. Clarke et al, "Measurements of Energetic Proton Transport through Magnetized Plasma from Intense Laser Interactions with Solids", Phys. Rev. Lett. 84, 670–673 (2000)
20. R.A. Staveley et al, "Intense High-Energy Proton Beams from Petawatt-Laser Irradiation of Solids", Phys. Rev. Lett. 85, 2945-2948 (2000)
21. L Robinson et al, "Radiation pressure acceleration of thin foils with circularly polarized laser pulses", New J. Phys.,10 013021 (2008)

22. O. Klimo et al, "Monoenergetic ion beams from ultrathin foils irradiated by ultrahigh-contrast circularly polarized laser pulses", Phys. Rev. ST Accel. Beams 11 031301 (2008)
23. X.Q. Yanet al, "Generating High-Current Monoenergetic Proton Beams by a Circularly Polarized Laser Pulse in the Phase-Stable Acceleration Regime", Phys. Rev. Lett. 100 135003 (2008)

Industrial Engagement

3.29 Cockcroft Institute (CI) Industrial Engagement

Swapan Chattopadhyay[1], Peter McIntosh[1] and Jonathan Smith[1,2]
[1] The Cockcroft Institute, Daresbury Science & Innovation Campus, Keckwick Lane, Daresbury, Warrington, Cheshire WA4 4AD, UK
[2] Tech-X UK Ltd.
Mail to: swapan@cockcroft.ac.uk

3.29.1 Introduction

The Cockcroft Institute has the charter of integrating the academic depth of university partners, the breadth of large scale facilities and national laboratory partners and societal applications via industrial engagement under one collaborative association and stewardship. The institute already has a 11-member strong Industrial Advisory Committee (IAC), with members from the Research Councils, Technology Strategy Board, relevant industries and expert professionals from the Energy, Healthcare and Security/Defense communities that have prepared a Technologies Readiness Map as well as a "Market Pull" analysis of the various offerings from the science and technology knowledge and associated skills base of particle accelerators and free electron lasers. In addition the institute has facilitated the formation of the UK base Tech-X UK Ltd. for the computational accelerator science company Tech-X,Inc.USA and has motivated local businesses (e.g. Shakespeare Engineering) to engage in superconducting radio frequency technology. The institute is engaging with the microwave industry for the development of unique microwave controls and power components. Finally it is interacting with the Health and Energy sectors for industry-led accelerator-based systems for proton/hadron therapy in UK and sustainable Thorium-based nuclear fission reactors driven by accelerators, towards which the ThorEA Association UK has been created by the UK community.

3.29.2 SRF Structures

The Cockcroft Institute (CI) is currently developing a variety of accelerator designs, which exploit the fundamental benefits of Superconducting RF (SRF) technology; whether it is for the optimization of modest gradient, CW, L-band accelerating structures for ALICE and NLS; high gradient, pulsed, L-band and C-band, accelerating and dipole mode structures for ILC; or low velocity, VHF accelerating structures for HIE-ISOLDE; all of which require specialist qualification, handling, forming,

machining, cleaning and validation processes in industry to ensure such devices can be successfully transferred and operated in a working accelerator environment. There is a distinct global shortage of appropriately recognised and validated commercial vendors who can deliver such specialist devices to the scientific community and so the CI has strived to engage with industry, both nationally and internationally, to ensure that the SRF requirements for such demanding projects can be appropriately maintained.

For the ALICE facility at Daresbury Laboratory, the SRF accelerating systems proposed at the design stage were in fact not commercially available and so subsequent discussions with Research Instruments GmbH in Germany (or ACCEL GmbH as it was at the time), identified an opportunity for licensing the FZD-Rossendorf ELBE cryomodule design, which would meet the requirements for the ALICE accelerator. Having successfully delivered two such cryomodules, which have operated on ALICE since Sept 2007 (see Figure 1), ACCEL now have a demonstrated and commercialized cryomodule solution for Energy Recovery Linac (ERL) applications.

Figure 1: ACCEL ERL cryomodule preparing to be installed on ALICE.

For the ILC project, the CI has lead the development of a C-band SRF crab cavity system for rotating the 500 GeV electron and positron bunches locally at the Interaction Point, to maximize collision luminosity. To provide a mechanism for validating both the crab cavity structure design and the precision Low Level RF (LLRF) control system that was developed, several single-cell dipole mode cavities were fabricated in industry. The CI at the time were building an array of SRF processing and testing facilities which included; chemical cleaning, high-pressure rinsing, ISO 4/5/6 clean rooms and a vertical test stand and so, when it came to placing an order with industry for these single-cell cavities, it was a requirement that CI staff could take part in the structure processing and qualification, thereby transferring critical skills from industry, to be then utilized by CI staff at Daresbury Laboratory. Niowave Inc in the USA were the only company approached who offered the ability to not only fabricate and qualify the SRF structures, but also to spend time training CI staff in the various cleaning and qualification stages (see Figure 2). The expertise developed has enabled CI staff to successfully complete the qualification of the ILC crab cavity system using the new SRF infrastructure at Daresbury, to performance levels which now exceed the stringent requirements for ILC.

Figure 2: CI staff being trained at Niowave Inc.

Nationally, the UK does not currently have a recognized vendor for fabrication of SRF structures for the scientific accelerator community. In order to try and instigate a mechanism whereby UK industry can learn from CI staff as to how SRF structures are handled and processed, an STFC Innovations Partnership Scheme grant has been secured with Shakespeare Engineering Ltd, to fabricate and qualify an L-band single-cell SRF structure. This will be the first bulk-niobium accelerating structure to have ever been built and qualified in the UK.

3.29.3 Compact Linac Applications

The design challenge for Compact Linac accelerating and dipole mode structures requires full understanding of surface wall losses in order to correctly predict the coupling between cells in the device, as well as S-parameter analysis and wakefield impedance suppression. Work being undertaken by Tech-X UK Ltd and CI will develop models that will help the understanding of these devices, and produce linacs which meet the needs of accelerator designers around the world (see Figure 3). With techniques that embrace modern software design practices and high performance computing clusters, problems in developing complex geometry models and parameterization of such models to converge on an optimum solution, solutions which previously were out of reach, are now becoming realisable.
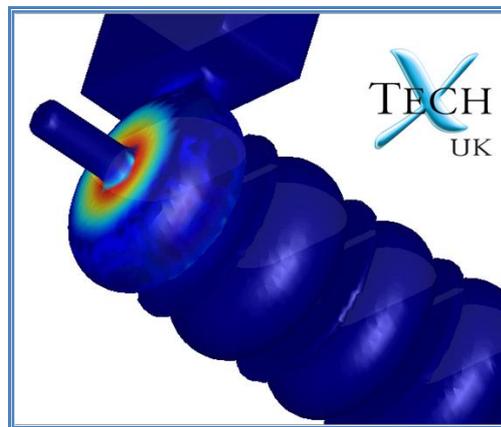
Figure 3: Compact linac design for security applications

The collaboration between Tech-X CI and e2v Technologies Ltd is also delivering the capability to simulate a complete magnetron startup, something which has been

performed with only limited success in the past, and to take this further to look at phase locking performance. If sufficient phase stability can be obtained from this phase locking process, it presents magnetrons as a much cheaper alternative to Klystrons as RF sources in the accelerator world. These developments are expected to flow into benefits to many UK and international producers of magnetrons.

CI and Tech-X supported work is also improving the capability we have to understand the multipactor effect. Multipactor is the primary cause of breakdown and failure in many classes of high power microwave devices. The collaboration is actively looking at RF power couplers at the SPL, and benchmarking experimental data taken from waveguide breakdown events to assess various techniques for circumventing the damage multipactor can cause and to ensure a 'right first time' design of accelerator components.

Tech-X in the US has already been working on multipactor in crab cavities, and is bringing its successes from this research to the problems being addressed by the UK community. The same phenomena is the cause of failure for many high power amplifiers, and the ability to simulate cavities in RF sources such as klystrons and IOTs, as well as in complete accelerators, is expected to lead to savings for manufacturers as well as those who operate such devices in the accelerator community.

3.29.4 Security Applications for Accelerators

Threats to society arising from unknown mobile cargo systems either in commercial, governmental or military transportation are higher than ever today, requiring smart, compact and cost effective inspection systems in bulk for diverse and distributed use. In particular, limited but successful experience in the past with X-ray sources derived from 'brehmstrahlung' radiation from a metal target irradiated by MeV energy electron beams, leads us to believe that a series of compact X-Ray sources are required for integration in a new series of cargo and vehicle inspection systems. The CI is collaborating with Rapiscan Systems for the development of these next generation cargo scanners.

3.29.5 Outlook

The recently commissioned (by the UK government) " Hauser Review" completed by the physicist and innovator Hermann Hauser , calls for the formation of technology innovation centers that will maximize the return on the scientific knowledge base of the academic institutions and national facilities in UK. The accelerator community in UK distributed amongst the universities, institutes, national laboratories is rising to this challenge by creating a national accelerator program that addresses the national and international grand challenges in Energy, Health and Security.

4 Workshop and Conference Reports

4.1 Strategy Workshop on High Power Laser Technology for Future Accelerators

A first strategy workshop was held at GSI Darmstadt, April 8-10, on the laser technology needed to meet the challenge of future accelerators that use or rely on very high average power lasers. The workshop was opened by Hartmut Eickhoff, Technical Director of GSI and Wim Leemans from LBNL, Chair of the newly established *Joint Task Force on Future Applications of Laser Acceleration.* The *Joint Task Force* operates under the umbrella of ICFA (*International Committee for Future Accelerators*) and ICUIL (*International Committee for Ultra Intense Lasers*) and invited experts on high power laser technology as well as accelerator technology and their applications to this workshop. The 47 participants came from China (1), France (4), Germany (18), Japan (4), Switzerland (2), the UK (4) and the US (14).

The main topics discussed were the laser performance needed for accelerator technology to support the most challenging present and future accelerator needs, as well as questions of laser architecture, laser material and optical components. At the workshop, accelerator and light source representatives outlined the top level laser requirements for potential laser-based accelerator applications, i.e. colliders, light sources and medical applications.

The largest challenge for laser technology comes from a laser-plasma e^+e^- collider with a center of mass energy as much as 10 TeV. The consensus in the world high energy physics community is that the next large collider after the LHC would be a TeV-scale lepton collider. Options currently under study include the ILC (0.5-1 TeV), CLIC (up to 3 TeV) and the muon collider (up to 4 TeV), all using RF technology. On the other hand, the very high gradients (~10 GeV/m) possible with laser acceleration open up new avenues to reach even higher energy and more compact machines. At this workshop participants discussed and set forth a set of beam and laser parameters for a 1-10 TeV, 10^{36} cm^{-2}s^{-1} e^+e^- collider based on two different technologies – laser plasma

acceleration (LPA) and direct laser acceleration (DLA). The main challenges to the practical achievement of laser acceleration are high average power (~100 MW), high repetition rate (kHz to MHz), and high efficiency (~40-60%) at a cost that ideally would be an order of magnitude lower than using RF based technology. The workshop also studied the laser requirements for a 200 GeV γγ collider, proposed as the first stage of a full scale ILC or CLIC. The required laser systems for such a collider may be within the reach of today's technology.

For light sources, lasers already play a significant role in existing facilities, and face new challenges with future light sources that aim at much higher repetition frequency. Ultrafast (femtosecond) lasers reaching 1-10 kW levels will be required for seeding and user driven experiments. Another important area is medical applications of laser acceleration of protons/ions and its potential to replace current technology used in tumour therapy. Such lasers are typically very high peak power (PW-class) and require special pulse shapes with very high temporal contrast. Again, multi-kW compact lasers will be needed.

Laser requirements for these applications are often many orders of magnitude beyond the capabilities of the lasers used in today's scientific demonstrations, i.e. MW's vs. 10's of W's. Laser science representatives at the workshop discussed and outlined how, with appropriate R&D, emerging 100-kW-class industrial lasers, 10-MW-class laser fusion energy technologies and MW-class defence laser systems might be adapted to meet these challenging requirements.

Results of the workshop, including parameter tables on laser technology requirements and goals will be compiled in a workshop report and submitted to ICFA and ICUIL for their approval, prior to public release.

5   Recent Doctoral Theses

5.1   Muon Capture Schemes for the Neutrino Factory

Stephen Brooks
University of Oxford, Trinity College, OX1 3BH, U.K.
Mail to: Stephen.brooks@stfc.ac.uk

Graduation Date: April 2010
Supervisors: Dr. J.H. Cobb and Dr. C.R. Prior

Abstract:

The proposed neutrino factory, a facility for precision measurements of neutrino oscillations, requires directional neutrino beams to reach the required sensitivities. Among the few sources of such beams is the decay of muons travelling at relativistic speeds; therefore an intense source of muons and subsequent rapid acceleration must be designed so they can reach the required energy before decaying.

This thesis investigates the design of several stages in this process: pion production from an energetic proton beam hitting a target and the decay of those pions to a beam of muons, confined by a channel of solenoids. Issues related to producing the original proton beam, the target efficiency, the arrangement of the solenoids and the start of

muon acceleration are all discussed in the context of eventual muon yield, with the target particle production and muon beam optics simulated by computer codes. The code MARS15 [1] is used for the target (and benchmarked against GEANT4 [2] and initial results from the HARP experiment [3]) and the author's code Muon1 [4] for muon tracking, with the techniques it uses also explained in the thesis.

To find the highest-yielding arrangement of magnets and accelerating components from the target onwards, Muon1 incorporates an optimisation feature where almost all parameters of the beamline can be varied. This produces a high-dimensionality search space where the best muon yield is sought using a genetic algorithm. As each individual evaluation of a design is itself a time-consuming simulation with tens of thousands of particles, the code has been deployed as a distributed computing project that is able to perform millions of simulations per optimisation.

5.2   3D Simulation Study of Space Charge Effects on High Intensity Cyclotrons

Jianjun Yang

Department of Engineering Physics, Tsinghua University, Beijing, China

Mail to: yangjianjun2000@tsinghua.org.cn

Abstract:

High intensity has maintained its prevailing position as one of the important research directions in the cyclotron development and constant efforts have been made and are still in progress to pursue higher beam current since the first cyclotron was built. Along with the steady increase of beam current, the beam collective effects would become stronger, among which the space charge effects, being the most significant collective effects in cyclotrons, are one of the main causes of beam loss and the activation of accelerator components. For high intensity isochronous cyclotrons, the space charge effects should include not only the interactions of the internal particles of a single bunch, but also the mutual interactions of neighboring multiple bunches in the radial direction. In compact AVF cyclotrons, the neighboring multi-bunch effects are particularly remarkable.

In this thesis, the space charge effects are studied quantitatively by numerical methods. Based on the beam dynamics analysis, a "Start-to-Stop" model and a "Central Bunch" model are established for compact AVF cyclotrons with multi-turn extraction and separated-sector cyclotrons with single-turn extraction respectively. In both models the neighboring bunch effects are included by multi-bunch tracking. On that basis, the parallel Particle-In-Cell based numerical simulation algorithms are studied and a new 3D object-oriented parallel code for large scale particle simulation in cyclotrons, OPAL-CYCL, is developed and validated by comparing with other similar codes. The usage of this code is not restricted to the study of space charge related issues, but it is also applicable to the conventional beam dynamics design and study of a cyclotron. The parallel scalability test shows that the code is functioning at high performance both on cluster systems and MPP systems.

To meet the running requirement of OPAL-CYCL, a new HPC cluster system of small scale is built at China Institute of Atomic Energy (CIAE).The Linpack test shows the parallel efficiency of up to 87% can be achieved on this system.

The high intensity beam dynamics problems in the 100MeV compact AVF cyclotron being constructed at CIAE are studied by using OPAL-CYCL. The simulation shows that for the initial matched beam at the exit of the central region given by the physical design, no massive beam loss would be caused by space charge effects when the extracted beam current is less than 1mA, and the beam current limit given by vertical space charge effects is about 10mA. Furthermore, the space charge related study in PSI 590MeV Ring is presented as well, for which the simulation shows the neighboring multiple bunches impose positive effects on this single-turn extraction cyclotron.

6   Forthcoming Beam Dynamics Events

6.1   49th ICFA Advanced Beam Dynamics Workshop on Electron Cloud Physics: ELOUD2010

The 49th ICFA Advanced Beam Dynamics Workshop will take place from October 8 to 12, 2010 at Cornell University, Ithaca, New York, USA.

The development of the electron cloud (EC) in accelerator vacuum systems remains a significant issue for the operation of present and planned high intensity accelerators. The interaction of the cloud with the beam can lead to single and multi-bunch instabilities, emittance growth, and betatron tune shifts.   The presence of the cloud in the beam chambers can result in a rapid rise in vacuum pressure, significant heat loads on cryogenic surfaces, and can interfere with beam diagnostics.   Since the last ECLOUD workshop in 2007, an intense R&D effort has been underway to further understand the physics of the EC and to investigate new methods to mitigate the EC effects.   The ECLOUD10 program will focus on: a review of EC observations at existing machines; recent experimental efforts to characterize the EC (including EC diagnostics, experimental techniques, characterization of mitigation methods, and characterization of beam instabilities and emittance growth); the status of EC physics models and simulation codes and their comparison to recently acquired experimental data; and, the mitigation requirements and potential performance limitations imposed by the EC on upgraded and future machines. In addition to the technical reports at the workshop, ECLOUD10 will present a set of introductory lectures for students and those new to the field on the opening day of the workshop.

The meeting will be held at the Statler Hotel on the campus of Cornell University overlooking picturesque Cayuga Lake. We are looking forward to a gathering where we can enjoy the beautiful foliage as Fall begins in the Finger Lakes region. The workshop will include a tour of the facilities at Wilson Laboratory.

Contact
ECLOUD10 Chair, Mark Palmer, Cornell University, USA
ecloud10@lepp.cornell.edu

6.2 16th International Workshop on Beam dynamics and Optimization: BDO2010

The 16th International Workshop *Beam Dynamics and Optimization* (BDO'2010) will be held in the St. Petersburg State University (St. Petersburg, Russia) June 28–30, 2010. It is organized by the Faculty of Applied Mathematics and Control Processes at St. Petersburg State University. For further information please visit the Workshop website:

http://www.bdo2010.compmath.spbu.ru/

Program Committee

       Chairperson — D. A. Ovsyannikov (Russia)

       A. Alisherov (Kyrghistan), S. Kawata (Japan), V.P. Stepanchuk (Russia), V.A. Belyakov (Russia), E.D. Kotina (Russia), Yu. A. Svistunov (Russia), M. Berz (USA), K. Makino (USA), A. Todd (USA), Yu.A. Budanov (Russia), F. Meot(France), E.I. Veremey (Russia), A.N. Dovbnya (Ukraine), A.D. Ovsyannikov (Russia), M.F. Vorogushin (Russia), A.P. Durkin (Russia), R. Ryne (USA), I.P. Yudin (Russia), R. Jameson (USA), P. Snopok (USA/Russia), A.P. Zhabko (Russia)

Organizing Committee

       Chairperson — E. D. Kotina (Russia)

       S.N. Andrianov (Russia), H. Mais (Germany), V.L. Uvarov (Ukraine), M. Berz (USA), V.V. Petrenko (Russia), Y. Yamazaki (Japan), N.S. Edamenko (Russia), V.A. Ploskikh (Russia), I.P. Yudin (Russia), N.V. Egorov (Russia), Yu. Senichev (Germany), A.V. Zherebtsov (Russia), V.P. Gorbachev (Russia), P. Snopok (USA/Russia), D.V. Zhukov (Russia), A.B. Kurzhanskiy (Russia)

Contacts

       Coordinator – D.V. Zhukov

       Secretary – A.G. Golovkina

       E-mail: bdo2010@apmath.spbu.ru

       Phone: +7(812)4284250

           +7(812)4284868

           +7(812)4284729

       Fax: +7(812)4287159

       Postal address: BDO'2010

              Saint-Petersburg State University

              Faculty of Applied Mathematics and Control Processes

              Universitetskij pr., 35

              Saint-Petersburg, 198504

              Russia

Scope

Traditionally the objective of the Workshop is to bring together mathematicians, physicists and engineers to present and discuss recent developments in the area of mathematical control methods, modeling and optimization and theory and design of

charged particle beams and plasma, parallel and distributed computing in accelerator physics.

Historical Overview

The series of workshops on Beam Dynamics and Optimization started in 1994. Since that, 14 workshops were held, either in St.Petersburg, or in Saratov and the 15th workshop (2008) took place in St. Petersburg, Florida, USA. In years 2004 and 2005 the BDO workshops were included as separate sections into the 8th International Computational Accelerator Physics Conference (ICAP 2004), and the International Conference "Stability and Control Processes (SCP 2005)", respectively. In 15-years time the workshop had developed into a full scale conference with more than 100 participants every time. Nevertheless, we are keeping the traditional and well-recognized name "BDO Workshop".

Technical Program
1. Beam Dynamics
2. Optimal Control Theory and Methods of Optimization
3. Mathematical Modeling of Electromagnetic Fields
4. Charged Particle Beam Generation
5. Plasma Control and Optimization
6. Applications of Accelerators
7. Code Development

Official Languages

The working languages of the BDO'2010 Workshop are English and Russian.

Sessions

Reports at the BDO'2010 Workshop may be presented in oral or poster form. The lecture hall for the oral session will be equipped with a PC-connected electronic projector. Please provide your presentations on CDs or memory sticks in Adobe PDF or MS PowerPoint format.

In the room for the poster session poster boards and material for attachment will be available.

Venue

The Workshop will be held in the New Conference Hall of the Faculty of Applied Mathematics & Control Processes (St. Petersburg, Staryj Petergof, Universitetskij pr., 35).

Dates and Deadlines
Registration and abstract submission deadline: March 21, 2010
Notification of acceptance: April 1, 2010
BDO'2010 Workshop: June 28–30, 2010

Registration

To register as a participant of the BDO'2010 Workshop please fill in the online registration form at the Workshop website:

http://www.bdo2010.compmath.spbu.ru/register.php

Abstracts Submission

Abstracts are to be prepared in LATEX or in Word (*.doc) and should not include any graphics. The size is limited by two pages. Your abstract should be send to the Organizing Committee using the online registration form. The deadline for submitting abstracts is March 21, 2010. The LATEX and Word templates are available at the Workshop website:

http://www.bdo2010.compmath.spbu.ru/abstract.html

Accommodation

We can arrange your accommodation at the hostel of St. Petersburg University (about 5-7 min by foot to the Workshop location). This is an economic accommodation (550 RUR* per night per person) in double rooms or in rooms for 3-4 persons (dependent of availability). Please inform us before the 1st April 2010 if you want us to book places for you, by e-mail: bdo2010@apmath.spbu.ru. Otherwise you can book a room at hotels in Peterhof. (Some information about the hotels is given at the Workshop website: http://www.bdo2010.compmath.spbu.ru/). Please book your accommodation there as soon as possible because June is a high season (White nights) in St. Petersburg.

*1 EUR = 40.6285 RUR
1 USD = 30.1510 RUR (the rate of exchange on 2010.02.20)

6.3 19th International Conference on Cyclotrons and Their Applications: Cyclotrons2010

The 19th international Conference on Cyclotrons and Their Applications (CYCLOTRONS'10) will take place at Lanzhou, P.R. China on September 6 – 10, 2010. The Institute of Modern Physics (IMP), affiliated to Chinese Academy of Sciences will be hosting the conference. The location of the conference will be at the Ning-Wo Zhuang Hotel in downtown Lanzhou. The conference will include a reception evening, oral presentations (invited talks and oral contributions), poster sessions, a conference banquet, a technical tour of IMP facilities and an option for a half day excursion.

The scientific program of the conference will include the following topics:
- Cyclotron applications
- Newly operating cyclotrons
- Operational cyclotrons: developments and status
- Facilities under construction
- Projects and proposals
- FFAG accelerators
- High beam intensity operation
- Radioactive beams
- Beam dynamics
- Ion sources , strippers and targets
- Radio frequency systems
- Magnet and vacuum
- Beam transport, diagnostics and control system

A conference web site will be available on March 1st 2010:

http://cyclotrons10.impcas.ac.cn

Conference Venue

The conference will be held at the Ning-Wo-Zhuang Hotel located in downtown Lanzhou, with advanced equipments, elegant decorations and satisfying environment, the venue provides participants warm services of fruitful scientific discussions in an informal and relaxed atmosphere. Details of the venue are available on the following web site:

http://www.gsnwzhotels.com/English/index.asp

Lanzhou, the capital of Gansu province, is a major stop on the ancient "Silk Road", located at the upper reaches of the Yellow River. It's an amazing city with a long history, offers many historic spots and interest places. Today, Lanzhou is an important heavy industrial base in the western China. In Lanzhou, everyone will be interesting in her unique charm. You can find the interesting information on the web site:

http://www.chinats.com/lanzhou/index.htm

Registration and Fee

All colleagues interested in the related fields of the conference are cordially invited to participate in the conference and present contributions in oral or poster format. All conference attendees are encouraged to complete the registration form on the conference web site via the JACoW SPMS system, which will be available on March 1st 2010.

Because the registration in time is crucial for organization of the conference, participant's cooperation will be highly appreciated. The reduced conference fee is EUR €550.00 (five hundred fifty EUROS) for payments which are received on or before August 6th 2010. After that date the registration fee will increase to EUR €600.00 (six hundred EUROS). A special reduced registration fee EUR €300.00 is offered to students. The registration fee for each accompanying person is EUR €200.00. The conference registration fee includes:

- Materials of conference including the abstract book and the proceedings
- Coffee breaks and lunch buffet
- Conference excursion and technical tour
- Reception and banquet
- Transportation between Lanzhou airport and the hotel

The reduced registration fee can be paid by transfer only. The conference bank account is:

Name: Institute of Modern Physics, Chinese Academy of Sciences
Bank of Deposit: Bank of China Gansu Branch
Account: 325127835688091038
Swift: BKCHCNBJ660

It is also possible to pay by cash or credit card at the conference desk when you arrival in Lanzhou.

Abstracts

Abstracts must be submitted to the SPMS system developed by the JACoW collaboration. Authors must register to the JACoW system before submission. The website for registration and submission will be available on March 1st 2010:

Hotel Accommodations

The conference hotel is the Ning-Wo-Zhuang Hotel. A number of rooms have been reserved for participants. Please make your reservations online by visiting hotel website:

http://www.gsnwzhotels.com/English/index.asp

Be sure to reference CYCLOTRONS'10 when making reservations so that you can get special rate!

Please do not hesitate to contact the conference secretary if you have any problem for the hotel reservation. Information on alternate hotels nearby will be available on the conference web page after March 1st 2010.

Visa Information

Participants (including the accompany person) are required a visa to enter P.R. China. Please contact local secretariat (mail to: cyclotrons@impcas.ac.cn) with the following information in order to receive the formal documents needed for the visa application.

****

1-First Name; 2-Family Name; 3-Sex; 4-Birthdate; 5-Nationality; 6-Affiliation and Position; 7-Postal Address; 8-Passport No.; 9-Embassy/Consulate to apply for Chinese VISA; 10-Planned date of entry and leaving China.

****

Then you will receive an invitation letter for the visa application from IMP and an official visa application form by regular mail. Please keep in mind that the visa application process could take up to more than one month in extreme cases. Please apply for your visa as early as possible.

Insurance

Attendees have to take care of proper health and personal liability insurance. No responsibility can be taken by the organizers.

Important Dates

Opening of Delegate Registration	March 1, 2010
Abstract Submission Available	March 1, 2010
Abstract Submission Deadline	June 15, 2010
Early Registration Deadline (€550.00)	August 6, 2010
Paper Submission Deadline	August 20, 2010

International Organizing Committee

P. Bertrand (GANIL), R. Bhandari (VECC), S. Brandenburg (KVI), L. Calabretta (INFN-LNS), J. Conradie (iThemba LABS), M. Craddock (TRIUMF), G. Dutto (TRIUMF), S. Gales (GANIL), K. Hatanaka (RCNP), P.

Heikkinen (JYFL), Y. Hirao (NIRS), Y.Jongen (IBA), M. Loiselet (UCL), C.Lyneis (LBNL), R. Maier (FZ-Jülich), F. Marti (NSCL/MSU), D. May (Texas A&M Univ.), Y. Mori (Kyoto Univ.), L. Onischenko (JINR), H. Schweickert (FZK), M. Seidel(PSI), Y.Yano (RIKEN), W. L. Zhan, IMP (Chairman)

Program Committee

P. Bertrand (GANIL), S. Brandenburg(KVI), L. Calabretta (INFN-LNS), M. Craddock (TRIUMF), A. Goto (RIKEN), Y. Jongen (IBA), C. Lyneis (LBNL), F. Marti (NSCL/MSU), Y.Mori (Kyoto Univ.), M. Seidel (PSI), W. L. Zhan (IMP), T.J. Zhang (CIAE), H.W. Zhao (IMP, Chairman)

Local Organizing Committee

X.H. Cai, H.L Chen, H.F. Hao, Y. He, Z.G.Hu, Q. Liang (Secretary), Y.Liu, L.J. Mao(Scientific secretary), M.T. Song, B. Wang, J.W. Xia, M. Xie, Z. Xu, H.W. Zhao, X.D. Yang, Y.J.Yuan (Chairman)

Contact

Please address any further questions to the conference scientific secretary:

Dr. Lijun Mao

Institute of Modern Physics (IMP), Chinese Academy of Sciences

509 Nanchang Road, Lanzhou, 730000, P.R. China

Tel: +86-931-4969221

Fax: +86-931-8272100

Email: cyclotrons@impcas.ac.cn

Conference Website: http://cyclotrons10.impcas.ac.cn

7 Announcements of the Beam Dynamics Panel

7.1 ICFA Beam Dynamics Newsletter

7.1.1 Aim of the Newsletter

The ICFA Beam Dynamics Newsletter is intended as a channel for describing unsolved problems and highlighting important ongoing works, and not as a substitute for journal articles and conference proceedings that usually describe completed work. It is published by the ICFA Beam Dynamics Panel, one of whose missions is to encourage international collaboration in beam dynamics.

Normally it is published every April, August and December. The deadlines are 15 March, 15 July and 15 November, respectively.

Categories of Articles

The categories of articles in the newsletter are the following:

1. Announcements from the panel.

2. Reports of beam dynamics activity of a group.

3. Reports on workshops, meetings and other events related to beam dynamics.

4. Announcements of future beam dynamics-related international workshops and meetings.

5. Those who want to use newsletter to announce their workshops are welcome to do so. Articles should typically fit within half a page and include descriptions of the subject, date, place, Web site and other contact information.

6. Review of beam dynamics problems: This is a place to bring attention to unsolved problems and should not be used to report completed work. Clear and short highlights on the problem are encouraged.

7. Letters to the editor: a forum open to everyone. Anybody can express his/her opinion on the beam dynamics and related activities, by sending it to one of the editors. The editors reserve the right to reject contributions they judge to be inappropriate, although they have rarely had cause to do so.

The editors may request an article following a recommendation by panel members. However anyone who wishes to submit an article is strongly encouraged to contact any Beam Dynamics Panel member before starting to write.

7.1.2 How to Prepare a Manuscript

Before starting to write, authors should download the template in Microsoft Word format from the Beam Dynamics Panel web site:

http://www-bd.fnal.gov/icfabd/news.html

It will be much easier to guarantee acceptance of the article if the template is used and the instructions included in it are respected. The template and instructions are expected to evolve with time so please make sure always to use the latest versions.

The final Microsoft Word file should be sent to one of the editors, preferably the issue editor, by email.

The editors regret that LaTeX files can no longer be accepted: a majority of contributors now prefer Word and we simply do not have the resources to make the conversions that would be needed. Contributions received in LaTeX will now be returned to the authors for re-formatting.

In cases where an article is composed entirely of straightforward prose (no equations, figures, tables, special symbols, etc.) contributions received in the form of plain text files may be accepted at the discretion of the issue editor.

Each article should include the title, authors' names, affiliations and e-mail addresses.

7.1.3 Distribution

A complete archive of issues of this newsletter from 1995 to the latest issue is available at

http://icfa-usa.jlab.org/archive/newsletter.shtml.

This is now intended as the primary method of distribution of the newsletter.

Readers are encouraged to sign-up for electronic mailing list to ensure that they will hear immediately when a new issue is published.

The Panel's Web site provides access to the Newsletters, information about future and past workshops, and other information useful to accelerator physicists. There are links to pages of information of local interest for each of the three ICFA areas.

Printed copies of the ICFA Beam Dynamics Newsletters are also distributed (generally some time after the Web edition appears) through the following distributors:

Weiren Chou	chou@fnal.gov	North and South Americas
Rainer Wanzenberg	rainer.wanzenberg@desy.de	Europe[++] and Africa
Susumu Kamada	susumu.kamada@kek.jp	Asia[**] and Pacific

[++] Including former Soviet Union.
[**] For Mainland China, Jiu-Qing Wang (wangjq@mail.ihep.ac.cn) takes care of the distribution with Ms. Su Ping, Secretariat of PASC, P.O. Box 918, Beijing 100039, China.

To keep costs down (remember that the Panel has no budget of its own) readers are encouraged to use the Web as much as possible. In particular, if you receive a paper copy that you no longer require, please inform the appropriate distributor.

7.1.4 Regular Correspondents

The Beam Dynamics Newsletter particularly encourages contributions from smaller institutions and countries where the accelerator physics community is small. Since it is impossible for the editors and panel members to survey all beam dynamics activity worldwide, we have some Regular Correspondents. They are expected to find interesting activities and appropriate persons to report them and/or report them by themselves. We hope that we will have a "compact and complete" list covering all over the world eventually. The present Regular Correspondents are as follows:

Liu Lin	Liu@lnls.br	LNLS, Brazil
Sameen Ahmed Khan	Rohelakan@yahoo.com	SCOT, Oman
Jacob Rodnizki	Jacob.Rodnizki@gmail.com	Soreq NRC, Israel
Rohan Dowd	Rohan.Dowd@synchrotron.org.au	Australian Synchrotron

We are calling for more volunteers as Regular Correspondents.

7.2 ICFA Beam Dynamics Panel Members

Name	eMail	Institution
Rick Baartman	baartman@lin12.triumf.ca	TRIUMF, 4004 Wesbrook Mall, Vancouver, BC, V6T 2A3, Canada
Marica Biagini	marica.biagini@lnf.infn.it	LNF-INFN, Via E. Fermi 40, Frascati 00044, Italy
Yunhai Cai	yunhai@slac.stanford.edu	SLAC, 2575 Sand Hill Road, MS 26, Menlo Park, CA 94025, U.S.A.
Swapan Chattopadhyay	swapan@cockcroft.ac.uk	The Cockcroft Institute, Daresbury, Warrington WA4 4AD, U.K.
Weiren Chou (Chair)	chou@fnal.gov	Fermilab, P.O. Box 500, Batavia, IL 60510, U.S.A.
Wolfram Fischer	wfischer@bnl.gov	Brookhaven National Laboratory, Bldg. 911B, Upton, NY 11973, U.S.A.
Yoshihiro Funakoshi	yoshihiro.funakoshi@kek.jp	KEK, 1-1 Oho, Tsukuba-shi, Ibaraki-ken, 305-0801, Japan
Miguel Furman	mafurman@lbl.gov	Center for Beam Physics, LBL, 1 Cyclotron Road, Berkeley, CA 94720-8211, U.S.A.
Jie Gao	gaoj@ihep.ac.cn	Institute for High Energy Physics, P.O. Box 918, Beijing 100049, China
Ajay Ghodke	ghodke@cat.ernet.in	RRCAT, ADL Bldg. Indore, Madhya Pradesh, 452 013, India
Ingo Hofmann	i.hofmann@gsi.de	High Current Beam Physics, GSI Darmstadt, Planckstr. 1, 64291 Darmstadt, Germany
Sergei Ivanov	ivanov_s@mx.ihep.su	Institute for High Energy Physics, Protvino, Moscow Region, 142281 Russia
Kwang-Je Kim	kwangje@aps.anl.gov	Argonne Nat'l Lab, Advanced Photon Source, 9700 S. Cass Avenue, Argonne, IL 60439, U.S.A.
In Soo Ko	isko@postech.ac.kr	Pohang Accelerator Lab, San 31, Hyoja-Dong, Pohang 790-784, South Korea
Alessandra Lombardi	alessandra.lombardi@cern.ch	CERN, CH-1211, Geneva 23, Switzerland
Yoshiharu Mori	mori@kl.rri.kyoto-u.ac.jp	Research Reactor Inst., Kyoto Univ. Kumatori, Osaka, 590-0494, Japan
Mark Palmer	mark.palmer@cornell.edu	Wilson Laboratory, Cornell University, Ithaca, NY 14853-8001, USA
Chris Prior	c.r.prior@rl.ac.uk	ASTeC Intense Beams Group, STFC RAL, Chilton, Didcot, Oxon OX11 0QX, U.K.
Yuri Shatunov	yu.m.shatunov@inp.nsk.su	Acad. Lavrentiev, prospect 11, 630090 Novosibirsk, Russia
Junji Urakawa	junji.urakawa@kek.jp	KEK, 1-1 Oho, Tsukuba-shi, Ibaraki-ken, 305-0801, Japan
Jiu-Qing Wang	wangjq@mail.ihep.av.cn	Institute for High Energy Physics, P.O. Box 918, 9-1, Beijing 100049, China
Rainer Wanzenberg	rainer.wanzenberg@desy.de	DESY, Notkestrasse 85, 22603 Hamburg, Germany

The views expressed in this newsletter do not necessarily coincide with those of the editors. The individual authors are responsible for their text.